EXPERIMED

İSTANBUL UNIVERSITY PRESS

EXPERIMED

Volume 15 • Issue 2 • August 2025

Indexing & Abstracting	SCOPUS
	Web of Science Core Collection - Emerging Sources Citation Index (ESCI)
	Web of Science - Biological Abstracts
	Web of Science - BIOSIS Previews
	TUBITAK ULAKBIM TR Index
	DOAJ (Directory of Open Access Journals)
	Chemical Abstracts Service (CAS)
	EBSCO Central & Eastern European Academic Source
	CAB Abstracts
	CABI Global Health
	SOBIAD

Editorial Management

Assoc. Prof. Ali Cihan TASKIN

Department of Lab Animal Science, Aziz Sancar Institute of Experimental Medicine, Istanbul University Istanbul, Turkiye
ataskin@istanbul.edu.tr

Assoc. Prof. Timur Hakan BARAK

Department of Pharmacognosy, Faculty of Pharmacy, Acıbadem Mehmet Ali Aydınlar University, Istanbul, Turkiye
timur.barak@acibadem.edu.tr

Statistics Editor   **Sevda OZEL YILDIZ**

Department of Biostatistics, Istanbul Medical Faculty, Istanbul University, Istanbul, Turkiye
sevda@istanbul.edu.tr

Editorial Board Members

Table of Contents

İSTANBUL
UNIVERSITY
PRESS

Experimed

Review Article

The Clinical Pathway of Human T-Lymphotropic Virus Type-1 (HTLV-1) from Infection to Leukemia: A Comprehensive Review

Abolfazl Jafari-Sales [1, 2, 3] ⓘ , Aylin Golestani [3, 4] ⓘ , Zahra Ghahremani [3, 4] ⓘ , Kosar Soleymanpour [3, 4] ⓘ ,
Kosar Hosseini-Karkaj [3, 4] ⓘ , Parya Rouhi [3, 4] ⓘ , Mehrdad Pashazadeh [3, 5] ⓘ ✉ , Hossein Bannazadeh Baghi [6, 7] ⓘ ,
Mohaddeseh Bahmani [7, 8] ⓘ

[1] Department of Microbiology, Kaz.C., Islamic Azad University, Kazerun, Iran
[2] Department of Microbiology, Ta.C., Islamic Azad University, Tabriz, Iran
[3] Infectious Diseases Research Center, TaMS.C., Islamic Azad University, Tabriz, Iran
[4] Department of Cellular and Molecular Biology, Ta.C., Islamic Azad University, Tabriz, Iran
[5] Department of Medical Laboratory Sciences and Microbiology, TaMS.C., Islamic Azad University, Tabriz, Iran
[6] Infectious and Tropical Diseases Research Center, Tabriz University of Medical Sciences, Tabriz, Iran
[7] Department of Virology, Tabriz University of Medical Sciences, Tabriz, Iran
[8] Center for Orthopedic Trans-Disciplinary Applied Research, Tehran University of Medical Sciences, Tehran, Iran

Abstract

Human T-lymphotropic virus type 1 (HTLV-1), a member of the Retroviridae family, is a pathogenic retrovirus that primarily includes two clinically relevant types: HTLV-1 and HTLV-2. HTLV-1 is etiologically linked to adult T-cell leukemia/lymphoma (ATLL), a highly aggressive hematological malignancy. The principal modes of HTLV-1 transmission are mother-to-child (predominantly via breastfeeding), sexual contact, and exposure to contaminated blood products. The viral oncoprotein Tax and HTLV-1 basic leucine zipper factor are central to the virus's oncogenic potential, orchestrating a cascade of genetic and molecular alterations that drive the clonal proliferation and malignant transformation of infected lymphocytes over a prolonged latent period, often spanning several years. Despite extensive research, the precise mechanisms underlying the clonal evolution and emergence of leukemic cells remain incompletely elucidated. Diagnosis typically relies on a two-step serological screening approach. While preventive strategies have been implemented, HTLV-1, like other retroviruses, persists as a lifelong infection, and no definitive cure or effective vaccine is currently available. This comprehensive review delineates the pathophysiological continuum from HTLV-1 infection to ATLL, emphasizing the molecular underpinnings of viral oncogenesis, the clinical relevance of early leukemia detection, and the current challenges in prevention and management.

✉ Corresponding author: Mehrdad Pashazadeh mehrdadpashazadeh85@gmail.com

Introduction

Leukemia, a clonal malignancy of hematopoietic stem and progenitor cells, ranks 15th in global cancer incidence and 11th in cancer-related mortality based on 2020 international statistics (1, 2). Human T-lymphotropic virus (HTLV) has been identified as one of the most potent oncogenic viruses, with HTLV type 1 (HTLV-1) implicated in a substantial spectrum of human diseases (3, 4). Alongside HTLV, other viruses such as hepatitis B virus, hepatitis C virus, Epstein-Barr virus, and human immunodeficiency virus are also recognized contributors to leukemia (5, 6). The World Health Organization (WHO) has recently designated HTLV-1 as a global health concern (7). A subset of patients with adult T-cell leukemia/lymphoma (ATLL) harbor HTLV-1 infection, with approximately 5% progressing to this aggressive malignancy (8, 9). The presence of HTLV-1 in ATLL is influenced by the host's genetic and epigenetic background (10). HTLV-1 persists in the host through clonal expansion or mitotic proliferation of infected cells, as well as direct cell-to-cell transmission of viral particles (11). Despite extensive research on HTLV and leukemia, challenges remain in isolating HTLV-1-infected cells and developing effective treatments. Rapid detection of HTLV-1 is crucial because early intervention can prevent disease progression and improve outcomes. This study aimed to elucidate the mechanisms of HTLV-1 pathogenesis and to review current therapeutic strategies for managing HTLV-1-associated infections and leukemia. Investigating the pathogenesis and risk factors of ATLL and evaluating novel diagnostic and therapeutic approaches are essential for advancing disease management. Such research will contribute to a deeper understanding of ATLL pathogenesis, diagnosis, and treatment, ultimately improving patient care for those affected by HTLV-1-associated malignancies.

Leukemia

Leukemia encompasses a group of malignancies that involve the spleen, bone marrow, lymphatic system, peripheral blood, and other hematopoietic tissues (12). In leukemia, the normal function of hematopoietic stem cells is disrupted, resulting in the incomplete and aberrant development of blood cells and the subsequent emergence of hematologic malignancies (13). Since the latter half of the nineteenth century, understanding of leukemia has significantly advanced. John Hughes Bennett reported the first documented case in the Edinburgh Medical and Surgical Journal in October 1845 (14). Leukemia accounts for approximately one-third of all cancers diagnosed in children (15). The four principal subtypes of leukemia are acute lymphocytic leukemia, acute myeloid leukemia, chronic lymphocytic leukemia, and chronic myeloid leukemia. Recent

epidemiological studies indicate an increasing incidence of leukemia in countries such as Germany, Korea (16), Japan, Canada, and the United Kingdom, as well as rising mortality rates in Ecuador, Belarus, Thailand, and the Philippines (17). Several risk factors have been identified, including advanced age, exposure to ionizing radiation, and contact with certain chemicals such as benzene (18-20). ATLL, a rare neoplasm, is classified into four clinical subtypes: acute, lymphoma, chronic and latent (21). According to the WHO, ATLL is defined as a mature peripheral T-cell neoplasm induced by HTLV-1 infection and is characterized by highly pleomorphic lymphoid cells (22). The clinical features of ATLL include leucocytosis, hepatosplenomegaly, lymphadenopathy, hypercalcemia, and multiple opportunistic infections. Additionally, the distinctive cell morphology in blood tests and immune-phenotyping results of blood or tissue samples are used for the accurate diagnosis of this disease (23). Other symptoms of ATLL include kidney dysfunction, neuropsychiatric disorders, and elevated lactate dehydrogenase levels. Skin lesions and visceral involvement in the bones, lungs, and gastrointestinal tract may also occur (24).

Human T-Lymphotropic Virus

HTLV is classified within the Orthoretrovirinae subfamily of the Retroviridae family (25). The first HTLV-1 was reported in 1980 (26). HTLV-1 is an enveloped, double-stranded RNA retrovirus that primarily infects lymphocytes, contributing to the pathogenesis of various diseases. Transmission occurs through sexual intercourse, injection, vertical transmission (notably via breastfeeding), blood transfusion, and transplantation of infected cells. Breastfeeding is recognized as the principal route of mother-to-child transmission. Approximately 10% of HTLV-1-infected individuals develop clinical symptoms during their lifetime (7, 27). The risk of HTLV-1 transmission via blood products, which may decrease the viability of infected lymphocytes, can be reduced by using blood plasma and cold storage (28). Epidemiologically, the incidence of HTLV-1 infection in women is about three times higher than in men (22). Clinical differentiation of HTLV-1 infection is primarily based on its association with ATLL and HTLV-1-associated myelopathy/tropical spastic paraparesis (HAM/TSP), a progressive, chronic neurological disorder. Only a minority of infected individuals develop these complications (29). HTLV-1 infection is also linked to inflammatory diseases such as uveitis, infective dermatitis, polyneuropathic, and tuberculosis, as well as certain rheumatic, autoimmune, and neuropsychiatric disorders (28, 30). The proviral load (PVL) of HTLV-1 is typically higher in individuals with HAM/TSP than

in asymptomatic carriers; however, an elevated PVL% is not invariably indicative of clinical disease, as it may also reflect subclinical proliferative or inflammatory processes (31).

Epidemiology

The development of serological techniques for detecting human antibodies against HTLV-1 and HTLV-2, as a result of the isolation of HTLV-1 and HTLV-2 strains, has enabled global characterization of their prevalence (32). HTLV-1 exhibits distinct geographic clustering, with highly endemic regions including the Caribbean, South America, Southwestern Japan, Australo-Melanesia, the Middle East and subtropical Africa particularly Southern Gabon. Europe's sole endemic focus is in Romania (3). Globally, an estimated 10 million individuals harbor HTLV-1, with tropical Africa accounting for approximately half of the infections. Hyper-endemic areas such as Gabon, Congo and Nigeria demonstrate prevalence rates reaching 10%–25% among elderly women. Despite Africa's status as the largest HTLV-1 reservoir, routine blood donor screening remains absent across the continent, whereas European nations like Spain and the UK mandate HTLV screening for organ donors (27, 33). In Southwest Asia, Iran reported the highest HTLV-1 burden, with an elevated prevalence concentrated in the Razavi Khorasan, South Khorasan, and Golestan provinces. Endemic foci include Mashhad (2.12% general population prevalence) (34), Neyshabur (7.25%) (35), Sabzevar (1.66%) (36), and Torbat-e-Heydarieh (1.25%) (37). Migration patterns have significantly influenced HTLV-1 epidemiology in England and Wales, where estimated cases rose from 14,900 in 1991 to 36,300 in 2021, driven largely by immigration from endemic regions such as Nigeria and Romania (33). HTLV-1 exhibits substantial genetic diversity and these genotypes may differ in various geographic distributions, with six genotypes (a, b, d, e, f, g), the greatest number of HTLV-1 genetic variations, identified in Africa alone (38). One of the most common clinical sequelae of the virus include HAM/TSP, affecting 2%–5% of infected individuals (39, 40).

Mechanisms of Human T-Lymphotropic Virus Type-1-Induced Carcinogenesis in Adult T-Cell Leukemia/Lymphoma

HTLV-1 infection is causally linked to ATLL, a malignancy arising from CD4+ T lymphocytes (41). Unlike other retroviruses, HTLV-1 predominantly spreads via cell-to-cell viral synapses (42, 43). Central to its oncogenicity are the viral proteins Tax and HTLV-1 basic leucine-zipper factor (HBZ), which drive genetic and epigenetic dysregulation (5). Chronic activation of the nuclear factor kappa B (NF-κB) pathway is essential for tumorigenesis.

The interaction between Tax and HBZ proteins in regulating the NF-κB pathway facilitates viral persistence in ATLL cells. Specifically, the Tax-1 protein acts as a potent activator of these transcription factors and promotes the proliferation of HTLV-1-transformed cell lines (44). Tax-mediated NF-κB activation results from the stimulation of a cytoplasmic mechanism that leads to the nuclear translocation of NF-κB. In addition, NF-κB can inhibit p53-independent apoptosis by interfering with oncogenic Ras activity (45). Genetic alterations or DNA hypermethylation frequently suppress Tax expression in ATLL, whereas somatic mutations in the T/B-cell receptor and NF-κB signaling pathways sustain NF-κB activation in ATLL (46). HBZ inhibits the canonical NF-κB pathway by suppressing DNA-binding capability and inducing proteasome degradation of the p65 subunit (47). P19 represents the matrix protein and p24 represents the capsid protein (48). Cell-to-cell transmission involves the envelope (Env), additional viral proteins such as p19 and nucleocapsid, and viral genomes (49). The expression level of glucose transporter 1, an HTLV-1 receptor molecule involved in the integration and entrance of the virus into the target cell, is directly correlated with infection (50). HTLV-1 binds to target cells through two receptors, neuropilin-1 and heparin sulfate proteoglycans (51). The transmembrane protein gp21 and the cell surface protein gp46 work together as a trimer to promote viral entry (52). The virus genome comprises the retroviral genes group-specific antigen (gag), pro, pol, and Env, which encode several viral structural proteins (53, 54). The majority of ATLL patients have tumor cells that express C-C chemokine receptor type 4 (CCR4) (55). CCR4 is primarily expressed by HTLV-1-infected T cells (56). In T cells infected with HTLV-1, Tax stimulates the production of the C-C motif chemokine ligand 22 (CCL22) and intercellular adhesion molecule 1 (ICAM-1). Among the ligands of CCR4 is CCL22. CCL22 stimulates lymphocyte function-associated antigen 1 (LFA-1) and draws T cells that express CCR4 to T cells infected with HTLV-1. Binding LFA-1 to ICAM-1 creates a viral synapse (57, 58). Once in the cytoplasm, reverse transcription converts viral RNA to double-stranded DNA (dsDNA). dsDNA is incorporated into the host's nuclear genome. This provirus's transcription factor is cellular RNA polymerase II. The resulting post-transcriptional regulatory mechanism is essential for viral mRNA splicing and trafficking. Viral mRNA is exported from the nucleus to the cytoplasm (59). There is a heterodimer (p51 and p66) in lieu of reverse transcription (60). Through the activity of virally encoded proteins, such as Tax, HTLV-1 promotes the clonal growth of virus-infected cells after infection (61) (Figure 1).
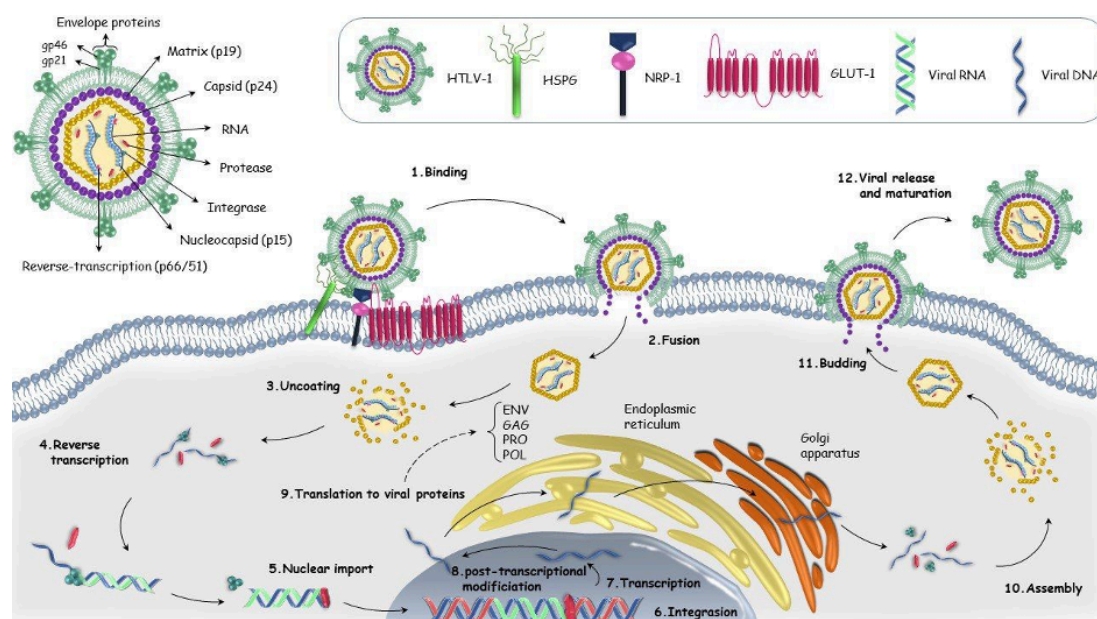
Figure 1. HTLV-1 and its entry into the host cell. HTLV-1 binds to target cells via interactions between its envelope glycoproteins (gp46 and gp21) and host receptors, including NRP1, HSPGs, and GLUT1. Following receptor engagement, the viral envelope mediates cell-to-cell fusion, facilitating the formation of a viral synapse a specialized structure critical for efficient viral transmission. The viral RNA genome is reverse-transcribed into double-stranded DNA (dsDNA), which integrates into the host nuclear genome as a provirus. Key viral proteins (e.g., Tax, HBZ) then drive the clonal expansion of infected T cells, a hallmark of HTLV-1 pathogenesis. HTLV-1: Human T lymphotropic virus type 1, HSPGs: Heparin sulfate proteoglycans, NRP1: Neuropilin-1, GLUT1: Glucose Transporter 1, Env: Envelope, gag: Group-specific antigen.

Diagnostic Approaches for Human T-Lymphotropic Virus Type-1 Infection and Adult T-cell Leukemia/Lymphoma Detection

Laboratory-based serological screening for HTLV-1 infection primarily employs enzyme-linked immunosorbent assay or particle agglutination assay as initial diagnostic tools. For samples exhibiting reactive, indeterminate, or discordant serological results, confirmatory testing is required, including western blot (WB), line immunoassay, and in-house molecular assays utilizing polymerase chain reaction (62). Antibody detection constitutes a cornerstone method for identifying HTLV-1 exposure (63), with WB serving as the gold standard for confirming reactivity to the gag gene-encoded proteins p24 (capsid) and p19 (matrix), demonstrating superior sensitivity in this context (40). Emergent biosensor-based technologies offer innovative, high-sensitivity platforms for the early-stage detection of infectious pathogens, including HTLV-1 (64). Notably, the ATLL lymphoma subtype can be identified through blood sampling before symptom manifestation, enabling preclinical diagnosis (65).

Prevention and Treatment

Currently, certain structural and non-structural protein segments of the virus are used to create vaccines. These elements are especially made to stimulate B cells, helper T lymphocytes, and cytotoxic T lymphocytes to produce a strong immune response. The search for an HTLV-1 vaccine is now examining a variety of strategies, such as viral vector vaccines, DNA vaccines, protein and peptide vaccines, dendritic cell-based vaccines, and mRNA vaccines (66). This improvement in many ATLL instances, particularly chronic ATLL, is thought to result from these two medicines' anti-proliferative rather than anti-viral properties, but the exact mechanism is yet unknown (67). New drugs such as mogamulizumab, lenalidomide, brentuximab vedotin (BV), tucidinostat, and valemetostat have been approved for the treatment of patients with relapsed or refractory ATLL (68). Mogamulizumab is a monoclonal antibody targeting CCR4 that enhances the initial response in ATLL by inducing antibody-dependent cellular cytotoxicity, with response rates of 50% in relapsed cases and 52% when combined with chemotherapy. Common adverse effects include infusion reactions and skin rashes, with more severe rashes correlated with a better prognosis (69, 70). Lenalidomide is an oral immunomodulatory drug with anti-proliferative and anti-tumor properties. Its direct target is a protein called Cereblon, which is essential for its anti-myeloma and anti-lymphoma effects. In a phase II study on relapsed ATLL patients, the overall response rate was 42%, with a complete response rate of 19%. The median progression-free survival was 3.8 months, and the median overall survival was 20.3 months. The most common severe adverse events included neutropenia, lymphocytopenia, anemia, and

thrombocytopenia (68, 71, 72). BV, an antibody-drug conjugate, consists of the microtubule inhibitor monomethyl auristatin E linked to the monoclonal antibody brentuximab, which targets CD30 (73). This drug exploits the increased expression of CD30 in the advanced stages of ATLL and its role in genomic instability, thereby enhancing the potential for CD30-targeted therapy in aggressive ATLL. Prospective studies are warranted to evaluate BV in ATLL (74, 75). Tucidinostat, a benzamide-class HDAC inhibitor, targets isoenzymes 1, 2, 3, and 10, exerting potent tumor suppression and immune modulation through epigenetic modifications. The major adverse effects include thrombocytopenia, neutropenia, and severe anemia. However, hematological toxicities and short duration of response limit its use, and combination therapies have been proposed (76, 77). Valemetostat, a selective dual inhibitor of EZH1/2, activates tumor suppressor genes by inhibiting histone H3K27 methylation The principal adverse effects include thrombocytopenia, anemia, lymphopenia, and severe neutropenia. Demonstrating significant anti-tumor activity, valemetostat holds promise for combination therapy approaches (78-80). When derived from bone marrow, peripheral blood, and umbilical cord blood, stem cells may be able to treat ATLL because they can develop into a variety of cell types and promote tissue regeneration (81). When treating HTLV-induced ATLL that is resistant to drugs that promote apoptosis, conventional chemotherapy has very little effect (82). In some cases, allogeneic stem cell transplantation is also used after chemotherapy (83). One of the usual methods of chemotherapy in ATLL is CHOP, which includes the drugs cyclophosphamide, doxorubicin, vincristine and prednisone (30). CCR4 signaling inhibition may be a treatment option for ATLL (84). Treatment of ATLL depends on the patient's symptoms and does not directly treat the viral infection (59).

Conclusion

HTLVs are oncogenic retroviruses implicated in the pathogenesis of diseases such as ATLL and HAM/TSP. The viral proteins Tax and HBZ play multifaceted roles in the development and progression of these disorders. Although most individuals infected with HTLV-1 remain asymptomatic throughout their lifetime and require no specific therapy, regular clinical monitoring is recommended to promptly identify disease onset. Given the therapeutic challenges associated with ATLL, there is a critical need for continued research into the molecular biology of HTLV-1 and the development of innovative treatment modalities. While chemotherapy remains a mainstay for ATLL management, it is not curative, and alternative strategies such as hematopoietic stem cell transplantation are under investigation. Targeting HBZ may represent a promising therapeutic avenue for

both HAM/TSP and ATLL. Future research should prioritize the development of targeted therapies, the refinement of early diagnostic techniques, and a deeper understanding of HTLV-1 molecular mechanisms to enhance disease control and improve patient outcomes.

List of Abbreviations

HTLV-1: Human T lymphotropic virus type 1, ATLL: Adult T cell leukemia/lymphoma, WHO: World Health Organization, HAM/TSP: HTLV-1-associated myelopathy/tropical spastic paraparesis, PVL: Proviral load, HBZ: HTLV-1 basic leucine zipper factor, NF-κB: Nuclear factor kappa B, Env: Envelope, gag: Group-specific antigen, CCR4: C-C chemokine receptor type 4, CCL22: C-C motif chemokine ligand 22, ICAM-1: Intercellular adhesion molecule 1, LFA-1: Lymphocyte function associated antigen 1, dsDNA: Double-stranded DNA, WB: Western blot, BV: Brentuximab vedotin

Author Details

Abolfazl Jafari-Sales
[1] Department of Microbiology, Kaz.C., Islamic Azad University, Kazerun, Iran

[2] Department of Microbiology, Ta.C., Islamic Azad University, Tabriz, Iran

[3] Infectious Diseases Research Center, TaMS.C., Islamic Azad University, Tabriz, Iran

0000-0002-5710-4076

Aylin Golestani
[3] Infectious Diseases Research Center, TaMS.C., Islamic Azad University, Tabriz, Iran

[4] Department of Cellular and Molecular Biology, Ta.C., Islamic Azad University, Tabriz, Iran

0009-0008-0886-9874

Zahra Ghahremani
[3] Infectious Diseases Research Center, TaMS.C., Islamic Azad University, Tabriz, Iran

[4] Department of Cellular and Molecular Biology, Ta.C., Islamic Azad University, Tabriz, Iran

0009-0002-9744-3707

Kosar Soleymanpour
[3] Infectious Diseases Research Center, TaMS.C., Islamic Azad University, Tabriz, Iran

[4] Department of Cellular and Molecular Biology, Ta.C., Islamic Azad University, Tabriz, Iran

0009-0002-2559-4645

Kosar Hosseini-Karkaj
[3] Infectious Diseases Research Center, TaMS.C., Islamic Azad University, Tabriz, Iran

[4] Department of Cellular and Molecular Biology, Ta.C., Islamic Azad University, Tabriz, Iran

0009-0001-1120-9665

Parya Rouhi
[3] Infectious Diseases Research Center, TaMS.C., Islamic Azad University, Tabriz, Iran

[4] Department of Cellular and Molecular Biology, Ta.C., Islamic Azad University, Tabriz, Iran

0009-0006-2944-8134

Mehrdad Pashazadeh
[3] Infectious Diseases Research Center, TaMS.C., Islamic Azad University, Tabriz, Iran

[5] Department of Medical Laboratory Sciences and Microbiology, TaMS.C., Islamic Azad University, Tabriz, Iran

0009-0005-0694-4592   ✉ mehrdadpashazadeh85@gmail.com

Hossein Bannazadeh Baghi
[6] Infectious and Tropical Diseases Research Center, Tabriz University of Medical Sciences, Tabriz, Iran

[7] Department of Virology, Tabriz University of Medical Sciences, Tabriz, Iran

0000-0002-2513-5361

Mohaddeseh Bahmani
[7] Department of Virology, Tabriz University of Medical Sciences, Tabriz, Iran

[8] Center for Orthopedic Trans-Disciplinary Applied Research, Tehran University of Medical Sciences, Tehran, Iran

REFERENCES

1. Du M, Chen W, Liu K, Wang L, Hu Y, Mao Y, et al. The global burden of leukemia and its attributable factors in 204 countries and territories: findings from the global burden of disease 2019 study and projections to 2030. J Oncol 2022; 2022(1): 1612702.

2. Wang W, An J, Zhao R, Geng X, Jiang W, Yan X, et al. Nanozymes: a new approach for leukemia therapy. J Mater Chem B 2024; 12(10): 2459-70.

3. Gessain A, Cassar O. Epidemiological aspects and world distribution of HTLV-1 infection. Front Microbiol 2012; 3: 388.

4. Martin F, Tagaya Y, Gallo R. Time to eradicate HTLV-1: an open letter to WHO. Lancet 2018; 391(10133): 1893-4.

5. Hatano Y, Ideta T, Hirata A, Hatano K, Tomita H, Okada H, et al. Virus-driven carcinogenesis. Cancers 2021; 13(11): 2625.

6. Haghtalab A, Hejazi M, Goharnia N, Yekanlou A, Hazhir K, Barghi A, et al. Investigating the correlation between prominent viruses and hematological malignancies: a literature review. Med Oncol 2024; 41(5): 102.

7. Rosadas C, Costa M, Senna K, Santos M, Taylor GP. Impact and economic analysis of human T-cell lymphotropic virus type 1 (HTLV-1)-targeted antenatal screening, England and Wales, 2021. Eurosurveillance 2024; 29(22): 2300537.

8. Gallo R, Mann D, Broder S, Ruscetti F, Maeda M, Kalyanaraman V, et al. Human T-cell leukemia-lymphoma virus (HTLV) is in T but not B lymphocytes from a patient with cutaneous T-cell lymphoma. Proc Natl Acad Sci 1982; 79(18): 5680-3.

9. Bangham CR. HTLV-1 persistence and the oncogenesis of adult T-cell leukemia/lymphoma. Blood, Am Soc Hematol 2023; 141(19): 2299-306.

10. Satou Y, Matsuoka M. Molecular and cellular mechanism of leukemogenesis of ATL: Emergent evidence of a significant role for HBZ in HTLV-1-induced pathogenesis. Leuk Res Treat 2012; 2012: 213653.

11. Mohanty S, Harhaj EW. Mechanisms of oncogenesis by HTLV-1 Tax. Pathogens 2020; 9(7): 543.

12. Salama MM, Aborehab NM, El Mahdy NM, Zayed A, Ezzat SM. Nanotechnology in leukemia: diagnosis, efficient-targeted drug delivery, and clinical trials. Eur J Med Res 2023; 28(1): 566.

13. Schoettler ML, Nathan DG. The pathophysiology of acquired aplastic anemia: current concepts revisited. Hematol/Oncol Clin North Am 2018; 32(4): 581-94.

14. Thomas X. First contributors in the history of leukemia. World J Hematol 2013; 2(3): 62-70.

15. Amani O, Mazaheri MA, Nejati V, Shamsian BS. Effect of cognitive rehabilitation on executive functions in adoles. Arch Rehabil 18(1): 73-82.

16. Sung H, Ferlay J, Siegel RL, Laversanne M, Soerjomataram I, Jemal A, et al. Global cancer statistics 2020: GLOBOCAN estimates of incidence and mortality worldwide for 36 cancers in 185 countries. Ca-Cancer J Clin 2021; 71(3): 209-49.

17. Huang J, Chan SC, Ngai CH, Lok V, Zhang L, Lucero-Prisno III DE, et al. Disease burden, risk factors, and trends of leukaemia: a global analysis. Front Oncol 2022; 12: 904292.

18. Creutzig U, Kutny MA, Barr R, Schlenk RF, Ribeiro RC. Acute myelogenous leukemia in adolescents and young adults. Pediatr Blood Cancer 2018; 65(9): e27089.

19. Ali Hailan YM, Al-Dubai HN, Yassin MA. Chronic myeloid leukemia following exposure to radioactive iodine (I131): a systematic review. Oncol 2023; 101(6): 362-8.

20. North CM, Schnatter AR, Rooseboom M, Kocabas NA, Dalzell A, Williams SD. Key event-informed risk models for benzene-induced acute myeloid leukaemia. Toxicol Lett 2021; 340: 141-52.

21. Ishitsuka K. Diagnosis and management of adult T-cell leukemia/lymphoma. Semin Hematol 2021; 58(2): 114-22.

22. Iwanaga M. Epidemiology of HTLV-1 infection and ATL in Japan: an update. Front Microbiol 2020; 11: 1124.

23. Cook L, Rowan A, Bangham C. Adult T-cell leukemia/lymphoma—pathobiology and implications for modern clinical management. Ann Lymphoma 2021; 5: 29.

24. El Hajj H, Tsukasaki K, Cheminant M, Bazarbachi A, Watanabe T, Hermine O. Novel treatments of adult T cell leukemia lymphoma. Front Microbiol 2020; 11: 1062.

25. Zhang L-l, Wei J-y, Wang L, Huang S-l, Chen J-l. Human T-cell lymphotropic virus type 1 and its oncogenesis. Acta Pharmacol Sin 2017; 38(8): 1093-103.

26. Poiesz BJ, Ruscetti FW, Gazdar AF, Bunn PA, Minna JD, Gallo RC. Detection and isolation of type C retrovirus particles from fresh and cultured lymphocytes of a patient with cutaneous T-cell lymphoma. Proc Natl Acad Sci 1980; 77(12): 7415-9.

27. Soriano V, de Mendoza C, Network SH. Screening for HTLV-1 infection should be expanded in Europe. Int J Infect Dis 2024; 140: 99-101.

28. Gonçalves DU, Proietti FA, Ribas JGR, Araújo MG, Pinheiro SR, Guedes AC, et al. Epidemiology, treatment, and prevention of human T-cell leukemia virus type 1-associated diseases. Clin Microbiol Rev 2010; 23(3): 577-89.

29. Verdonck K, González E, Van Dooren S, Vandamme A-M, Vanham G, Gotuzzo E. Human T-lymphotropic virus 1: recent knowledge about an ancient infection. Lancet Infect Dis 2007; 7(4): 266-81.

30. Eusebio-Ponce E, Anguita E, Paulino-Ramirez R, Candel FJ. HTLV-1 infection: An emerging risk. Pathogenesis, epidemiology, diagnosis and associated diseases. Rev Española Quimioter 2019; 32(6): 485-96.

31. Taylor GP, Evans W, Rosadas C. High HTLV-1 Proviral load predates and predicts HTLV-1-associated disease: literature review and the London experience. Pathogens 2024; 13(7): 553.

32. Ishak R, de Oliveira Guimarães Ishak M, Vallinoto ACR. The challenge of describing the epidemiology of HTLV in the Amazon region of Brazil. Retrovirology 2020; 17: 4.

33. de Mendoza C, Taylor G, Gessain A, Thoma-Kress AK, Bangham C, Vesterbacka J, et al. Virology, pathogenesis, epidemiology and clinical management of HTLV-1 infection. Proceedings of the 30th HTLV European research network (HERN 2023). NeuroImmune Pharmacol Ther 2024; 3(1): 61-9.

34. Rafatpanah H, Hedayati-Moghaddam MR, Fathimoghadam F, Bidkhori HR, Shamsian SK, Ahmadi S, et al. High prevalence of HTLV-I infection in Mashhad, Northeast Iran: a population-based seroepidemiology survey. J Clin Virol 2011; 52(3): 172-6.

35. Hedayati-Moghaddam M, Fathimoghadam F, Mashhadi IE, Soghandi L, Bidkhori H. Epidemiology of HTLV-1 in Neyshabour, northeast of Iran. Iran Red Crescent Med J 2011; 13(6): 424–7

36. Azarpazhooh MR, Hasanpour K, Ghanbari M, Rezaee SR, Mashkani B, Hedayati-Moghaddam MR, et al. Human T-lymphotropic virus type 1 prevalence in northeastern Iran, Sabzevar: an epidemiologic-based study and phylogenetic analysis. AIDS Res Hum Retroviruses 2012; 28(9): 1095-101.

37. Hedayati-Moghaddam MR, Jafarzadeh Esfehani R, El Hajj H, Bazarbachi A. Updates on the epidemiology of the human T-cell leukemia virus type 1 infection in the countries of the eastern mediterranean regional office of the world health organization with special emphasis on the situation in Iran. Viruses 2022; 14(4): 664.

38. Gessain A, Ramassamy J-L, Afonso PV, Cassar O. Geographic distribution, clinical epidemiology and genetic diversity of the human oncogenic retrovirus HTLV-1 in Africa, the world's largest endemic area. Front Immunol 2023; 14: 1043600.

39. Eatemadi M, Boustani R. the comparative therapeutic effects of danazol with multivitamin in HTLV-I associated myelopathy. Med J Mashhad Univ Med Sci 2005; 48(87): 69-74.

40. Martín-Dávila P, Fortún J, López-Vélez R, Norman F, Montes de Oca M, Zamarrón P, et al. Transmission of tropical and geographically restricted infections during solid-organ transplantation. Clin Microbiol Rev 2008; 21(1): 60-96.

41. Wu W, Cheng W, Chen M, Xu L, Zhao T. HTLV-1 bZIP factor (HBZ): Roles in HTLV-1 oncogenesis. Bing du xue bao 2016; 32(2): 235-42.

42. Pique C, Jones KS. Pathways of cell-cell transmission of HTLV-1. Front Microbiol 2012; 3: 378.

43. Matsuoka M. Human T-cell leukemia virus type I (HTLV-I) infection and the onset of adult T-cell leukemia (ATL). Retrovirology 2005; 2: 27.

44. Fochi S, Mutascio S, Bertazzoni U, Zipeto D, Romanelli MG. HTLV deregulation of the NF-κB pathway: An update on tax and antisense proteins role. Front Microbiol 2018; 9: 285.

45. Li XH, Gaynor RB. Regulation of NF-κB by the HTLV-1 Tax protein. Gene Expr 2018; 7(4-5-6): 233–45.

46. Harhaj EW, Giam CZ. NF-κB signaling mechanisms in HTLV-1-induced adult T-cell leukemia/lymphoma. FEBS J 2018; 285(18): 3324-36.

47. Ma G, Yasunaga J-i, Matsuoka M. Multifaceted functions and roles of HBZ in HTLV-1 pathogenesis. Retrovirology 2016; 13: 16.

48. Tu JJ, King E, Maksimova V, Smith S, Macias R, Cheng X, et al. An HTLV-1 envelope mRNA vaccine is immunogenic and protective in New Zealand rabbits. J Virol 2024; 98(2): e01623-23.

49. Maksimova V, Panfil AR. Human T-cell leukemia virus type 1 envelope protein: post-entry roles in viral pathogenesis. Viruses 2022; 14(1): 138.

50. Manel N, Battini J-L, Sitbon M. Human T cell leukemia virus envelope binding and virus entry are mediated by distinct domains of the glucose transporter GLUT1. J Biol Chem 2005; 280(32): 29025-9.

51. Al-Saleem J, Dirksen WP, Martinez MP, Shkriabai N, Kvaratskhelia M, Ratner L, et al. HTLV-1 Tax-1 interacts with SNX27 to regulate cellular localization of the HTLV-1 receptor molecule, GLUT1. PLoS One 2019; 14(3): e0214059.

52. Hatayama Y, Yamaoka Y, Morita T, Jeremiah SS, Miyakawa K, Nishi M, et al. Development of a monoclonal antibody targeting HTLV-1 envelope gp46 glycoprotein and its application to near-infrared photoimmuno-antimicrobial strategy. Viruses 2022; 14(10): 2153.

53. Hoshino H. Cellular factors involved in HTLV-1 entry and pathogenicit. Front Microbiol 2012; 3: 222.

54. Giam C-Z, Pasupala N. NF-κB-Induced R-Loops and genomic instability in HTLV-1-Infected and adult T-cell leukemia cells. Viruses 2022; 14(5): 877.

55. Fujii K, Sakamoto Y, Masaki A, Murase T, Tashiro Y, Yonekura K, et al. Immunohistochemistry for CCR4 C-terminus predicts CCR4 mutations and mogamulizumab efficacy in adult T-cell leukemia/lymphoma. J Pathol Clin Res 2021; 7(1): 52-60.

56. Yoshie O, Fujisawa R, Nakayama T, Harasawa H, Tago H, Izawa D, et al. Frequent expression of CCR4 in adult T-cell leukemia and human T-cell leukemia virus type 1–transformed T cells. Blood 2002; 99(5): 1505-11.

57. Yoshie O. CCR4 as a therapeutic target for cancer immunotherapy. Cancers 2021; 13(21): 5542.

58. Nejmeddine M, Bangham CR. The HTLV-1 virological synapse. Viruses 2010; 2(7): 1427-47.

59. Martin JL, Maldonado JO, Mueller JD, Zhang W, Mansky LM. Molecular studies of HTLV-1 replication: an update. Viruses 2016; 8(2): 31.

60. Tardiota N, Jaberolansar N, Lackenby JA, Chappell KJ, O'Donnell JS. HTLV-1 reverse transcriptase homology model provides structural basis for sensitivity to existing nucleoside/nucleotide reverse transcriptase inhibitors. Virol J 2024; 21(1): 14.

61. Tebbi CK. Etiology of acute leukemia: A review. Cancers 2021; 13(9): 2256.

62. Gomes Y, Caterino-de-Araujo A, Campos K, Gonçalves MG, Leite AC, Lima MA, et al. Loop-mediated isothermal amplification (LAMP) assay for rapid and accurate confirmatory diagnosis of HTLV-1/2 infection. Viruses 2020; 12(9): 981.

63. Hjelle B, Wilson C, Cyrus S, Bradshaw P, Lo J, Schammel C, et al. Human T-cell leukemia virus type II infection frequently goes undetected in contemporary US blood donors. Blood 1993; 81(6): 1641–4.

64. Kamali P, Zandi M, Ghasemzadeh-Moghaddam H, Fani M. Comparison between various biosensor methods for human T-lymphotropic virus-1 (HTLV-1) detection. Mol Biol Rep 2022; 49(2): 1513-7.

65. Rowan AG, Dillon R, Witkover A, Melamed A, Demontis M-A, Gillet NA, et al. Evolution of retrovirus-infected premalignant T-cell clones prior to adult T-cell leukemia/lymphoma diagnosis. Blood 2020; 135(23): 2023-32.

66. Letafati A, Bahari M, Ardekani OS, Jazi NN, Nikzad A, Mahdavi B, et al. HTLV-1 vaccination Landscape: Current developments and challenges. Vaccine X 2024; 19: 100525.

67. Bangham CR, Ratner L. How does HTLV-1 cause adult T-cell leukaemia/lymphoma (ATL)? Curr Opin Virol 2015; 14: 93-100.

68. Makiyama J, Ishitsuka K, Munakata W, Maruyama D, Nagai H. An update on the developments in the treatment of adult T-cell leukemia–lymphoma: current knowledge and future perspective. Jpn J Clin Oncol 2023; 53(12): 1104-11.

69. Ishida T, Utsunomiya A, Iida S, Inagaki H, Takatsuka Y, Kusumoto S, et al. Clinical significance of CCR4 expression in adult T-cell leukemia/lymphoma: Its close association with skin involvement and unfavorable outcome1. Clin Cancer Res 2003; 9(10): 3625-34.

70. Sakamoto Y, Ishida T, Masaki A, Murase T, Yonekura K, Tashiro Y, et al. CCR4 mutations associated with superior outcome of adult T-cell leukemia/lymphoma under mogamulizumab treatment. Blood 2018; 132(7): 758-61.

71. Gribben JG, Fowler N, Morschhauser F. Mechanisms of action of lenalidomide in B-cell non-Hodgkin lymphoma. J Clin Oncol 2015; 33(25): 2803-11.

72. Ishida T, Fujiwara H, Nosaka K, Taira N, Abe Y, Imaizumi Y, et al. Multicenter phase II study of lenalidomide in relapsed or recurrent adult T-cell leukemia/lymphoma: ATLL-002. J Clin Oncol 2016; 34(34): 4086-93.

73. Katz J, Janik JE, Younes A. Brentuximab vedotin (SGN-35). Clin Cancer Res 2011; 17(20): 6428-36.

74. Nakashima M, Yamochi T, Watanabe M, Uchimaru K, Utsunomiya A, Higashihara M, et al. CD30 characterizes polylobated lymphocytes and disease progression in HTLV-1–infected individuals. Clin Cancer Res 2018; 24(21): 5445-57.

75. Nakashima M, Utsunomiya A, Watanabe T, Horie R, Uchimaru K. The oncogenic driving force of CD30 signaling-induced chromosomal instability in adult T-cell leukemia/lymphoma. Cancer Sci 2023; 114(4): 1556-68.

76. Ning Z-Q, Li Z-B, Newman MJ, Shan S, Wang X-H, Pan D-S, et al. Chidamide (CS055/HBI-8000): a new histone deacetylase inhibitor of the benzamide class with antitumor activity and the ability to enhance immune cell-mediated tumor cell cytotoxicity. Cancer Chemother Pharmacol 2012; 69: 901-9.

77. Utsunomiya A, Izutsu K, Jo T, Yoshida S, Tsukasaki K, Ando K, et al. Oral histone deacetylase inhibitor tucidinostat (HBI-8000) in patients with relapsed or refractory adult T-cell leukemia/lymphoma: Phase IIb results. Cancer Sci 2022; 113(8): 2778-87.

78. Margueron R, Reinberg D. The polycomb complex PRC2 and its mark in life. Nature 2011; 469(7330): 343-9.

79. Yamagishi M, Hori M, Fujikawa D, Ohsugi T, Honma D, Adachi N, et al. Targeting excessive EZH1 and EZH2 activities for abnormal histone methylation and transcription network in malignant lymphomas. Cell Rep 2019; 29(8): 2321-37. e7.

80. Izutsu K, Makita S, Nosaka K, Yoshimitsu M, Utsunomiya A, Kusumoto S, et al. An open-label, single-arm phase 2 trial of valemetostat for relapsed or refractory adult T-cell leukemia/lymphoma. Blood 2023; 141(10): 1159-68.

81. Gholamzad A, Khakpour N, Gholamzad M, Sarvandani MRR, Khosroshahi EM, Asadi S, et al. Stem cell therapy for HTLV-1 induced adult T-cell leukemia/lymphoma (ATLL): A comprehensive review. Pathol-Res Pract 2024; 255: 155172.

82. Utsunomiya A, Choi I, Chihara D, Seto M. Recent advances in the treatment of adult T-cell leukemia-lymphomas. Cancer Sci 2015; 106(4): 344-51.

83. Malpica L, Pimentel A, Reis IM, Gotuzzo E, Lekakis L, Komanduri K, et al. Epidemiology, clinical features, and outcome of HTLV-1–related ATLL in an area of prevalence in the United States. Blood Adv 2018; 2(6): 607-20.

84. Nakagawa M, Schmitz R, Xiao W, Goldman CK, Xu W, Yang Y, et al. Gain-of-function CCR4 mutations in adult T cell leukemia/lymphoma. J Exp Med 2014; 211(13): 2497-505.

Experimed

Review Article　　　　　　　　　　　　　　　　　　　　　　　　　ô **Open Access**

The Exosome Complex in Health and Disease: A Multifaceted Regulator of RNA Homeostasis

Esra Nur Demirtas [1, 2] , Selcuk Sozer Tokdemir [1]

[1] Department of Genetics, Aziz Sancar Institute of Experimental Medicine, Istanbul University, Istanbul, Turkiye
[2] Institute of Graduate Studies in Health Sciences, Istanbul University, Istanbul, Turkiye

Abstract　　　The RNA exosome complex is a multi-subunit ribonuclease complex that participates in RNA degradation, processing, and quality control. In recent years, mutations and dysregulation in the subunits of this complex, which play significant roles in RNA metabolism, have been associated with neurodegenerative diseases, hematological malignancies, and solid tumors. This review discusses the contributions of genes encoding both the catalytic and non-catalytic subunits of the exosome complex to cellular homeostasis, development, and disease pathogenesis. In addition to its roles in RNA homeostasis, the complex also plays a role in maintaining the stability of genomic-resolving DNA:RNA hybrids, regulating telomere integrity, and facilitating homologous recombination. Considering the current literature, this review highlights the potential of RNA exosomes as biomarkers for disease diagnosis and as therapeutic targets for developing new treatment approaches.

Keywords　　　RNA exosome complex · ExosC · RNA degradation · Therapy

INTRODUCTION

The RNA exosome complex (ExosC) is key in regulating RNA metabolism. The system ensures RNA quality by processing and degrading different types of RNA. Located in both the nucleus and cytoplasm, ExosC helps to maintain cellular homeostasis and indirectly supports genome stability by resolving DNA:RNA hybrids (R-loops) and stabilizing telomeres. ExosC functions mainly include quality control of coding and non-coding RNAs, degradation of defective transcripts, and processing of precursor RNAs (1, 2). Although the contribution of ExosC to RNA metabolism is clear, studies on its contribution to disease pathobiology have accelerated in the last decade.

ExosC has been linked to several diseases, including neurodegenerative disorders (3), autoimmune diseases (4), and cancer, and its disruption has been associated with genomic instability (5), uncontrolled proliferation (6), and tumor progression (7). It has been shown that changes detected in exosome subunits in hematological cancers (8, 9) and solid cancers (10) cause them to act as oncogenic drivers or tumor suppressors (10, 11). This review explores the potential of targeting RNA exosome subunits or their specific functions for diagnostic and therapeutic purposes by integrating insights into disease-associated dysfunctions and subunit-specific roles. We aim to inspire further research and novel therapeutic approaches by bridging fundamental biology with clinical implications.

The Structure and Function of the RNA Exosome Complex

ExosC is an 11-subunit protein assembled in the nucleus and cytoplasm (Figure 1). In the nucleus, it facilitates the degradation of RNAs and processes precursors of 5.8S rRNA and other stable RNAs (12). ExosC ensures intracellular homeostasis in the cytoplasm by degrading mRNA (13, 14).

The complex features a unique cap region, the S1/KH ring, comprising exosome components (EXOSC) of EXOSC1, EXOSC2, and EXOSC3 subunits (Figure 1). Below the cap lies the PH-like ring structure, formed by catalytically inactive subunits EXOSC4 to EXOSC9 (collectively called EXO-9). EXO-9 interacts with the two catalytic subunits, EXOSC10 and DIS3, which mediate RNA degradation and processing (15). DIS3, which has three subtypes in humans, is found in the nucleus and cytoplasm, whereas EXOSC10 is enriched in the nucleus (16). RNA enters the ExosC through a gap at the apex of the S1/KH cap and exits via a gap at the base of the PH ring. There are three pathways for RNA interaction: substrates may bypass the channels in the complex body and directly reach EXOSC10 (17, 18), RNA can pass through the channel to reach DIS3 (18–20), or RNA can directly bind to DIS3 without entering the complex (21).

The RNA Exosome Complex in Cellular Stress and DNA Damage Response

The RNA exosome complex plays an important role in maintaining cellular homeostasis by ensuring RNA quality control and preventing the accumulation of toxic RNA species (1, 22). Functional disorders in ExosC cause R-loop formation (23), RNA:DNA hybrid structures that cause transcription-replication conflicts, replication fork stalling, and DNA double-stranded breaks (DSBs) (24). The loss of EXOSC10 function with exoribonuclease activity contributes to tumorigenesis and genomic instability owing to R-loop formation (25). Mutations in the subunit DIS3, which has both endo- and exoribonuclease activity, cause transcriptional stress by preventing the degradation of dysfunctional RNA products (26, 27).

EXOSC plays a critical role in DNA repair. Marin-Vicente et al. showed that during homologous recombination, EXOSC10 localizes at the site of damage and facilitates the uptake of RAD51 into DSBs (28). On the other hand, its depletion makes cancerous cells sensitive to radiation (28, 29).

In addition, EXOSC9 causes stress resistance by promoting the formation of stress granules (30). EXOSC3 upregulation promotes tumor progression by activating pro-inflammatory pathways by stimulating IFNGR1, MYD88, NFκBIA, and STAT3 expression (31). EXOSC is a promising therapeutic target in cancer biology because of its dual roles in genomic stability, stress resistance, and inflammation.

The Roles of RNA Exosome Complex Subunits in Cancer

ExosC subunits play critical roles in various cancers. In colorectal cancer, EXOSC2, EXOSC3, and EXOSC4 are upregulated. The upregulation of EXOSC4 induces metastasis and proliferation, whereas its inhibition leads to cell cycle arrest in the G1 phase (32–34). EXOSC8 disrupts tumor suppressors such as p53 (35), and copy number variation (CNV) gain is associated with poor overall survival (36). In addition, EXOSC10 degrades CYLD deubiquitinase mRNA in colorectal cancer and promotes tumor progression by increasing c-Jun N-terminal kinase (JNK) activity (37). Conversely, EXOSC2 facilitates proliferation, migration, and angiogenesis in breast cancer by activating the Wnt/β-catenin pathway (11). However, EXOSC3 exhibits protective roles against breast cancer by potentially mitigating oncogenic pathways (10), whereas
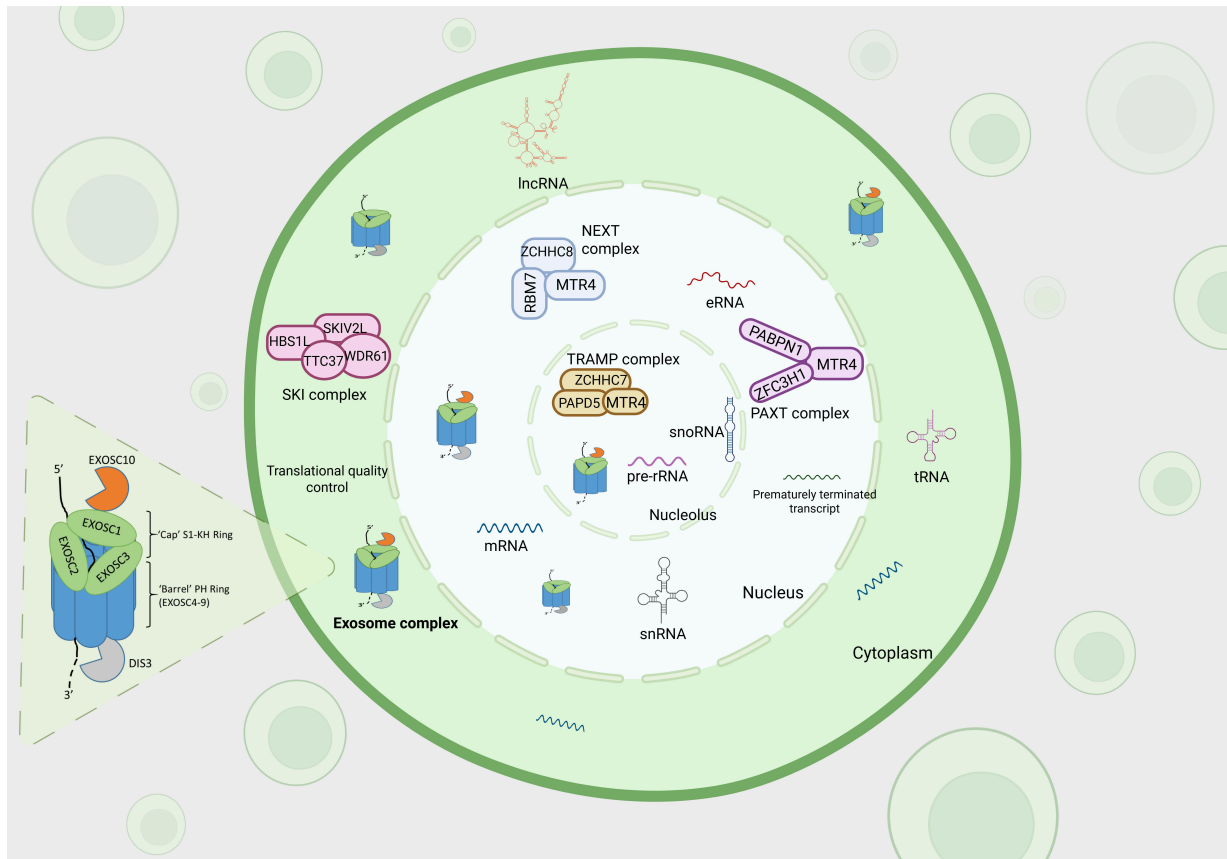
Figure 1. Illustration of the RNA exosome complex inside a cell, including its localization, cofactors, and substrates. The RNA exosome complex is located in the nucleolus, nucleus, and cytoplasm. In the nucleolus, the exosome complex contains the EXOSC10 subunit but lacks DIS3 and interacts with TRAMP complex cofactors, allowing pre-rRNA and snoRNA to bind to the complex. In contrast, the exosome complex located in the nucleus is mediated by the NEXT and PAXT complex for mRNA, snRNA, and eRNA, prematurely terminated transcript binding, and combines with the DIS3. The NEXT complex targets short-lived RNAs, whereas PAXT targets long and polyadenylated RNAs. The SKI complex acts as a cofactor in the cytoplasm, allowing mRNAs to bind to its cap region. The exosome complex is accompanied by DIS3 and DIS3L proteins in the cytoplasm. Abbreviations: TRAMP: Trf–Air–Mtr4 polyadenylation; NEXT: nuclear exosome targeting; PAXT: poly(A) tail exosome targeting; snoRNA: small nucleolar RNA; snRNA: small nuclear RNA; mRNA: messenger RNA; tRNA: transfer RNA; eRNA: enhancer RNA; lncRNA: long non-coding RNA) (Created in BioRender. Demirtaş, E. (2025) https://BioRender.com/g37v632)

EXOSC9 supports metastasis and therapy resistance by degrading telomeric RNAs (38).

In kidney renal clear cell carcinoma, EXOSC1 promotes DNA damage and mutations, thereby contributing to poor patient outcomes (39). EXOSC5 drives tumor proliferation in colorectal cancer (40). In pancreatic cancer, subunits such as EXOSC2 and EXOSC4 support tumor progression by promoting proliferation and survival (41, 42), with EXOSC9 and EXOSC10 playing roles in stress resistance and tumor maintenance (30, 42). In gastric cancer, EXOSC3 and EXOSC5 are associated with poor prognosis (43), with EXOSC3 incorporated into relapse-free survival models (44).

In hematological cancers, multiple myeloma frequently exhibits frequent *DIS3* mutations, disrupting RNA processing and cell proliferation (45), whereas *EXOSC1* is identified as a harmful gene in mantle cell lymphoma (46). In endometrial cancer, EXOSC5 activates c-MYC and enhances cancer stem cell properties (47), while EXOSC10 is linked to aggressive

phenotypes (48). Hepatocellular carcinoma shows contrasting roles for EXOSC8, where it acts protectively and improves survival, whereas EXOSC5 supports tumor growth via the STAT3 pathway (49, 50). Other cancers, such as epithelial ovarian cancer, involve EXOSC4, whose over-expression drives aggressive tumor behavior (51). In esophageal squamous cell carcinoma, EXOSC2 prevents malignant progression by degrading oncogenic RNAs (52).

The findings indicate that specific RNA exosome components might function as oncogenes or tumor suppressors, depending on the cancer type and cellular context. The carcinogenic potential of exosome components was demonstrated by the correlation between poor prognosis and over-expression of EXOSC1 in renal cancer (39) and EXOSC10 in hepatocellular carcinoma (53). On the other hand, DIS3 loss-of-function mutations disrupt RNA processing, accumulating abnormal transcripts, and promoting the development of tumors in hematological malignancies like multiple myeloma

(54). The intricacy of RNA exosome biology and the requirement for context-specific research to clarify its roles in oncogenesis are reflected in these dual roles.

The RNA Exosome and Beyond: Connections to Other Diseases

Although primarily studied in the context of cancer, the RNA exosome complex also plays a critical role in the pathogenesis of several non-cancerous diseases, including neurodegenerative disorders, immune dysregulation, and developmental syndromes. Mutations or dysregulation of specific RNA exosome subunits often result in widespread RNA accumulation, toxic RNA species, and disrupted RNA homeostasis, which are hallmark features of these conditions.

Neurodegenerative Diseases

The RNA exosome participates in the degradation of defective mitochondrial RNAs, and any disturbances to this task could disrupt the function of mitochondrial dysfunction, an essential factor in neurodegenerative diseases such as Parkinson's disease and amyotrophic lateral sclerosis (ALS).

Because the RNA exosome complex controls alternative splicing (55), mutations in this complex can cause defective splicing patterns and loss of control of mRNA abundance in neurons (56). Mutations in *EXOSC3* and *EXOSC8* have been strongly associated with pontocerebellar hypoplasia (PCH), spinal muscular atrophy (SMA), and cerebellar hypoplasia, disorders characterized by impaired motor function and progressive neuronal loss (3, 57–60). EXOSC3 loss and mutations contribute to neurodegeneration by causing defective rRNA processing and modulation of R-loop formation (23, 61). In a study of 22 infants, Boczonadi et al. detected a homozygous non-sense mutation in EXOSC8. They showed that the mutation disrupted RNA metabolism in oligodendrocytes, causing them to produce abnormal proteins and to undergo neurodegeneration (3). In ALS and frontotemporal dementia (FTD), accumulation of GGGGCC repeats in the *C9orf72* gene leads to the production of toxic di-peptide repeat proteins (62). By detecting that EXOSC10 and DIS3 cleave these hexanucleotide repeats, Kawabe et al. showed that EXOSC has therapeutic potential to reduce RNA toxicity (63).

Autoimmune and Inflammatory Diseases

ExosC dysfunction triggers immune dysregulation by inducing inflammatory pathways. The disruption of endogenous immunostimulatory genes in the absence of SKIV2L (a cytoplasmic RNA helicase cofactor) leads to the activation of type I interferons, laying the groundwork for systemic autoimmune diseases (64). RNA accumulation causes inflammation and developmental abnormalities in congenital disorders, and similar effects are observed in trichohepatoenteric syndrome, a rare congenital disorder associated with SKIV2L and EXOSC2 deficiencies (65). ExosCs are important for the maintenance of immune homeostasis.

Developmental and Genetic Disorders

ExosC participates in early embryogenesis and differentiation is necessary for normal development (66). EXOSC2 knockout in a zebrafish model disrupted neuronal development by disrupting the mRNA loop. Rapamycin treatment, which modulates mRNA stability through the mTOR signaling pathway, can partially reverse this effect (67). In addition, the downstream effects of modified *EXOSC1* splicing affect vascular pathophysiology and play a role in ischemic stroke (68).

Therapeutic Implications of Targeting the RNA Exosome Complex

The devastating consequences of ExosC dysfunction make it an attractive therapeutic target in diseases. Targeting ExosC subcomponents or cofactors can inhibit the mechanisms that promote tumor formation and render cancer cells susceptible to treatment. Kammler et al. determined that the subunit EXOSC10 with exoribonucleolytic activity is a target for chemotherapeutics such as 5-fluorouracil (5-FU), which induces cytotoxicity by increasing the accumulation of RNA substrates. HeLa cells lacking EXOSC10 became sensitive to 5-FU and showed impaired growth and increased RNA substrate levels (69). Therefore, EXOSC10 expression is critical for enhancing the efficacy of current therapies. Targeting the accumulation of R-loops that trigger replication stress with ribonuclease-active subunits of the complex may reduce genomic instability caused by defective DNA damage repair pathways. Molecules targeting ExosC-mediated R-loop resolution are promising for new drug discovery.

For cancers harboring ExosC dysfunction, a combined treatment approach using PARP and ExosC inhibitors may contribute to the selective death of cancer cells with homologous recombination defects. Marin-Vicente et al. found that EXOSC10 depletion causes RAD51 to be unable to be recruited to the damaged site, disrupting DNA double-stranded break repair, thus making cancer cells susceptible to radiation and DNA-damaging agents (28). Modulation of DIS3 expression provides a different treatment strategy to ensure RNA homeostasis involving enhancer RNAs, promoter upstream transcripts (PROMPTs), and early cleavage and

Table 1. The role of ExosC in cancer, neurodegenerative disease and syndromes.

GENE	DISEASE/CONDITION	POTENTIAL EFFECT	REFERENCES
EXOSC1	Pontocerebellar hypoplasia	Stump protein	(71, 72)
EXOSC2	Short stature, Hearing loss, Retinitis pigmentosa, and distinctive Facies (SHRF)	Impaired RNA metabolism Altered activities in the autophagy pathway	(73, 74)
EXOSC3	Pontocerebellar hypoplasia	Cerebellar and spinal motor neuron development and degeneration.	(75)
	Non-small cell lung cancer	Prediction of NSCLC survival	(76)
	Thrombotic Microangiopathy	Prevention of response to eculizumab treatment	(77)
EXOSC4	Tongue Cancer	biological markers for predicting lymph node metastasis	(78)
	Diffuse large B-cell lymphoma	shorter overall survival and progression-free survival	(79)
	Luminal B/Her2 breast cancer	Colony formation, cell invasion, and mammosphere formation of breast cancer cells	(80)
	Neurodevelopmental defects	Biallelic variant that impairs RNA exosome function	(81)
EXOSC5	Delayed development	Reduced eye/head size, edema, and shortened and curved bodies	(82)
	CABAC syndrome (cerebellar ataxia, brain abnormalities, and cardiac conduction defects)	Thrombotic microangiopathy	(77)
	Prostate cancer	Abiraterone-resistant gene	(83)
EXOSC6	Cerebral amyloid angiopathy	Potential drivers of pathological processes	(84)
EXOSC8	Pontocerebellar hypoplasia	Alterations in mRNA metabolism, hypomyelination with spinal muscular atrophy, and cerebellar hypoplasia	(3)
	Head and neck squamous cell carcinoma	ERS-related biomarkers for predicting immunotherapy response	(85)
EXOSC9	Pontocerebellar hypoplasia	Cerebellar atrophy with spinal motor neuronopathy	(86–88)
	Breast cancer	Support the growth of endocrine therapy-resistant HR+ breast cancer cells.	(38)
		Promising biomarker of response to PARP inhibitors	
EXOSC10	Frontotemporal lobar degeneration (FTLD) and Amyotrophic Lateral Sclerosis (ALS)	Degradation of pathogenic C9orf72-derived repeat RNA	(63)
	Oocyte development	depletion of the ovarian reserve by EXOSC10 inactivation	(89)
DIS3	Premature ovarian insufficiency	Aberrant ovarian development and egg chamber degeneration	(90)
	Male fertility	Disruption of early germline cell development	(91)
	Breast cancer	Target gene to increase major histocompatibility complex I (MHC-I) expression	(92)
		High DIS3 expression leads to cancer cell survival	
		Poor prognosis of breast cancer	

polyadenylation products (PCPA) to prevent the degradation of tumor suppressor RNAs and target oncogenic RNAs.

In addition, the non-catalytic subunits of ExosC can serve as diagnostic and prognostic biomarkers. Elevated levels of EXOSC1 and EXOSC4 subunits were associated with poor renal cell carcinoma (39) and colorectal cancer (33), respectively. These findings provide important tools for patient stratification and treatment response monitoring.

In addition to traditional chemotherapy and radiotherapy treatment methods, synthetic lethality approaches targeting DNA repair and ExosC function can be applied, which may help combat therapeutic resistance.

Therapeutic Insights Across Diseases

ExosC is a potential target for neurodegenerative and inflammatory diseases because it balances RNA metabolism and maintains cell homeostasis. Results from cancer studies targeting EXOSC10 to eliminate toxic RNA species have shown

that this complex is also promising for diseases other than cancer. In ALS and frontotemporal dementia (FTD), Bush et al. designed repetitive RNA-targeted small molecules to target the destruction of unwanted RNAs by ExosC. In the C9ALS/FTD mouse model, these small molecules crossing the blood-brain barrier also prevented the production of di-peptide repeat proteins, thus alleviating disease pathology (70). Likewise, the subsequent development of therapeutic strategies to prevent the generation of pathogenic repeat sequence-containing RNA forms by targeting ExosC function improvement could be implemented in other repeat sequence diseases, like Huntington's disease, myotonic dystrophy, Fragile X syndrome, spinocerebellar ataxia, and Friedreich's ataxia. These results indicate that ExosC is associated with diverse biological processes and diseases other than cancer. Additional studies are required to clarify the potential contribution of ExosC to neurodegeneration, immune dysregulation, and developmental disorders. An improved understanding of how ExosC contributes to the pathogenesis of these conditions may provide vital insights into both disease mechanisms and the development of new therapeutic strategies.

DISCUSSION

ExosC is classified as a ribonuclease complex and can facilitate RNA processing and degradation to maintain RNA homeostasis and genomic stability; thus, ExosC plays an instrumental role in minimizing replication stress by ensuring that R-loop structures are resolved and contributing to the repair of DSBs via the process of homologous recombination. If defects in EXOSC10 or DIS3 impair ExosC function, unresolved R-loops accumulate, causing replication stress and inadequate DNA damage repair. The involvement of the complex in homologous recombination (HR) makes it a promising target in tumors with HR deficiencies, particularly in combination with PARP inhibitors. Cancer and neuroscience studies have shown that mutations and expression changes in ExosC subunits are associated with transcriptional stress, genomic instability, inflammation, cancer cell growth, proliferation, and metastasis processes (Table 1). In addition, the fact that it promotes the formation of stress granules can increase the stress resistance of cancer cells and maintain their survival. Therefore, ExosC subunits are important targets of targeted therapies. The most important difficulty in ExosC studies is that the specific and non-canonical roles of each subunit in the disease remain unclear.

CONCLUSION

ExosC is a vital RNA regulatory mechanism for cancer and other diseases. The disruption of ExosC causes loss of homeostasis and can serve as a potential therapeutic target.

Detailed studies will delineate the roles of specific subunits and identify treatments that modulate complex dysfunction. In conclusion, ExosC subunits represent an exciting potential biomarker and therapeutic target and may be a pioneer for novel therapies, particularly in the fields of oncology and neurodegeneration.

Author Details

Esra Nur Demirtas
¹ Department of Genetics, Aziz Sancar Institute of Experimental Medicine, Istanbul University, Istanbul, Turkiye

² Institute of Graduate Studies in Health Sciences, Istanbul University, Istanbul, Turkiye

 0000-0002-3533-0697

Selcuk Sozer Tokdemir
¹ Department of Genetics, Aziz Sancar Institute of Experimental Medicine, Istanbul University, Istanbul, Turkiye

 0000-0002-5035-4048   ✉ ssozer@istanbul.edu.tr

REFERENCES

1. Kilchert C, Wittmann S, Vasiljeva L. The regulation and functions of the nuclear RNA exosome complex. Nat Rev Mol Cell Biol 2016; 17(4): 227–39.

2. Ogami K, Suzuki HI. Nuclear RNA exosome and pervasive transcription: Dual sculptors of genome function. Int J Mol Sci2021; 22(24): 13401.

3. Boczonadi V, Müller JS, Pyle A, Munkley J, Dor T, Quartararo J, et al. EXOSC8 mutations alter mRNA metabolism and cause hypomyelination with spinal muscular atrophy and cerebellar hypoplasia. Nat Commun 2014; 5(1): 1–13.

4. Blin J, Fitzgerald KA. Perspective: The RNA exosome, cytokine gene regulation and links to autoimmunity. Cytokine 2015; 74(2): 175–80.

5. Chan YA, Hieter P, Stirling PC. Mechanisms of genome instability induced by RNA-processing defects. Trends Genet 2014; 30(6): 245–53.

6. McIver SC, Katsumura KR, Davids E, Liu P, Kang YA, Yang D, et al. Exosome complex orchestrates developmental signaling to balance proliferation and differentiation during erythropoiesis. Elife 2016; 5: e17877.

7. Taniue K, Tanu T, Shimoura Y, Mitsutomi S, Han H, Kakisaka R, et al. RNA Exosome component EXOSC4 amplified in multiple cancer types is required for the cancer cell survival. Int J Mol Sci 2022; 23(1): 496.

8. Desterke C, Bennaceur-Griscelli A, Turhan AG. DIS3 mutation in RUNX1-mutated AML1 confers a highly dismal prognosis in AML by repressing sister chromatid cohesion. Blood 2019; 134(Supp 1): 1454.

9. Todoerti K, Ronchetti D, Favasuli V, Maura F, Morabito F, Bolli N, et al. DIS3 mutations in multiple myeloma impact the transcriptional signature and clinical outcome. Haematologica 2022; 107(4): 921.

10. Yan X, You SN, Chen Y, Qian K. Construction and validation of a newly prognostic signature for CRISPR-Cas9-based cancer dependency map genes in breast cancer. J Oncol 2022; 2022: 4566577.

11. Lv CG, Cheng Y, Zhang L, Wu GG, Liang CY, Tao Z, et al. EXOSC2 mediates the pro-tumor role of WTAP in breast cancer cells via activating the Wnt/β-catenin signal. Mol Biotechnol 2024; 66(9): 2569–82.

12. Vanacova S, Stef R. The exosome and RNA quality control in the nucleus. EMBO Rep 2007; 8(7): 651–7.

13. Houseley J, LaCava J, Tollervey D. RNA-quality control by the exosome. Nat Rev Mol Cell Biol 2006; 7(7): 529–39.

14. Schneider C, Leung E, Brown J, Tollervey D. The N-terminal PIN domain of the exosome subunit Rrp44 harbors endonuclease activity and tethers Rrp44 to the yeast core exosome. Nucleic Acids Res 2009; 37(4): 1127.

15. Makino DL, Baumgärtner M, Conti E. Crystal structure of an RNA-bound 11-subunit eukaryotic exosome complex. Nature 2013; 495(7439): 70–5.

16. Davidson L, Francis L, Cordiner RA, Eaton JD, Estell C, Macias S, et al. Rapid depletion of DIS3, EXOSC10, or XRN2 reveals the immediate impact of exoribonucleolysis on nuclear RNA metabolism and transcriptional control. Cell Rep 2019; 26(10): 2779–91.e5.

17. Makino DL, Schuch B, Stegmann E, Baumgärtner M, Basquin C, Conti E. RNA degradation paths in a 12-subunit nuclear exosome complex. Nature 2015; 524(7563): 54–8.

18. Zinder JC, Wasmuth E V, Lima CD. Nuclear RNA exosome at 3.1 Å reveals substrate specificities, RNA paths, and allosteric inhibition of Rrp44/Dis3. Mol Cell 2016; 64(4): 734–45.

19. Liu JJ, Bratkowski MA, Liu X, Niu CY, Ke A, Wang HW. Visualization of distinct substrate-recruitment pathways in the yeast exosome by EM. Nat Struct Mol Biol 2014; 21(1): 95–102.

20. Han J, van Hoof A. The RNA exosome channeling and direct access conformations have distinct in vivo functions. Cell Rep 2016; 16(12): 3348–58.

21. Gerlach P, Schuller JM, Bonneau F, Basquin J, Reichelt P, Falk S, et al. Distinct and evolutionary conserved structural features of the human nuclear exosome complex. Elife. 2018; 7: e38686.

22. Gudipati RK, Xu Z, Lebreton A, Séraphin B, Steinmetz LM, Jacquier A, et al. Extensive degradation of RNA precursors by the exosome in wild-type cells. Mol Cell 2012; 48(3): 409–21.

23. de Amorim JL, Leung SW, Haji-Seyed-Javadi R, Hou Y, Yu DS, Ghalei H, et al. The putative RNA helicase DDX1 associates with the nuclear RNA exosome and modulates RNA/DNA hybrids (R-loops). J Biol Chem 2024; 300(2): 105646.

24. Papadopoulos D, Solvie D, Baluapuri A, Endres T, Ha SA, Herold S, et al. MYCN recruits the nuclear exosome complex to RNA polymerase II to prevent transcription-replication conflicts. Mol Cell 2022; 82(1): 159–76. e12.

25. Pefanis E, Wang J, Rothschild G, Lim J, Kazadi D, Sun J, et al. RNA exosome-regulated long non-coding RNA transcription controls super-enhancer activity. Cell 2015; 161(4): 774–89.

26. Favasuli VK, Ronchetti D, Silvestris I, Puccio N, Fabbiano G, Traini V, et al. DIS3 depletion in multiple myeloma causes extensive perturbation in cell cycle progression and centrosome amplification. Haematologica 2024; 109(1): 231–44.

27. Szczepińska T, Kalisiak K, Tomecki R, Labno A, Borowski LS, Kulinski TM, et al. DIS3 shapes the RNA polymerase II transcriptome in humans by degrading a variety of unwanted transcripts. Genome Res 2015; 25(11): 1622–33.

28. Marin-Vicente C, Domingo-Prim J, Eberle AB, Visa N. RRP6/EXOSC10 is required for the repair of DNA double-strand breaks by homologous recombination. J Cell Sci 2015; 128(6): 1097–107.

29. Domingo-Prim J, Endara-Coll M, Bonath F, Jimeno S, Prados-Carvajal R, Friedländer MR, et al. EXOSC10 is required for RPA assembly and controlled DNA end resection at DNA double-strand breaks. Nat Commun 2019; 10(1): 2135.

30. Yoshino S, Matsui Y, Fukui Y, Seki M, Yamaguchi K, Kanamori A, et al. EXOSC9 depletion attenuates P-body formation, stress resistance, and tumorigenicity of cancer cells. Sci Reports 2020; 10(1): 9275.

31. Tsuda M, Noguchi M, Kurai T, Ichihashi Y, Ise K, Wang L, et al. Aberrant expression of MYD88 via RNA-controlling CNOT4 and EXOSC3 in colonic mucosa impacts generation of colonic cancer. Cancer Sci 2021; 112(12): 5100–13.

32. Wang YX, Li YZ, Zhao WL, Zhang ZY, Qian XL, He GY. STX2 drives colorectal cancer proliferation via upregulation of EXOSC4. Life Sci 2020; 263: 118597.

33. Pan Y, Tong JHM, Kang W, Lung RWM, Chak WP, Chung LY, et al. EXOSC4 functions as a potential oncogene in development and progression of colorectal cancer. Mol Carcinog 2018; 57(12): 1780–91.

34. de Wit M, Kant H, Piersma SR, Pham T V, Mongera S, van Berkel MPA, et al. Colorectal cancer candidate biomarkers identified by tissue secretome proteome profiling. J Proteomics 2014; 99: 26–39.

35. Cui K, Gong L, Zhang H, Chen Y, Liu B, Gong Z, et al. EXOSC8 promotes colorectal cancer tumorigenesis via regulating ribosome biogenesis-related processes. Oncogene 2022; 41(50): 5397–410.

36. Cui K, Liu C, Li X, Zhang Q, Li Y. Comprehensive characterization of the rRNA metabolism-related genes in human cancer. Oncogene 2019; 39(4): 786–800.

37. Sun L, Patai Á V., Hogenson TL, Fernandez-Zapico ME, Qin B, Sinicrope FA. Irreversible JNK blockade overcomes PD-L1-mediated resistance to chemotherapy in colorectal cancer. Oncogene 2021; 40(32): 5105–15.

38. Quttina M, Waiters KD, Khan AF, Karami S, Peidl AS, Babajide MF, et al. Exosc9 initiates SUMO-dependent lncRNA TERRA degradation to impact telomeric integrity in endocrine therapy insensitive hormone receptor-positive breast cancer. Cells 2023; 12(20): 2495.

39. Liu Q, Xiao Q, Sun Z, Wang B, Wang L, Wang N, et al. Exosome component 1 cleaves single-stranded DNA and sensitizes human kidney renal clear cell carcinoma cells to poly(ADP-ribose) polymerase inhibitor. Elife 2021; 10: e69454.

40. Pan H, Pan J, Song S, Ji L, Lv H, Yang Z. EXOSC5 as a novel prognostic marker promotes proliferation of colorectal cancer via activating the ERK and AKT pathways. Front Oncol 2019; 9: 643. Erratum in: Front Oncol 2021; 11: 670041.

41. Makler A, Narayanan R. Mining exosomal genes for pancreatic cancer targets. Cancer Genomics Proteomics 2017; 14(3): 161–72.

42. Taniue K, Tanu T, Shimoura Y, Mitsutomi S, Han H, Kakisaka R, et al. RNA exosome component exosc4 amplified in multiple cancer types is required for the cancer cell survival. Int J Mol Sci 2022; 23(1): 496.

43. Chen X, Huang Y, Liu J, Lin W, Chen C, Chen Y, et al. EXOSC5 promotes proliferation of gastric cancer through regulating AKT/STAT3 signaling pathways. J Cancer 2022; 13(5): 1456–67.

44. Cho JY, Lim JY, Cheong JH, Park YY, Yoon SL, Kim SM, et al. Gene expression signature-based prognostic risk score in gastric cancer. Clin Cancer Res 2011; 17(7): 1850–7.

45. Tomecki R, Drazkowska K, Kucinski I, Stodus K, Szczesny RJ, Gruchota J, et al. Multiple myeloma-associated hDIS3 mutations cause perturbations in cellular RNA metabolism and suggest hDIS3 PIN domain as a potential drug target. Nucleic Acids Res 2014; 42(2): 1270–90.

46. Zhang W, Zhu J, He X, Liu X, Li J, Li W, et al. Exosome complex genes mediate RNA degradation and predict survival in mantle cell lymphoma. Oncol Lett 2019; 18(5): 5119–28.

47. Huang YH, Wang WL, Wang PH, Lee H Te, Chang WW. EXOSC5 maintains cancer stem cell activity in endometrial cancer by regulating the NTN4/integrin β1 signalling axis. Int J Biol Sci 2024; 20(1): 265–79.

48. Attarha S, Andersson S, Mints M, Souchelnytskyi S. Individualised proteome profiling of human endometrial tumours improves detection of new prognostic markers. Br J Cancer 2013; 109(3): 704–13.

49. Nichols CA, Gibson WJ, Brown MS, Kosmicki JA, Busanovich JP, Wei H, et al. Loss of heterozygosity of essential genes represents a widespread class of potential cancer vulnerabilities. Nat Commun 2020; 11(1): 2517.

50. Zhang Y, Yang X, Hu Y, Huang X. Integrated bioinformatic investigation of EXOSCs in hepatocellular carcinoma followed by the preliminary validation of EXOSC5 in cell proliferation. Int J Mol Sci 2022; 23(20): 12161.

51. Xiong C, Sun Z, Yu J, Lin Y. Exosome component 4 promotes epithelial ovarian cancer cell proliferation, migration, and invasion via the Wnt pathway. Front Oncol 2021; 11: 797968.

52. Zhang Y, Chen C, Liu Z, Guo H, Lu W, Hu W, et al. PABPC1-induced stabilization of IFI27 mRNA promotes angiogenesis and malignant progression in esophageal squamous cell carcinoma through exosomal miRNA-21-5p. J Exp Clin Cancer Res 2022; 41(1): 111.

53. Meng ZY, Fan YC, Zhang CS, Zhang LL, Wu T, Nong MY, et al. EXOSC10 is a novel hepatocellular carcinoma prognostic biomarker: a comprehensive bioinformatics analysis and experiment verification. PeerJ 2023; 11: e15860.

54. Chapman MA, Lawrence MS, Keats JJ, Cibulskis K, Sougnez C, Schinzel AC, et al. Initial genome sequencing and analysis of multiple myeloma. Nature 2011; 471(7339): 467–72.

55. Zhang L, Wan Y, Huang G, Wang D, Yu X, Huang G, et al. The exosome controls alternative splicing by mediating the gene expression and assembly of the spliceosome complex. Sci Reports 2015; 5: 13403.

56. Mauger O, Scheiffele P. Beyond proteome diversity: alternative splicing as a regulator of neuronal transcript dynamics. Curr Opin Neurobiol 2017; 45: 162–8.

57. Di Giovambattista AP, Jácome Querejeta I, Ventura Faci P, Rodríguez Martínez G, Ramos Fuentes F. Familial EXOSC3-related pontocerebellar hypoplasia. An Pediatr (Barc) 2017; 86(5): 284–6.

58. Spyridakis AC, Cao Y, Litra F. A rare case of pontocerebellar hypoplasia type 1b with literature review. Cureus. 2022; 14(7): e27098.

59. Zaki MS, Abdel-Ghafar SF, Abdel-Hamid MS. A missense variant in EXOSC8 causes exon skipping and expands the phenotypic spectrum of pontocerebellar hypoplasia type 1C. J Hum Genet 2024; 69(2): 79–84.

60. Müller JS, Burns DT, Griffin H, Wells GR, Zendah RA, Munro B, et al. RNA exosome mutations in pontocerebellar hypoplasia alter ribosome biogenesis and p53 levels. Life Sci Alliance 2020; 3(8): e202000678.

61. Gillespie A, Gabunilas J, Jen JC, Chanfreau GF. Mutations of EXOSC3/Rrp40p associated with neurological diseases impact ribosomal RNA processing functions of the exosome in S. cerevisiae. RNA 2017; 23(4): 466–72.

62. Uozumi R, Mori K, Gotoh S, Miyamoto T, Kondo S, Yamashita T, et al. PABPC1 mediates degradation of C9orf72-FTLD/ALS GGGGCC repeat RNA. iScience 2024; 27(3): 109303.

63. Kawabe Y, Mori K, Yamashita T, Gotoh S, Ikeda M. The RNA exosome complex degrades expanded hexanucleotide repeat RNA in C9orf72 FTLD/ALS. EMBO J 2020; 39(19): e102700.

64. Eckard SC, Rice GI, Fabre A, Badens C, Gray EE, Hartley JL, et al. The SKIV2L RNA exosome limits activation of the RIG-I-like receptors. Nat Immunol 2014; 15(9): 839–45.

65. Fabre A, Martinez-Vinson C, Goulet O, Badens C. Syndromic diarrhea/tricho-hepato-enteric syndrome. Orphanet J Rare Dis 2013; 8: 5.

66. Srinivasan S, He X, Mirza S, Mager J. Exosome complex components 1 and 2 are vital for early mammalian development. Gene Expr Patterns 2024; 51: 119346.

67. Yatsuka H, Hada K, Shiraishi H, Umeda R, Morisaki I, Urushibata H, et al. Exosc2 deficiency leads to developmental disorders by causing a nucleotide pool imbalance in zebrafish. Biochem Biophys Res Commun 2020; 533(4): 1470–6.

68. Zhou H, Huang L, Liang L, Chen L, Zou C, Li Z, et al. Identification of an mirna regulatory network and candidate markers for ischemic stroke related to diabetes. Int J Gen Med 2021; 14: 3213–23.

69. Kammler S, Lykke-Andersen S, Jensen TH. The RNA exosome component hRrp6 is a target for 5-fluorouracil in human cells. Mol Cancer Res 2008; 6(6): 990–5.

70. Bush JA, Meyer SM, Fuerst R, Tong Y, Li Y, Benhamou RI, et al. A blood–brain penetrant RNA-targeted small molecule triggers elimination of r(G4C2)exp in c9ALS/FTD via the nuclear RNA exosome. Proc Natl Acad Sci U S A 2022; 119(48): e2210532119.

71. Damseh NS, Obeidat AN, Ahammed KS, Al-Ashhab M, Awad MA, van Hoof A. Pontocerebellar hypoplasia associated with p.Arg183Trp homozygous variant in EXOSC1 gene: A case report. Am J Med Genet Part A 2023; 191(7): 1923–8.

72. Somashekar PH, Kaur P, Stephen J, Guleria VS, Kadavigere R, Girisha KM, et al. Bi-allelic missense variant, p.Ser35Leu in EXOSC1 is associated with pontocerebellar hypoplasia. Clin Genet 2021; 99(4): 594–600.

73. Di Donato N, Neuhann T, Kahlert AK, Klink B, Hackmann K, Neuhann I, et al. Mutations in EXOSC2 are associated with a novel syndrome characterised by retinitis pigmentosa, progressive hearing loss, premature ageing, short stature, mild intellectual disability and distinctive gestalt. J Med Genet 2016; 53(6): 419–25.

74. Yang X, Bayat V, Didonato N, Zhao Y, Zarnegar B, Siprashvili Z, et al. Genetic and genomic studies of pathogenic EXOSC2 mutations in the newly described

disease SHRF implicate the autophagy pathway in disease pathogenesis. Hum Mol Genet 2020; 29(4): 541–53.

75. Wan J, Yourshaw M, Mamsa H, Rudnik-Schöneborn S, Menezes MP, Hong JE, et al. Mutations in the RNA exosome component gene EXOSC3 cause pontocerebellar hypoplasia and spinal motor neuron degeneration. Nat Genet 2012; 44(6): 704–8.

76. Lu G, Liu H, Wang H, Tang X, Luo S, Du M, et al. Potentially functional variants of INPP5D and EXOSC3 in immunity B cell-related genes are associated with non-small cell lung cancer survival. Front Immunol 2024; 15: 1440454.

77. Wijnsma KL, Schijvens AM, Bouwmeester RN, Aarts LAM, van den Heuvel L (Bert) P, Haaxma CA, et al. Mutations in genes encoding subunits of the RNA exosome as a potential novel cause of thrombotic microangiopathy. Int J Mol Sci 2024; 25(14): 7604.

78. Huynh NCN, Pham AL, Pham NVT, Le PHN. Differential gene expression analysis of The Cancer Genome Atlas messenger ribonucleic acid sequencing data from male patients with and without lymph node metastasis in tongue cancer. Arch Orofac Sci 2024; 19(2): 127–39.

79. Hong JQ, Huang QH, Huang ZY, Fan LP, Lin QY, Huang HB. Expression and clinical significance of exosome component 4 in newly diagnosed patients with diffuse large B-cell lymphoma. Zhongguo Shi Yan Xue Ye Xue Za Zhi 2023; 31(6): 1684–9.

80. Wang N, Miao X, Lu W, Ji Y, Zheng Y, Meng D, et al. RUNX3 exerts tumor-suppressive role through inhibiting EXOSC4 expression. Funct Integr Genomics 2024; 24(3): 1–12.

81. Fasken MB, Leung SW, Cureton LA, Al-Awadi M, Al-Kindy A, van Hoof A, et al. A biallelic variant of the RNA exosome gene, EXOSC4, associated with neurodevelopmental defects impairs RNA exosome function and translation. J Biol Chem 2024; 300(8): 107571.

82. Slavotinek A, Misceo D, Htun S, Mathisen L, Frengen E, Foreman M, et al. Biallelic variants in the RNA exosome gene EXOSC5 are associated with developmental delays, short stature, cerebellar hypoplasia and motor weakness. Hum Mol Genet 2020; 29(13): 2218–39.

83. Huang Y, Cen Y, Wu H, Zeng G, Su Z, Zhang Z, et al. Nodularin-R synergistically enhances abiraterone against castrate- resistant prostate cancer via PPP1CA inhibition. J Cell Mol Med 2024; 28(22): e70210.

84. Perez CM, Gong Z, Yoo C, Roy D, Deoraj A, Felty Q. Inhibitor of DNA binding protein 3 (ID3) and nuclear respiratory factor 1 (NRF1) mediated transcriptional gene signatures are associated with the severity of cerebral amyloid angiopathy. Mol Neurobiol 2024; 61(2): 835–82.

85. Fan X, Yang X, Guo N, Gao X, Zhao Y. Development of an endoplasmic reticulum stress-related signature with potential implications in prognosis and immunotherapy in head and neck squamous cell carcinoma. Diagn Pathol 2023; 18(1): 1–14.

86. Burns DT, Donkervoort S, Müller JS, Knierim E, Bharucha-Goebel D, Faqeih EA, et al. Variants in EXOSC9 disrupt the RNA exosome and result in cerebellar atrophy with spinal motor neuronopathy. Am J Hum Genet 2018; 102(5): 858–73.

87. Sakamoto M, Iwama K, Sekiguchi F, Mashimo H, Kumada S, Ishigaki K, et al. Novel EXOSC9 variants cause pontocerebellar hypoplasia type 1D with spinal motor neuronopathy and cerebellar atrophy. J Hum Genet 2020; 66(4): 401–7.

88. Bizzari S, Hamzeh AR, Mohamed M, Al-Ali MT, Bastaki F. Expanded PCH1D phenotype linked to EXOSC9 mutation. Eur J Med Genet 2020; 63(1): 103622.

89. Demini L, Kervarrec C, Guillot L, Com E, Lavigne R, Kernanec PY, et al. Inactivation of Exosc10 in the oocyte impairs oocyte development and maturation, leading to a depletion of the ovarian reserve in mice. Int J Biol Sci 2023; 19(4): 1080.

90. Kline BL, Siddall NA, Wijaya F, Stuart CJ, Orlando L, Bakhshalizadeh S, et al. Functional characterization of human recessive DIS3 variants in premature ovarian insufficiency. Biol Reprod 2025; 112(1): 102-18.

91. Wang Z, Wu D, Xu X, Yu G, Li N, Wang X, et al. DIS3 ribonuclease is essential for spermatogenesis and male fertility in mice. Development 2024; 151(13): dev202579. Erratum in: Development 2024; 151(17): dev204238.

92. Li X, Ruan Z, Yang S, Yang Q, Li J, Hu M. Bioinformatic-experimental screening uncovers multiple targets for increase of MHC-I expression through activating the interferon response in breast cancer. Int J Mol Sci 2024; 25(19): 10546.

Experimed

Research Article

Open Access

Effects of Ozone Therapy and Ozonated Olive Oil on Bacterial Translocation in an Experimental Burn Model

Ayten Basak Kilic [1] ✉, Osman Hakan Kocaman [2], Feryal Gun Soysal [2]

[1] Department of Pediatric Surgery, Elite Medical Center, Doha, Qatar
[2] Department of Pediatric Surgery, Istanbul Medical Faculty, Istanbul University, Istanbul, Turkiye

Abstract

Objective: Ozone therapy may reduce the complications associated with bacterial translocation. This study evaluated the effects of ozone therapy on bacterial translocation and intestinal mucosal damage in a rat model of scald burns.

Materials and Methods: Thirty-two Wistar albino rats were divided into four groups. After inducing third-degree burns, Group A (control) received no treatment, Group B received rectal ozone, Group C was treated with ozonated olive oil topically, and Group D received pure olive oil. Blood, liver, mesenteric lymph nodes (MLN), and intestinal samples were cultured, and histopathological examinations were conducted on the terminal ileum sections.

Results: Group A had significantly higher bacterial translocation rates in blood cultures (p=0.033). Groups A and D showed higher bacterial growth in MLN samples compared to Groups B and C (p=0.000). Similarly, the growth rate observed in the liver samples of Group D rats was significantly higher than that in the other groups (p=0.001). Histopathological analysis revealed the most severe mucosal damage in Group A (p=0.000), while Group C exhibited the least damage and no bacterial growth.

Conclusions: Our findings clearly demonstrated that ozone therapy, particularly ozonated olive oil, significantly reduces bacterial translocation and intestinal mucosal damage in burn injuries, suggesting its potential therapeutic role in the management of such injuries.

Keywords   Burn · Ozone (O₃) · Ozone therapy · Bacterial translocation · Rat

INTRODUCTION

Burns are defined as injuries to the skin or other tissues caused by thermal, chemical, electrical, or radiation sources. The prevalence of burn-related deaths varies widely across different regions due to epidemiological and socio-economic factors (1). However, they remain a leading cause of substantial morbidity and injury-related deaths, particularly in low- and middle-income countries. Worldwide, burn-related mortality is documented at approximately 18.27%, and burns account for an estimated 180,000 deaths annually (1, 2).

The primary causes of mortality following severe burn injuries include systemic inflammatory response syndrome (SIRS), bacterial infections, and subsequent sepsis (3). Bacterial translocation is a critical phenomenon in the pathophysiology of burn injuries. It involves the passage of bacteria from the gastrointestinal tract to extra-intestinal sites, such as the bloodstream, mesenteric lymph nodes, and other organs. This process is driven by increased intestinal ischaemia, permeability, dysbiosis, and immune suppression following severe burns. The translocation of gut bacteria can trigger systemic infections and sepsis, significantly complicating the clinical management of burn patients (4).

Ozone therapy has been explored as a therapeutic intervention due to its anti-bacterial, anti-viral, anti-fungal, anti-inflammatory, and immune-modulating properties. Ozone (O_3) is a tri-atomic oxygen molecule with potent oxidizing capabilities, making it effective against a wide range of pathogens (5). Therapeutically, ozone can be applied topically, injected subcutaneously, or administered systemically. In the context of burn injuries, ozone therapy has shown promise in enhancing wound healing by improving oxygen transport, reducing infection rates, and modulating inflammatory responses (6).

Research has demonstrated that ozone can accelerate the healing of second-degree burns by increasing tissue oxygenation, enhancing fibroblast activity, and reducing the microbial load in the wound bed. Moreover, ozone therapy has been associated with a decrease in healing time and a reduction in the incidence of burn wound infections (6, 7). Overall, the therapeutic potential of ozone in the management of burn injuries is supported by evidence indicating its effectiveness in improving clinical outcomes and mitigating complications associated with bacterial translocation and systemic infections (6-8). Therefore, we aimed to evaluate the effects of ozone therapy on bacterial translocation and intestinal mucosal changes following experimentally induced scald burns with hot water in rats.

MATERIALS AND METHODS

This prospective study was performed with the Institutional Review Board protocol approval date 29.07.2010 and number 124 in Istanbul University, Aziz Sancar Institute of Experimental Medicine (DETAE), Department of Experimental Animal Biology and Biomedical Application Techniques. In the present study, 32 female Wistar-Albino rats weighing between 180 and 220 grams, were used. All animals included in the experiment were non-pregnant and in a healthy condition, confirmed by veterinary examination before the study.

Before burn induction, the animals were housed in group Plexiglas cages to allow social interaction under controlled environmental conditions (temperature: 22 ± 2 °C, humidity: 40-60%, 12-hour light/dark cycle). Each cage housed 3–4 rats, allowing sufficient space for movement and access to food and water *ad libitum*. Following burn induction, all animals were housed individually in transparent, separate cages to prevent wound contamination, minimize stress, and ensure accurate health monitoring, in accordance with established experimental protocols.

Experimental Burn Induction

Following anesthesia with 100 mg/kg ketamine HCL administered intramuscularly, the rats' dorsal skin was shaved (4 cm×4 cm), covering approximately 35%-40% of the total body surface area (TBSA). The percentage of affected was calculated based on standard body surface estimation methods for rodents.

A third-degree burn injury was induced by immersing the shaved dorsal area in boiling water (100 °C) for 12 seconds while maintaining proper temperature control. This technique is a widely accepted method for creating full-thickness burns in experimental models (9). To confirm the creation of third-degree burns, clinical symptoms such as eschar formation, absence of capillary refill, and insensitivity to pain stimuli were observed. Additionally, histopathological examination of the burned tissue demonstrated complete epidermal and dermal necrosis, consistent with the characteristics of third-degree burns (10). Prior to burn induction, fluid resuscitation was performed using lactated Ringer's solution. The total fluid volume was calculated based on the Parkland formula (Total fluid volume (mL) = 4 mL × kg × TBSA (%)), considering the average rat body weight. Accordingly, 3 mL of the lactated Ringer's solution was administered intraperitoneally to mitigate fluid loss and maintain hemodynamic stability. To manage potential pain, tramadol (Contramal®) was administered at 5 mg/kg and mixed into the drinking water post-burn induction.

Surgical Method and Sample

The animals were divided into four groups. The experimental groups were designed to evaluate the effects of different ozone therapy methods on bacterial translocation and intestinal mucosal integrity following burn injury. A control group was included to assess the natural progression of burn-related damage, while the treatment groups were structured to compare the efficacy of rectal ozone gas and ozonated olive oil application. Additionally, a pure olive oil group was incorporated to differentiate the effects of ozone from the potential influence of the vehicle itself.

The treatment protocol was designed for five days based on the bacterial translocation timeline following burn injury. Previous studies have shown that gram-negative bacterial translocation begins around day 3 post-injury and peaks within the first week (11). Five days after the experimental burn induction procedure, all animals were euthanized under general anesthesia following sample collection. Euthanasia was performed via cervical dislocation. Blood samples (2 mL) were obtained directly from the heart through cardiac puncture following laparotomy. Additionally, liver, mesenteric lymph nodes, and intestinal tissue samples were collected under sterile conditions. A sample was also taken from the terminal ileum approximately 2 cm from the ileocecal valve for histopathological examination in all animals.

Burn Group (Group A) (n=8): This control group did not receive any further treatment after the experimental third degree burn induction (Picture 1).

Picture 1. Representative image of the burn wound on day 5 in the control group. The wound area shows the progression of untreated full-thickness burn injury, with visible eschar formation and tissue necrosis.

Rectal Ozone Application Group (Group B) (n=8): Following the experimental burn induction procedure, all burned animals in this group received 10 mL of ozone gas at 5 ng/mL rectally once daily for 5 days (Picture 2). Ozone gas administration was performed using a no:6 feeding tube, which was carefully inserted 1-2 cm into the rectum. The gas was delivered slowly, and to prevent leakage, the tube was kept in place for 30 seconds before removal (12).

Picture 2. Rectal ozone application in the experimental rat model. Ozone gas was administered rectally using a No:6 feeding tube to ensure controlled and standardised delivery.

Ozonated Olive Oil Application Group (Group C) (n=8): After the experimental burn induction, this Group of animals was administered 10 mL of ozonated olive oil (Kirlangic Olive Oil - Anadolu Group A.S., Turkiye), prepared using an ozone generator, applied topically to the burned area three times daily (Picture 3). The ozonated olive oil was freshly prepared before each application. The preparation involved bubbling ozone gas continuously at a low flow rate through pure olive oil for 12-24 hours until saturation was achieved, resulting in a gel-like consistency. This method is consistent with the minor ozonation technique. The final concentration of ozone in the olive oil was approximately 700-1000 mg/L, ensuring effective therapeutic dosing. The ozonated olive oil was stored in dark-coloured glass bottles to maintain its stability and efficacy (13).
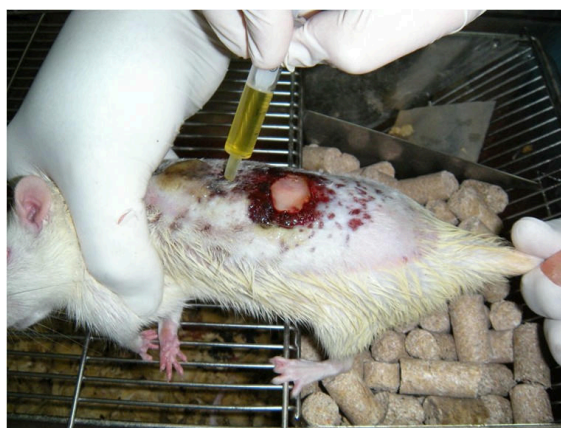
Picture 3. Ozonated olive oil application to the burn area. The oil was freshly prepared and applied topically three times daily to evaluate its effects on wound healing and bacterial translocation.

Pure Olive Oil Application Group (Group D) (n=8): After the experimental burn induction, over five days, 10 mL of pure olive oil (Kirlangic Olive Oil - Anadolu Group A.S., Turkiye) was applied three times daily to the burned skin of all animals.

Data Collection

Microbiological Evaluation: Blood, liver, mesenteric lymph nodes (MLN), and intestinal samples from each animal were cultured under aerobic and anaerobic conditions. To prevent air contact, the samples for culture were placed in appropriate deoxygenated transport media. Bacteria were isolated using standard microbiological methods. Bacterial growths in the MLN, liver, and blood cultures were evaluated as indications of bacterial translocation in each group.

Histopathological Evaluation: A 1 cm segment of the ileum, approximately 2 cm from the ileocecal valve, was fixed in 4% buffered formaldehyde. After 24 hours, the fixed tissue was processed into paraffin blocks. Sections of 3-5 microns from the paraffin blocks were stained with Hematoxylin and Eosin (H&E) and examined under a light microscope. In the histopathological assessment and staging of changes in the intestinal villus structure, blunting of villus tips, flattening, and shortening of the villi were considered (Table 1). Stages from 1 to 4 were assigned to show the changes in the structure of the intestinal mucosa villi. The staging score for each group was determined by multiplying the number of animals at each stage by their respective stage points, resulting in a histopathological score (14).

Table 1. Staging of changes in the intestinal mucosal villus structure.

Stage	Score	Structural Changes
1	1	Normal mucosal structure
2	2	Mild blunting, shortening, and edema in the villi
3	3	Pronounced flattening and shortening of the villi
4	4	Significant villus irregularity and hyperplasia in the lymph follicles

Statistical Analyses

The data were analyzed using SPSS (Statistical Package for the Social Sciences) software for Windows, version 21.0, provided by IBM in Armonk, NY, USA. The analysis involved summarizing individual and aggregate data using descriptive statistics, which included means, standard deviations, medians (ranging from minimum to maximum), frequency distributions, and percentages. The normality of the data distribution was assessed using the Kolmogorov-Smirnov test. For variables with a normal distribution, comparisons were made using the Student's t-test and ANOVA. For non-normally distributed variables, the Mann–Whitney and Kruskal-Wallis tests were employed to compare the groups. Categorical variables were evaluated using the Chi-Square test. Correlations were examined using either Spearman's Rho or Pearson tests. p values of <0.05 were considered statistically significant.

RESULTS

The comparison of culture growths between groups A, B, C, and D across blood, MLN, and liver samples revealed significant differences in bacterial translocation. In Group A, 87.5% (7/8) of the blood and MLN samples showed bacterial growth, while the liver samples had a growth rate of 25.0% (2/8). Group B displayed bacterial translocation in 12.5% (1/8) of the blood samples, 25.0% (2/8) of MLN samples, and 25.0% (2/8) of the liver samples. Group C had no bacterial growth in any of the samples, with all blood, MLN, and liver samples being sterile (0%, 0/8, respectively). Group D exhibited bacterial growth in 37.5% (3/8) of the blood samples, 100.0% (8/8) of MLN samples, and 87.5% (7/8) of the liver samples. Additionally, flora bacteria were observed in the intestines of all rats in the entire sample groups. The comparison of culture growths between groups across blood, MLN, and liver samples, with specific bacterial species and their counts detailed in the Table 2. Following the bacteriological study, it was found that the growth rate observed in the blood cultures of Group A rats was statistically significantly higher compared to the growth rates observed in the blood cultures of Groups D, B, and C rats (p=0.033). When evaluating the growth rates in MLN samples, it was determined that the growth rates observed in Groups A and D were statistically significantly higher than those in Groups B and C (p=0.000, for both). Similarly, the growth rate observed in the liver samples of Group D rats was significantly higher than that in Groups A, B, and C rats (p=0.001, for all) (Figure 1).
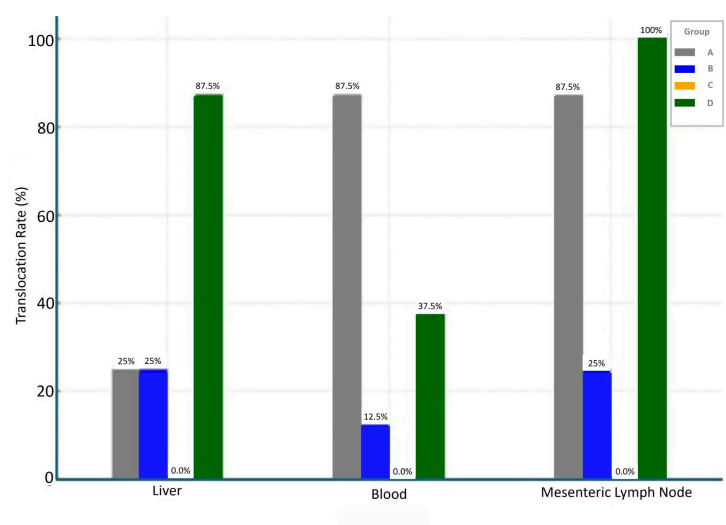
Figure 1. Bacterial translocation rates between groups.

In our study, particularly in Group A rats, a macroscopic examination of the intestines revealed that the intestines appeared pale and dull, the intestinal walls were thinned, and there was noticeable dilation (Picture 4). Additionally, according to the histopathological evaluations in Group A rats, microscopic examination of the mucosal villous structure revealed that no animals had a normal mucosal villous structure. Upon microscopic examination of the intestinal sections, in Group A rats, stage 2 changes were detected in one animal (Figure 2), stage 3 in three animals, and stage 4 in four animals (Figure 3). In Group B, four animals exhibited normal mucosal villus structure, three showed stage 2 changes, and one displayed stage 3 changes. In Group C, seven animals had normal mucosal villus structure, and one had stage 2 changes. In group D, two animals had normal mucosal villus structure, and six had stage 2 changes. Therefore, it has been determined that the mean mucosal damage calculated in the control group (Group A: 3.38) is statistically significantly higher compared to other treatment groups (Group B: 1.13, Group C: 0.25 and Group D: 1.5) (df_{total}=31; F=15.50; p=0.000).
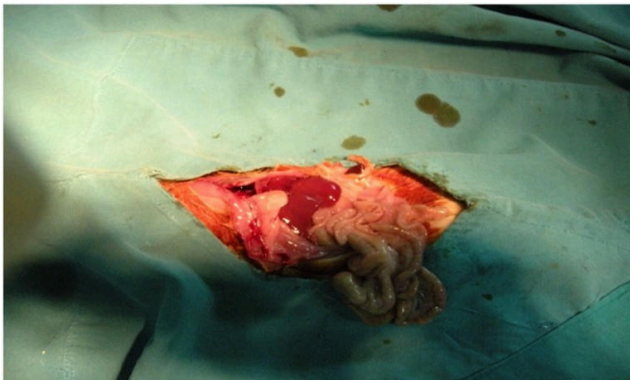
Picture 4. In rats with induced burns (Group A), the intestines were dilated, oedematous, and have a dull appearance.
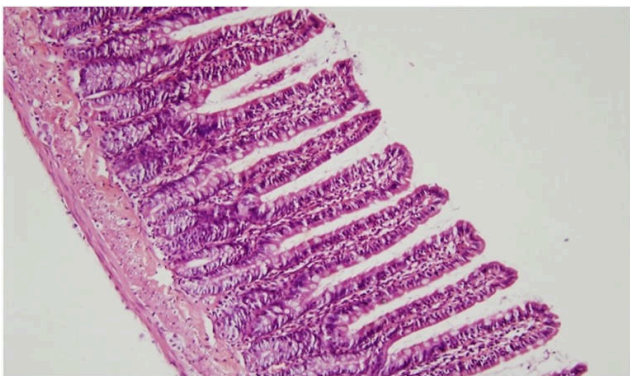
Figure 2. A normal villous structure and minimal lymphocyte infiltration were observed (Hematoxylin and Eosin (H&E), x125) (Stage 2).

DISCUSSION

The impact of ozone therapy on bacterial translocation in burn injuries presents promising yet complex outcomes. Several studies have explored the multifaceted role of ozone in modulating post-injury infection and inflammation. Published data indicate that ozone therapy significantly enhances wound healing through increased angiogenesis and fibroblast activity. Pchepiorka et al. demonstrated that wounds treated with ozone showed higher angiogenesis and fibroplasia compared with the control groups, indicating enhanced healing processes (15). Moreover, ozone therapy's efficacy in reducing oxidative stress and inflammation is well-documented in published data. In a study by Erginel et al., an increased dosage of ozone significantly reduced inflammatory processes and intestinal mucosal damage in a rat model of ischemia/reperfusion injury (16). Furthermore, Liu et al. showed that hyperbaric oxygen treatment alleviated intestinal histological damage, reduced mucosal permeability, and prevented bacterial translocation in rats (17). Additionally, the effects of ozone on burn wounds specifically highlight its efficacy in reducing bacterial load and promoting tissue regeneration. A 2021 study by Karakaya et al. (18) reported the impact of subcutaneous ozone therapy on the healing of second-degree burn wounds in 72 male Sprague-Dawley rats. The rats were divided into three groups: control, silver sulfadiazine, and ozone, each further assessed on days 7 and 14. Superficial partial-thickness burns were induced on the rats' lower backs. The control group received saline injections daily, the silver sulfadiazine group had daily dressings with the compound, and only the ozone group received daily subcutaneous ozone injections. Histopathological assessments revealed that the ozone group had markedly improved wound healing and higher tissue hydroxyproline levels compared with the other groups.
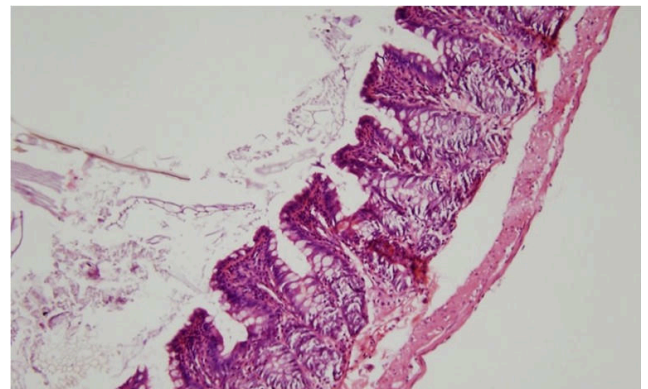
Figure 3. Thinning of the mucosa and pronounced thickening, flattening, shortening, and lymphocyte infiltration in the villi are presented (Hematoxylin and Eosin (H&E), x125) (Stage 4).

Table 2. Comparison of culture growths between the groups.

Group	Blood n (%)	MLN n (%)	Liver n (%)
A	· 7/8 Growths (87.5%)	· 7/8 Growths (87.5%)	· 2/8 Growths (25.0%)
	S. aureus (n=3)	*Enterococcus spp.* (n=1)	*Enterococcus* (n=1)
	Enterobacter spp. (n=2)	*Enterobacter spp.* (n=1)	*Enterobacter spp.* (n=1)
	Mix (n=2)	*E. coli* (n=1)	
		Acinetobacter (n=1)	
		Mix (n=3)	
B	· 1/8 Growth (12.5%)	· 2/8 Growths (25.0%)	· 2/8 Growths (25.0%)
	P. mirabilis (n=1)	*P. mirabilis* (n=1)	*S. aureus* (n=2)
		Mix (n=1)	
C	· 0/8 Sterile (0.0%)	· 0/8 Sterile (0.0%)	· 0/8 Sterile (0.0%)
D	· 3/8 Growths (37.5%)	· 8/8 Growths (100.0%)	· 7/8 Growths (87.5%)
	S. aureus (n=2)	*Enterococcus spp.* (n=1)	*Enterobacter spp.* (n=1)
	Enterobacter spp. (n=1)	Mix (n=7)	*Enterococcus spp.* (n=1)
			Mix (n=5)

MLN: Mesenteric lymph nodes

Researchers concluded that subcutaneous ozone therapy can enhance the healing of second-degree burn wounds more effectively, indicating its potential as a beneficial treatment in burn care (18). In the present study, histopathological evaluations revealed significantly severe mucosal damage in Group A (control group), which did not receive any further treatment following the burn induction, characterized by thinning and dilation of the mucosa. Furthermore, no animals had a normal mucosal villous structure in Group A rats. In contrast, the rectal ozone group (Group B) and the ozonated olive oil group (Group C) exhibited significantly less mucosal damage, particularly Group C, highlighting ozone therapy's protective effects on the intestinal mucosa. These effects likely stem from ozone's anti-oxidative and anti-inflammatory properties.

However, published data evaluating the anti-bacterial efficacy of ozone therapy on bacterial translocation after burn injuries are limited and remain a point of debate. Some studies suggest that while ozone therapy aids in wound healing, its direct impact on bacterial elimination can be limited. Ozturk et al. observed that although ozone had positive effects on inflammatory and oxidant profiles, it did not significantly reduce bacterial counts in a vascular graft infection model caused by Methicillin-resistant *Staphylococcus aureus* (MRSA) (19). On the contrary, Emre et al. evaluated the effectiveness of ozone therapy on hydrofluoric acid (HF)-induced skin burns in 20 male Wistar Albino rats. The rats were divided into two groups of ten: an experimental group and a control group. The experimental group received topical ozonized liquid vaseline (20 μg O_3/mL) for seven days following HF application, while the control group was treated with a saline solution. The results indicated significantly higher epithelial proliferation and collagen formation in the experimental group than in the control group, which showed higher infiltration levels. These findings demonstrated that ozone therapy significantly improves tissue repair in HF-induced skin burns in rats, indicating its potential as an effective first aid treatment for chemical burns (6). Supportively, Khidirov et al. conducted a study to explore the impact of ozone therapy on burn sepsis treatment in 130 cases with thermal injuries. These patients were grouped into four categories. The first group, comprising 50 patients with burn sepsis, received a combination of traditional treatments and intravenous ozonized saline solution (4.0 mg/L) administered daily in 200 mL doses for 10 days. The second group (n=30) was treated with only traditional methods. The third group included 30 burn patients without sepsis who received a combination of traditional treatments and ozone therapy. The fourth group (n=20) involved burn cases without sepsis, and received only traditional treatments. The study found that the group receiving ozone therapy (n=50, 38.5%) demonstrated significant and earlier improvements in inflammation and wound healing than the control groups. Notably, the sepsis group treated with ozone exhibited a sustained increase in catalase levels and enhanced anti-oxidant activity, improvements that were not seen in the sepsis group without ozone therapy. Researchers reported that combining routine therapy with ozone treatment statistically lowered the overall mortality from 72.5% to 45%. The researchers concluded that ozone therapy effectively treats burn sepsis and reduces

microbial contamination. Moreover, researchers also noted that it is a simple, cost-effective treatment that reduces the duration of treatment and hospitalization (20). Moreover, Bostanci et al. evaluated the impact of rectal ozone therapy on bacterial translocation in an experimental colitis model. The rats were randomly assigned to three groups: sham, control, and ozone treatment. Researchers assessed tissue damage and measured the levels of oxidative stress markers in the colon and liver tissue. In addition, blood cultures were collected to determine bacterial translocation. Researchers documented that ozone treatment significantly reduced tissue damage compared with the control group. Moreover, bacterial translocation was reported to be less prevalent in the ozone treatment group than in the control group, affecting various tissues including the liver, MLN, portal vein, spleen, and systemic blood. Ultimately, researchers concluded that the use of rectal ozone therapy increased the anti-oxidant activity and improved the function of key enzymes that protect against oxidative stress, which was measured by oxidative stress markers including glutathione-s-transferase, superoxide dismutase, glutathione, and malondialdehyde. This therapy also promotes better healing of tissue damage and significantly reduces bacterial translocation to tissues (21). In accordance with published data, Group A (control group) exhibited the highest bacterial translocation rates, with significant bacterial growth in the blood, MLN, and liver samples in our study. The cultures from tissue and blood in the group treated with pure olive oil showed similarities with the control group. Conversely, the rectal ozone group (Group B) and the ozonated olive oil group (Group C) showed significantly reduced bacterial translocation, with Group C exhibiting no bacterial growth in any samples. This suggests that topical ozonated olive oil is highly effective in preventing bacterial translocation, consistent with the findings on ozone's anti-bacterial properties.

In conclusion, our findings clearly demonstrated that ozone therapy, particularly ozonated olive oil, significantly reduces bacterial translocation and intestinal mucosal damage following severe burn injury in rats. These findings suggest a potential therapeutic role for ozone in the management of burn injuries. Further studies should be performed with larger sample groups to delineate the specific conditions and dosages under which the ozone therapy method can be most effective, particularly in preventing bacterial translocation and optimizing its clinical application in burn injuries.

Ethics Committee Approval	Ethical approval was obtained from the Istanbul University Local Ethics Committee for Animal Experiments (approval number: 124; approval date: 29.07.2010).

Author Details

Ayten Basak Kilic
[1] Department of Pediatric Surgery, Elite Medical Center, Doha, Qatar

(iD) 0009-0003-1114-8983 ✉ basaksezginer@yahoo.com

Osman Hakan Kocaman
[2] Department of Pediatric Surgery, Istanbul Medical Faculty, Istanbul University, Istanbul, Turkiye

(iD) 0000-0002-8072-5292

Feryal Gun Soysal
[2] Department of Pediatric Surgery, Istanbul Medical Faculty, Istanbul University, Istanbul, Turkiye

(iD) 0000-0001-7712-6849

REFERENCES

1. Opriessnig E, Luze H, Smolle C, Draschl A, Zrim R, Giretzlehner M, et al. Epidemiology of burn injury and the ideal dressing in global burn care – Regional differences explored. Burns 2023; 49(1): 1–14.

2. World Health Organization. Burns. World Health Organization; 2023 Oct 13. Available from: https://www.who.int/news-room/fact-sheets/detail/burns

3. Sallam HS, Urvil P, Savidge TC, Chen JD. Ghrelin abates bacterial translocation following burn injury by improving gastric emptying. Neurogastroenterol Motil 2020; 32(2): e13742.

4. Alikulov RT, Djemileva EI, Mansurov ZZ. Early diagnosis and principles of treatment of sepsis in severely burned patients. Boffin Academy 2024; 2(1): 252–6.

5. Martusevich AK, Peretyagin SP, Ruchin MV, Struchkov AA. Ozone therapy in patients with burn disease. J Biomed Sci Eng 2018; 11(2): 27–35.

6. Aslan NE, Erol H, Balcıoğlu E, Yalçın B. Efficiency of ozone (O_3) therapy on experimental acidic skin burns in rats. Vet Méx 2024; 11(1): 2–10.

7. El-Tobgy K. Ozone therapy in burns: our experience in Egypt. J Ozone Ther 2019; 3(4): 12.

8. Furqatovich AR, Karabaevich KK, Muxiddinovich TF. Burn sepsis – a terrible complication of thermal injury. J Biomed Pract 2022; 7(6): 372-75.

9. Moyliev G, Yunuskhodjaev A, Saidov S, Babakhanov O, Mirsultanov J. To study references and analysis of an experimental model for skin burns in rats. The Scientific Temper 2024; 15(1): 13.

10. Junior JKM, Gragnani A, Ramos MCC, Ferreira L. Rat: an experimental model for burns – a systematic review. Acta Cir Bras 2012; 27(6): 417–23.

11. Feng Y, Wang D, Wang K, Leng X, Xiao H, Guo D, et al. Role of lymphatics in bacterial translocation from intestine in burn rats. Zhonghua Shao Shang Za Zhi 2011; 27(1): 49–53.

12. Kocaman H, Erginel B, Onder SY, Soysal FG, Keskin E, Celik A, et al. The role of ozone therapy in hepatic fibrosis due to biliary tract obstruction. Eur J Pediatr Surg 2016; 26(1): 133–7.

13. Anzolin AP, da Silveira-Kaross NL, Bertol CD. Ozonated oil in wound healing: what has already been proven? Med Gas Res 2020; 10(1): 54–9.

14. Söfteland J, Hellström M, Oltean M. The development of intestinal preservation injury: a comparison between porcine and rat intestines. Transplantation 2017; 101(6S2): S28.

15. Pchepiorka R, Moreira MS, da Silva Lascane NA, Catalani LH, Allegrini Jr S, de Lima NB. Effect of ozone therapy on wound healing in the buccal mucosa of rats. Arch Oral Biol 2020; 119: 104889.

16. Erginel B, Yanar F, Ilhan B, Yüksel S, Mikailo P, Berker N, et al. Is the increased ozone dosage a key factor for its anti-inflammatory effect in an experimental model of mesenteric ischemia? Turk J Trauma Emerg Surg 2023; 29: 1069–74.

17. Liu X, Liang F, Song W, Diao X, Zhu W, Yang J. Effect of Nrf2 signaling pathway on the improvement of intestinal epithelial barrier dysfunction by hyperbaric oxygen treatment after spinal cord injury. Cell Stress Chaperones 2021; 26: 433–41.

18. Karakaya E, Akdur A, Ayvazoğlu Soy E, Araz C, Ok Atilgan A, Özturan Özer, et al. Effect of subcutaneous topical ozone therapy on second-degree burn wounds in rats: an experimental study. J Burn Care Res 2021; 42(6): 1243–53.

19. Ozturk B, Kurtoglu T, Durmaz S, Kozaci LD, Abacigil F, Ertugrul B, et al. The effects of ozone on bacterial growth and thiol-disulphide homeostasis in vascular graft infection caused by MRSA in rats. Acta Cir Bras 2017; 32: 219–28.

20. Khidirov LF, Pulotov BB, Saydilov SU. Effect of ozone therapy on the course of burn sepsis. J Coryphaeus Sci 2024; 6(1): 209–17.

21. Bostanci ME, Avci O, Tas A, Koc T, Gursoy S, Silig Y. The effect of rectal ozone use on bacterial translocation and oxidative stress in experimental colitis model. Experimed 2022; 12(2): 66–73.

Experimed

Research Article　　　　　　　　　　　　　　　　　　　　**Open Access**

In vitro Efficacy of Sumac (*Rhus Coriaria*) Extracts Against *Leishmania tropicana* and *Leishmania mexicana*: A Preliminary Study from Turkiye

Ergun Mete [1] , Yener Ozel [2] ✉, Hilal Bardakci [3] , Cenk Durmuskahya [4] , Aylin Koseler [5] , Ozgur Kurt [6]

[1] Department of Medical Microbiology, Faculty of Medicine, Pamukkale University, Denizli, Turkiye
[2] Department of Medical Microbiology, Faculty of Medicine, Balikesir University, Balikesir, Turkiye
[3] Department of Pharmacognosy, Faculty of Pharmacy, Fenerbahce University, Istanbul, Turkiye
[4] Department of Forest Engineering, Faculty of Forestry, Izmir Kâtip Celebi University, Izmir, Turkiye
[5] Department of Biophysics, Faculty of Medicine, Pamukkale University, Denizli, Turkiye
[6] Department of Medical Microbiology, School of Medicine, Acibadem University, Istanbul, Turkiye

Abstract

Objective: Cutaneous leishmaniasis (CL) is a common clinical manifestation of leishmaniasis. Here, *the in vitro* anti-leishmanial efficacy of sumac extracts was tested for the first time on both *Leishmania (L.) tropica* and *L. mexicana* isolates using *Rhus (R.) coriaria* plant, which was collected in western Anatolia.

Materials and Methods: The dried and powdered fruits of *R. coriaria* were macerated in acetone, ethyl alcohol, and ethyl alcohol-water mixture at room temperature for two days. The pooled extracts were evaporated under reduced pressure and lyophilized form for the study. Isolates of *L. tropica* and *L. mexicana* in Acibadem University R&D Laboratory were initially thawed and cultivated in NNN medium. Assessments were made using the haemocytometer and MTT methods at 24 and 48 h, compared with meglumine antimoniate as the control group.

Results: For *L. tropica*, the effective concentration ranges of the extracts and the infusion were found to be 578.13-289.06 µg/mL and 289.06-144.53 µg/mL, respectively. For *L. mexicana*, the ranges were found to be 289.06-144.53 µg/mL and 144.53-72.27 µg/mL, respectively. It was shown that all extracts of *R. coriaria* were effective against both *L. tropica* and *L. mexicana* in higher doses, compared to meglumine antimoniate.

Conclusion: An interesting finding was that higher sumac doses were required to eliminate *L. tropica* of the Old World, compared to *L. mexicana* of the New World. In addition, the aqueous alcohol extract showed efficacy that lasted for 48 h in half doses compared to others in *L. tropica*. Further assessments for both the identification of the active compounds within *R. coriaria* and their efficacy *in vivo* are planned.

Keywords　　*Leishmania* · Cutaneous leishmaniasis · Sumac · *Rhus coriaria*

✉ Corresponding author: Yener Ozel yener_ozel@hotmail.com

INTRODUCTION

Leishmaniasis is a common parasitic disease in the tropical and subtropical regions of the world, which is caused by flagellated protozoa of the *Leishmania* genus and transmitted by the sandflies (*Phlebotomus* sp. in the Old World and *Lutzomyia* sp. in the New World) (1). It appears with different clinical manifestations in humans, which are mainly cutaneous form (cutaneous leishmaniasis-CL) and visceral form which may go deadly in left untreated and the mucocutaneous form that is mostly limited in South America. Leishmaniasis is currently endemic in 99 countries today, with around 1.2 million reported cases, and CL constitutes almost 70% of all cases in the world, annually (1-3). There has been a constant increase in the incidence of leishmaniasis in many parts of the world lately, due to many factors including the refugee problem, global warming-associated longer survival of vectors in nature and expansion of the neighbourhoods to the original habitats of arthropods (4). Therefore, changes in environmental factors, vector-parasite as well as parasite-host interactions may all cause alterations in the epidemiology of leishmaniasis in many regions of the world (1, 4).

Today, it is documented that CL cases are predominantly caused by *Leishmania (L.) tropica* in the Old World and *L. mexicana* in the New World (3, 5). Skin lesions start with a small papule after the bite of a sandfly, which gradually turns into a painless nodule and ulcer overlaid by a large crust. These lesions may shrink in time even without a treatment but leave a remarkable scar tissue (5). It has also been reported that the presence of *Leishmania* virus inside the causative *Leishmania* species may aggravate the clinical manifestation of CL (6). Therefore, it is essential to apply anti-leishmanial therapy on CL lesions over 2 cm. Pentavalent antimonial compounds have long been used as the first-line agents in leishmaniasis treatment; however, there is an emerging resistance against them and their efficacy has declined in many endemic regions, such as India (4, 5). Thus, new drug trials have been conducted in many laboratories around the world to offer new options for leishmaniasis treatment, using both natural and synthetic compounds.

It is estimated that there are almost 250,000-500,000 medicinal plant species in the world, but only 6% of them have had their biological activities evaluated (7). Today, clinical trials and empirical studies on medicinal plants have been conducted in different parts of the world, especially in Asian countries (8-11). Anatolia is rich in medicinal plants, and many of them have been used in traditional medicine for centuries (10). Among them, sumac (*Rhus (R.) coriaria* L.*) has been used traditionally as a spice and a flavouring agent in Anatolia, while it has also been used as a medicine owing to its anti-oxidant, anti-inflammatory, hypoglycemic, hypolipidemic and anti-microbial activities (10-12). In addition to its use as a culinary herb and tanning agent in Mediterranean countries, sumac has also been used for thousands of years as a traditional medicine for the treatment of several diseases, including cancer. Lately, its anti-parasitic activities on *L. major* were demonstrated as well (13). However, more studies are required to test its efficacy on leishmaniasis treatment.

In the present study, the anti-leishmanial efficacies of different extracts and the infusion form of *R. coriaria* were tested *in vitro* against both *L. tropica* and *L. mexicana*, the leading causative agents of CL in the Old and the New World, respectively.

MATERIALS AND METHODS

Leishmania Isolates: The *L. tropica* isolate was initially isolated from a CL patient in Manisa province, stored in liquid nitrogen in the Parasite Bank located in Manisa Celal Bayar University, Faculty of Medicine, and confirmed as *L. tropica* after species-specific polymerase chain reaction (PCR) (MHOM/AZ/1974/SAF-K27). The *L. mexicana* isolate used in the study was initially purchased from ATCC (MNYC/B7/62/M379). Both species were kept at –80°C in Acibadem University's R&D Lab until the day of the trial. A total of 1x10^8/mL of *L. tropica* and *L. mexicana* promastigotes were used during the assessments. Both isolates were removed from the liquid nitrogen tank under appropriate conditions, and after viability control, they were inoculated first in NNN medium and then in RPMI-1640 medium, supplemented with 15% fetal bovine serum (FBS), 1% penicillin-streptomycin (penicillin, 10,000 units/mL-streptomycin, 10 mg/mL) and 0.2% gentamicin (50 mg/mL). Promastigote reproduction was checked on consecutive days and following the detection of a minimum of 10 promastigotes in each microscopic field, the FBS content was dropped to 10% (14). Cultures were kept in an incubator at 25°C.

Plant Material: The fruits of fresh sumac plant samples were collected on the 5th of September 2023, in Kusadasi, a county located 110 km on the south of Izmir province in western Anatolia (Figure 1). The remaining plant samples are kept in the Herbarium of Ege University Faculty of Pharmacy Department of Pharmacognosy in Izmir (Herbarium No: 1672). The fruits were collected and identified by Prof. Dr. Cenk Durmuşkahya. Grinded sumac samples were transferred to the R&D Laboratory of Acibadem University Faculty of Pharmacy for the preparation of the alcohol, water-alcohol, acetone and infusion extracts for the study. Here, the air-dried and powdered fruits of *R. coriaria* (130 g) were macerated with acetone (1500 mL), EtOH (1500 mL), and the mixture of

EtOH:H$_2$O (1:1) (1500 mL) separately at room temperature for 2 days. The filtered extracts were evaporated under reduced pressure and lyophilized to obtain the crude extracts (acetone: 35.31 g, yield 27.1%; EtOH: 33.15 g, yield 25.5%; EtOH:H$_2$O: 19.8 g, yield 19.8%). Moreover, infusion of the *R. coriaria* was also prepared from 2 g of plant material with 100 mL of freshly boiled water, representing the typical quantity consumed by tea drinkers and lyophilized (5 g, yield 25%).
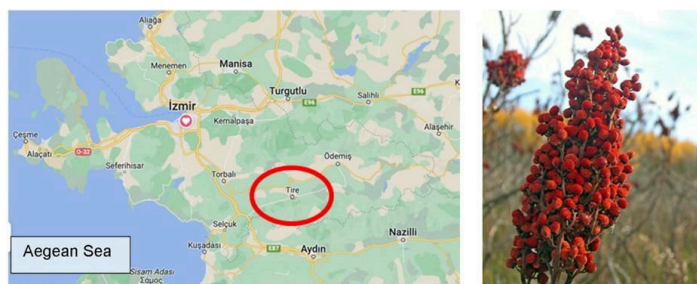
Figure 1. Location of Kusadasi County in western Anatolia where the sumac samples were collected

Application of the *In vitro* Assessments: Following the preparation of *R. coriaria* extracts and both *L. tropica* and *L. mexicana* promastigotes (1x10^8/mL each), they were mixed and incubated at room temperature in different test plates. Assessments were made using the haemocytometer and MTT methods as described at 24 and 48 h, in comparison with meglumine antimoniate as the control drug (concentration range: 300-0.19 µg/mL), the primary choice in leishmaniasis treatment today. All chemicals and references used in the trials were purchased from Sigma Chemical Co. (St. Louis, MO, USA). The dilutions used in the *in vitro* test were calculated according to the amount of *R. coriaria* content in the extracts and were assessed within the range of 18.07 µg/mL and 2312.48 µg/mL, according to the preliminary assessments.

Statistical Analyses

All statistical analyses were performed using IBM SPSS Statistics for Windows, Version 25.0 (IBM Corp., Armonk, NY, USA). The results were assessed by Student's t-test and false discovery rate (FDR) correction was performed during the assessments. Statistical differences identified as p<0.05 were considered significant.

RESULTS

The findings of the assessments are presented in Table 1. For *L. tropica*, the effective concentration ranges of the extracts and the infusion were found to be 578.13-289.06 µg/mL and 289.06-144.53 µg/mL, respectively. For *L. mexicana*, the ranges were found to be 289.06-144.53 µg/mL and 144.53-72.27 µg/mL, respectively. The effective concentration values of the

control agent, meglumine antimoniate, were within the range of 25-12.5 µg/mL for both *L. tropica* and *L. mexicana* strains at the same time points.

Table 1. Activity of *R. coriaria* extracts on *L. tropica* and *L. mexicana* at the 24th and 48th hours

Type of the Sumac Extract	24th Hour (µg/mL)		48th Hour (µg/mL)	
	L. tropica	*L. mexicana*	*L. tropica*	*L. mexicana*
Ethyl Alcohol	578.13	144.53	289.06	72.27
Aqueous Alcohol (1:1)	289.06	144.53	144.53	72.27
Acetone	578.13	144.53	289.06	72.27
Infusion	578.13	289.06	289.06	144.53
Positive control (meglumine antimoniate)	25.0	25.0	12.5	12.5

DISCUSSION

The incidence of CL has been on the rise, not only in the old but also in the new World. This is mainly due to environmental factors such as global warming and human activities such as the global refugee problem and increased housing in rural regions where people are exposed to vectors more often (4). In addition, the causative agents of leishmaniasis, the *Leishmania* species may go hybridized to adapt to these changing environmental conditions in nature, including the change in vectors; this hybridization process may complicate the diagnosis and treatment of leishmaniasis cases as the available diagnostic methods and/or treatment options may become ineffective.

Pentavalent antimonial drugs, developed in the 1940s, are still the primary agents of leishmaniasis treatment in many regions of the world (5). Yet, emerging resistance in leishmaniasis against these antimonial compounds is a potential threat to clinical cases. Indeed, alternative drugs such as amphotericin B and pentamidine, which are preferred mostly for visceral infections, are reported as highly toxic for many patients (3). Therefore, there is an urgent need for new and effective drugs for leishmaniasis treatment.

Natural compounds are the primary sources of research in leishmaniasis treatment studies (8). Almost one of each three approved drugs in the market are natural products or semi-synthetic derivatives, while 30% are currently the synthetic molecules based on natural products or pharmacophores developed from natural compounds (15). It is noteworthy that 65% of the 15 anti-parasitic drugs approved by health authorities between 1981 and 2006 were natural products or their derivatives.

In different cultures and countries, medicinal plants have been used to treat parasitic diseases, including leishmaniasis

(2). Plant derivatives or extracts could provide valuable sources for new medical agents and for anti-leishmanial activity testing, which showed promising results (2, 4). Sumac (*R. coriaria*) is one of these important plant species widely used as a spice and medicinal plant in Turkiye.

R. coriaria belongs to the Anacardiaceae family and is found in the temperate and tropical regions of the world. Today, the increasing awareness of the positive effects of sumac on human health is boosting its consumption (10, 11). Sumac contains various compounds including organic acids, proteins, essential oils, vitamins, and minerals, and it may exert strong anti-microbial and anti-cancer activities in varying degrees through its different extracts (8-10). In addition, *R. coriaria* has anti-oxidant properties, as it is rich in gallic acid and its derivatives, which make it an important substance for the food industry as a natural anti-microbial (5, 10-13).

Despite the presence of many studies in the literature that indicate the anti-bacterial and anti-oxidant properties of *R. coriaria*, the number of studies that show its anti-leishmanial activity is currently limited. In a study conducted by Camacho et al. (2003), methanol extracts obtained from the leaves, bark, and seeds of *R. aucheri* Boiss were reported to be effective against *L. donovani* at concentrations of 55.85 μg/mL, 171 μg/mL, and 141.87 μg/mL, respectively, with high selectivity (SI=2.55) (8). Similarly, a recent study by Ashoori et al. (2020) extensively evaluated the anti-leishmanial and anti-bacterial potential of the hydroalcoholic extract of *R. coriaria* fruits *in vitro*. This study demonstrated a pronounced leishmanicidal effect of the extract, particularly against *L. major* promastigotes and amastigotes, with IC_{50} values of 147 μg/mL and 233 μg/mL, respectively (13). In recent years, nanotechnological approaches have emerged as promising alternatives for treating *Leishmania* infections (16). In this context, the green synthesis of haematite (Fe_2O_3) nanoparticles using *Rhus punjabensis* has been achieved, with the nanoparticles exhibiting free radical scavenging, anti-oxidant, and potent anti-bacterial activities, owing to the binding of functional groups from the plant extract to their surfaces (17).

In the present study, the *in vitro* efficacy of sumac (*R. coriaria*) was investigated against two leading causative agents of the Old World and the New World cutaneous leishmaniasis, *L. tropica* and *L. mexicana*, respectively. It was shown that all extracts of *R. coriaria* were effective against these *Leishmania* species in relatively higher doses, within 144.53 μg/mL and 578.13 μg/mL, compared to meglumine antimoniate (25 μg/mL). An interesting finding was that higher sumac doses were required to eliminate *L. tropica* compared with *L.*

mexicana in this *in vitro* assessment. In other words, *R. coriaria* extracts were totally effective at half doses against *L. mexicana* compared with *L. tropica*. This study showed that the aqueous alcohol extract was effective at lower doses (289.06 μg/mL and 144.53 μg/mL for *L. tropica* and *L. mexicana*, respectively) compared with the other extracts. The fact that this effect continued at 48 h, along with the 24 h mark, was considered important in terms of the continuity and stability of the effect. These findings are particularly encouraging for the potential development of sumac-based treatment options for leishmaniasis. The sustained efficacy of the aqueous alcohol extract makes it a promising candidate for further investigation, potentially leading to more effective and practical treatment options.

In this study, different extracts of sumac (alcohol, aqueous-alcohol, infusion, acetone) were found to be effective against *L. tropica* promastigotes, the primary target of the study, to a degree comparable to the reference drug glucantime. In a further comparison, it was determined that the aqueous-alcohol extract of sumac, which was found to be the most effective, was much more potent against *L. mexicana* than *L. tropica*, eradicating *L. mexicana* promastigotes even when administered at half the dose. It is believed that future studies on the anti-leishmanial effects of sumac may be beneficial not only for the treatment of leishmaniasis in the Old World but also in the New World. The study's findings suggest that sumac-based treatments could hold promise for combating leishmaniasis not only in regions where *L. tropica* is prevalent but also in areas affected by *L. mexicana*. This has significant implications for developing more broadly effective treatments for this global health concern.

In conclusion, the aqueous alcohol extract of sumac was found to be at least as effective as meglumine antimoniate against *L. tropica* promastigotes under *in vitro* conditions. The most important limitation of this study is that the extracts were investigated only under *in vitro* conditions. The next step involves investigating the active compounds within the extract that could serve as potential drug candidates and testing them using *in vivo* models. Obtaining successful results in this stage would strengthen the possibility of a new drug option for this common neglected tropical disease, leishmaniasis.

Y.O., H.B., C.D., A.K., O.K.; Critical Revision of Manuscript – C.D., A.K., O.K.; Final Approval and Accountability – C.D., A.K., O.K.

Author Details

Ergun Mete
[1] Department of Medical Microbiology, Faculty of Medicine, Pamukkale University, Denizli, Turkiye

ⓘ 0000-0002-0854-2440

Yener Ozel
[2] Department of Medical Microbiology, Faculty of Medicine, Balikesir University, Balikesir, Turkiye

ⓘ 0000-0001-6618-8251   ✉ yener_ozel@hotmail.com

Hilal Bardakci
[3] Department of Pharmacognosy, Faculty of Pharmacy, Fenerbahce University, Istanbul, Turkiye

ⓘ 0000-0001-8799-6565

Cenk Durmuskahya
[4] Department of Forest Engineering, Faculty of Forestry, Izmir Kâtip Celebi University, Izmir, Turkiye

ⓘ 0000-0002-8092-9770

Aylin Koseler
[5] Department of Biophysics, Faculty of Medicine, Pamukkale University, Denizli, Turkiye

ⓘ 0000-0003-4832-0436

Ozgur Kurt
[6] Department of Medical Microbiology, School of Medicine, Acibadem University, Istanbul, Turkiye

ⓘ 0000-0001-5575-588X

REFERENCES

1. Özbilgin A, Gencoglan G, Tunali V, Çavus I, Yıldırım A, Gündüz C et al. Refugees at the crossroads of continents: A molecular approach for cutaneous leishmaniasis among refugees in Turkey. Acta Parasitol 2020; 65(1): 136–43.

2. Saki J, Biranvand E, Arjmand R. The in vitro anti-Leishmania effect of *Zingiber officinale* extract on promastigotes and amastigotes of *Leishmania major* and *Leishmania tropica*. Turkiye Parazitol Derg 2022; 46(2): 91-6.

3. Özbilgin A, Töz S, Harman M, Günaştı Topal S, Uzun S, Okudan F et al. The current clinical and geographical situation of cutaneous leishmaniasis based on species identification in Turkey. Acta trop 2019; 190: 59–67.

4. Kurt Ö, Özbilgin A, Petersen E, Ergönül Ö. An update on the imported cutaneous Leishmaniasis in Europe. Infect Dis Clin Microbiol 2023; 5(1): 59-62.

5. Aronson NE, Copeland NK, Magill AJ. Leishmania Species: Visceral (Kala-Azar), Cutaneous, and Mucosal Leishmaniasis. Mandell GL, Bennette JE, Dolin R, editors. Madell, Douglas, and Bennett's Principles and Practice of Infectious Diseases. Elsevier; 2020. p.3321-39.

6. Kurt Ö, Mansur N, Çavuş İ, Özcan O, Batir MB, Gündüz C et al. First report and *in silico* analysis of *Leishmania* virus (LRV2) identified in an autochthonous Leishmania major isolate in Turkey. New Microbiol 2019; 42(1): 64-7.

7. Gurib-Fakim A. Medicinal plants: traditions of yesterday and drugs of tomorrow. Mol Aspects Med 2006; 27(1): 1-93.

8. Camacho MDR, Phillipson JD, Croft SL, Solis PN, Marshall SJ, Ghazanfar SA. Screening of plant extracts for antiprotozoal and cytotoxic activities. J Ethnopharmacol 2003; 89(2-3): 185-91.

9. Soosaraei M, Fakhar M, Hosseini Teshnizi S, Ziaei Hezarjaribi H, Banimostafavi ES. Medicinal plants with promising antileishmanial activity in Iran: a systematic review and meta-analysis. Ann Med Surg (Lond) 2017; 21: 63-80.

10. Karadaş Ö, Yılmaz İ, Geçgel U. Sumak (*Rhus coriaria* L.) meyvesinin fizikokimyasal ozellikleri. TUJES, 2020; 21(2): 87-94.

11. Alsamri H, Athamneh K, Pintus G, Eid AH, Iratni R. Pharmacological and antioxidant activities of *Rhus coriaria* L. (Sumac). Antioxidants (Basel) 2021; 10(1): 73.

12. Sakhr K, El Khatib S. Physiochemical properties and medicinal, nutritional and industrial applications of Lebanese Sumac (Syrian Sumac - *Rhus coriaria*): A review. Heliyon 2020; 6(1): e03207.

13. Ashoori F, Fakhar M, Goli HR, Mirzaee F, Faridnia R, Kalani H, et al. Antileishmanial and antibacterial activities of the hydroalcoholic extract of *Rhus coriaria* L. Ann Parasitol 2020; 62(2): 157-63.

14. Bhattacharya J, Chandra G, Hati AK. A simple method for cryopreservation of Leishmania donovani promastigotes. Indian J Med Res 1991; 93: 245-6.

15. Calixto JB. The role of natural products in modern drug discovery. An Acad Bras Cienc 2019; 91: e20190105

16. Özel Y, Çavuş İ, Yilmaz U, Tokay F, Bağdat S, Özbilgin A, Ünlü M, Vardar Ünlü G. Hibrit gümüş nanoparçacik komplekslerinin sitotoksik ve antilayşmanyal aktivitesinin araştirilmasi: Leishmania türlerine karşi potansiyel ilaç adayları [Investigation of cytotoxic and antileishmanial activity of hybrid silver nanoparticle complexes: potential drug candidates against leishmania species]. Mikrobiyol Bul. 2024; 58(2): 182-95.

17. Naz S, Islam M, Siddiqa A, Rasheed R, Sadaf S, Zia M. Phytomediated synthesis of hematite nanoparticles from Rhus punjabensis extract: Characterization and biomedical potential. J Mol Struct 2019; 1185: 1–7.

Experimed

Research Article

Open Access

Application and Clinical Results of Minimally Invasive Surgery in Patients with Uterine Fibroids: A Single-Centre Study in Azerbaijan

Akbar Ibrahimov [1] ✉, Fidan Novruzova [1], Abuzar Gaziyev [1], Aygun Hasanova [1], Mushviq Hasanov [1]

[1] Azerbaijan Medical University, Baku, Azerbaijan

Abstract

Objective: This single-centre retrospective study aimed to evaluate the efficacy, safety, and clinical outcomes of laparoscopic myomectomy laparoscopic myomectomy (LM) for uterine fibroids in a resource-limited clinical setting.

Materials and Methods: The medical records of 406 patients with uterine leiomyomas who underwent laparoscopic myomectomy between 2019 and 2024 were analyzed. Data included myoma characteristics (localization, number, and size), intraoperative parameters, complications, and postoperative outcomes (symptom resolution and fertility rates).

Results: Among the 406 procedures, most patients were nulliparous (81.8%) and presented with abnormal uterine bleeding (69.7%). The mean diameter of the largest fibroid was 6.2 ± 2.1 cm, with a range of 3–10 cm, with solitary fibroids in 62.3% of cases. Subserosal (48.1%) and intramural (41.4%) localizations were the most common. Intraoperative blood loss was <100 mL in 52.5% of the cases. Laparoscopic resection was successfully completed in 394 cases (97.0%), while 12 cases (3.0%) required conversion to laparotomy due to dense adhesions, intraoperative hemorrhage, or technical limitations. At the 12-month follow-up, symptom resolution rates were 92.1% for bleeding, 88.6% for pelvic pressure, and 76.9% for infertility, with 33.3% of fertility-seeking patients achieving pregnancy.

Conclusion: Laparoscopic myomectomy demonstrated safety and efficacy as a primary treatment for uterine fibroids in resource-limited settings, with high symptom resolution and favorable fertility outcomes. This minimally invasive approach should be prioritized where surgical expertise is available, even in low-equipment environments.

Keywords Minimally invasive surgery · Uterine fibroids · Laparoscopic myomectomy · Fertility preservation · Resource-limited settings

✉ Corresponding author: Akbar Ibrahimov dr.akbaribrahimov3@gmail.com

INTRODUCTION

Leiomyomas are the predominant benign tumors found in the uterus in women worldwide (1). Most cases are asymptomatic and do not require surgical intervention (2). However, in some instances, these fibroids may cause clinical complications such as irregular uterine bleeding, pelvic discomfort, infertility, or pregnancy loss (3). For symptomatic individuals seeking to preserve fertility, myomectomy has emerged as a preferred surgical intervention over hysterectomy (4). Increasing patient awareness of aesthetic outcomes and minimally traumatic procedures have further encouraged minimally invasive surgical (MIS) techniques when an operation is indicated (5, 6).

The current literature has demonstrated the practicability, security, and aesthetic advantages of laparoscopic myomectomy (7). Nonetheless, laparoscopic myomectomy is a technically challenging treatment marked by a steep learning curve and the risk of significant complications, as indicated in studies (8). The mini-laparotomy approach has been implemented as a minimally invasive alternative to laparoscopic myomectomy to tackle these issues (9). However, clinical studies have shown that the mini-laparotomy technique does not provide equivalent benefits regarding decreased hospital stay, expedited postoperative recovery, or enhanced aesthetic results (10).

The approaches for myomas comprise expectant management, pharmacological agents, hysteroscopic myomectomy, abdominal or laparoscopic myomectomy, laparoscopic hysterectomy, UAE, and focused ultrasound (11). In many low-income countries, the implementation of minimally invasive laparoscopic procedures remains limited due to financial limitations and a lack of surgeons with specialized training in advanced laparoscopic techniques (12, 13). However, access to focused ultrasound and medical therapies, such as GnRH agonists or selective progesterone receptor modulators, is restricted for most patients due to expensiveness and limited availability. Consequently, open abdominal surgeries—particularly abdominal myomectomy—remain the primary treatment modality, with hysterectomy also continuing to be clinically useful in specific cases. This trend reflects the general systemic issues in healthcare infrastructure and resource allocation within low-income nations.

The purpose of this research was to demonstrate the efficacy of laparoscopic myomectomy in the surgical management of uterine fibroids in patients who suffer from severe symptoms in a resource-limited clinical setting.

MATERIALS AND METHODS

This investigation constitutes a retrospective, single-centre scientific study analyzing clinical data from 406 patients diagnosed with uterine leiomyomas who underwent laparoscopic myomectomy procedures between 2019 and 2024. The research was approved by the Ethics Committee of the Azerbaijan Medical University. The research was conducted in the Oncology Department of Azerbaijan Medical University, a tertiary care facility located in Baku, Azerbaijan, utilizing hospital records gathered over a 5-year observational period to evaluate surgical management patterns and patient characteristics. Preoperative assessment included transvaginal ultrasound and MRI to document the number, size (maximum diameter), and location (subserosal, intramural, submucosal) of the fibroids. Inclusion criteria for laparoscopic resection were fibroid size ≤10 cm (single) or ≤6 cm (multiple, up to 5 fibroids) and non-cervical location. Patients with fibroids >10 cm, diffuse uterine involvement (>5 fibroids), or suspected malignancy were excluded. Laparoscopic myomectomy was performed under general anesthesia using a four-port technique (one 10-mm umbilical port, two 5-mm lateral ports, and one 5-mm suprapubic port). After establishing the pneumoperitoneum (12 mmHg), the fibroid(s) were localized. The HOHL uterine manipulator with an atraumatic tip was used in all cases included in this study. After the establishment of the pneumoperitoneum, the fibroid was identified, and bilateral uterine artery clipping was performed to minimize bleeding. The serosa and pseudocapsule were incised using monopolar energy, followed by enucleation with blunt and sharp dissection, followed by layered suturing of the myometrial defect with absorbable vicryl sutures. Hemostasis was confirmed, uterine artery clips were extracted, and the pelvis was irrigated before closure.

A systematic clinical chart was created and used to collect data from the hospital medical records database. The data consisted of socio-demographic variables, clinical parameters, length of hospitalization, and types of surgical procedures performed. Comprehensive details on the operating procedures are documented in the operating theatre register.

Statistical Analyses

Data were inputted and analyzed using the Statistical Package for the Social Sciences (SPSS) IBM version 25.0 (Armonk, NY, USA). Frequencies and percentages were computed for the category variables. The p-value was accepted as lower than 0.05 as significant.

Table 1. Demographic characteristics of the participants

Criteria	(n)	(%)
Age		
<30	26	6.4
30-35	151	37.2
36-40	140	34.5
>40	89	21.9
Pregnancy status		
0	332	81.8
1	55	13.6
2	16	3.9
>2	3	0.7
Family status		
Married	211	52.0
Unmarried	195	48.0

Table 2. Clinical presentation of the participants

Symptoms	(n)	(%)
Abnormal uterine bleeding	283	69.7
Pelvic mass	80	19.7
Infertility	33	8.1
Pressure	10	2.5

Table 3. Length of the symptomatic period

Duration (month)	(n)	(%)
<12	38	9.4
12-36	284	70
48-72	72	17.7
>72	12	2.9

RESULTS

A total of 406 laparoscopic myomectomy were performed during the study period. Table 1 presents the demographic characteristics of the participants. The participants had a mean age of 36.0 ± 5.0 years, aged 25 to 50 years. The parity range ranged from 0 to 3. Approximately 52% were married, and 291 individuals (71.7%) were aged between 30 and 40 years, with the 30-35 year age group (37.7%) slightly surpassing the 36-40 year age group (34.5%). most women were nulliparous (81.8%). Abnormal uterine bleeding (69.7%) was the predominant presenting symptom, with most symptoms (70%) persisting for 1-3 years before presentation. These are illustrated in Table 2 and Table 3, respectively. In most cases, 213 (52.5%) experienced a blood loss of less than 100 mL during the procedures. Localization, number, and diameter of the myomas are illustrated in Table 4.

Table 4. Characteristics of myomas

Criteria	(n)	(%)
Localization		
Subserosal	253	62.3
Intramural	117	28.8
Submucosal	36	8.9
Number of myomas		
1-3	301	74.1
≥4	105	25.9
Diameter of the myoma (cm)		
<5	142	35.0
5-8	218	53.7
>8	46	11.3

Localization

Subserosal fibroids accounted for 62.3% (n=253), intramural for 28.8% (n=117), and submucosal for 8.9% (n=36). Number of myomas: the majority of patients (74.1%, n=301) had 1–3 fibroids, while 25.9% (n=105) had ≥4 fibroids.

Diameter

The mean diameter of the largest fibroid was 6.2 ± 2.1 cm, with a range of 3–10 cm. Laparoscopic resection was successfully completed in 394 cases (97.0%), while 12 cases (3.0%) required conversion to laparotomy due to dense adhesions, intraoperative hemorrhage, or technical limitations.

Intraoperative complications occurred in 12 patients (3.0%), including intraoperative hemorrhage (n=5, 1.2%), conversion to laparotomy due to dense adhesions (n=4, 1.0%), and technical limitations (n=3, 0.7%) (Table 5). Morcellation was not performed intra-abdominally, so posterior colpotomy was performed to extract the fibroids. The posterior colpotomy approach for fibroid extraction demonstrated excellent healing outcomes with minimal scarring, no large abdominal incisions, and faster recovery times compared with traditional extraction methods. This technique proved to be an optimal choice for tissue removal, contributing to the overall success of the minimally invasive approach and patient satisfaction with the cosmetic outcomes.

Postoperative complications included febrile morbidity (n=9, 2.2%), wound infection (n=6, 1.5%), and re-laparoscopy for hematoma evacuation (n=2, 0.5%). If we look at the complication rates with prior studies, our conversion rate (1.0%) aligns with the <2% reported in high-income settings. Follow-up data at 12 months postoperatively demonstrated the resolution of abnormal uterine bleeding in 91.2% (258/283) of patients and the resolution of pelvic pressure in 90% (9/10) (Table 6). Among infertile patients (n=33), 21 (63.6%) achieved

Table 5. Intraoperative blood loss during laparoscopic myomectomy

Blood loss (mL)	(n)	(%)
<100	213	52.5
100–200	142	35.0
>200	51	12.5

Table 6. Postoperative outcomes at 12 months

Outcome	(n)	(%)
Resolution of the abnormal uterine bleeding	258	91.2
Resolution of the pelvic mass	72	90.0
Resolution of the pelvic pain	9	90.0
Pregnancy rate (infertility)	21	63.6
Regular menstruation	267	94.3

Table 7. Comparative outcomes of myomectomy techniques

Parameter	Laparoscopic (n=406)	Abdominal (n=200)	Mini-Laparotomy (n=100)	p value
Operative time (min)	85 ± 20	120 ± 30	90 ± 25	<0.01
Blood loss (mL)	98 ± 45	250 ± 80	150 ± 60	<0.001
Postop pain (VAS)	3.2 ± 1.1	5.8 ± 1.5	4.5 ± 1.3	<0.001
Hospital stay (days)	1.5 ± 0.7	3.5 ± 1.2	2.0 ± 0.9	<0.001
Recurrence rate (%)	8.1	12.5	10.0	0.15

pregnancy within 2 years post-surgery. Regular menstruation was restored in 94.3% (267/283) of the patients with preoperative menstrual irregularities. Comparative analysis revealed significantly shorter operative times (p<0.01) and reduced blood loss (p<0.001) in the laparoscopic myomectomy compared with the abdominal approach (Table 7).

DISCUSSION

According to current evidence, laparoscopic myomectomy provides a fertility-preserving option compared with hysterectomy while effectively decreasing the symptoms related to leiomyomas (14). While traditional laparotomy is the standard surgical procedure for myomectomy, innovations in minimally invasive methods have created modified approaches. The techniques include mini-laparotomy (skin incisions of 4–8 cm), ultra-mini-laparotomy (incisions ≤4 cm), laparoscopy, laparoscopically assisted laparotomy, natural orifice laparoscopy, and single-port laparoscopically assisted

transumbilical ultra-mini-laparotomy (15). The results of this study highlight the benefits of laparoscopic myomectomy compared with conventional laparotomy in the management of uterine leiomyomas. Although this study did not assess long-term recurrence rates due to its retrospective design and limited follow-up period, the perioperative benefits of laparoscopic myomectomy—such as reduced blood loss, shorter hospital stays, and improved aesthetic outcomes —align with global trends favoring MIS procedures. The study exhibited a shortened operational length, reduced intraoperative blood loss, decreased postoperative pain, accelerated recovery, improved aesthetic outcomes and decreased recurrence rates. In conclusion, MIS procedures, as demonstrated in this study, constitute a sustainable and successful alternative to traditional laparotomy for the management of symptomatic leiomyomas in reproductive-aged cases. Our findings demonstrate that laparoscopic myomectomy is achievable in low-equipment clinics despite infrastructural challenges. Although limited access to advanced equipment (e.g., morcellator bags, ligasure) necessitated manual tissue extraction, this did not compromise safety. Operative times (mean: 95±25 min) reflected standardized techniques.

This study's limitations include its retrospective design and exclusion of larger/complex fibroids. Nevertheless, our criteria reflect the pragmatic triaging in equipment-limited clinics, where prioritizing cases with higher technical success rates optimizes outcomes. Future studies should explore the cost-effectiveness and long-term fertility outcomes.

All surgical strategies must be arranged for the individual, considering the patient's fertility desire. Laparoscopic myomectomy should be a standard surgical procedure in low-income nations, hence requiring all gynaecologists to train in minimally invasive techniques to address the increasing patient population. Moreover, it is recommended that all obstetricians and gynaecologists acquire knowledge of recent breakthroughs in minimally invasive surgery. An awareness programme should be implemented to educate women about the minimally invasive methods and the possibility of preserving fertility in low-equipment clinics.

CONCLUSION

Laparoscopic myomectomy demonstrated high efficacy in symptom resolution (91.2% for abnormal bleeding, 63.6% pregnancy rate) with an acceptable complication profile (7.2% overall), supporting its role as a primary option for uterine fibroids in low-resource settings. Our study indicates that laparoscopic myomectomy is a safe and effective option for managing uterine myomas, with advantages such as

reduced intraoperative blood loss, shorter operative time, and faster recovery. MIS should be promoted for uterine fibroid treatment in low-equipment clinics. Laparoscopic myomectomy is a safe and effective option for symptomatic uterine fibroids in low-equipment clinics when performed by trained surgeons within defined size/number parameters. Our results emphasize the importance of context-specific protocols and investment in laparoscopic training and equipment to expand access. While challenges such as equipment costs persist, strategic prioritization of cases and skill development can mitigate barriers, offering patients a minimally invasive alternative to traditional laparotomy. Healthcare institutions in similar clinics should prioritize MIS training programmes to address systemic gaps in surgical care.

Consequently, laparoscopic myomectomy appears to be a reasonable primary option for the management of uterine myomas because it is a safe and well-established technique, mainly when appropriate equipment or a skilled operator is available.

Author Details

Akbar Ibrahimov
[1] Azerbaijan Medical University, Baku, Azerbaijan

0009-0007-8780-6400   dr.akbaribrahimov3@gmail.com

Fidan Novruzova
[1] Azerbaijan Medical University, Baku, Azerbaijan

0009-0005-3970-451X

Abuzar Gaziyev
[1] Azerbaijan Medical University, Baku, Azerbaijan

0009-0008-5755-2021

Aygun Hasanova
[1] Azerbaijan Medical University, Baku, Azerbaijan

0009-0009-5162-5143

Mushviq Hasanov
[1] Azerbaijan Medical University, Baku, Azerbaijan

0000-0003-4213-6769

REFERENCES

1. Yang Q, Ciebiera M, Bariani MV, Ali M, Elkafas H, Boyer TG, et al. Comprehensive review of uterine fibroids: developmental origin, pathogenesis, and treatment. Endocr Rev 2022; 43(4): 678-719.

2. Stewart EA, Nowak RA. Uterine fibroids: hiding in plain sight. Physiology (Bethesda) 2022; 37(1): 16-27.

3. Sundermann AC, Velez Edwards DR, Bray MJ, Jones SH, Latham SM, Hartmann KE. Leiomyomas in pregnancy and spontaneous abortion: a systematic review and meta-analysis. Obstet Gynecol 2017; 130(5): 1065-72.

4. Li YT, Yeh CC, Chao HT, Wang PH. Preservation of the uterus. Taiwan J Obstet Gynecol 2015; 54(6): 799-800.

5. Fonseca MCM, Castro R, Machado M, Conte T, Girao M. Uterine artery embolization and surgical methods for the treatment of symptomatic uterine leiomyomas: a systemic review and meta-analysis followed by indirect treatment comparison. Clin Ther 2017; 39(7): 1438-55.e2.

6. Havryliuk Y, Setton R, Carlow JJ, Shaktman BD. Symptomatic fibroid management: systematic review of the literature. JSLS 2017; 21(3): e2017.00041.

7. Huang HY, Liu YC, Li YC, Kuo HH, Wang CJ. Comparison of three different hemostatic devices in laparoscopic myomectomy. J Chin Med Assoc 2018; 81(2): 178-82.

8. Li YT, Chang WH, Wang PH. Laparoscopy-aided myomectomy. J Obstet Gynaecol Res 2010; 36(4): 922.

9. Wen KC, Chen YJ, Sung PL, Wang PH. Comparing uterine fibroids treated by myomectomy through traditional laparotomy and 2 modified approaches: ultraminilaparotomy and laparoscopically assisted ultraminilaparotomy. Am J Obstet Gynecol 2010; 202(2): 144.e1-8.

10. Shin DG, Yoo HJ, Lee YA, Kwon IS, Lee KH. Recurrence factors and reproductive outcomes of laparoscopic myomectomy and minilaparotomic myomectomy for uterine leiomyomas. Obstet Gynecol Sci 2017; 60(2): 193-9.

11. Donnez J, Dolmans MM. Uterine fibroid management: from the present to the future. Hum Reprod Update 2016; 22(6): 665-86.

12. Ibrahimov AM, Gaziyev AYU. Surgical and oncological outcomes in women with endometrial cancer treated via minimally invasive surgery – a single-center study in low-income country. World Med Biol 2024; 3(89): 66-70.

13. Ibrahimov A. Application and clinical results of minimally invasive surgery based on pathohistological criteria in uterine cancer: A single center study in a low-income country. Actual Gyn 2024; 16: 70-4.

14. Cezar C, Becker S, di Spiezio Sardo A, Herrmann A, Larbig A, Tanos V, et al. Laparoscopy or laparotomy as the way of entrance in myoma enucleation. Arch Gynecol Obstet 2017; 296(4): 709-20.

15. Baekelandt J. Transvaginal natural-orifice transluminal endoscopic surgery: a new approach to myomectomy. Fertil Steril 2018; 109(1): 179.

Experimed

Research Article

Evaluation of Electroencephalography Signals in Alzheimer's Disease Using Coherence Analysis and Persistent Homology
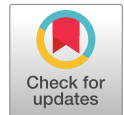
Mustafa Bayrak [1,2] 🆔 ✉, Omer Bahadir Eryilmaz [3] 🆔 , Cihan Katar [4,5] 🆔 , Atilla Uslu [2] 🆔

[1] Institute of Graduate Studies in Health Sciences, Istanbul University, Istanbul, Türkiye
[2] Department of Physiology, Istanbul Faculty of Medicine, Istanbul University, Istanbul, Türkiye
[3] School of Computer Science, University of Birmingham, Birmingham, UK
[4] Department of Electrical Electronics Engineering, Faculty of Engineering, Turkish-German University, Istanbul, Türkiye
[5] Department of Electronics and Communication Engineering, Faculty of Electrical and Electronics Engineering, Istanbul Technical University, Istanbul, Türkiye

Abstract

Objective: This study aimed to use a new approach, namely persistent homology, to analyse electroencephalogram (EEG) coherence and identify the alterations in brain connectivity in patients with Alzheimer's disease (AD).

Materials and Methods: We applied persistent homology to the distance maps that we created using the EEG coherence values from five different frequency bands in order to determine if there are disruptions specific to these bands in patients diagnosed with AD.

Results: Our findings revealed that the features extracted using persistent homology were significantly different in two bands (delta and theta) between AD patients and subjects in the healthy control (HC) group. Furthermore, the machine learning algorithms using these topological features achieved accurate classification results. This suggests that persistent homology may be a useful adjunct in the diagnosis of AD.

Conclusion: We have demonstrated the potential of persistent homology in identifying AD-related changes in brain connectivity, which are the most clearly present in the theta and delta bands. Larger datasets should be used in future research to determine the clinical relevancy of this method.

Keywords   Alzheimer's disease · EEG · Coherence · Persistent homology

INTRODUCTION

Dementia has become one of the leading causes of death in recent years, and with a rapidly ageing global population, its prevalence is expected to rise (1). Alzheimer's disease (AD) accounts for the majority of dementia cases and it is characterised by progressive memory loss (2).

Memory impairment is usually the first symptom of AD and it typically begins after the age of 65 years. Disease progression is accompanied by executive dysfunction, impairment in judgement, loss of insight, visuospatial problems, language deficits and other neurological and psychiatric symptoms (3). Currently, no cure is available for AD, but there are treatment options intended to mitigate certain symptoms of the disease.

Histopathological examination is required to establish a definitive diagnosis of AD, but it is usually not used in clinical practice (4). Clinicians generally use neuropsychological tests, neuroimaging techniques, and molecular biomarkers when diagnosing patients with AD. Although it is not used in the routine evaluation, several studies suggest that electroencephalogram (EEG) might add confidence to the diagnosis and, as a non-invasive and relatively cheap technique, it could prove to be a valuable tool in discovering potential biomarkers for the disease (5, 6).

Because the visual assessment of EEG signals is somewhat subjective, various quantitative analyzing techniques have been used to evaluate the EEG data to help with the diagnosis of neurological disorders including AD (7-10). The analysis of quantitative EEG in Alzheimer's disease typically involves the extraction of features such as absolute power, relative power, coherence, sample entropy, and Lempel-Ziv complexity using signal processing techniques including the fast fourier transform (FFT), Welch's method, coherence analysis, and wavelet transform. These features are subsequently used in classification tasks employing traditional machine learning algorithms, such as support vector machine (SVM), random forest (RF), and k-nearest neighbours (kNN)- as well as advanced deep learning approaches, including convolutional neural networks (CNN), recurrent neural networks (RNN), and autoencoders (11). A consistent finding in numerous quantitative EEG studies is an increase in the slow frequency band (delta and theta) power, a decrease in the fast frequency band (alpha and beta) power and a reduction in the alpha band coherence in AD. (10, 12, 13). These findings were shown to be correlated with the disease severity (14), Mini-Mental State Examination (MMSE) scores (15), and different cognitive functions (16).

Functional connectivity analysis is one of the most commonly used quantitative EEG analysis methods. It measures

Table 1. A comparison of the traditional coherence analysis and topological data analysis

Traditional Coherence Analysis	Topological Data Analysis
Based on Fourier transforms, spectral analysis, and correlation	Based on the algebraic topology and computational geometry
Limited to pairwise, linear interactions	Captures non-linear, higher-order structures and multiscale patterns in the data
Requires a fixed or manually chosen threshold	No need for an arbitrarily chosen threshold
Gives coherence values ranging from 0 to 1 between the channel pairs	Provides persistence diagrams showing the birth and death of topological features
Easy to interpret	Interpretation requires training

coherence, which indicates the level of correlation between two signals in the frequency domain, providing insights into their functional connectivity (17). While traditional coherence analysis examines the pairwise relationships between electrodes, topological data analysis (TDA) enables the investigation of relationships beyond simple pairwise interactions, extending to structures such as triangles, tetrahedra, and higher-dimensional formations (18). A comparison of the two methods is shown in Table 1. One of the principal methods of TDA is persistent homology. It examines the evolution of the topological features across multiple scales (18). It extends classical homology by not only identifying the presence of features such as connected components, loops, and voids but also quantifying their persistence across different levels of detail. This makes persistent homology particularly effective for understanding the structure of data embedded in high-dimensional spaces.

TDA has been used to extract topological features from EEG signals for various clinical applications such as detection of delirium (19), attention deficit hyperactivity disorder (ADHD) classification (20), identification of EEG characteristics in children with sleep apnoea (21), and discrimination of epileptic from the non-epileptic EEG signals (22). In recent years, it has been suggested that TDA, especially persistent homology, may prove to be useful in the diagnosis of AD (23). In our study, we used persistent homology with a coherence-derived distance metric to compute H_1 persistence to differentiate between the AD and HC groups. Given that AD is often associated with reduced coherence in certain frequency bands and brain regions, using a tool from TDA, we were able to evaluate the functional connectivity without being limited to pairwise interactions and arbitrarily determined thresholds, as is often the case with the traditional coherence-based methods. Choosing persistent homology over traditional coherence in our analysis allowed us to represent high-dimensional EEG data with compact

yet informative topological features that we then used for classification. The features extracted via persistent homology, which exhibited notable differences in the slower brain waves, were subsequently employed as input to various machine learning algorithms. These algorithms achieved accurate classification results, demonstrating the effectiveness of the topological features in distinguishing between the AD and HC groups.

MATERIALS AND METHODS

Dataset

We used the dataset provided by Miltiadous et al. (24). There were eyes-closed resting-state EEG recordings of 65 participants in this dataset. The demographic and clinical features of the participants are presented in Table 2.

The duration of each recording was approximately 13.5 min for the AD group (min=5.1, max=21.3) and 13.8 min for the HC group (min=12.5, max=16.5) and the total duration of the recordings was 485.5 min for the AD group and 402 min for the HC group.

The EEG signals recorded from the 19 channels were pre-processed following the steps described in Miltiadous et al. (24). The first step of the pre-processing was re-referencing the signals to the average of A1-A2. Subsequently, a Butterworth band-pass filter (0.5–45 Hz) was applied to achieve noise reduction. The ASR routine was then used for automatic artefact rejection. Independent component analysis (ICA) decomposed the signals into 19 components, with the eye and jaw artefacts automatically removed. The baseline correction was applied to reduce the high-frequency artefacts as the last step. We used these pre-processed EEG data in our analysis.

Coherence Analysis

As the first step in the coherence analysis, FFT was used to transform the signals into the frequency domain, and subsequently these signals were divided into five widely studied frequency bands: Delta (1–4 Hz), Theta (4–8 Hz), Alpha (8–12 Hz), Beta (12–25 Hz), and Gamma (25–45 Hz) bands. Coherence, more specifically, magnitude-squared coherence,

was computed for each frequency band according to the following formula:

$$C_{xy}(f) = \frac{|P_{xy}(f)|^2}{P_{xx}(f)P_{yy}(f)} \tag{1}$$

where $C_{xy}(f)$ is the coherence value between the x and y signals at an f frequency, $P_{xy}(f)$ is the cross-spectrum, which represents the shared power between x and y at an f frequency, $P_{xx}(f)$ is the power spectrum density for the x signal, and $P_{yy}(f)$ is the power spectrum density for the y signal.

The coherence values range between 0 and 1. The closer a value is to 1, stronger the synchronisation is, which means that the two signals are associated with the same functional activity. In contrast, values near 0 imply the absence of functional connectivity between the corresponding brain regions. For this analysis, coherence was evaluated in the sensor space, reflecting functional connectivity patterns based on the spatial arrangement of the EEG electrodes.

The EEG signals were first epoched into 2-s windows with 50% (1-s) overlap, following a standard segmentation strategy for the time-frequency analysis. Within each epoch, the magnitude-squared coherence between the electrode pairs was estimated using the Welch method with a Hann window of 2 s. All recordings exceeded 5 min in length, ensuring sufficient overlapping segments for stable coherence estimation across participants.

The computed coherence values were then used to construct distance maps, where the distance between two electrodes was defined as follows:

$$Distance = 1 - Coherence \tag{2}$$

These distance maps are used as inputs for persistent homology, which will be explained in the following subsection, to characterise EEG channel interactions across each frequency band at varying scales.

Persistent Homology

Persistent homology was applied to the distance maps obtained from the coherence analysis, capturing higher-order connectivity patterns beyond the pairwise relationships between the EEG channels. These maps represent the functional connectivity, where each value indicates the relationship between the electrode pairs.

To analyse the topology of the distance maps, a mathematical structure called a simplicial complex was constructed. Simplicial complexes are composed of basic building blocks known as simplices (e.g., vertices, edges, triangles, and higher-dimensional analogs). The most widely used method for constructing simplicial complexes from point clouds is the Vietoris-Rips filtration, which operates as follows:

Table 2. Demographic and clinical features of the participants

	AD Group	HC Group
Number of individuals	36	29
Age, year, mean ± SD	66.4 ± 7.9	67.9 ± 5.4
Gender (Male/Female)	12/24	18/11
MMSE score, mean ± SD	17.75 ± 4.5	30.0 ± 0.0

AD: Alzheimer's disease, HC: Healthy control, MMSE: Mini Mental State Examination, SD: Standard deviation.
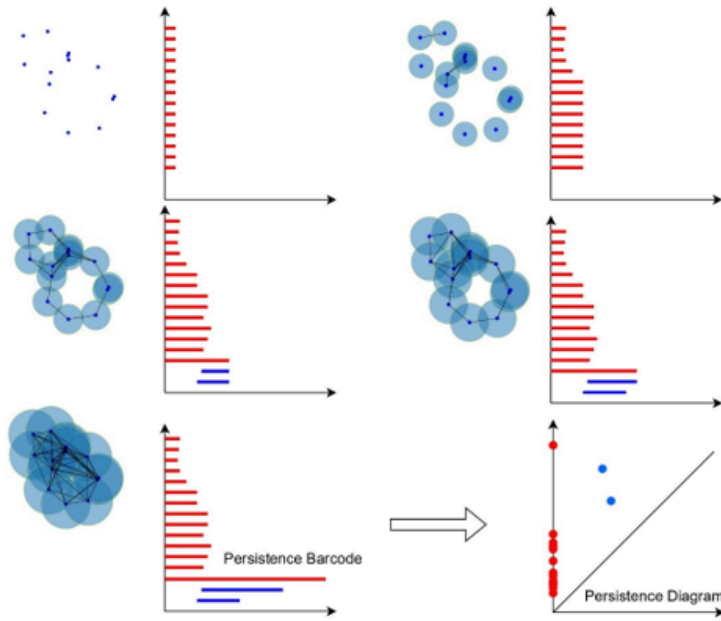
Figure 1. Persistent homology on a 2D point cloud

- Points are connected by edges if their pairwise distance is within a threshold a (the scale parameter).
- Higher-dimensional simplices, such as triangles and tetrahedra, are added based on the connections of the lower-dimensional simplices.

Increases in the scale parameter a are accompanied by the addition of new simplices to the complex, resulting in a nested sequence of simplicial complexes ($S_{a1} \subseteq S_{a2}$ for $a_1 < a_2$). Persistent homology captures the appearance of topological features (e.g., connected components, loops) at specific scales, referred to as their "birth," and their disappearance at another scale, termed "death." The persistence of a feature is defined as the difference between its death and birth scales, representing its lifespan across varying resolutions.

These topological features are categorised based on their dimension: H_0 (zero-dimensional homology) represents connected components, H_1 (one-dimensional homology) stands for loops or holes, and H_2 (two-dimensional homology) captures enclosed voids. This pattern extends to higher dimensions, where H_n describes the n-dimensional cavities within the data.

Features with high persistence are interpreted as robust and meaningful structures in the data, whereas those with low persistence are often attributed to noise or sampling artefacts. This process is illustrated in Figure 1, which shows a sequence of the Vietoris–Rips complexes constructed at increasing scale values. As the scale increases, topological features such as connected components and loops emerge,

merge, or vanish. These changes are visualised using barcode diagrams, where red bars represent H_0 features and blue bars represent H_1 features. The corresponding persistence diagram summarises all features by plotting their birth and death scales. Features that persist over a wide range of scales appear farther from the diagonal and are considered topologically significant.

Wasserstein Distance

The Wasserstein distance is a metric that quantifies the cost of transforming one distribution into another. If the two distributions are similar, the cost will be lower. Therefore, it is a widely used metric for comparing persistence diagrams.

Given the two distributions P and Q, the Wasserstein distance is defined as

$$W(P,Q) = \inf_{\gamma \in \Gamma(P,Q)} \sum_{(p,q) \in \gamma} |p - q|_p, \qquad (3)$$

where:

- (P, Q): The set of all possible matchings between points in the persistence diagrams P and Q, including points matched to the diagonal.

  p: The p-norm distance between points p ∈ P and q ∈ Q.

In this study, we chose $p=2$, where the distance metric simplifies to the Euclidean distance. If p is set to ∞, the distance corresponds to the *bottleneck distance*, which captures the maximum difference between the matched points. The flexibility in choosing p allows for different

interpretations of the similarity between the persistence diagrams.

Figure 2 shows the difference in the persistence diagrams between the AD and HC groups based on the Wasserstein distance (p=2).

Statistical Analysis

To compare the persistence values extracted from the persistence diagrams between the AD and HC groups, we used Welch's t-test for five EEG frequency bands. The test was conducted on three persistence features: the mean of the birth scales, the mean of the death scales, and the mean of the persistence values (death – birth scales). Welch's t-test was chosen as it does not assume equal variances between the two groups. For each comparison, we reported the t-statistic (t), indicating the magnitude and direction of the difference, and the p-value, determining whether the difference had statistical significance (p<0.0001).

Classification

In this study, machine learning algorithms were employed for classification using the persistence features extracted via persistent homology. These were multilayer perceptron (MLP), SVM, kNN (k=7) and logistic regression. The performance of these algorithms was evaluated on the basis of accuracy (overall correctness), sensitivity (true positive rate), specificity (true negative rate), and F1 score (balance between precision and recall) using K-fold cross-validation.
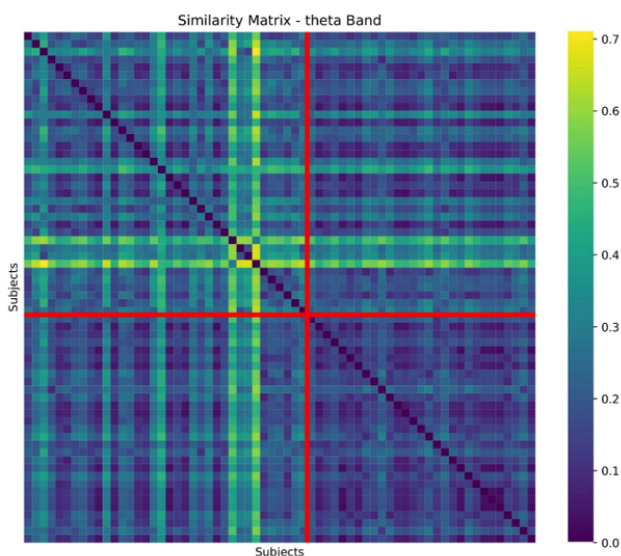
Table 3. Mean Wasserstein distances of H_1 persistence within and between the AD and HC groups across frequency bands

Band	Mean within the AD Group	Mean within the HC Group	Mean between Groups
Delta	0.0712	0.0201	0.0479
Theta	0.2632	0.1423	0.2182
Alpha	0.3322	0.3853	0.3742
Beta	0.2225	0.3187	0.2902
Gamma	0.1446	0.1842	0.1711

AD: Alzheimer's disease, HC: Healthy control.

RESULTS

The heatmap in Figure 2 shows that the persistence diagrams of the HC group (lower right section) are highly similar based on the Wasserstein distance, indicating consistent H_1 persistence within the group. This suggests that persistence diagrams capture the key differences between groups.

Moreover, we found that in the delta and theta bands, the mean H_1 birth, death, and persistence features differed significantly between the HC and AD groups, as shown in Table 3.

The AD group exhibited higher birth, death, and persistence values in the delta and theta bands compared with the HC group (p<0.0001). In contrast, the alpha and beta bands showed reduced birth and death values in the AD group. The persistence features in these bands are less affected. There were no significant differences detected in the gamma band. These findings reveal that the most significant changes in brain activity in AD occur in the slower brain waves.

Table 4 shows the statistical analysis of the persistence features across the EEG frequency bands for the AD and HC groups. In the delta and theta bands, birth, death, and persistence values were significantly higher in the AD group (p<0.0001). In the alpha and beta bands, birth and death values were lower in AD patients. In the gamma band, no significant differences were observed. This implies that high-frequency brain activity is less affected.

The results of the machine learning algorithms using topological features extracted via persistent homology as input, along with a comparison of their performance to that of algorithms using features derived from relative band power for distinguishing AD from HC, are presented in Table 5. The best performing relative band power-based model, i.e., LightGBM achieved an accuracy of 76.43% and an F1 score of 76.12% (24), and several classifiers trained on topological features exceeded these results. Notably, both the k-Nearest Neighbours (kNN) and Support Vector Machine (SVM with linear kernel) classifiers trained on topological features

Figure 2. Wasserstein distance matrix of H_1 persistence features from theta band coherence

Table 4. Statistical analysis of the persistence features across the frequency bands

Frequency Band	Feature	Mean Values		T-test Results	
		AD Group	HC Group	T-statistic	p value
Delta	Birth	0.0668	0.0343	6.0027	<0.0001
	Death	0.0819	0.0399	6.2044	<0.0001
	Persistence	0.0151	0.0056	5.1096	<0.0001
Theta	Birth	0.2022	0.1339	8.7890	<0.0001
	Death	0.2497	0.1495	9.1735	<0.0001
	Persistence	0.0475	0.0256	5.6515	<0.0001
Alpha	Birth	0.3157	0.3730	–3.9829	0.0001
	Death	0.3804	0.4491	–4.0787	0.0001
	Persistence	0.0647	0.0761	–1.8391	0.0666
Beta	Birth	0.3877	0.4182	–1.7555	0.0801
	Death	0.4453	0.4919	–2.3635	0.0187
	Persistence	0.0576	0.0737	–2.3972	0.0171
Gamma	Birth	0.4378	0.4514	–0.5464	0.5853
	Death	0.4870	0.4957	–0.3268	0.7441
	Persistence	0.0492	0.0443	0.9613	0.3373

AD: Alzheimer's disease, HC: Healthy control.

reached an accuracy of 81.50%, with the SVM also yielding the highest F1 score of 79.50%.

DISCUSSION

Our results show that the delta and theta waves exhibit increased persistence, which may be indicative of pathological overactivity (25). Higher persistence values indicate altered slow wave activity, which is associated with cognitive decline. This increased persistence may be interpreted as a sign of abnormal neural synchronization or potential compensatory mechanisms. Alpha and beta waves show reduced persistence, indicating decreased neural complexity and desynchronization, which may reflect an impairment in cognitive performance (26). Thus, by capturing these differences, persistence homology may present a new way to understand the effects of AD on brain dynamics. These results show that the altered slow-wave activity and disrupted neural synchronization seen in AD patients can be identified using the persistence features in the theta and delta bands.

While previous literature has primarily identified a decrease in pairwise coherence in the alpha band (5), our study highlighted the theta band when examining beyond pairwise relations, such as H_1 persistence, revealing distinct features that differentiate AD patients. The extracted topological features from the theta band showed significant alterations in functional connectivity among patients with AD.

EEG connectivity measures demonstrate higher diagnostic accuracy compared with traditional EEG power analysis and conventional AD biomarkers (27). While traditional coherence analysis has been extensively used in EEG research, it primarily captures pairwise relationships and does not account for higher-dimensional structures. In contrast, TDA, particularly persistent homology, provides a more comprehensive understanding of EEG connectivity by identifying complex topological patterns that coherence analysis alone cannot detect.

The use of persistent homology has enabled the identification of distinctive features in EEG data. TDA-based methods have shown potential for enhancing EEG-based diagnostic techniques, particularly in differentiating AD from normal brain activity. It is effective in the early detection of the disease and characterisation of disease severity (28, 29). Our results show that machine learning algorithms utilising topological features as input demonstrated superior performance in distinguishing between the AD and HC groups compared to those employing features derived from relative band power.

Table 5. Classification performance using different feature extraction and classification methods for distinguishing AD patients from HC subjects.

Feature Type	Classification Method	Accuracy %	Sensitivity %	Specificity %	F1 Score %
Relative Band Power	LightGBM	76.43	76.01	76.16	76.12
	SVM	73.14	71.89	75.98	73.74
	kNN (k=7)	71.23	69.67	74.19	72.81
	MLP	73.12	73.00	74.63	74.82
Topological	MLP	79.40	71.40	89.30	78.80
	Logistic Regression	80.00	74.30	86.00	78.90
	kNN (k=7)	81.50	68.90	96.00	78.20
	SVM (linear kernel)	81.50	71.40	92.70	79.50

SVM: Support vector machine, kNN: k-Nearest neighbours, MLP: Multilayer perceptron.

However, while topological analysis successfully uncovers high-dimensional relationships, it still lacks the capability to precisely localise the specific brain regions where these loops form. Further advancements in methodological frameworks may help address this limitation, thereby refining the interpretability of topological features in clinical applications.

CONCLUSION

In this study, coherence analysis and persistent homology methods were used to differentiate between patients diagnosed with AD and healthy individuals based on EEG data. By examining the topology of coherence in the electrode space, we demonstrated that meaningful features could be extracted. Unlike traditional metrics, our approach analyses the overall topological structure rather than individual pairwise relationships, revealing significant associations with the disease.

Our findings suggest that the TDA methods provide a promising approach for EEG-based Alzheimer's diagnosis. Future research can further explore the applicability of this methodology by evaluating it on different EEG frequency bands and larger datasets, potentially enhancing its clinical relevance.

Ethics Committee Approval		In our study we have made use of a freely available open access database. I accept and declare that no violation of ethical rules was made in the preparation and publication process of the study.
Peer-review		Externally peer-reviewed.
Author Contributions		Conception/Design of Study – M.B., O.B.E., C.K., A.U.; Data Acquisition – M.B., O.B.E., C.K., A.U.; Data Analysis/ Interpretation – M.B., O.B.E., C.K., A.U.; Drafting Manuscript M.B., O.B.E., C.K., A.U.; Critical Revision of Manuscript – M.B., O.B.E., C.K., A.U.; Final Approval and Accountability – M.B., O.B.E., C.K., A.U.
Conflict of Interest		The authors declare no conflict of interest.
Financial Disclosure		The authors declare that they received no financial support for this study.

Author Details

Mustafa Bayrak
[1] Institute of Graduate Studies in Health Sciences, Istanbul University, Istanbul, Turkiye

[2] Department of Physiology, Istanbul Faculty of Medicine, Istanbul University, Istanbul, Turkiye

0009-0006-7601-1584   ✉ mustafabayrakphd@gmail.com

Omer Bahadir Eryilmaz
[3] School of Computer Science, University of Birmingham, Birmingham, UK

0009-0006-2229-6254

Cihan Katar
[4] Department of Electrical Electronics Engineering, Faculty of Engineering, Turkish-German University, Istanbul, Turkiye

[5] Department of Electronics and Communication Engineering, Faculty of Electrical and Electronics Engineering, Istanbul Technical University, Istanbul, Turkiye

0000-0003-1247-9082

Atilla Uslu
[2] Department of Physiology, Istanbul Faculty of Medicine, Istanbul University, Istanbul, Turkiye

0000-0003-1351-1072

REFERENCES

1. Ulep MG, Saraon SK, McLea S. Alzheimer disease. J Nurse Pract 2018; 14(3): 129-35.

2. Ballard C, Gauthier S, Corbett A, Brayne C, Aarsland D, Jones E. Alzheimer's disease. Lancet 2011; 377(9770): 1019-31.

3. Harwood DG, Sultzer DL, Wheatley MV. Impaired insight in Alzheimer disease: association with cognitive deficits, psychiatric symptoms, and behavioral disturbances. Cogn Behav Neurol 2000; 13(2): 83-8.

4. Khachaturian ZS. Diagnosis of Alzheimer's disease. Archives Neurol 1985; 42(11): 1097-105.

5. Cassani R, Estarellas M, San-Martin R, Fraga FJ, Falk TH. Systematic review on resting-state EEG for Alzheimer's disease diagnosis and progression assessment. Dis Markers 2018; 2018: 5174815.

6. Kulkarni N, Bairagi VK. Diagnosis of Alzheimer disease using EEG signals. Int J Eng Res 2014; 3(4): 1835-8.

7. Gawel M, Zalewska E, Szmidt-Sałkowska E, Kowalski J. The value of quantitative EEG in differential diagnosis of Alzheimer's disease and subcortical vascular dementia. J Neurol Sci 2009; 283(1-2): 127–33.

8. Garn H, Waser M, Deistler M, Schmidt R, Dal-Bianco P, Ransmayr G, et al. Quantitative EEG in Alzheimer's disease: Cognitive state, resting state and association with disease severity. Int J Psychophysiol 2014; 93(3): 390–7.

9. Yener GG, Leuchter AF, Jenden D, Read SL, Cummings JL, Miller BL. Quantitative EEG in frontotemporal dementia. Clin Electroencephalogr 1996; 27(2): 61-8.

10. Jelic V, Shigeta M, Julin P, Almkvist O, Winblad B, Wahlund LO. Quantitative electroencephalography power and coherence in Alzheimer's disease and mild cognitive impairment. Dement Geriatr Cogn Disord 1996; 7(6): 314-23.

11. Ouchani M, Gharibzadeh S, Jamshidi M, Amini M. A review of methods of diagnosis and complexity analysis of Alzheimer's disease using EEG signals. BioMed Res Int 2021; 2021: 5425569.

12. Lizio R, Vecchio F, Frisoni GB, Ferri R, Rodriguez G, Babiloni C. Electroencephalographic rhythms in Alzheimer's disease. Int J Alzheimer's Dis 2011; 2011: 927573.

13. Fischer MH, Zibrandtsen IC, Høgh P, Musaeus CS. Systematic review of EEG coherence in Alzheimer's disease. J Alzheimers Dis 2023; 91(4): 1261-72.

14. Kowalski JW, Gawel M, Pfeffer A, Barcikowska M. The diagnostic value of EEG in Alzheimer disease: correlation with the severity of mental impairment. Clin Neurophysiol 2001; 18(6): 570-5.

15. Onishi J, Suzuki Y, Yoshiko K, Hibino S, Iguchi A. Predictive model for assessing cognitive impairment by quantitative electroencephalography. Cogn Behav Neurol 2005; 18(3): 179-84.

16. Van der Hiele K, Vein AA, Reijntjes RH, Westendorp RG, Bollen EL, Van Buchem MA, et al. EEG correlates in the spectrum of cognitive decline. Clin Neurophysiol 2007; 118(9): 1931-9.

17. French CC, Beaumont JG. A critical review of EEG coherence studies of hemisphere function. Int J Psychophysiol 1984; 1(3): 241-54.

18. Carlsson G. Topology and data. Bull Am Math Soc 2009; 46(2): 255-308.

19. Yamanashi T, Kajitani M, Iwata M, Crutchley KJ, Marra P, Malicoat JR, et al. Topological data analysis (TDA) enhances bispectral EEG (BSEEG) algorithm for detection of delirium. Sci Rep 2021; 11(1): 304.

20. Cai T, Zhao G, Zang J, Zong C, Zhang Z, Xue C. Topological feature search method for multichannel EEG: Application in ADHD classification. Biomed Signal Process Control 2025; 100: 107153.

21. Sathyanarayana A, Manjunath S, Perea JA. Topological data analysis based characteristics of electroencephalogram signals in children with sleep apnea. J Sleep Res 2025: e70017.

22. Piangerelli M, Rucco M, Tesei L, Merelli E. Topological classifier for detecting the emergence of epileptic seizures. BMC Res Notes 2018; 11: 1-7.

23. Rutkowski TM, Abe MS, Sugimoto H, Otake-Matsuura M. Mild cognitive impairment detection with machine learning and topological data analysis applied to EEG time-series in facial emotion oddball paradigm. In2023 45th Annual International Conference of the IEEE Engineering in Medicine & Biology Society (EMBC) 2023 (pp. 1-4). IEEE.

24. Miltiadous A, Tzimourta KD, Afrantou T, Ioannidis P, Grigoriadis N, Tsalikakis DG, et al. A dataset of scalp EEG recordings of Alzheimer's disease, frontotemporal dementia and healthy subjects from routine EEG. Data 2023; 8(6): 95.

25. Abuhassan K, Coyle D, Belatreche A, Maguire L. Compensating for synaptic loss in Alzheimer's disease. J Comput Neurosci 2014; 36: 19-37.

26. Fonseca LC, Tedrus GMAS, Prandi LR, Almeida AM, Furlanetto DS. Alzheimer's disease: Relationship between cognitive aspects and power and coherence EEG measures. Arq Neuro-Psiquiatr 2011; 69(6): 875–81.

27. Musaeus CS, Engedal K, Høgh P, Jelic V, Mørup M, Naik M, et al. Oscillatory connectivity as a diagnostic marker of dementia due to Alzheimer's disease. Clin Neurophysiol 2019; 130(10): 1889-99.

28. Duan F, Huang Z, Sun Z, Zhang Y, Zhao Q, Cichocki A, et al. Topological network analysis of early Alzheimer's disease based on resting-state EEG. IEEE Trans Neural Syst Rehabil Eng 2020; 28(10): 2164-72.

29. Fan M, Yang AC, Fuh JL, Chou CA. Topological pattern recognition of severe Alzheimer's disease via regularized supervised learning of EEG complexity. Front Neurosci 2018; 12: 685.

Experimed

Research Article

Open Access

Clinical Significance of Cytogenetic Abnormalities Detected by FISH in CLL: Insights from a Real-World Single-Centre Cohort

Ayse Gul Bayrak Tokac [1] ✉, Simge Erdem [2] , Gulcin Bagatir [1] , Ender Coskunpinar [3] , Kubra Gunduz [3] ,
Okan Cetin [2] , Abdullah Savas [2] , Mustafa Nuri Yenerel [2] , Sukru Palanduz [1]

[1] Division of Medical Genetics, Department of Internal Medicine, Istanbul Faculty of Medicine, Istanbul University, Istanbul, Turkiye
[2] Division of Hematology, Department of Internal Medicine, Istanbul Faculty of Medicine, Istanbul University, Istanbul, Turkiye
[3] Department of Medical Biology, School of Medicine, Health Sciences University, Istanbul, Turkiye

Abstract

Objective: Chronic lymphocytic leukemia (CLL) is a hematologic malignancy that predominantly affects the elderly. This study aimed to investigate cytogenetic alterations that could be used for risk assessment and treatment decisions in patients with CLL in relation to clinical parameters and outcomes.

Materials and Methods: Peripheral blood samples from 101 CLL patients either newly diagnosed or previously diagnosed but untreated were analyzed using interphase fluorescence *in situ* hybridization (I-FISH) method with a CLL panel probe set. The associations among cytogenetic abnormalities, clinical features, treatment indications, and outcomes were statistically evaluated.

Results: FISH analysis revealed statistically significant associations between specific cytogenetic abnormalities and clinical features. del(13q) and ATM deletion were significantly associated with large/symptomatic/progressive lymphadenopathy (LAP); ATM deletion was also linked to progressive splenomegaly. Regarding the causes of death, P53 deletion was significantly associated with secondary solid neoplasms and acute decompensated heart failure; trisomy 12 with disease progression and secondary solid neoplasms; and immunoglobulin heavy chain gene (IGH) rearrangement with tumor lysis syndrome. No significant difference in the overall survival was observed between the treated and untreated CLL patients.

Conclusion: If validated in larger, multicenter cohorts, the novel associations identified between cytogenetic abnormalities and both treatment indications and causes of death could help guide the management of CLL.

Keywords Chronic lymphocytic leukemia · Fluorescence in situ hybridization · Prognosis · Cytogenetic abnormalities · Clinical marker

✉ Corresponding author: Ayse Gul Bayrak Tokac abayrak@istanbul.edu.tr

INTRODUCTION

Chronic lymphocytic leukemia (CLL), which originates from B cells, is the most common neoplasm in adults. It has significant clinical and genetic heterogeneity that influences disease progression. The median age at diagnosis is 70 years, with a male predominance. Approximately 10% of CLL cases occur in individuals under 45 years of age (1). 70-80% of CLL patients are asymptomatic at the time of diagnosis. The watch and wait approach is the standard of care for this subgroup, with nearly one-third never requiring intervention during their lifetime (2).

Clinically, CLL is staged using the Rai and Binet classification systems, which assess lymphadenopathy, splenomegaly/ hepatomegaly, and hematologic parameters such as anemia or thrombocytopenia (3, 4).

Approximately 2-10% of patients develop Richter's syndrome (RS) - a progression to a high-grade aggressive lymphoma. In 95-99% of these cases, the transformation is to diffuse large B-cell lymphoma (DLBCL), in 0.5-5% to Hodgkin's Lymphoma (HL), and less frequently to plasmablastic lymphoma (5).

Genetic abnormalities are critical prognostic markers and play an important role in determining the right treatment decisions in CLL. Interphase fluorescence *in situ* hybridization (I-FISH) is the most effective method for detecting cytogenetic abnormalities, with approximately 80% sensitivity (6). Standard I-FISH panels screen for trisomy 12, del(13)(q14.3), del(11)(q22.3) (*ATM* gene deletion), and del(17)(p13.1) (TP53/P53 gene deletion). Some panels also include del(6)(q23) (*MYB* gene deletion) and immunoglobulin heavy chain (IGH) genes rearrangements. The prognostic impact of each abnormality is different (6, 7). These abnormalities are also associated with RS, which worsens the prognosis of the patient (8).

In this single-centre cohort study, we investigated the prognostic significance of cytogenetic abnormalities detected by I-FISH in patients with CLL. By correlating these genetic alterations with clinical parameters, treatment indications, and survival outcomes, we aimed to identify specific FISH-detectable aberrations that enhance risk stratification and inform therapeutic decisions in real-world settings.

MATERIALS AND METHODS

Study Population

Peripheral blood samples were collected from 101 patients with CLL, either newly diagnosed or previously diagnosed but treatment-naïve. None of the patients were receiving cytotoxic therapy at the time of sampling, and all had no history of other malignancies. Informed consent was obtained from each patient before participation. The study protocol was approved by the Clinical Research Ethics Committee (Decision date/number: November 17, 2023/23), in accordance with the Declaration of Helsinki.

I-FISH Analysis

I-FISH was performed using the direct culture method in accordance with our laboratory's standard procedures. Peripheral blood samples from the patients were drawn into sodium heparinized tubes. For each patient, 0.1 mL of blood was added to a polystyrene tube containing 5 mL of RPMI 1640 medium. Then, the tubes were centrifuged at 3,000 rpm for six minutes, and the supernatant was removed. The pellet was resuspended in 8 mL of a 0.075 M potassium chloride (KCl) solution and incubated at 37 °C for 15 min. Following the second centrifugation and removal of the supernatant, the pellet was resuspended in 8 mL of the fixative (Carnoy's solution: 3:1 methanol/acetic acid) and centrifuged again. The supernatant was removed. This procedure was repeated three times. Finally, the resulting pellet was vortexed, spread onto a microscope slide for each target, and air-dried at room temperature for 10 min.

The CLL panel probe set with the I-FISH method was applied to the patients according to the manufacturer's instructions. For each patient, 200 interphase nuclei were evaluated. Analyses were evaluated with the Isis Fluorescent Imaging System (Metasystems, Germany). The CLL FISH Panel was used for interphase FISH analysis; Alpha satellite 12 plus (Cytocell, UK) for trisomy 12, D13S319 plus deletion (Cytocell, UK) for 13q deletion, and P53 (TP53)/ATM combination (Cytocell, UK) for 17p/11q deletions, IGH plus breakapart (Cytocell, UK) for IGH rearrangements (deletion/translocation) and *MYB* gene deletion (Cytocell, UK) for 6q deletion.

Statistical Analyses

SPSS 20.0 (SPSS Inc., Chicago, IL, USA) was used for the statistical analysis. Shapiro-Wilk and Levene's tests were used to investigate the continuous variables. ANOVA and t-test were used for the parametric variables; Mann–Whitney U and Kruskal-Wallis tests were used for the non-parametrical variables. Categorical data were examined with chi-square tests. Correlations between expression data and clinical parameters were evaluated using Pearson's correlation coefficient.

RESULTS

Of the 101 CLL patients included, 40 (39.6%) were female and 61 (60.4%) were male, yielding a male:female ratio of 1.52. The mean age was 59.7 years (range: 35-86). Clinical follow-up

revealed that 38 patients (37.6%) did not require treatment, 62 (61.4%) received treatment, and 1 patient (1%) was lost to follow-up. According to the Rai staging system, patients were classified as stage 0 (n=39, 38.6%), stage I (n=27, 26.7%), stage II (n=19, 18.8%), stage III (n=9, 8.9%), and stage IV (n=7, 6.9%). Based on the Binet staging system, 69 patients (68.3%) were in stage A, 17 (16.8%) in stage B, and 15 (14.9%) in stage C. The clinical findings of the patients are presented in Table 1.

Comparisons between RAI stages of the patients and treatment indications demonstrated significant associations with progressive lymphocytosis, progressive bone marrow failure, and refractory autoimmune hemolytic anemia (p=0.01, p=0.0003, p=0.00009, respectively). According to the Binet staging system, a significant relationship was found between progressive bone marrow failure and refractory autoimmune hemolytic anemia (p=0.0003 and p=0.01, respectively) (Table 2).

Cytogenetic abnormalities were detected in 64 patients (63.4%), whereas 37 patients (36.6%) had no detectable abnormalities for the regions examined by I-FISH. The frequency of specific abnormalities was as follows: (13q) deletion in 42 patients (41.6%), ATM deletion in 9 patients (8.9%), (P53) deletion in 9 patients (8.9%), trisomy 12 in 13 patients (12.9%), IGH rearrangement in 12 patients (11.9%), and MYB deletion in 1 patient (1%). Images from the CLL FISH panel are shown in Figure 1. A total of 19 patients (18.8%) harbored two or more abnormalities, with the 13q deletion most frequently co-occurring with other abnormalities (Table 3).

When comparing patients' treatment indications with their FISH abnormality results, a significant association was found between 13q deletion and bulky/symptomatic/progressive lymphadenopathy (LAP) (p=0.01), as well as between ATM deletion and both bulky/symptomatic/progressive LAP (p=0.05) and progressive splenomegaly (p=0.03) (Table 4).

During follow-up, 28 patients (27.7%) died (25 of the 63 patients from the treated group and 3 of the 37 patients from the untreated group). The survival statistics (mean and median) are detailed in Table 5. Kaplan–Meier analysis revealed no statistically significant difference in survival between the treated and untreated patients (p=0.154) (Figure 2).

Infection was the leading cause of death with a rate of 8%. Notably, P53 deletion was significantly associated with secondary solid neoplasms (p=0.003) and acute decompensated heart failure (p=0.03); trisomy 12 correlated with disease progression (p=0.0001) and secondary solid neoplasms (p=0.02); and IGH rearrangements were linked to tumor lysis syndrome (p=0.006) (Table 6).

Table 1. Clinical findings of the patients

Characteristic	n = 101
Age at diagnosis, mean ± SD (range)	59.7 ± 10.7 (35-86)
Gender, n(%)	
Female	40 (39.6)
Male	61 (60.4)
Binet stage, n(%)	
A	69 (68.3)
B	17 (16.8)
C	15 (14.9)
Rai stage, n(%)	
0	39 (38.6)
1	27 (26.7)
2	19 (18.8)
3	9 (8.9)
4	7 (6.9)
Number of untreated patients, n(%)	38 (37.6)
Binet stage	
A	30 (78.9)
B	6 (15.4)
C	2 (5.1)
Rai stage	
0	22 (57.9)
1	7 (17.9)
2	6 (15.4)
3	2 (5.1)
4	1 (2.7)
Number of treated patients, n(%)	62 (61.4)
Binet stage	
A	38 (61.3)
B	11 (17.7)
C	13 (21)
Rai stage	
0	16 (25.8)
1	20 (32.3)
2	13 (20.9)
3	7 (11.3)
4	6 (9.7)
Number of patients with an unknown treatment status, n(%)	1 (0.99)
Alive, n (%)	
Yes	73 (72.3)
No	28 (27.7)
Mean time to first treatment (months), mean (range)	26.95 (1-119)
Overall survival (months), mean (range)	86 (29-201)
Patients ≥65 years	55.9
Patients between the ages of 50-65	95
Patients ≤50 years	102.7

Table 2. Comparison of the patient's clinical phase results and reasons for therapy

| Reason for the therapy | Clinical phase | | | |
| | Rai stage | | Binet stage | |
	n	p value	n	p value
progressive lymphocytosis	101	**0.01***	101	0.76
progressive bone marrow failure	101	**0.0003***	101	**0.0003***
b symptoms	101	0.796	101	0.44
bulky/symptomatic/progressive LAP	101	0.07	101	0.39
unresponsive to therapy autoimmune hemolytic anemia	101	**0.00009***	101	**0.01***
unresponsive to therapy ITP	101	0.78	101	0.49
progressive splenomegaly	101	0.63	101	0.62
symptomatic/progressive splenomegaly	101	0.44	101	0.16

* Significant difference (p≤0.05); LAP: lymphadenopathy; ITP: immune thrombocytopenic purpura.

Six patients developed RS. Among these, one patient had no detected abnormalities, two had ATM deletion, one had both 13q deletion and IGH rearrangement, another had 13q deletion and trisomy 12, and one had IGH rearrangement. A correlation was found between the time elapsed from diagnosis to death and the RS (p=0.07). The reason for treatment in 3 of 6 patients with RS was bulky/symptomatic/progressive LAP.

DISCUSSION

CLL is the most common type of leukemia. Although most patients are over 65 years of age at the time of diagnosis, approximately 10% are younger than 45 years and a male predominance (male:female ratio 1.9:1) (1).

In our cohort of 101 CLL patients, the mean age was slightly younger 59.7 years (range: 35-86). Nevertheless, the proportion of patients under the age of 45 (8.9%) and the male:female ratio (1.52) remained consistent with the literature.

CLL is a heterogeneous disease diagnosed via blood tests and flow cytometry, with patients monitored until the need for treatment (1). The presence of genetic abnormalities provides valuable prognostic information in CLL requiring therapy (9).

Trisomy of chromosome 12 is one of the most frequent cytogenetic abnormalities (approximately 20%) and remains the only abnormality in 40-60% of cases. Its prognostic significance is debated. It is typically related to shorter survival in the intermediate risk group (10, 11). However, according to the results of a nine-year follow-up of 250 CLL patients with untreated trisomy 12, these patients were reported to have increased CD38 positivity and an atypical immunophenotype, as well as a high incidence of thrombocytopenia, RS, and secondary malignancies (12). It is hypothesized that concurrent NOTCH1 mutations intensify

Table 3. Genetic abnormalities detected in patients by I-FISH testing

FISH abnormalities	Patient n	Percentage (%)
(13q) deletion*	42	41.6
sole abnormality	27	
with one or more abnormalities	15	
ATM deletion	9	8.9
sole abnormality	4	
with one or more abnormalities	5	
(P53) deletion	9	8.9
sole abnormality	7	
with one or more abnormalities	2	
(12) trisomy	13	12.9
sole abnormality	5	
with one or more abnormalities	8	
IGH rearrangement	12	11.9
sole abnormality	3	
with one or more abnormalities	9	
MYB deletion (sole abnormality)	1	1
Complex FISH abnormalities	19	18.8
(13q) monoallelic deletion + ATM deletion	4	3.96
(13q) monoallelic deletion + P53 deletion	2	1.98
(12) trisomy + IGH rearrangement	2	1.98
(13q) deletion + IGH rearrangement	3	2.97
(12) trisomy + (13q) biallelic deletion	2	1.98
(12) trisomy + (13q) monoallelic deletion	2	1.98
(13q) trisomy + IGH rearrangement	1	0.99
(12) trisomy + P53 deletion + IGH rearrangement	1	0.99
(13q) monoallelic deletion + ATM deletion + IGH rearrangement	1	0.99
(12) trisomy + (13q) monoallelic deletion + IGH rearrangement	1	0.99

* 13q deletions are biallelic in only 2 patients and monoallelic in the other 40 patients.

prognosis and that trisomy 12 alone may predispose to disease progression and subsequent alterations such as TP53 and NOTCH1 (11, 13).

In our cohort, trisomy 12 was present in 13 patients (12.9%), and in five cases (38.5%) was the only abnormality. These rates were consistent with the literature findings. The other abnormalities accompanying trisomy 12 were 13q deletion, IGH rearrangement, and P53 deletion. We also identified a significant correlation between trisomy 12 abnormalities and disease progression as well as the development of secondary solid neoplasms.

13q deletion is observed in approximately 50% of CLL patients, either mono- or biallelic. Although it is

Table 4. Comparison of patients' FISH abnormalities results and reasons for therapy

	FISH abnormalities											
	(13q) deletion		ATM deletion		(P53) deletion		(12) trisomy		IGH rearrangement		MYB deletion	
Reason for the therapy	n	p value	n	p value	n	p value	n	p value	n	p value	n	p value
progressive lymphocytosis	15	0.08	4	0.20	3	0.63	3	0.75	2	0.40	1	0.09
progressive bone marrow failure	3	0.30	1	0.98	1	0.98	1	0.69	2	0.49	0	0.72
B symptoms	5	0.78	1	0.98	2	0.25	1	0.69	0	0.19	0	0.72
bulky/symptomatic/progressive LAP	17	**0.01***	5	**0.05***	4	0.24	2	0.28	2	0.36	0	0.53
Unresponsive to therapy autoimmune hemolytic anemia	3	0.39	0	0.47	1	0.37	1	0.62	0	0.40	0	0.81
unresponsive to therapy ITP	2	0.37	1	0.13	0	0.58	0	0.49	0	0.51	0	0.86
progressive splenomegaly	1	0.80	1	**0.03***	0	0.65	0	0.58	0	0.60	0	0.88
symptomatic/progressive splenomegaly	3	0.66	0	0.43	0	0.43	1	0.77	2	0.09	0	0.80

* Significant difference (p≤0.05); LAP: lymphadenopathy; ITP: immune thrombocytopenic purpura.

Table 5. Mean and median survival time of patients

Treatment	Mean[a]				Median			
	Estimate	Std. Error	95% confidence interval		Estimate	Std. Error	95% confidence interval	
			Lower Bound	Upper Bound			Lower Bound	Upper Bound
No	222.333	21.647	179.906	264.761	.	.	.	.
Yes	180.053	14.491	151.651	208.455	147.000	4.429	138.318	155.682
Overall	190.634	14.333	162.541	218.727	150.000	4.667	140.853	159.147

[a] Estimation is limited to the largest survival time if it is censored.

Table 6. Comparison of patients' FISH abnormalities results and the cause of death

	FISH abnormalities											
	(13q) deletion		ATM deletion		(P53) deletion		(12) trisomy		IGH rearrangement		MYB deletion	
Cause of death	n	p value	n	p value	n	p value	n	p value	n	p value	n	p value
Disease progression	1	0.49	1	0.24	0	0.52	3	**0.0001***	1	0.40	0	0.83
Secondary Solid Neoplasm	0	0.08	0	0.52	2	**0.003***	2	**0.02***	1	0.40	0	0.83
Infection	5	0.21	2	0.09	1	0.71	0	0.25	1	0.95	0	0.76
Acute Decompensated Heart Failure	1	0.80	0	0.65	1	**0.03***	0	0.58	0	0.60	0	0.88
Other: Hepatitis	0	0.22	0	0.65	0	0.65	0	0.58	1	0.09	0	0.88
Tumor lysis syndrome	0	0.39	0	0.75	0	0.75	0	0.69	1	**0.006***	0	0.92

* Significant difference (p≤0.05)

clinically heterogeneous, its presence in the absence of additional cytogenetic abnormalities is considered a favorable prognostic marker (11). It is also a protective factor that reduces the risk of RS development (8). The deletion region at 13q14 spans an area from 300 kbp to 70 Mbp, including the *DLEU1, DLEU2, RB1,* and *TRIM13* genes, as well as microRNAs (miRs 15a and 16-1) (7). A higher number of deleted cells (>70) and the larger deletions shorten the treatment-free intervals. It has been reported that mono/biallelic deletion has no effect on prognosis. Although the 13q deletion is isolated in 36% of patients, it frequently accompanies other abnormalities (14).

Consistent with previous studies, we detected 13q deletion in 42 patients (41.6%) in our cohort. Among those, 27 patients (64%) had it as the sole abnormality. This rate was higher than that reported in the literature. In patients with two or more abnormalities, the 13q deletion frequently co-occurred. We newly identified a significant association between 13q deletion and bulky/symptomatic/progressive lymphadenopathy in the treated patients. To our knowledge, this relationship has not been reported in the literature.
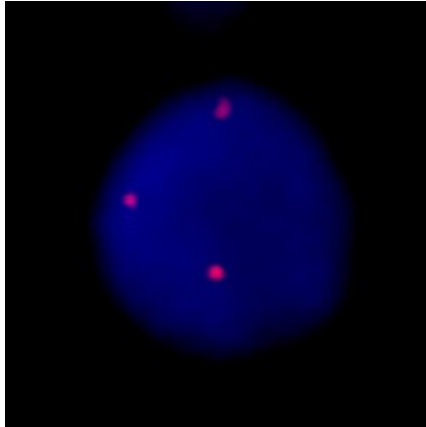
a. Trisomy 12 (red signal D12Z3, 12p11.1-q11.1; three red signals indicate trisomy 12).
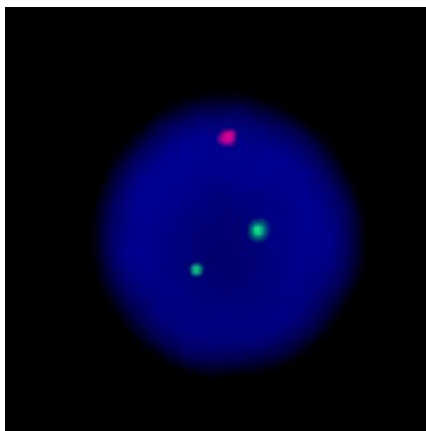
b. Del
(13q) (red signal 13q14.2-q14.3, green signal 13q34; 1R,2G signal indicates a deletion in 13q).
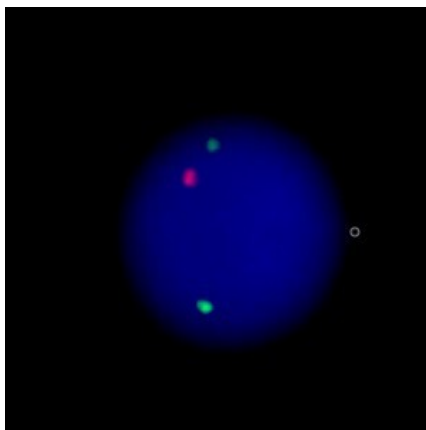
c. del (17p) (red signal P53(17p13), green signal ATM(11q22.3); 1R,2G signal indicates P53 deletion and normal ATM presence).
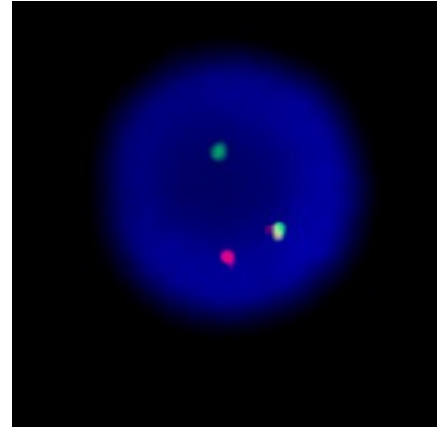
d. IGH rearrangement (red signal IGHC, 14q32.3, green signal IGHV, 14q32.3 ; 1F,1R,1G signal indicates rearrangement).
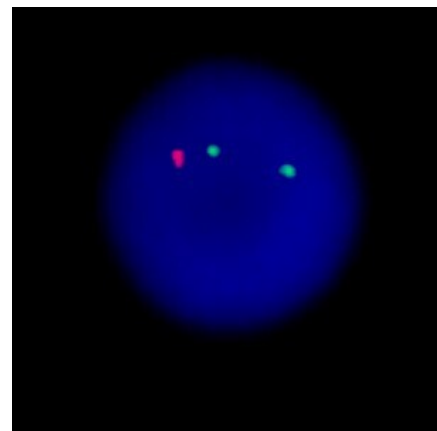
e. del (6q) (red signal 6q23.3, green signal D6Z1, 6p11.1-q11.1 ; 1R,2G signal indicates MYB deletion).

Figure 1. FISH images of different patients.

The 11q deletion, observed in 5-20% of CLL cases, is a highly heterogeneous locus ranging from 2 to 20 megabase pairs (Mb) in the 22.3-q23.1 segment interval. It includes the *ATM, ACAT, BIRC3, CUL5, EXPH2, FRDX1, H2AX, KDELC2, MRE11, NPAT, RAB39,* and *RDX* genes. While the 11q deletion results in the loss of the *ATM* tumor suppressor gene in CLL, other genes within this region are also thought to contribute to the disease pathogenesis. It is linked to an early onset, poor prognosis, unmutated IGH variable (*IGHV*) genes, and lymphadenopathy (11, 15). It is also a risk factor for the development of RS (8). Mutations in the *ATM* gene are detected in approximately 30% of CLL patients with del 11q. Furthermore, mutations and deletions in the *BIRC3* gene, which is located near the *ATM* gene at 11q22, have been identified in 4% at diagnosis and 24% in fludarabine-resistant patients. This provides evidence that the *BIRC3* gene is associated with the chemotherapy-resistant CLL phenotype (7, 11).
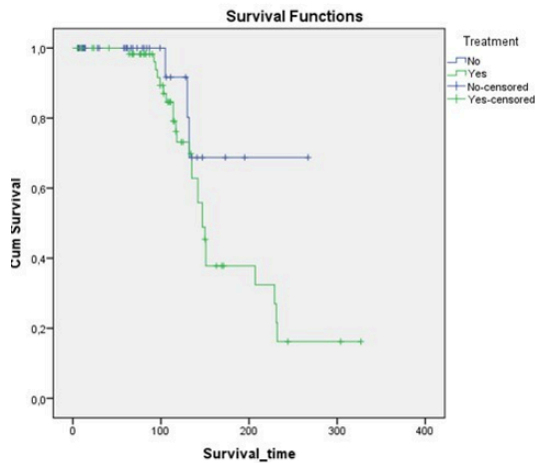
Figure 2. Kaplan–Meier plots of survival estimate for CLL patients who received and did not receive treatment.

When we compared our findings with published data, we found that the 11q deletion rate (8.9%) in our study was consistent with previously reported values. This abnormality was identified as the sole cytogenetic finding in four patients (44.4%). In our cohort, ATM deletion was frequently accompanied by 13q deletion. There was a significant association between ATM deletion and bulky/symptomatic/progressive LAP, consistent with the literature, and with progressive splenomegaly, which has not been previously reported.

The del (17p) abnormality, seen in approximately 5-10% of newly diagnosed CLL patients and in 40-50% of those with relapsed or refractory disease, results in the loss of the tumor suppressor gene *P53* (*TP53*). This deletion, which is associated with a poor prognosis, also confers resistance to treatment. In addition to deletions, somatic gene mutations were detected in the p53 gene. These mutations are observed in approximately 10% of CLL patients and are often associated with p53 deletion (16, 17). Biallelic loss of the *p53* gene, defined as the deletion of one allele and mutation of the other, disrupts the protective barrier against genomic instability, leading to increased DNA damage (18). Notably, CLL patients with monoallelic *TP53* abnormalities exhibit better survival compared with those with biallelic alterations (19). Approximately 40% of patients with p53 abnormalities have biallelic loss. While the mutation frequency is low in untreated CLL patients, it is higher among those who experience disease progression and develop treatment resistance. Although the prognostic impact of *TP53* deletion and mutation is independent, the presence of both abnormalities is associated with a shorter time to first treatment, progression-free survival, and overall survival (20).

In our study, p53 deletion was identified in nine patients (8.9%), which is lower than the frequency reported in the literature. This abnormality was the only cytogenetic finding in seven patients (77.7%). When the causes of death were compared with the FISH abnormalities, a significant association was observed between p53 deletion and both secondary solid neoplasms and acute decompensated heart failure.

The 6q deletion is observed in approximately 3-7% of CLL cases and is typically considered a secondary abnormality within a complex karyotype. It is rarely detected as an isolated aberration (21–23). The 6q deletion region is highly heterogeneous and contains genes with different breakpoints. In patients with CLL, this deletion most frequently occurs between q21 and q23 (24). The minimal deleted region detected by array comparative genomic hybridization (array CGH) included the *SCML4, SEC63, STM1, NR2E1, SNX3, LACE1,* and *FOXO3* genes at 6q21, spanning 107.7–108.7 Mb. It has been reported that the *FOXO3* gene triggers apoptosis by regulating the expression of genes required for cell death. It shows low expression with 6q21 deletion and may represent a potential target for therapy in CLL (23). The 6q23 deletion, which involves the *MYB* gene (the most frequently investigated *MYB* gene), is more prevalent among patients with advanced-stage CLL (25), but remains rare in treatment-naïve patients, who tend to have shorter survival (22).

In our study, MYB deletion was detected in only one patient, representing a lower frequency than that reported in the literature. This patient was clinically diagnosed with RAI stage II and Binet stage A disease and required treatment 22 months after diagnosis.

IGH rearrangements are an important cytogenetic abnormality in CLL. Deletions, translocations, and mutations involving the *IGH* gene can be detected. Translocations of the IGH locus on 14q32 are seen with a frequency of 4-9% in CLL. *BCL2* (18q21) and *BCL3* (19q13) are the most common recurrent partner genes (26). CLL patients with 14q32 rearrangements typically have a shorter treatment-free interval (27). Approximately 60% of CLL patients have a mutation in the *IGHV* gene. In these patients, the disease tends to progress more slowly, usually does not require early treatment, and is associated with a favorable prognosis (28, 29). In contrast, patients without IGHV mutations exhibited high expression of CD38, ZAP-70, and CD49d as well as had a more aggressive disease with shorter overall survival. Unlike other genetic markers in CLL, the IGHV mutation status remains stable over the course of the disease. This observation suggests the existence of two distinct biological subtypes of CLL according to the IGHV mutation status, which plays a role in the pathogenesis of the

disease (28). Del (14q), which is associated with trisomy 12, has also been linked to the unmutated IGHV status, NOTCH1 mutations, and shorter treatment-free survival (29).

In our study, the frequency of IGH rearrangements was higher than that previously reported in the literature, at 11.9%. In nine of the 12 patients (75%) with IGH rearrangements, the abnormality was associated with one or more additional cytogenetic alterations. The other abnormalities accompanying the IGH rearrangements were 13q deletion, trisomy 12, ATM, and P53 deletions. Furthermore, a significant association was found between IGH rearrangement and tumor lysis syndrome when the causes of death were analyzed in relation to the FISH results.

Most patients with CLL are asymptomatic at diagnosis and are monitored without immediate treatment (1).

In our study, 38 of 101 patients (37.6%) did not receive treatment, 62 (61.4%) received treatment, and one patient (1%) was lost to follow-up, with the treatment status unknown. Among those who received treatment, 23 patients (37.1%) initiated therapy within 12 months of diagnosis, 16 (25.8%) between 12 and 24 months, and 23 (37.1%) after more than 24 months. The mean treatment-free survival was 26.95 months (range: 1-119). The overall survival was 55.9 months for patients aged ≥65 years, 95 months for those aged 50-65 years, and 102.7 months for patients aged ≤50 years.

In a study of 1143 CLL patients, the causes of death in 225 patients who died were reported as disease progression (46%), other causes unrelated to CLL (27%), secondary solid neoplasms (19%) and infection (8%) (30).

In our study, 28 of 101 patients (27.7%) died. The cause of death was unknown in 8 cases. In the remaining 20 patients, the most common cause of death was infection (8%). The infection-related mortality rate in our cohort was consistent with that reported in the literature.

In the literature, del (11q) and del (17p) have been reported as risk factors for the development of RS, whereas del (13q) has been described as a protective factor associated with lower risk (8).

In our study, among the 6 patients who developed RS, 1 had no cytogenetic abnormality, 2 had ATM deletions, 1 had both 13q deletion and IGH rearrangement, 1 had 13q deletion with trisomy 12, and 1 had IGH rearrangement. No statistically significant associations were identified.

Given the clinical heterogeneity of CLL, a multifaceted approach is required for disease monitoring and prognosis prediction. Although CLL is generally characterized by advanced age and prolonged survival without treatment, our cohort exhibited a younger average age at diagnosis.

The findings of our single-centre study were largely consistent with previously published data. However, the novel associations we observed between cytogenetic abnormalities and both treatment indications and causes of death could help guide the CLL management if validated in larger, multicenter cohorts.

Author Details

Ayse Gul Bayrak Tokac
[1] Division of Medical Genetics, Department of Internal Medicine, Istanbul Faculty of Medicine, Istanbul University, Istanbul, Turkiye

 0000-0003-2228-0632   ✉ abayrak@istanbul.edu.tr

Simge Erdem
[2] Division of Hematology, Department of Internal Medicine, Istanbul Faculty of Medicine, Istanbul University, Istanbul, Turkiye

 0000-0001-8095-5445

Gulcin Bagatir
[1] Division of Medical Genetics, Department of Internal Medicine, Istanbul Faculty of Medicine, Istanbul University, Istanbul, Turkiye

 0000-0002-4685-6686

Ender Coskunpinar
[3] Department of Medical Biology, School of Medicine, Health Sciences University, Istanbul, Turkiye

 0000-0002-1003-5544

Kubra Gunduz
[3] Department of Medical Biology, School of Medicine, Health Sciences University, Istanbul, Turkiye

 0000-0003-0824-2357

Okan Cetin
[2] Division of Hematology, Department of Internal Medicine, Istanbul Faculty of Medicine, Istanbul University, Istanbul, Turkiye

 0000-0003-1672-4743

Abdullah Savas
[2] Division of Hematology, Department of Internal Medicine, Istanbul Faculty of Medicine, Istanbul University, Istanbul, Turkiye

 0009-0008-5221-0938

Mustafa Nuri Yenerel
[2] Division of Hematology, Department of Internal Medicine, Istanbul Faculty of Medicine, Istanbul University, Istanbul, Turkiye

 0000-0002-6473-1342

Sukru Palanduz
[1] Division of Medical Genetics, Department of Internal Medicine, Istanbul Faculty of Medicine, Istanbul University, Istanbul, Turkiye

 0000-0002-9435-009X

REFERENCES

1. Hallek M. Chronic lymphocytic leukemia: 2025 update on the epidemiology, pathogenesis, diagnosis, and therapy. Am J Hematol 2025; 100(3): 450-80.
2. Shadman M. Diagnosis and treatment of chronic lymphocytic leukemia: a review. JAMA 2023;329(11): 918-32.
3. Rai KR, Sawitsky A, Cronkite EP, Chanana AD, Levy RN, Pasternack BS. Clinical staging of chronic lymphocytic leukemia Blood 1975; 46(2): 219-34.
4. Binet JL, Auquier A, Dighiero G, Chastang C, Piguet H, Goasguen J, et al. A new prognostic classification of chronic lymphocytic leukemia derived from a multivariate survival analysis. Cancer 1981; 48(1): 198-206.
5. Tadmor T, Levy I. Richter transformation in chronic lymphocytic leukemia: update in the era of novel agents. Cancers (Basel) 2021; 13(20): 5141.
6. Döhner H, Stilgenbauer S, Benner A, Leupolt E, Kröber A, Bullinger L, et al. Genomic aberrations and survival in chronic lymphocytic leukemia. N Engl J Med 2000; 343(26): 1910-6.
7. Rosenquist R, Cortese D, Bhoi S, Mansouri L, Gunnarsson R. Prognostic markers and their clinical applicability in chronic lymphocytic leukemia: where do we stand? Leuk Lymphoma 2013; 54(11): 2351-64.
8. Innocenti I, Benintende G, Tomasso A, Fresa A, Autore F, Larocca LM, et al. Richter transformation in Chronic Lymphocytic Leukemia. Hematol Oncol 2023; 41(3): 293-300.
9. Van Dyke DL, Werner L, Rassenti LZ, Neuberg D, Ghia E, Heerema NA, et al. The Dohner fluorescence in situ hybridization prognostic classification of chronic lymphocytic leukaemia (CLL): the CLL Research Consortium experience. Br J Haematol 2016; 173(1): 105-13.
10. Roos-Weil D, Nguyen-Khac F, Chevret S, Touzeau C, Roux C, Lejeune J, et al. FILO working group. Mutational and cytogenetic analyses of 188 CLL patients with trisomy 12: A retrospective study from the French Innovative Leukemia Organization (FILO) working group. Genes Chromosomes Cancer 2018; 57(11): 533-40.
11. Puiggros A, Blanco G, Espinet B. Genetic abnormalities in chronic lymphocytic leukemia: where we are and where we go. Biomed Res Int 2014; 2014: 435983.
12. Strati P, Abruzzo LV, Wierda WG, O'Brien S, Ferrajoli A, Keating MJ. Second cancers and Richter transformation are the leading causes of death in patients with trisomy 12 chronic lymphocytic leukemia. Clin Lymphoma Myeloma Leuk 2015; 15(7): 420-27.
13. Del Giudice I, Rossi D, Chiaretti S, Marinelli M, Tavolaro S, Gabrielli S, et al. NOTCH1 mutations in +12 chronic lymphocytic leukemia (CLL) confer an unfavorable prognosis, induce a distinctive transcriptional profiling and refine the intermediate prognosis of +12 CLL. Haematologica 2012; 97(3): 437-41.
14. Van Dyke DL, Shanafelt TD, Call TG, Zent CS, Smoley SA, Rabe KG, et al. A comprehensive evaluation of the prognostic significance of 13q deletions in patients with B-chronic lymphocytic leukaemia. Br J Haematol 2010; 148(4): 544-50.
15. Stankovic T, Skowronska A. The role of ATM mutations and 11q deletions in disease progression in chronic lymphocytic leukemia. Leuk Lymphoma 2014; 55(6): 1227-39.
16. De Viron E, Michaux L, Put N, Bontemps F, Van Den Neste E. Present status and perspectives in functional analysis of p53 in chronic lymphocytic leukemia. Leuk Lymphoma 2012; 53(8): 1445-51.
17. Te Raa GD, Kater AP. TP53 dysfunction in CLL: Implications for prognosis and treatment. Best Pract Res Clin Haematol 2016; 29(1): 90-9.
18. Kwok M, Agathanggelou A, Davies N, Stankovic T. Targeting the p53 pathway in CLL: state of the art and future perspectives. Cancers (Basel) 2021; 13(18): 4681.
19. Malcikova J, Smardova J, Rocnova L, Tichy B, Kuglik P, Vranova V, et al. Monoallelic and biallelic inactivation of TP53 gene in chronic lymphocytic leukemia: selection, impact on survival, and response to DNA damage. Blood 2009; 114(26): 5307-14.
20. Catherwood MA, Gonzalez D, Donaldson D, Clifford R, Mills K, Thornton P. Relevance of TP53 for CLL diagnostics. J Clin Pathol 2019; 72(5): 343-46.
21. Cuneo A, Rigolin GM, Bigoni R, De Angeli C, Veronese A, Cavazzini F, et al. Chronic lymphocytic leukemia with 6q- shows distinct hematological features and intermediate prognosis. Leukemia 2004; 18(3): 476-83.
22. Audil HY, Hampel PJ, Van Dyke DL, Achenbach SJ, Rabe KG, Smoley SA, et al. The prognostic significance of del6q23 in chronic lymphocytic leukemia. Am J Hematol 2021; 96(6): E203-E206.
23. Jarosova M, Hruba M, Oltova A, Plevova K, Kruzova L, Kriegova E, et al. Chromosome 6q deletion correlates with poor prognosis and low relative expression of FOXO3 in chronic lymphocytic leukemia patients. Am J Hematol 2017; 92(10): E604-E607.
24. Qiu HX, Xu W, Cao XS, Zhou M, Shen YF, Xu YL, et al. Cytogenetic characterisation in Chinese patients with chronic lymphocytic leukemia: a prospective, multicenter study on 143 cases analysed with interphase fluorescence in situ hybridisation. Leuk Lymphoma 2008; 49(10): 1887-92.

25. Wang DM, Miao KR, Fan L, Qiu HR, Fang C, Zhu DX, et al. Intermediate prognosis of 6q deletion in chronic lymphocytic leukemia. Leuk Lymphoma 2011; 52(2): 230-37.

26. Cavazzini F, Ciccone M, Negrini M, Rigolin GM, Cuneo A. Clinicobiologic importance of cytogenetic lesions in chronic lymphocytic leukemia. Expert Rev Hematol 2009; 2(3): 305-14.

27. Davids MS, Vartanov A, Werner L, Neuberg D, Dal Cin P, Brown JR. Controversial fluorescence in situ hybridization cytogenetic abnormalities in chronic lymphocytic leukaemia: new insights from a large cohort. Br J Haematol 2015; 170(5): 694-703.

28. Montserrat E, Bauman T, Delgado J. Present and future of personalized medicine in CLL. Best Pract Res Clin Haematol 2016; 29(1): 100-10.

29. Wan Mohamad Zamri WN, Mohd Yunus N, Abdul Aziz AA, Zulkipli NN, Sulong S. Perspectives on the application of cytogenomic approaches in chronic lymphocytic leukaemia. diagnostics (Basel) 2023; 13(5): 964.

30. Strati P, Parikh SA, Chaffee KG, Kay NE, Call TG, Achenbach SJ, et al. Relationship between co-morbidities at diagnosis, survival and ultimate cause of death in patients with chronic lymphocytic leukaemia (CLL): a prospective cohort study. Br J Haematol 2017; 178(3): 394-402.

İSTANBUL UNIVERSITY PRESS

Experimed

Research Article

Open Access

Relationship between Cyberbullying, Victimization and Depression among High School Students in Turkiye

Cem Uysal [1] ✉, Tugba Cobanoglu [2] , Neslim Guvendeger Doksat [3] , Zeliha Yildirim [4] , Humeyra Aslan [5] , Mahi Aslan [6] , Feyza Inceoglu [7] , Oguz Polat [8]

[1] Department of Forensic Medicine, Dicle University, Diyarbakir, Turkiye
[2] Department of Child Psychiatry, Turgut Ozal University, Malatya, Turkiye
[3] Department of Psychology, Beykent University, Istanbul, Turkiye
[4] Council of Forensic Medicine, Diyarbakir Group Presidency, Diyarbakir, Turkiye
[5] Council of Forensic Medicine, Yozgat Branch Office, Yozgat, Turkiye
[6] Institute of Health Sciences, Department of Forensic Science, Acibadem Mehmet Ali Aydinlar University, Istanbul, Turkiye
[7] Department of Biostatistics, Faculty of Medicine, Malatya Turgut Ozal University, Malatya, Turkiye
[8] Department of Forensic Medicine, Acibadem Mehmet Ali Aydinlar University, Istanbul, Turkiye

Abstract

Objective: This study aimed to investigate the relationship between depression, cyberbullying, and cybervictimization among high school students in the Diyarbakir region during the post-pandemic period of COVID-19.

Materials and Methods: A total of 1,985 high school students (1,057 females and 928 males), aged 13 to 18, from the Diyarbakir province participated in this cross-sectional survey. Participants completed the Bullying and Cyberbullying Scale for Adolescents (BCS-A) and the Beck Depression Inventory (BDI). Sociodemographic characteristics and computer and internet usage behaviours were evaluated as factors influencing the scale scores.

Results: Cyberbullying was found to be more prevalent among male students with higher access to digital devices (computers, phones, tablets) and longer internet use, particularly those whose mothers had higher education levels. Conversely, elevated BDI scores were observed among female students in the tenth grade who attended public schools, had more than four siblings, and had limited access to technological resources. Statistically significant positive correlations were identified between the BDI scores and both the bullying perpetration and victimization scores.

Conclusion: This study highlights the growing impact of digital aggression on adolescent mental health in Turkiye and underscores the importance of targeted forensic-psychiatric screening and early preventive strategies in high school populations.

Keywords Cyberbullying · Cybervictimization · Adolescent Mental Health · Beck Depression Inventory (BDI) · Internet Use · COVID-19 Pandemic

✉ Corresponding author: Cem Uysal drcemuysal@gmail.com

INTRODUCTION

Bullying and its adverse effects are now widely acknowledged as significant public health concerns worldwide (1). As technology has become more embedded in daily life, bullying behaviors have evolved into new digital forms, commonly referred to as cyberbullying (2, 3). This form of aggression encompasses repeated, intentional actions carried out via digital platforms—such as mocking, exclusion, public shaming, rumor dissemination, or non-consensual disclosure of personal information (4).

The rapid proliferation of social media, particularly among adolescents, has increased their vulnerability to such behaviors (5). For instance, a recent nationwide study in the United States reported that 46% of teenagers between 13 and 17 years had experienced at least one incident of cyberbullying (6). Global estimates vary significantly, with prevalence rates ranging from 14% to 58%.

Unlike conventional bullying, which typically occurs in physical settings, cyberbullying is often anonymous and might happen at any time, making it more persistent and difficult to address (7, 8). The lasting visibility of online content can intensify psychological harm, leading to severe emotional distress (9). Victims of cyberbullying are more likely to experience self-injurious behavior, suicidal ideation, and even attempts at suicide (10).

Cyberbullying is therefore characterized by repetitive and intentional acts of aggression using electronic communication, with considerable potential for perceived and actual harm to the individual (11). While digital technologies provide new avenues for communication, they also present unique risks for harmful interpersonal behaviors that require targeted public health and educational interventions.

In Turkiye, despite the growing digital engagement among adolescents, regionally grounded data on cyberbullying and its psychological impacts remain limited. Given the increased reliance on digital education during and after the COVID-19 pandemic, high school students have become particularly vulnerable to cyber aggression. Therefore, this study was designed to address the gap in localized data and to examine the interaction between cyberbullying, victimization, and depression levels in a representative adolescent population.

MATERIALS AND METHODS

Participants

This study used a cross-sectional survey to investigate how common cyberbullying and cybervictimization are among high school students in the province of Diyarbakir, Turkiye, and

how these experiences play out. Prior to data collection, the research team obtained ethical approval from the Non-Interventional Research Ethics Committee at Dicle University, Faculty of Medicine. After receiving approval from the Provincial Directorate of National Education, they randomly selected public high schools from the area.

In accordance with national education research protocols and as permitted by the Ministry, participation was considered ethically acceptable within the institutional framework approved by the local education authority. The survey was conducted anonymously, and participation was entirely voluntary. The target population consisted of students in grades 9 to 11, an age group identified as particularly susceptible to online risks due to increased internet use for education and communication during the COVID-19 pandemic.

Demographic Characteristics

The demographic characteristics of the study samples are presented in Table 1. A total of 1,985 students participated, consisting of 1,057 females and 928 males. Age distribution included 412 students aged 14, 799 aged 15, and 633 aged 16. Most participants were in the 10th grade (n=153), and the majority were attending public schools (n=1,695).

In terms of familial and socioeconomic indicators, 1,006 students reported having more than four siblings. The mothers of the participants had varying levels of education: 326 were illiterate, 456 had completed primary school, and 341 were university graduates. The fathers' educational levels also varied, with 388 primary school, 450 high school, and 441 university graduates.

Tests: Bullying, being bullied and beck depression inventory (BDI) scales were applied in the survey.

Bullying and Cyberbullying Scale for Adolescents (BCS-A): Thomas et al. created the BCS-A to measure both bullying and victim experiences in teenagers between 12 and 18 years old (12). The original scale showed strong internal consistency across its different areas. For the victimization subscale, the Cronbach's alpha scores were 0.72 for physical, 0.92 for verbal, 0.66 for relational, and 0.83 for cyberbullying. For the bullying subscale, the scores were 0.69 for physical, 0.92 for verbal, 0.69 for relational, and 0.92 for cyber forms.

Later, a Turkish version of the BCS-A was translated and validated by Ozbey and Basdas (13). They designed two matching forms, each with 13 items that covered the same four categories. In the Turkish version, all factor loadings were strong—above 0.630 in the victim section and 0.679 in the bullying section. Reliability scores (Cronbach's alpha) ranged from 0.606 to 0.806 for victimization and from 0.616 to 0.815

for bullying. These numbers suggest that the scale works well in Turkish too.

Table 1. Demographics information of the participants

Variables	Group	Number	Percentage
Gender	Female	1,057	53.2
	Male	928	46.8
Age, years	13	28	1.4
	14	412	20.8
	15	799	40.3
	16	633	31.9
	17	99	5.0
	18	14	0.7
Class	9	684	34.5
	10	1,153	58.1
	11	148	7.5
School	State School	1,695	85.4
	Private School	290	14.6
Number of Siblings	0	7	0.4
	One	63	3.2
	2	368	18.5
	3	541	27.3
	≥4	1,006	50.7
Mother's Education Status	Illiterate	326	16.4
	Literate	211	10.6
	Primary School	456	23.0
	Middle School	260	13.1
	High School	300	15.1
	University	341	17.2
	Master/ PhD	91	4.6
Father's Education Status	Illiterate	104	5.2
	Literate	103	5.2
	Primary School	388	19.5
	Middle School	349	17.6
	High School	450	22.7
	University	441	22.2
	Master/ PhD	150	7.6
Parents' Marital Status	Married	1,833	92.3
	Divorced	77	3.9
	Stepmother	10	0.5
	Stepfather	7	0.4
	Mother Not Alive	13	0.7
	Father Not Alive	45	2.3
Personal Computer	Yes	500	25.2
	No	1,485	74.8
Personal Mobile Phone	Yes	1,232	62.1
	No	753	37.9

Variables	Group	Number	Percentage
Internet	Yes	1,236	62.3
		345	17.4
	No	1,016	51.2
Do you do homework online?	Yes	1,215	61.2
	No	315	15.9
Do you play games on the internet?	Yes	534	26.9
	No	1,194	60.2
Do you access social networks on the internet?	Yes	991	49.9
	No	994	50.1
Other	Yes	216	10.9
	No	1,769	89.1

BDI: BDI is a widely used 21-question self-report tool for measuring how severe someone's depressive symptoms are. Each question is scored on a scale from 0 to 3, with higher scores showing stronger symptoms. The Turkish version has been tested and found to be reliable. According to Hisli and Onalan et al., it has an internal consistency score of 0.80 (14, 15).

Validity and Reliability

To ensure these tools are trustworthy and meaningful for the study, researchers looked at how consistent and valid they are. Reliability was checked using Cronbach's alpha for the main tools: the BDI, the bullying scale, and the cyberbullying victimization scale. These results are detailed in Table 2.

To check if the tools used in the study were measuring what they were supposed to, two main stats were used: Composite reliability (CR) and average variance extracted (AVE). CR looks at how well the items on a scale reflect the bigger concept they're meant to measure. It's like Cronbach's alpha, and a score of 0.70 or higher usually means it's reliable. AVE, on the other hand, shows how much of the total variation in responses is explained by the concept being measured. A value above 0.50 suggests that the scale has good convergent validity—basically, that everything fits together well.

When checking the reliability of the tools, Cronbach's alpha scores came out strong, ranging from 0.90 to 1.00, which points to excellent internal consistency. These scores were based on

Table 2. Descriptive statistics of scale scores

Points	Mean ± SD	Min - Max	Cronbach α	AVE	CR
Cyberbullying Victimization	6.5 ± 2.99	0 - 25	0.934	0.55	0.86
Cyberbullying	6.15 ± 3.2	0 - 25	0.779	0.67	0.91
BDI	24.54 ± 16.59	0 - 80	0.863	0.51	0.96

SD: Standard Deviation; Min: Minimum; Max: Maximum; CR: Composite reliability; AVE: Average Variance Extracted; BDI: Beck Depression Inventory.

Table 3. Comparison of scale scores according to sociodemographic data

Variables	Groups	Cyberbullying Victimization		Cyberbullying		BDI	
		Mean ± SD	M (Min - Max)	Mean ± SD	M (Min - Max)	Mean ± SD	M (Min - Max)
Gender	Female	6.37 ± 2.69	5(0-25)	5.73 ± 2.41	5(0-25)	25.85 ± 14.78	23(0-80)
	Male	6.64 ± 3.29	5(0-25)	6.64 ± 3.85 [a]	5(0-25)	23.05 ± 18.32 [a]	19(0-80)
p value		0.596*		**0.001***		**0.001***	
Age	13	7.57 ± 3.58	6(5-18)	7.75 ± 5.04	5(5-25)	30.46 ± 21.2	26.5(1-80)
	14	6.5 ± 2.89	5(0-25)	6.00 ± 2.74	5(0-25)	22.57 ± 15.26	20(0-80)
	15	6.44 ± 2.97	5(0-25)	5.91 ± 2.83	5(0-25)	24.46 ± 16.27	21(0-80)
	16	6.44 ± 2.94	5(2-25)	6.48 ± 3.82	5(0-25)	25.56 ± 17.23	23(0-80)
	17	6.99 ± 3.56	5(5-25)	6.15 ± 2.43	5(0-16)	25.12 ± 18.47	21(0-80)
	18	7.14 ± 3.11	6(5-14)	6.64 ± 3.75	5(5-19)	25.29 ± 14.17	23.5(6-55)
p value		0.120**		0.051**		0.093**	
Class	9	6.46 ± 2.87	5(0-25)	6.11 ± 2.91	5(0-25)	22.72 ± 16.2	19(0-80)
	10	6.52 ± 3.1	5(0-25)	6.16 ± 3.4	5(0-25)	25.83 ± 16.86 [a]	23(0-80)
	11	6.53 ± 2.68	5(5-19)	6.34 ± 2.93	5(0-25)	22.92 ± 15.35	20(0-80)
p value		0.517 **		0.051**		**0.001****	
School	State	6.53 ± 3.06	5(0-25)	6.14 ± 3.24	5(0-25)	25.34 ± 17.16	22(0-80)
	Private	6.33 ± 2.54	5(5-24)	6.22 ± 2.98	5(5-25)	19.9 ± 11.77 [a]	18.5(0-71)
p value		0.383*		0.076*		**0.001***	
Number of Siblings	0	10.17 ± 7.86	6.5(5-25)	6.00 ± 2.45	5(5-11)	31.67 ± 26.39	27(2-80)
	1	6.86 ± 3.73	6(5-25)	6.37 ± 3.17	5(5-25)	26.24 ± 17.78	23(0-80)
	2	6.57 ± 3.3	5(2-25)	6.44 ± 3.75	5(0-25)	21.19 ± 14.06	18(0-80)
	3	6.48 ± 2.56	5(5-21)	6.30 ± 3.16	5(0-25)	23.56 ± 16.24	20(0-80)
	≥4	6.44 ± 2.98	5(0-25)	5.96 ± 3.00 [a]	5(0-25)	26.14 ± 17.27 [a]	23(0-80)
p value		0.202**		**0.004****		**0.001****	
Mother's Education	Illiterate	6.44 ± 2.88	5(0-25)	5.91 ± 2.88	5(0-25)	27.26 ± 19.14	23(0-80)
	Literate	6.13 ± 2.97	5(0-25)	6.06 ± 3.31	5(0-25)	26.61 ± 17.42	23(0-80)
	Primary	6.55 ± 2.99	5(0-25)	6.04 ± 3.1	5(0-25)	26.06 ± 16.69	23(0-80)
	Middle school	6.56 ± 3.15	5(0-25)	6.06 ± 2.97	5(0-25)	25.2 ± 17.58	21(0-80)
	High school	6.78 ± 3.07 [a]	5(5-25)	6.07 ± 2.71	5(5-25)	24.07 ± 15.35	21(0-80)
	University	6.56 ± 3.14	5(4-25)	6.55 ± 3.84	5(5-25)	20.07 ± 12.81 [a]	18(0-80)
	Master's/PhD	5.97 ± 1.82	5(5-14)	6.88 ± 3.84 [a]	5(5-25)	18.89 ± 13.3 [a]	18(0-70)
p value		**0.024****		**0.006****		**0.001****	
Father's Education	Illiterate	6.85 ± 3.84	5(4-25)	6.65 ± 3.77	5(5-25)	29.36 ± 19.3 [a]	24(0-80)
	Literate	6.28 ± 2.12	5(4-14)	6.27 ± 3.59	5(5-25)	25.79 ± 16.26	24(0-80)
	Primary	6.43 ± 3.04	5(0-25)	5.66 ± 2.37 [a]	5(0-25)	26.78 ± 17.3	23(0-80)
	Middle school	6.55 ± 3.26	5(0-25)	5.99 ± 3.04	5(0-25)	25.94 ± 18.22	22(0-80)
	High school	6.46 ± 2.78	5(3-25)	6.18 ± 3.13	5(0-25)	25.19 ± 16.86	21(0-80)
	University	6.63 ± 3.14	5(4-25)	6.41 ± 3.58	5(5-25)	21.14 ± 13.38	20(0-80)
	Master's/PhD	6.2 ± 2.1	5(5-15)	6.57 ± 3.64	5(5-25)	19.28 ± 13.76 [b]	17(0-70)
p value		0.718**		**0.006 ****		**0.001****	
Parent's Marital Status	Married	6.48 ± 2.97	5(0-25)	6.12 ± 3.15	5(0-25)	24.59 ± 16.73	21(0-80)
	Divorced	6.82 ± 3.48	5(3-25)	6.95 ± 4.7	5(5-25)	23.12 ± 14.95	21(0-80)
	Stepmother	9.1 ± 5.47	6(5-18)	5.9 ± 1.66	5(5-9)	35 ± 16.17	29.5(19-64)
	Stepfather	5.29 ± 0.49	5(5-6)	6.14 ± 3.02	5(5-13)	17.57 ± 12.11	22(0-32)
	Mother Not Alive	6.69 ± 1.7	6(5-11)	6.54 ± 3.53	5(5-18)	27 ± 18.2	24(7-80)
	Father Not Alive	6.16 ± 2.31	5(5-17)	6.07 ± 2.29	5(5-14)	22.96 ± 12.89	18(2-56)
p value		0.220 **		0.745 **		0.258 **	

Superscripts ([a,b]) show the differences within the group. There is no difference in the measurement that takes place with the same letters. SD: Standard Deviation; M: Median; Min: Minimum; Max: Maximum; BDI: Beck Depression Inventory; *: Mann-Whitney U Test; **: Kruskal-Wallis Test.

Table 4. Comparison of scale scores according to computer use

Variables	Groups	Cyberbullying Victimization		Cyberbullying		BDI	
		Mean ± SD	Median (Min - Max)	Mean ± SD	Median (Min - Max)	Mean ± SD	Median (Min - Max)
Number of Computers at Home	One	6.3 ± 2.82	5(0-25)	5.52 ± 1.99 [a]	5(0-25)	28.73 ± 19.19 [a]	24(0-80)
	Two	6.62 ± 3.15	5(0-25)	6.32 ± 3.56	5(0-25)	24.36 ± 15.93 [b]	22(0-80)
	Three	6.63 ± 3.06	5(0-25)	6.58 ± 3.62 [b]	5(0-25)	22.73 ± 14.65 [c]	20(0-80)
	≥4	6.41 ± 2.81	5(5-25)	6.33 ± 3.38	5(5-25)	20.12 ± 13.79	18(0-80)
p value		0.279 **		**0.001****		**0.00****	
Having a Personal Computer	Yes	6.62 ± 3.17	5(0-25)	6.75 ± 3.99	5(0-25)	21.7 ± 15.17	19(0-80)
	No	6.46 ± 2.93	5(0-25)	5.95 ± 2.86 [a]	5(0-25)	25.5 ± 16.94 [a]	22(0-80)
p value		0.356*		**0.001***		**0.001***	
Having a Personal Mobile Phone	Yes	6.56 ± 3.04	5(0-25)	6.42 ± 3.58	5(0-25)	23.22 ± 16.14	20(0-80)
	No	6.4 ± 2.9	5(0-25)	5.73 ± 2.4 [a]	5(0-25)	26.7 ± 17.09 [a]	23(0-80)
p value		0.279*		**0.001***		**0.001***	
Having a Personal Tablet	Yes	6.4 ± 2.95	5(0-25)	6.32 ± 3.46	5(0-25)	22.31 ± 15.5	20(0-80)
	No	6.54 ± 3.01	5(0-25)	6.08 ± 3.08 [a]	5(0-25)	25.52 ± 16.96 [a]	22(0-80)
p value		0.412*		**0.039***		**0.001***	
Having an Internet	Yes	6.56 ± 3.19	5(0-25)	6.38 ± 3.48	5(0-25)	23.75 ± 15.96	21(0-80)
	No	6.39 ± 2.63	5(0-25)	5.79 ± 2.66 [a]	5(0-25)	25.82 ± 17.49 [a]	22(0-80)
p value		0.961*		**0.001***		**0.011***	
How Do You Connect to the Internet?	Home	6.5 ± 3.05	5(0-25)	6.2 ± 3.21	5(0-25)	23.6 ± 15.76	21(0-80)
		6.7 ± 3.16	5(0-25)	6.35 ± 3.8	5(0-25)	25.59 ± 16.92	23(0-80)
	Mobile Phone	6.18 ± 2.57	5(2-25)	5.8 ± 2.65	5(0-25)	26.4 ± 18.44	23(0-80)
	Tablet	6.8 ± 2.56	6(3-15)	6 ± 1.9	5(5-15)	26.48 ± 18.23	26(0-80)
	Computer	7.23 ± 3.72	5(5-18)	6.38 ± 3.18	5(5-14)	29.46 ± 21.79	31(4-80)
p value		0.053 **		0.139 **		0.063 **	
Is your internet usage supervised?	Yes	6.4 ± 2.7	5(0-25)	5.99 ± 2.7	5(0-25)	24.15 ± 16.43	21(0-80)
	No	6.6 ± 3.24	5(0-25)	6.31 ± 3.61	5(0-25)	24.91 ± 16.74	22(0-80)
p value		0.884*		0.641*		0.224*	
How often do you use the internet?	Always	6.9 ± 3.52 [a]	5(4-25)	7.23 ± 4.66 [a]	5(0-25)	27.19 ± 18.45	23(0-80)
	> 3 hours online daily	6.66 ± 3.16 [a]	5(2-25)	6.23 ± 3.08	5(0-25)	26.13 ± 15.18	24(0-80)
	2-3 hours online daily	6.36 ± 2.78	5(0-25)	5.86 ± 2.63	5(0-25)	22.13 ± 15.19 [a]	19(0-80)
	≤ one hour online daily	6 .00± 2.11	5(0-18)	5.54 ± 1.8	5(0-19)	23.13 ± 17.43	20(0-80)
	Online every 2-3 days	6.08 ± 2.44	5(0-15)	5.21 ± 0.96	5(0-8)	23.58 ± 13.24	22.5(2-80)
	Once a week	6.30 ± 2.2	5(4-13)	5.38 ± 0.92	5(5-9)	26.68 ± 22.58	21(0-80)
	Rarely	6.82 ± 3.59	5(5-25)	5.69 ± 2.72	5(5-25)	27.42 ± 17.41	23(0-80)
p value		**0.007****		**0.001****		**0.001****	

Superscripts ([a,b,c]) show the differences within the group. There is no difference in the measurement that takes place with the same letters. SD: Standard Deviation; M: Median; Min: Minimum; Max: Maximum; BDI: Beck Depression Inventory; *: Mann-Whitney U Test; **: Kruskal-Wallis Test.

factor loadings obtained through exploratory factor analysis (EFA). EFA helps uncover hidden patterns or "factors" among a group of related items, trimming things down to the core ideas. The results backed up the tools' reliability and showed that they were valid in terms of structure.

Statistical Analyses

All statistical analyses were performed using SPSS version 25 (SPSS Inc., Chicago, IL, USA). First, the Kolmogorov–Smirnov test was run to see if the data followed a normal curve. Depending on how the data were spread out, results were shown as mean ± standard deviation or as median with the lowest and highest values included.

To check for differences between the two separate groups, the researchers used the Mann–Whitney U test. If they needed to compare more than two groups, they used the Kruskal–Wallis test. Furthermore, when this test showed a significant result, they followed up with a post hoc test using the Bonferroni correction to keep things accurate and avoid false positives.

To understand how the different scale scores were related to each other, Pearson's correlation coefficient was used. Any p-value below 0.05 was seen as a sign that the result was statistically significant.

RESULTS

A comparison of the test scores and demographic data of the students participating in the study is presented in Table 3. The female BDI score was significantly higher than that of the males, and the male bullying scale score was significantly higher than that of the females (p=0.001). The BDI scores of those in the tenth grade were significantly higher than those in the ninth grade. The BDI score of those who attended public school was significantly higher than those who attended private school. The bullying scale scores of those with more than four siblings were significantly lower than those with one or three siblings. The BDI score of those with more than four siblings was higher than that of those with two or three siblings, and the BDI score of those with one sibling was higher than that of those with two siblings. The bullying scale scores of those whose mothers were master's/doctoral graduates were higher than those whose mothers were illiterate. The BDI score of those whose mothers were master's/doctoral graduates and whose mothers were university graduates was significantly lower than that of others. The bullying scale scores of those whose fathers were university graduates and whose fathers were masters/doctoral graduates were higher than those whose fathers were primary school graduates. The BDI scores of those whose fathers were university graduates and whose fathers were masters/doctoral graduates were significantly lower than those of the other groups. There was no significant difference in terms of other parameters and test scores.

The relationships between the test scores, computer use, and internet habits of the students participating in the study are presented in Table 4. The bullying scale scores of those who had more than one computer at home were significantly higher than those who had one computer at home. As the number of computers at home increased, the BDI score decreased significantly. The bullying scale scores were higher among those who had a personal computer than those who did not, those who had a personal mobile phone than those who did not, those who had a personal tablet than those who did

Table 5. Examining the relationships between scale scores by correlation analysis

Points	Value	BDI	Cyberbullying
Cyberbullying Victimization	r	0.265	0.392
	p	**0.001**	**0.001**
Cyberbullying	r	0.247	
	p	0.043	

r: Pearson correlation analysis; p: Statistical significance; BDI: Beck Depression Inventory.

Table 6. Regression analysis of the relationship between scale total scores in groups

Dependent	Independent	R²	F test	p₁ value	β₁	t- test	p₂ value
BDI	**Still**	0.028	28.189	0.001*	**18.978**	19.357	**0.001***
	Stop by				0.968	7.223	**0.001***
	To do				−0.118	−0.946	0.344

BDI: Beck Depression Inventory; R² : Explanatory Coefficient; **p₁<0.05: F test result for the significance of the model; β₁: Non-standardized regression coefficients; *p₂<0.05: t test result for the significance of the regression coefficients.

did not, and those who had an internet connection compared to those who did not. BDI scores were lower among those who had a personal computer than those who did not, those who had a personal mobile phone than those who did not, those who had a personal tablet than those who did not, and those who had an internet connection compared to those who did not. The bullying scale score of those who were constantly connected to the Internet was significantly higher than that of the other groups who were connected to the Internet for less than 3 hours a day. The BDI score of those who were constantly connected to the internet and who were connected for more than 3 hours was higher than those who were connected for 2-3 hours a day and less than an hour a day. No significant difference was observed in terms of other parameters and test scores.

Correlations and regression analysis between test scores are given in Table 5 and 6. There were low positive correlations between BDI and bullying scale and being bullied scale scores. There was a moderate positive correlation between bullying and being bullied scale scores.

DISCUSSION

In this study, the internet use and related cyberbullying, cyberbullying victimization and BDI scores of 1,985 high school students in Diyarbakir, Turkiye were evaluated. BDI scores were higher for women than for men, for those who studied in public schools than for those who studied in private schools and for those whose mothers and fathers had lower education levels than those who did not. Additionally, those who did not own a personal computer, tablet, phone, or internet had higher BDI scores than those who did. Moreover, a positive

significant relationship was determined between exposure to cyberbullying and BDI scores.

Extensive research has consistently linked bullying involvement—whether as a victim, perpetrator, or both—to adverse mental health outcomes and reduced life satisfaction (16-18). Victims of bullying frequently display internalizing symptoms such as anxiety, depression, fearfulness, and social withdrawal, whereas perpetrators tend to exhibit externalizing behaviours including aggression, delinquency, and impulsivity (19-21). Adolescents who occupy dual roles—as both bullies and victims—appear to be at even greater psychological risk, showing elevated levels of both internalizing and externalizing problems (22).

The rise in cyberbullying has paralleled the increasing integration of internet technologies into the daily lives of adolescents, particularly those belonging to Generation Z (23). A cross-national analysis involving over 180,000 adolescents from 35 countries found that individuals from cultures valuing self-expression reported lower rates of bullying behavior, while all forms of bullying exposure were associated with decreased quality of life (24). Evidence suggests that adolescents who experience cybervictimization may respond through avoidance, denial, or even retaliatory bullying (25). Moreover, cybervictimization has been linked to elevated risks of stress, substance abuse, low self-esteem, suicidal ideation, and feelings of shame or rage (26). In alignment with these findings, our study identified a significant positive correlation between cyberbullying exposure and depressive symptomatology, as measured by BDI scores. These results underscore the necessity of implementing educational and clinical interventions that promote adolescent awareness of cyber aggression and ensure access to appropriate psychiatric care.

Understanding the factors that influence both cyberbullying perpetration and victimization is essential for designing targeted interventions. Although some research has suggested that girls are more frequent victims and boys more often perpetrators of cyber aggression (27), other studies indicate a more nuanced picture. For instance, while Cook et al. and Slonje and Smith reported no significant gender differences in exposure, Guo and Unver & Koc noted that males may demonstrate higher levels of perpetration (8, 28-30). In contrast, other analyses, including those by Yigit et al. and Kowalski et al., found mixed or inconclusive patterns (2, 31). A recent meta-analysis highlighted gender as a moderate factor in predicting cyberbullying, with males tending to engage more in perpetration and females being more susceptible to victimization . In our study, male students were significantly more likely to engage in cyberbullying

behaviors than females, which aligns with previous findings in the Turkish context. However, no gender-based difference was observed in cyberbullying victimization. Similarly, age was not found to significantly influence bullying dynamics, consistent with studies limited to adolescent populations (32, 33).

Another noteworthy finding of our study relates to the influence of sibling numbers on cyberbullying dynamics. Prior work by Chen et al. suggested that sibling presence may offer a protective buffer against online aggression, possibly due to emotional or digital peer support (34). Supporting this, Cagirkan and Bilek reported lower cyberbullying scores among students with two or more siblings (35). In our analysis, students with four or more siblings exhibited significantly lower bullying scale scores than those with fewer siblings. However, the BDI scores presented a more complex picture: while students with no siblings had the highest depression scores, even those with more than four siblings showed elevated BDI scores compared to students with two or three siblings. This suggests that while a greater number of siblings may be associated with reduced cybervictimization, it does not uniformly buffer against depressive symptoms. The inverse relationship observed between depression severity and the number of siblings—especially in single-child households—may reflect additional psychological vulnerabilities associated with isolation or reduced familial interaction.

Prior research has consistently demonstrated that owning personal electronic devices and engaging in prolonged internet use are key predictors of increased exposure to cyber aggression (2, 36). A Turkish study noted that adolescents who possess a computer at home and use it for leisure activities tend to have higher levels of both cyberbullying perpetration and victimization. Similarly, adolescents who spend more than four hours online daily or engage in internet use after 11:00 p.m. have been reported to score significantly higher on cyberbullying-related scales (29, 37).

Cagirkan and Bilek further observed that students with their own mobile phones and private internet access are more likely to engage in cyberbullying (35). Our findings are in alignment, indicating that adolescents with access to personal devices (computers, tablets, and smartphones) and unrestricted internet connectivity reported higher levels of perpetration. Interestingly, no statistically significant association was observed between device ownership and cybervictimization. Moreover, frequent and extended internet usage—exceeding two to three hours per day—was associated with elevated scores in cyberbullying, victimization , and depressive symptoms (as measured by the BDI).

Adolescents often refrain from reporting negative online experiences to their parents, fearing restrictions on internet access or mobile phone use (25). This lack of disclosure undermines parental control efforts. Korkmaz reported that approximately half of adolescents use the Internet without supervision and that unsupervised youth are significantly more prone to engage in cyberbullying (38). Dehue et al. also found that many parents remain unaware of their children's experiences with cyber aggression (39). Although our study did not establish a significant relationship between parental internet monitoring and cyberbullying outcomes, this may reflect a broader pattern of inadequate digital oversight and limited parental awareness.

CONCLUSION

The findings of this study demonstrate a significant positive correlation between depressive symptom severity, as measured by the BDI, and both cyberbullying perpetration and victimization scores. Furthermore, a statistically meaningful relationship was identified between being a victim of cyberbullying and subsequently engaging in perpetration, indicating that victims may transition into offenders over time.

These results highlight the cyclical and escalating nature of cyber aggression among adolescents, underscoring the urgent need for comprehensive preventive strategies. Protecting vulnerable youth from cyber violence and interrupting the victim-to-perpetrator trajectory requires a multifaceted approach. Educational initiatives should emphasize digital literacy, personal rights, privacy protections, and responsible online behavior from an early age. Moreover, national legal frameworks must be promptly updated to address violations related to online harassment and infringement of digital freedoms.

Author Details

Cem Uysal
[1] Department of Forensic Medicine, Dicle University, Diyarbakir, Turkiye
🆔 0000-0002-7373-9725   ✉ drcemuysal@gmail.com

Tugba Cobanoglu
[2] Department of Child Psychiatry, Turgut Ozal University, Malatya, Turkiye
🆔 0000-0001-5611-2739

Neslim Guvendeger Doksat
[3] Department of Psychology, Beykent University, Istanbul, Turkiye
🆔 0000-0002-5896-0165

Zeliha Yildirim
[4] Council of Forensic Medicine, Diyarbakir Group Presidency, Diyarbakir, Turkiye
🆔 0000-0001-5441-4901

Humeyra Aslan
[5] Council of Forensic Medicine, Yozgat Branch Office, Yozgat, Turkiye
🆔 0000-0002-8749-2399

Mahi Aslan
[6] Institute of Health Sciences, Department of Forensic Science, Acibadem Mehmet Ali Aydinlar University, Istanbul, Turkiye
🆔 0000-0001-9470-1294

Feyza Inceoglu
[7] Department of Biostatistics, Faculty of Medicine, Malatya Turgut Ozal University, Malatya, Turkiye
🆔 0000-0003-1453-0937

Oguz Polat
[8] Department of Forensic Medicine, Acibadem Mehmet Ali Aydinlar University, Istanbul, Turkiye
🆔 0000-0001-8454-6817

REFERENCES

1. Olweus D. Bullying at school: what we know and what we can do. Oxford, UK Blackwell; 1993.

2. Kowalski RM, Giumetti GW, Schroeder AN, Lattanner MR. Bullying in the digital age: a critical review and meta-analysis of cyberbullying research among youth. Psychol Bull 2014; 140(4): 1073-137.

3. Wang J, Iannotti RJ, Nansel TR. School bullying among adolescents in the United States: physical, verbal, relational, and cyber. J Adolesc Health 2009; 45(4): 368-75.

4. Yang X, Huang Y, Li B. Attachment anxiety and cyberbullying victimization in college students: the mediating role of social media self-disclosure and the moderating role of gender. Front Psychol 2023; 14: 1274517.

5. Orben A, Przybylski AK. The association between adolescent well-being and digital technology use. Nat Hum Behav 2019; 3(2): 173-82.

6. Shao IY, Al-Shoaibi AAA, Testa A, Ganson KT, Baker FC, Nagata JM. The Association between family environment and subsequent risk of cyberbullying victimization in adolescents. Acad Pediatr 2024; 24(6): 957-62.

7. Cassidy W, Faucher C, Jackson M. Cyberbullying among youth: A comprehensive review of current international research and its implications and application to policy and practice. School Psychol Int 2013; 34(6): 575-612.

8. Slonje R, Smith PK. Cyberbullying: another main type of bullying? Scand J Psychol 2008; 49(2): 147-54.

9. Vandebosch H, Van Cleemput K. Defining cyberbullying: a qualitative research into the perceptions of youngsters. Cyberpsychol Behav 2008; 11(4): 499-503.

10. John A, Glendenning AC, Marchant A, Montgomery P, Stewart A, Wood S, et al. Self-harm, suicidal behaviours, and cyberbullying in children and young people: systematic review. J Med Internet Res 2018; 20(4): e129.

11. Hinduja S, Patchin JW. Bullying, cyberbullying, and suicide. Arch Suicide Res 2010; 14(3): 206-21.

12. Thomas HJ, Scott JG, Coates JM, Connor JP. Development and validation of the bullying and cyberbullying scale for adolescents: A multi-dimensional measurement model. Br J Educ Psychol 2019; 89(1): 75-94.

13. Ozbey H, Basdas O. Psychometric properties of the Turkish version of the Bullying and Cyber Bullying Scale for Adolescents (BCS-A). Psychiatry Res 2020; 289: 112994.

14. Hisli N. A study on the validity of Beck Depression Inventory (Beck Depresyon Envanterinin geçerliliği üzerine bir çalışma.). Psikoloji Dergisi 1988; 6: 118-22.

15. Onalan G, Onalan R, Selam B, Akar M, Gunenc Z, Topcuoglu A. Mood scores in relation to hormone replacement therapies during menopause: a prospective randomized trial. Tohoku J Exp Med 2005; 207(3): 223-31.

16. Chou WJ, Wang PW, Hsiao RC, Hu HF, Yen CF. Role of school bullying involvement in depression, anxiety, suicidality, and low self-esteem among adolescents with high-functioning autism spectrum disorder. Front Psychiatry 2020; 11: 9.

17. Gobina I, Zaborskis A, Pudule I, Kalnins I, Villerusa A. Bullying and subjective health among adolescents at schools in Latvia and Lithuania. Int J Public Health 2008; 53(5): 272-6.

18. Naveed S, Waqas A, Aedma KK, Afzaal T, Majeed MH. Association of bullying experiences with depressive symptoms and psychosocial functioning among school going children and adolescents. BMC Res Notes 2019; 12(1): 198.

19. Durbeej N, Ssegonja R, Salari R, Dahlberg A, Fabian H, Sarkadi A. Preschool-level socio-economic deprivation in relation to emotional and behavioural problems among preschool children in Sweden. Scand J Public Health 2024; 52(8): 978-87.

20. Gustafsson BM, Proczkowska-Bjorklund M, Gustafsson PA. Emotional and behavioural problems in Swedish preschool children rated by preschool teachers with the Strengths and Difficulties Questionnaire (SDQ). BMC Pediatr 2017; 17(1): 110.

21. Haltigan JD, Vaillancourt T. Joint trajectories of bullying and peer victimization across elementary and middle school and associations with symptoms of psychopathology. Dev Psychol 2014; 50(11): 2426-36.

22. Fekkes M, Pijpers FI, Verloove-Vanhorick SP. Bullying behavior and associations with psychosomatic complaints and depression in victims. J Pediatr 2004; 144(1): 17-22.

23. Craig W, Boniel-Nissim M, King N, Walsh SD, Boer M, Donnelly PD, et al. Social media use and cyber-bullying: a cross-national analysis of young people in 42 countries. J Adolesc Health 2020; 66(6S): S100-S8.

24. Yin H, Han Z, Li Y. Traditional bullying, cyberbullying, and quality of life among adolescents in 35 countries: Do cultural values matter? Soc Sci Med 2024; 340: 116499.

25. Aksaray S. Cyberbullying. J Cukurova Univ Inst Social Sci 2011; 20(2): 405-32.

26. Martinez-Monteagudo MC, Delgado B, Garcia-Fernandez JM, Ruiz-Esteban C. Cyberbullying in the university setting. Relationship with emotional problems and adaptation to the university. Front Psychol 2019; 10: 3074.

27. Zhu C, Huang S, Evans R, Zhang W. Cyberbullying among adolescents and children: a comprehensive review of the global situation, risk factors, and preventive measures. Front Public Health 2021; 9: 634909.

28. Cook EE, Nickerson AB, Werth JM, Allen KP. Service providers' perceptions of and responses to bullying of individuals with disabilities. J Intellect Disabil 2017; 21(4): 277-96.

29. Guo S. A Meta-analysis of the predictors of cyberbullying perpetration and victimization. Psychol Schools 2016; 53(4): 432-53.

30. Ünver H, Koç Z. An investigation of the relationship between cyberbullying, problematic internet use, and risky online behaviors. Türk Eğitim Bilimleri Dergisi 2017; 15(2): 117-40.

31. Yiğit MF, Keskin S, Yurdugül H. Investigating the relationship between cyberbullying and perceived family support in middle-school students in relation to gender, frequency of internet use, and grade. Addicta: Turkish J Addictions 2018; 5(2): 249-84.

32. Juvonen J, Gross EF. Extending the school grounds?–Bullying experiences in cyberspace. J Sch Health 2008; 78(9): 496-505.

33. Wolak J, Mitchell KJ, Finkelhor D. Does online harassment constitute bullying? An exploration of online harassment by known peers and online-only contacts. J Adolesc Health 2007; 41(6 Suppl 1): S51-8.

34. Chen Q, Lo CKM, Zhu Y, Cheung A, Chan KL, Ip P. Family poly-victimization and cyberbullying among adolescents in a Chinese school sample. Child Abuse Negl 2018; 77: 180-7.

35. Cagirkan B, Bilek G. Cyberbullying among Turkish high school students. Scand J Psychol 2021; 62(4): 608-16.

36. Ybarra ML, Diener-West M, Leaf PJ. Examining the overlap in internet harassment and school bullying: implications for school intervention. J Adolesc Health 2007; 41(6 Suppl 1): S42-50.

37. Nixon CL. Current perspectives: the impact of cyberbullying on adolescent health. Adolesc Health Med Ther 2014; 5: 143-58.

38. Korkmaz A. Cyberbullying: new violence from physical to virtual. Fiction 2016; 24(2): 74-85.

39. Dehue F, Bolman C, Vollink T. Cyberbullying: youngsters' experiences and parental perception. Cyberpsychol Behav 2008; 11(2): 217-23.
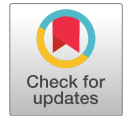
Experimed

Research Article

Accuracy of Procalcitonin in the Diagnosis of Bacteremia and Discrimination from Contamination

Nuket Hayirlioglu [1] 🔟 , Ayse Demet Kaya [2] 🔟 , Deniz Sertel Selale [3] 🔟 ✉, Mine Aydin Kurc [4] 🔟 , Gamze Varol [5] 🔟

[1] Darica Farabi Training and Research Hospital Microbiology Laboratory, Kocaeli, Turkiye
[2] Department of Medical Microbiology, Faculty of Medicine, Istanbul Okan University, Istanbul, Turkiye
[3] Department of Microbiology and Clinical Microbiology, Faculty of Medicine, Istinye University, Istanbul, Turkiye
[4] Department of Medical Microbiology, Faculty of Medicine, Namik Kemal University, Tekirdag, Turkiye
[5] Department of Public Health, Faculty of Medicine, Namik Kemal University, Tekirdag, Turkiye

Abstract

Objective: In this study, we aimed to evaluate the concordance of blood culture with procalcitonin (PCT) alone and together with C-reactive protein (CRP) in detecting bacteremia and the diagnostic performance of these biomarkers to differentiate contamination from true bacteremia.

Materials and Methods: The medical records of 310 patients were analysed retrospectively. Advia Centaur XP immunoassay system and Au analysers were used to determine PCT and CRP levels, respectively. BacT/Alert 3D60 hemoculture system was used to incubate blood specimens, and VITEK 2 compact was used to identify isolated strains.

Results: The accuracy of PCT and CRP in detecting bacteremia were found to be 68.1% and 36.4%, respectively, and combining PCT and CRP had no added value. In analysis of receiver operating characteristic (ROC), the area under the ROC curve (AUROC) values of PCT and CRP were found to be 0.889 and 0.779 in discriminating the culture-negative group from the culture-positive group, and 0.645 and 0.502 in discriminating bacteremia from contamination, respectively.

Conclusion: PCT is a reliable marker that can be used to detect bacteremia. However, its discriminative power was low in differentiating true bacteremia from contamination. Therefore, PCT levels alone should not be used to rule out blood culture contamination.

Keywords   Procalcitonin · CRP · Blood cultures · Bacteremia · Contamination

✉ Corresponding author: Deniz Sertel Selale deniz.sertel@istinye.edu.tr

INTRODUCTION

Bacteremia, if treatment is delayed, may progress to sepsis, septic shock, and death. Therefore, prompt diagnosis is of great importance. In diagnosis, blood culture is considered as the gold standard, but long incubation times (>24 hours), false-positive results due to contamination and unacceptably high false-negative results have created the need for the search for rapid and accurate tests (1-3).

Acute-phase reactants (APRs) have been commonly used as biomarkers indicating infections as they are present in the serum in case of injury and inflammation (1, 4). However, very few can discriminate bacterial infection from inflammation due to non-infectious causes, and information regarding their ability to differentiate true bacteremia from contamination is either unavailable or limited. One of the most commonly used APRs is C-reactive protein (CRP). CRP is predominantly produced by the liver and its concentration in the bloodstream increases gradually in response to pro-inflammatory cytokines, principally interleukin-6 (IL-6), which is produced in case of inflammation due to infection or other causes (4, 5).

Procalcitonin (PCT), the prohormone of calcitonin, is synthesized ubiquitously in response to systemic inflammatory stimuli, particularly bacterial infection (4-7). In detecting bacterial infections, PCT has a number of advantages over other commonly used biomarkers such that it increases rapidly after bacterial infections (rises up to detectable levels in serum within 2–6 hours following stimulation), it has a long half-life (can be detected for up to 7 days), and viral infections or autoimmune diseases do not increase its levels. In addition, PCT levels in the serum coincide with the infection's severity (PCT levels increases parallel to the severity of the infection) and production is not affected by anti-inflammatory and immunosuppressive states (5, 8, 9). These properties of PCT make it a plausible choice as an indicator of severe bacterial infections and bacteremia; hence, PCT is a commonly used biomarker for predicting sepsis due to bacterial infection (4-7). Serum PCT levels have also been considered for guiding antibiotic therapy and for monitoring the prognosis of the disease and the efficacy of the treatment (10, 11). Although there are a few studies that have shown that PCT can also be used in differentiating bacteremia from contamination, this feature should be verified with additional studies before using it in clinical practice.

Besides the clear benefits of PCT over the other APRs including CRP, PCT levels alone are not sufficient to make critical decisions. Therefore, we examined and compared the diagnostic accuracy of PCT alone and together with CRP in detecting bacteremia and their performance in distinguishing bacteremia from contamination.

MATERIALS and METHODS

Study Design and Settings

The Kocaeli University Ethical Committee of Non-Invasive Clinical Research reviewed and approved this study (Approval no: GOKAEK-2017/4.09) and the ethical standards of the Helsinki were followed.

The study was carried out at Darica Farabi Training and Research Hospital throughout a six-month study period. The medical records of patients with suspected blood stream infection were retrospectively reviewed provided that the levels of PCT and CRP were investigated and blood culture had been performed simultaneously. Only data of the patients in whom PCT, CRP, and blood cultures were assayed simultaneously were included. Patients were excluded if the results of any of the tests were not available.

Blood Culture, PCT, and CRP Analysis

Blood samples were inoculated in hemoculture vials of the automated hemoculture system BacT/Alert3D60 (Biomerieux) and incubated for up to seven days. Bacteria isolated from positive cultures were identified using the VITEK2 compact (Biomerieux) system. Blood cultures were considered negative if no growth was observed at the end of the seventh day. Isolation of skin microbiota members (coagulase-negative *Staphylococcus* [CoNS], *Corynebacterium* spp, *Propionibacterium acnes*, etc) were considered as contamination unless isolates that had similar antibiograms were isolated from more than one blood culture taken at two different times (12-14).

Advia Centaur XP immunoassay system (Siemens) was used for detecting PCT levels and Au 680 and Au 5800 analysers (Beckman Coulter) were used for detecting CRP levels. If the levels of CRP or PCT were undetectable, a value equal to the threshold of detection was assigned. For CRP, the cut-off value was accepted as 5mg/dL. The PCT cut-offs used was 5ng/mL, 2ng/mL, and 10ng/mL.

Blood cultures were considered as the reference test, and the accuracy of PCT and CRP was determined by comparing the results of these tests with those of the blood culture.

To assess whether including CRP test has any added value, PCT and CRP results were analysed in combination. If both PCT and CRP tests were positive, the result was considered positive, but if any of the tests were negative, the result was accepted as negative.
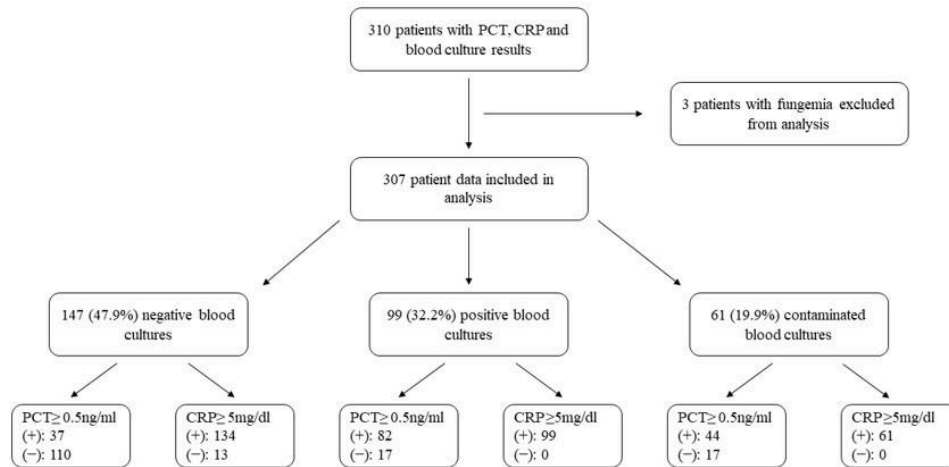
Figure 1. Flow diagram of the included cases. PCT: Procalcitonin; CRP: C-reactive protein

Statistical Analyses

The SPSS 20.0 (SPSS Inc., Chicago, IL, USA) package program was used to evaluate the data. The sensitivity, specificity, and positive- and negative-predictive values were calculated in the methodological analysis. Categorical variables were compared using Pearson Chi-square test and Fisher's exact test. One-way analysis of variance (ANOVA) was performed, and Post Hoc Bonferroni correction was applied to compare the measurement values of more than two groups. The accuracy of PCT and CRP in discriminating culture positive from culture negative and culture positive from contamination were determined by receiver operating characteristic (ROC) analysis. p value was accepted below 0.05 as significant.

RESULTS

During the six-month study period, PCT, CRP, and blood cultures were concomitantly assayed in 310 patients. Data of three patients were excluded because *Candida* spp. were grown in the blood cultures. The mean age was 66.60 ± 16.61 (range: 18-96), and the gender distribution was 48.5% female and 51.5% male. Patients were categorised into three groups regarding the blood culture results: culture positive (n=99, 32.2%), culture negative (n=147, 47.9%) and contamination (n=61, 19.9%) (Figure 1). Culture-positive group was again divided into 2 groups as Gram positive bacteremia (n=55) and Gram negative bacteremia (n=44). Among Gram positive bacteria isolated from blood cultures, *Staphylococcus aureus* (n=21) was the predominant species, followed by *Enterococcus faecalis* (n=20), *Enterococcus faecium* (n=11) and *Enterococcus cloacae* (n=1). Among Gram negative bacteria, *Klebsiella pneumoniae* (n=18) ranked first, followed by *Escherichia coli* (n=16), *Acinetobacter baumannii* (n=8), *Pseudomonas*

aeruginosa (n=1), and *Serratia marcescens* (n=1). All bacteria in the contamination group were CoNS.

The mean, minimum and maximum PCT and CRP levels were assessed and compared among the groups (Table 1). In the culture-negative group, PCT and CRP levels were significantly lower (p<0.001) than in the culture-positive and contamination groups. Although the mean PCT and CRP concentrations were lower in the contamination group in comparison to the culture-positive group, Gram positive and Gram negative bacteremia group, the difference was not significant statistically (p=1.00). The PCT and CRP levels in the Gram negative bacteremia group were slightly above the levels detected in the Gram positive bacteremia group, but the difference was not statistically meaningful (p=1.00).

Table 1. Mean, minimum and maximum PCT and CRP values among the groups.

Groups	Mean ± Standard Deviation (min-med-max)	
	PCT (ng/mL)	CRP (mg/dL)
Contamination (n=61)	9.87 ± 23.36	177.07 ± 86.21
	(0.01-1.10-101.00)	(9.20-177.20-347.70)
Culture positive (n=99)	13.23 ± 20.76	178.71 ± 88.97
	(0.10-4.68-101.00)	(9.80-178.30-411.90)
Gram-positive bacteremia (n=56)	12.80 ± 21.85	173.43 ± 88.33
	(0.12-3.98-101.00)	(9.80-179.25-411.90)
Gram-negative bacteremia (n=43)	13.78 ± 19.50	185.59 ± 90.36
	(0.10-6.43-90.60)	(44.00-177.90-368.97)
Culture-negative (n=147)	1.06 ± 3.26	87.95 ± 86.85
	(0.00-0.14-23.04)	(0.40-63.00-421.60)
p value*	<0.001	<0.001

* One-way analysis of variance with Post Hoc Bonferroni correction was applied. Statistically significant difference was present only between culture-negative group vs culture positive, contamination, Gram-positive bacteremia and Gram-negative bacteremia groups. PCT: Procalcitonin; CRP: C-reactive protein.

In comparison to the reference blood culture, PCT was found to be 82.8% sensitive and 61.1% specific when 0.5 ng/mL was used as the cut-off. As for CRP, sensitivity was 100% and specificity was 6.2%. The specificity of PCT increased markedly when higher cut-off values were used, but the sensitivity declined. When 2 ng/mL was used as the cut-off, sensitivity decreased to 64.7% and specificity increased to 83.2%. When 10 ng/mL was used as cutt-of, sensitivity decreased dramatically to 36.4% and specificity increased further to 91.8% (Table 2). On the basis of these results, the optimal PCT threshold for detecting bacteremia was considered to be 0.5 ng/mL.

Table 2. Diagnostic accuracy of PCT and CRP in detecting bacteremia

	PCT			CRP
Cut-off value	0.5 ng/mL	2 ng/mL	10 ng/mL	5 mg/dL
Sensitivity, (95% CI)	82.8 (75-90)	64.7 (55-74)	36.4 (27-46)	100 (100-100)
Specificity, (95% CI)	61.1 (54-67)	83.2 (78-88)	91.8 (88-95)	6.2 (3-10)
PPV, (95% CI)	50.3 (43-58)	64.7 (55-74)	67.9 (55-80)	33.6 (28-39)
NPV, (95% CI)	88.2 (83-93)	83.2 (78-88)	75.2 (70-81)	100 (100-100)
Accuracy, (95% CI)	68.1 (63-73)	77.2 (73-82)	73.4 (69-79)	36.4 (31-42)

PCT: Procalcitonin; CRP: C-reactive protein; CI: Confidence interval; PPV: Positive predictive value; NPV: Negative predictive value.

The diagnostic performance of PCT (0.5 ng/mL) and CRP (5 mg/dL) was compared between Gram positive bacteremia group and Gram negative bacteremia group. The diagnostic accuracy of PCT in detecting Gram positive and Gram negative bacteremia was 65.8% (95% CI=60-72) and 64.7% (95% CI=59-71). CRP detected Gram positive and Gram negative bacteremia with 25.9% (95% CI=21-31) and 22.6% (95% CI=17-28) accuracy, respectively. A statistically significant difference was not found for both tests.

The diagnostic accuracy of the PCT-CRP combination (accuracy 68.1%) was analysed but the results did not differ from the PCT test alone (accuracy 68.1%); hence, including the CRP test had no added value.

In the ROC analysis, the area under the ROC curve (AUROC) values of PCT and CRP in discriminating the culture-positive group from the culture-negative group were 0.889 and 0.779, respectively (Figure 2). In distinguishing the culture-positive from the contamination group, PCT had an AUROC of 0.645, and CRP had an AUROC of 0.502 (Figure 3).
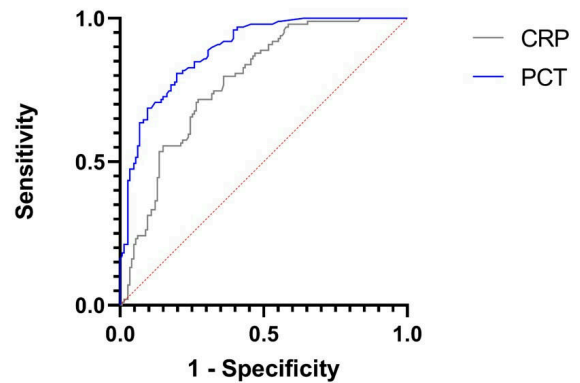
Figure 2. ROC analysis of the PCT and CRP for distinguishing culture-positive from culture-negative. ROC: Receiver operating characteristic; PCT: Procalcitonin; CRP: C-reactive protein
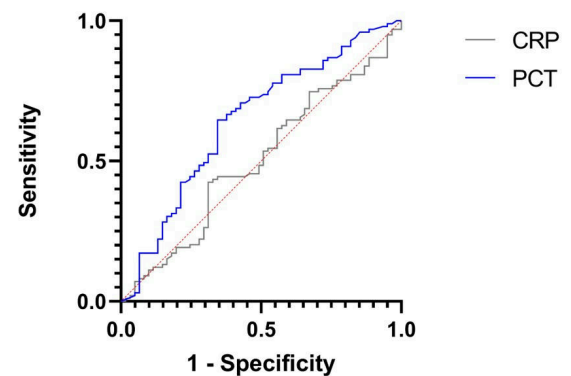
Figure 3. ROC analysis of PCT and CRP for distinguishing culture-positive from contamination. ROC: Receiver operating characteristic; PCT: Procalcitonin; CRP: C-reactive protein

DISCUSSION

Our results have shown that PCT can be used as a reliable biomarker for detecting bacteremia, but its discriminative power is low in distinguishing true bacteremia from contamination.

Multiple studies have investigated the diagnostic performance of PCT and CRP, but relatively few have investigated their ability to distinguish between true bacteremia and contamination (15-18). Schuetz and colleagues were the first to investigate the diagnostic accuracy of PCT to discriminate blood culture contamination from bloodstream infection. In this prospective study conducted in a small cohort (n=40), PCT was found to be an early and accurate biomarker that can aid in distinguishing bloodstream infection from contamination due to CoNS (15). Following this research, a limited number of studies were conducted analysing the capability of PCT and CRP to distinguish bacteremia and contamination (16-18). These studies have found PCT to be superior to CRP and a reliable marker that

can accurately differentiate bacteremia from contamination (16-18). Interestingly, in these studies, PCT and CRP performed better at differentiating true bacteraemia from contamination than discriminating culture-positive from culture-negative (Table 3) (16-18). In a recent study, the usefulness of PCT in diagnosing blood culture contamination was evaluated (19). This study used 0.1 ng/mL as the threshold and concluded that PCT levels below 0.1 ng/mL was a reliable biomarker in determining contamination of blood cultures in hospitalised patients (19).

Table 3. Diagnostic performance of PCT and CRP to discriminate culture positive (CP) from culture negative (CN) and CP from contamination

Study	CP/Cont (% Cont)	CP vs CN		CP vs. Cont	
		AUROC PCT	AUROC CRP	AUROC PCT	AUROC CRP
Present study	99/61 (38.1)	0.889	0.779	0.645	0.502
Oksuz et al.[16]	88/49 (35.8)	0.755	0.601	0.864	0.744
Iqbal-Mirza et al.[17]	154/112 (42.1)	NA	NA	0.983	0.639
Jeong S et al.[18]	331/156 (40.3)	0.76	0.64	0.86	0.65

PCT: Procalcitonin; CRP: C-reactive protein; CP: Culture positive; CN: Culture negative; Cont: Contamination; ROC: Receiver operating characteristic; AUROC: Area under the ROC curve; NA: Not available.

In our study, PCT performed well in discriminating culture negative from culture positive, but its performance was poor in discriminating true bacteremia from contamination, and the performance of CRP was lower than that of PCT in both regards. The AUROC of PCT and CRP in distinguishing culture-positive from contamination was lower than that in other studies with a similar design. Conversely, in discriminating culture-positive from culture-negative, we found the performance of PCT and CRP to be better than reported in the aforementioned studies (Table 3). The reason behind this difference is not clear. It is possible that in certain patients, isolated CoNS might be misidentified as contaminants. To implicate CoNS and other common contaminants as the cause of bacteremia, two or more positive blood cultures were required, but in 17 out of 61 (27.9%) patients, from whom CoNS were isolated, only one sample of blood was drawn for culture; therefore, according to our criteria these were classified as contaminants.

A number of studies have investigated the efficiency of using PCT concentration to discriminate bacteremia or sepsis due to Gram positive and Gram negative pathogens. In our study, the PCT concentrations did not significantly vary among bacteremia caused by Gram negative and Gram positive bacteria. This finding is in line with studies of Oksuz et al. (16) and Kim et al. (20) but discordant with the studies of Engel et al. (21) Svaldi et al. (22), Jeong et al. (18), Leli et al. (23), Yan et

al. (24), Ogawa et al. (25) and Dincer et al. (26). In some studies, statistically significant differences were observed even in between bacteremia due to different species of Gram negative bacteria (23, 24).

Although PCT is explicitly more specific for infections caused by bacteria compared to most other APRs, it is still far from being perfect, therefore we also analysed the diagnostic accuracy of the PCT-CRP combination. However, combining PCT with CRP did not have any added value in regards of specificity. Thus, according to our findings, if sepsis due to bacterial infection is suspected, the PCT test alone will be sufficient for the presumptive diagnosis.

Due to its retrospective nature, information regarding certain factors that can influence the PCT levels like baseline characteristics and comorbidities of, and the treatment applied to the patients were not available and therefore could not be assessed. Furthermore, all the data were obtained from inpatients and antibiotic therapy is frequently applied to hospitalised patients which may result in lower PCT concentrations either by direct effect or by lowering the microbial load, also it may cause false negative results in blood culture (27). Although the impact of underlying diseases and treatments applied could not be assessed, the factors that influence PCT and CRP concentrations have been well established in numerous studies conducted previously, and the purpose of this study was to assert the accuracy of PCT and CRP as independent parameters in diagnosing bacteremia and discrimination from contamination.

An important challenge that physicians face in patients with sepsis is to decide whether the cause is a bacterial agent, or not. Guidelines and algorithms regarding the use of PCT levels to initiate and terminate antibiotic treatment in patients with sepsis have been established, and in 2017, the Food and Drug Administration cleared the use of procalcitonin tests in determining whether to initiate or terminate antibiotic treatment in patients with sepsis and lower respiratory tract infections (27-29). Although few studies have shown that PCT can effectively distinguish true bacteremia from contamination, no algorithms have been proposed. This may be due to the fact that the number of studies that have been conducted on this topic is insufficient. To contribute to the literature, we conducted this retrospective study in a training and research hospital in Turkiye.

Our study results demonstrate that PCT can be used in the presumptive diagnosis of bacteremia as a reliable biomarker and is clearly a better option than CRP. To differentiate Gram positive and -negative pathogens, we cannot propose a cut-off value that can be used because no significant difference was found between the two groups. Discriminating true

bacteremia from contamination promptly is vital, particularly for hospital-acquired infections, in which bacteria frequently regarded as contaminants may be the cause of the infection. The diagnostic performance of PCT was poor in differentiating true bacteremia from contamination; hence, PCT levels alone cannot be used in deciding whether the isolate is the cause or a contaminant. Biomarkers, including PCT, can contribute, but the available data are not sufficient. Therefore, prospective studies with large cohorts should be conducted to establish a reliable diagnostic algorithm.

Author Details

Nuket Hayirlioglu
[1] Darica Farabi Training and Research Hospital Microbiology Laboratory, Kocaeli, Turkiye
0000-0003-1975-4884

Ayse Demet Kaya
[2] Department of Medical Microbiology, Faculty of Medicine, Istanbul Okan University, Istanbul, Turkiye
0000-0001-8224-8242

Deniz Sertel Selale
[3] Department of Microbiology and Clinical Microbiology, Faculty of Medicine, Istinye University, Istanbul, Turkiye
0000-0001-8437-3557   ✉ deniz.sertel@istinye.edu.tr

Mine Aydin Kurc
[4] Department of Medical Microbiology, Faculty of Medicine, Namik Kemal University, Tekirdag, Turkiye
0000-0002-5053-4276

Gamze Varol
[5] Department of Public Health, Faculty of Medicine, Namik Kemal University, Tekirdag, Turkiye
0000-0002-3490-3406

REFERENCES

1. Smith DA, Nehring SM. Bacteremia. In: StatPearls [Internet]. Treasure Island (FL): StatPearls Publishing; 2023 Jan. (PMID: 28723008). Available from: https://www.ncbi.nlm.nih.gov/books/NBK441979/ Accessed November 13, 2022.

2. Hoeboer SH, van der Geest PJ, Nieboer D, Groeneveld AB. The diagnostic accuracy of procalcitonin for bacteraemia: a systematic review and meta-analysis. Clin Microbiol Infect 2015; 21(5): 474-81.

3. Peters RP, van Agtmael MA, Danner SA, Savelkoul PH, Vandenbroucke-Grauls CM. New developments in the diagnosis of bloodstream infections. Lancet Infect Dis 2004; 4(12): 751-60.

4. Markanday A. Acute phase reactants in infections: Evidence-based review and a guide for clinicians. Open Forum Infect Dis 2015; 2(3): ofv098.

5. Nishikawa H, Shirano M, Kasamatsu Y, Morimura A, Iida K, Kishi T, et al. Comparative usefulness of inflammatory markers to indicate bacterial infection-analyzed according to blood culture results and related clinical factors. Diagn Microbiol Infect Dis 2016; 84(1): 69-73.

6. Guo SY, Zhou Y, Hu QF, Yao J, Wang H. Procalcitonin is a marker of gram-negative bacteremia in patients with sepsis. Am J Med Sci 2015; 349(6): 499-504.

7. Thomas-Rüddel DO, Poidinger B, Kott M, Weiss M, Reinhart K, Bloos F. MEDUSA study group. Influence of pathogen and focus of infection on procalcitonin values in sepsis patients with bacteremia or candidemia. Crit Care 2018; 22(1): 128.

8. El-Azeem AA, Hamdy G, Saraya M, Fawzy E, Anwar E, Abdulattif S. The role of procalcitonin as a guide for the diagnosis, prognosis, and decision of antibiotic therapy for lower respiratory tract infections. Egypt J Chest Dis Tuberc 2013; 62(4): 687-95.

9. Aabenhus R, Jensen JU. Procalcitonin-guided antibiotic treatment of respiratory tract infections in a primary care setting: are we there yet? Prim Care Respir J 2011; 20(4): 360-7.

10. Bréchot N, Hékimian G, Chastre J, Luyt CE. Procalcitonin to guide antibiotic therapy in the ICU. Int J Antimicrob Agents 2015; 46 Suppl 1: S19-24.

11. Jin M, Khan AI. Procalcitonin: uses in the clinical laboratory for the diagnosis of sepsis. Lab Med 2010; 41(3): 173–7.

12. Tokars JI. Predictive value of blood cultures positive for coagulase-negative staphylococci: implications for patient care and health care quality assurance. Clin Infect Dis 2004; 39(3): 333-41.

13. Hall KK, Lyman JA. Update review of blood culture contamination. Clin Microb Rev 2006; 19: 788-802.

14. Clinical and Laboratory Standarts Institute. Principles and procedures for blood cultures. Approved Guideline. M47-A, Vol. 27 No. 17. Clinical and Laboratory Standards Institute; 2007. Wayne, PA.

15. Schuetz P, Mueller B, Trampuz A. Serum procalcitonin for discrimination of blood contamination from bloodstream infection due to coagulase-negative staphylococci. Infection 2007; 35(5): 352-5.

16. Oksuz L, Somer A, Salman N, Erk O, Gurler N. Procalcitonin and C-reactive protein in differantiating to contamination from bacteremia. Braz J Microbiol 2015; 45(4): 1415-21.

17. Zafar Iqbal-Mirza S, Serrano Romero de Ávila V, Estévez-González R, Rodríguez-González D, Heredero-Gálvez E, Julián-Jiménez A. Ability of procalcitonin to differentiate true bacteraemia from contaminated blood cultures in an emergency department. Enferm Infecc Microbiol Clin (Engl Ed) 2019; 37(9): 560-8.

18. Jeong S, Park Y, Cho Y, Kim HS. Diagnostic utilities of procalcitonin and C-reactive protein for the prediction of bacteremia determined by blood culture. Clin Chim Acta 2012; 413(21-22): 1731-6.

19. Berthezène C, Aissa N, Manteaux AE, Guéant JL, Oussalah A, Lozniewski A. Accuracy of procalcitonin for diagnosing peripheral blood culture contamination among patients with positive blood culture for potential contaminants. Infection 2021; 49(6): 1249-55.

20. Kim MH, Lim G, Kang SY, Lee WI, Suh JT, Lee HJ. Utility of procalcitonin as an early diagnostic marker of bacteremia in patients with acute fever. Yonsei Med J 2011; 52: 276-81.

21. Engel A, Steinbach G, Kern P, Kern WV. Diagnostic value of procalcitonin serum levels in neutropenic patients with fever: comparison with interleukin-8. Scand J Infect Dis 1999; 31: 185-9.

22. Svaldi M, Hirber J, Lanthaler AI, Mayr O, Faes S, Peer E, et al. Procalcitonin-reduced sensitivity and specificity in heavily leucopenic and immunosuppressed patients. Br J Haematol 2001; 115(1): 53-7.

23. Leli C, Ferranti M, Moretti A, Al Dhahab ZS, Cenci E, Mencacci A. Procalcitonin levels in gram-positive, gram-negative, and fungal bloodstream infections. Dis Markers 2015; 2015: 701480.

24. Yan ST, Sun LC, Jia HB, Gao W, Yang JP, Zhang GQ. Procalcitonin levels in bloodstream infections caused by different sources and species of bacteria. Am J Emerg Med 2017; 35(4): 579-83.

25. Ogasawara S, Saito N, Hirano R, Minakawa S, Kimura M, Kayaba H. Clinical relevance of procalcitonin values in bacteremia. J Infect Chemother 2020; 26(10): 1048-53.

26. Dinçer ŞD, Zeyinli ÜO, Ayaş M, Aksaray S. Can high procalcitonin levels be a biomarker for detecting multidrug-resistant Gram-negative bacteremia? J Health Sci Med 2023; 6(6): 1162-9.

27. Schuetz P, Albrich W, Mueller B. Procalcitonin for diagnosis of infection and guide to antibiotic decisions: past, present and future. BMC Med 2011; 9: 107.

28. Paudel R, Dogra P, Montgomery-Yates AA, Coz Yataco A. Procalcitonin: A promising tool or just another overhyped test? Int J Med Sci 2020; 17(3): 332-7.

29. Janković R, Stojanović M, Božov H, Domi R, Ivančan V, Karišik M et al. Procalcitonin guided antibiotic stewardship: A Balkan expert consensus statement. Acta Clin Croat 2023; 62: 36-44.
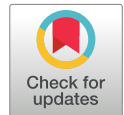
Experimed

Research Article

Open Access

Preliminary Study: Physiological Responses to a Single Bout of Nordic Walking Exercise in Patients with Pre-hypertensive Post-menopausal Women

Emine Kilic-Toprak [1] ✉, Ebru Tekin [2] , Yalin Tolga Yaylali [3] , Fatma Unver [4] , Aysegul Cort [5] ,
Melek Bor-Kucukatay [1]

[1] Department of Physiology, Faculty of Medicine, Pamukkale University, Kinikli, Denizli, Turkiye
[2] Department of Therapy and Rehabilitation, Bigadic Vocational School, Balikesir University, Bigadic, Balikesir, Turkiye
[3] Department of Cardiology, Faculty of Medicine, Pamukkale University, Denizli, Turkiye
[4] Faculty of Physiotherapy and Rehabilitation, Pamukkale University, Kinikli, Denizli, Turkiye
[5] Department of Biochemistry, Faculty of Medicine, Pamukkale University, Kinikli, Denizli, Turkiye

Abstract

Objective: Cardiovascular diseases are a significant cause of morbidity and mortality globally, particularly among post-menopausal women who face heightened risk. Exercise is recognized for its preventive benefits on cardiovascular health and enhancement of vascular function; yet, the effects of various exercise modalities remain inadequately understood. This study aimed to assess alterations in erythrocyte deformability, total oxidant/antioxidant status (TOS/TAS), oxidative stress index (OSI), and serum levels of leptin and irisin in pre-hypertensive post-menopausal women following one session of Nordic walking (NW) exercise.

Materials and Methods: The study cohort comprised 11 post-menopausal women with pre-hypertension (mean age 57.91 ± 7.23 years) and 12 age-matched healthy women (mean age 55.17 ± 5.29 years). Venous blood was taken before and just after the exercise session. The deformability of red blood cells (RBCs) was assessed using an ektacytometer. TOS/TAS, irisin, and leptin were quantified using commercial assays.

Results: A session of NW exercise did not influence oxidative stress indices or blood levels of irisin and leptin; nevertheless, erythrocyte deformability assessed at 30.00 Pa significantly increased post-exercise (p=0.043).

Conclusion: Our findings indicate that enhanced RBC deformability after an acute session of NW may facilitate blood flow.

Keywords Red blood cell deformability · Nordic walking exercise · Oxidative stress · Irisin and Leptin

INTRODUCTION

Pre-hypertension is associated with cognitive decline, increased left ventricular mass, and arteriosclerosis (1). Currently, the advised intervention for pre-hypertension is lifestyle modification. Weight reduction, sodium limitation, increased physical activity, cessation of smoking, and abstinence from alcohol exemplify lifestyle modifications (2).

Menopause correlates with an age-dependent increase in artery damage and a decrease in muscle strength, thereby increasing the risk of cardiovascular disease. Thus, reducing arterial damage and lowering blood pressure may be advantageous in decreasing the incidence of cardiovascular disease in post-menopausal women with pre-hypertension (3).

Exercise has been allowed to mitigate age-related cardiovascular disease risk factors. Nordic walking (NW) is an aerobic workout that has attained considerable popularity as a form of physical activity. In contrast to walking, it offers the benefit of using the upper body and arms, hence alleviating stress on the hips, knees, and feet (4).

Hemorrheology is a scientific discipline that investigates the characteristics of blood flow and the interactions between blood and blood arteries. Deformability of red blood cells (RBCs) is essential for their function in oxygen delivery, as indicated by an elevated elongation index (EI) (5). Enhanced EI at a specific shear stress signifies increased cellular deformability. Articles on the impacts of exercise on RBC deformability show variability attributed to differences in exercise volume and intensity, studied population and the devices used to measure deformability (6). Diseases such as diabetes, hypercholesterolemia, and hypertension may lead to diminished RBC deformability because of heightened oxidative stress or reduced NO bioavailability (7).

The removal of free radicals by antioxidant enzymes and substances is often balanced by the production of free radicals. In the human body, oxidative pathway components can be quantified from biological samples; however, this procedure may be expensive and time-consuming. The assessment of the total oxidant status (TOS) and total antioxidant status (TAS), which reflect the cumulative and interaction influences of oxidant and antioxidant substances, provide a more thorough approach for evaluating the oxidant/antioxidant equilibrium. There are very few clinical studies investigating oxidative stress and the antioxidant system with NW exercise (8, 9).

Proteins and other cytokines secreted by the skeletal muscle are called "myokines." Myokines greatly enhance the contact between the muscle and adipose tissue, liver and pancreas.

Leptin and irisin are markers of glucose metabolism and control, and are linked to visceral obesity (10). Although no studies have examined the acute exercise response on irisin in post-menopausal women, research has examined the impact of acute exercise on leptin levels in this population (11, 12). The data mentioned above show that obesity and being overweight are significant problems for women after menopause. This study was conducted because of the considerable acceptance of physical activity through NW training (13). Research indicates that NW training, used as a body composition intervention, is most effective when supervised by trainers (14).

Nonetheless, the impact of NW on red blood cell deformability, TOS, TAS, oxidative stress index (OSI), and the levels of leptin and irisin has not yet been investigated in pre-hypertensive post-menopausal women. This study aimed to investigate the acute effects of a single session of NW exercise on erythrocyte deformability, oxidative stress markers (TOS/TAS, OSI), and serum levels of leptin and irisin in pre-hypertensive post-menopausal women.

MATERIALS AND METHODS

The work protocol adhered to the ethical principles established in the 1975 Declaration of Helsinki (ethical approval no: 60116787-020/5756). All participants received a comprehensive written and verbal description of the potential risks and advantages of participation.

Patients

In our study, patients exhibiting systolic blood pressure (SBP) ranging from 120 to 129 mmHg and diastolic blood pressure (DBP) below 80 mm Hg were classified as having high blood pressure (formerly known as pre-hypertension) (1). The exclusion criteria were as follows: SBP of 180 mmHg or more and/or DBP of 90 mmHg or more, current anti-hypertensive medications used, presence of rheumatoid arthritis, diabetes mellitus and inability to obtain approval from a primary care physician to participate in the study.

Twenty-three post-menopausal women with pre-hypertension (mean age 56.48 ± 6.30 years) participated in the study. Individuals who had not engaged in regular physical activity in the last six months were included in the study. Participants were randomly assigned to two groups: NW (n=11; mean age 57.91 ± 7.23 years) and control (n=12; mean age 55.17 ± 5.29 years). All participants were required to provide medical documentation confirming their eligibility for physical activity, and the groups were similar in terms of physical fitness and consistent with a sedentary lifestyle.

Anthropometric Assessments

Height in centimeters was measured using a stadiometer with the participant in the inspiratory phase in the anatomical position. This measurement was performed with an accuracy of ±1 mm in centimeters.

On the first day of the study, body composition was assessed using a TANITA (BC-480) body composition analyzer while participants wearing lightweight shorts and a t-shirt. Participants were asked to wear the same attire for each subsequent measurement session. Special attention was given to ensure that all participants maintained a consistent posture throughout the measurements. To enhance the conductivity, the steel platform where the participants placed their feet was cleaned with a damp cloth before each measurement. Additionally, participants were instructed to fast for a minimum of 8 h before undergoing the assessments.

Aerobic Test: Prediction of Maximum Oxygen Uptake capacity (VO$_{2max}$) by Cooper 12-minute Run/Walk Test

The subjects spent 12 minutes running on a 400 m circular track. Their desire to complete as many laps as possible drove them. The finish line was marked, and the total number of laps was tallied. The VO$_{2max}$ was predicted using the following equation once the distance in meters was translated to kilometers (15).

$$VO_{2max} = (22.351 \times \text{distance [km]}) \times 11.288$$

Sit and Reach Test

The sit-and-reach test was utilized to assess the flexibility of the lumbar extensors, hip extensors, gastrocnemius and hamstring muscles with a sit-and-reach test box. Participants, having removed their shoes, took their places on the bench, guaranteeing. Their toes were oriented upward. They were directed to extend the measuring ruler progressively by bending at the hips and extending forward maximally while maintaining fully extended legs. Participants were asked to maintain this maximum position for 2 s. The test was conducted thrice, and the highest score, measured in centimeters, was used for analysis (16).

Grip Strength Measurement

The hand grip strength was assessed using a calibrated digital Jamar dynamometer (Performance Health, Warrenville, IL). Participants were required to exert maximum force three times with each hand while maintaining the elbows at a 90-degree flexion and the wrists in a neutral posture. The optimal value was observed (17).

Exercise Protocol

Exercise sessions were conducted outdoors on a flat surface, beginning with a 10-to 12 min warm-up period. During the warm-up, each movement was performed in 4–6 repetitions to reduce muscle stiffness and maintain joint range of motion. Following the warm-up, the participants engaged in 50 min of NW, a full-body aerobic exercise performed with specially designed poles, involving the coordinated use of both the upper and lower extremity muscles. The walks were conducted during the spring , between 2:00 PM and 4:00 PM. Throughout the study, the weather conditions were characterized by moderate temperature levels. This technique includes not only forward walking but also technical aspects that require motor coordination and attention, such as correct pole placement, synchronization of arm and leg movements, maintaining appropriate stride length, and sustaining rhythmic movement throughout the activity. To ensure familiarity with the exercise, the participants were shown instructional videos and participated in a 5-min familiarization session before the walking session. The walks were conducted using a Polar M200 wrist-based heart rate (HR) tracking watch with GPS, which measures the HR. The single session NW program was conducted at a mean HR of 40-55% of the maximum age-related HR (18).

HRmax = 206 - 0.88 x (age)

[(HRmax - HRrest) x (0.4 to 0.55)] + HRrest

8-10 mL of venous blood was collected from the pre-hypertension group before and immediately after exercise and the control group only once.

Blood Samples

8-10 mL of venous blood was collected from the antecubital vein into tubes [EDTA (1.5 mg/mL)] from the pre-hypertension group before and immediately after exercise and the control group only once for analysis of complete blood count and hemorheological parameters. Venous blood samples (10 mL) were collected before the exercise, following an 8 h fasting period in the morning before any physical activity. Additionally, participants rested for at least 10 min in a seated position before blood collection. The samples were conveyed to the Physiology Laboratory in appropriate tubes and under proper transportation conditions, where hemorheological tests were performed within 3 h in accordance with the manual of hemorheological laboratory procedures (19). Blood samples (4-5 mL) were obtained in yellow top tubes containing gel (which includes a coagulation activator and separator) for the measurement of biochemical parameters, oxidative stress indicators, and serum levels of irisin and leptin. Blood was

centrifuged at 7260 rpm for 6 min, after which the serum was removed and preserved at −80 °C.

Measurements of Erythrocyte Deformability

RBC deformability was assessed using laser diffraction analysis with an ektacytometer (Laser-Assisted Optical Rotational Cell Analyzer [LORCA], RR Mechatronics, Hoorn, The Netherlands). The system and methodology have been described in detail, previously (20). Briefly, a low hematocrit (Hct) suspension of RBCs in an isotonic, viscous medium (4% polyvinylpyrrolidone 360 solution; molecular weight 360 kDa; Sigma P5288, St. Louis, MO, USA) was subjected to shear stress within a Couette system comprising a glass cup and a rotating bob, creating a 0.3 mm gap. A laser beam was passed through the sheared suspension, and the resulting diffraction pattern was analyzed by a microcomputer. The EI was calculated using the formula $EI = (L - W)/(L + W)$, where L and W represent the major and minor axes of the elliptical diffraction pattern, respectively. The EI values were recorded at nine shear stress levels ranging from 0.3 to 30 Pa, revealing consistent deformability trends across the groups at all shear rates. All measurements were performed at 37 °C (21, 22).

Assessment of the TOS/TAS and OSI

The serum TOS was measured using a fully automated, colorimetric method developed by Erel (23). In this assay, oxidants present in the serum oxidize the ferrous ion–O-dianisidine complex to the ferric ion, a reaction that is enhanced in the presence of glycerol. The resulting ferric ions formed a colored complex with xylenol orange in an acidic medium. The intensity of the color, measured spectrophotometrically, is directly proportional to the total amount of oxidant molecules (e.g., lipids, proteins) in the serum. The assay was calibrated using hydrogen peroxide, and the results were expressed in micromolar hydrogen peroxide equivalents per liter (μmol H_2O_2 equiv/L).

The serum TAS was evaluated using another automated colorimetric method developed by Erel (24). In this method, hydroxyl radicals generated by the Fenton reaction react with the colorless substrate O-dianisidine to form a bright yellowish-brown dansyl radical. Upon the addition of a serum sample, the antioxidant components inhibit this oxidative reaction, thereby preventing the formation of color. The degree of suppression reflects the serum's total antioxidant capacity. Results are expressed as millimoles of Trolox equivalent per liter (mmol Trolox/L).

Serum Exercise (irisin, leptin) Levels Assessment

Irisin and leptin levels were determined using ELISA Kits (Shanghai, YL Biotech Co.). According to the manufacturer's protocols, the commercial kits used were specific for measuring irisin and leptin in human samples. The detection limit was 5.0 pg/mL for the kits.

Statistical Analyses

A power analysis was performed based on the expected results. Accordingly, when at least 22 participants (at least 11 per group) were included in the study, that would result in 80% power with 95% confidence level (%5 type 1 error rate) and the effect size was dz = 6.84. Statistical analyses were performed using GraphPad Prism software, version 6 (GraphPad Software, La Jolla, CA, USA). One-way ANOVA and independent samples t test were applied to normally distributed data, while Kruskal-Wallis and Mann–Whitney U tests were used for non-normally distributed data. Statistical significance was defined as $p<0.05$.

RESULTS

Effect of NW on Physiological and Clinical Assessment Variables

Physiological and clinical assessment variables such as anthropometric measurements, blood pressure characteristics, functional fitness components, biochemical data, and hematological parameters were all within normal ranges at the start of the study and did not show any statistically significant differences between the groups (Table 1-5). All of the participants completed the exercise protocol session without any complications.

The study enrolled 11 pre-hypertensive post-menopausal women (mean age was 57.91 ± 7.23 years) and 12 age-matched pre-hypertensive post-menopausal women controls (mean age was 55.17 ± 5.29 years).

Erythrocyte Deformability Values

RBC deformability was determined as EI. The differences between before and after the exercise regarding EI values were not statistically significant except at 30.00 Pa shear stress value in patients with pre-hypertension EI values measured at 30.00 Pa increased after the NW exercise (p=0.043). The Hct value was increased after the exercise compared to before exercise (p = 0.008) (Table 6).

TOS/TAS and OSI Values

The TOS, TAS, and OSI of the participants in response to one session of the NW exercise and the control group are

Table 1. Anthropometric measurements of the participants

Parameters	Controls (n=12)	The NW exercise (n=11)	p
Age (years)	55.17 ± 5.29	57.91 ± 7.23	0.379
Body height (cm)	156.83 ± 3.1	155.82 ± 5.49	0.413
Body weight (kg)	73.73 ± 12.75	72.36 ± 11.47	0.566
BMI (kg/cm²)	30.02 ± 4.69	29.68 ± 3.4	0.928
Percentage body fat (%)	38.65 ± 7.52	38.23 ± 5.58	0.601
Body muscle mass (kg)	42.32 ± 3.31	42.04 ± 3.99	1.000
Body fat mass (kg)	29.35 ± 9.94	28.14 ± 8.2	0.566
Total body water (kg)	32.63 ± 3.13	32.37 ± 3.13	1.000
Arm circumference (cm)	31.5 ± 3.49	34.8 ± 3.62	0.268
Forearm circumference (cm)	25.43 ± 2.52	27.3 ± 1.79	0.202
Wrist circumference (cm)	17.14 ± 1.07	17 ± 0.71	0.876
Chest circumference (cm)	105.43 ± 10.52	106.2 ± 6.72	1.000
Abdominal circumference (cm)	100.91 ± 14.74	100.72 ± 11.8	0.882
Hip circumference (cm)	112.09 ± 11.58	110.61 ± 8.56	0.941
Thigh circumference (cm)	56.57 ± 5.26	58.2 ± 7.76	0.876
Calf circumference (cm)	38 ± 3.86	39.4 ± 3.34	0.639
Ankle circumference (cm)	23.5 ± 3.12	23 ± 1.54	0.876

Values are expressed as mean ± standard deviation. NW: Nordic walking; BMI: Body mass index.

Table 2. Blood pressure characteristics of the participants

Parameters	Controls (n=12)	Before the NW exercise (n=11)	After the NW exercise (n=11)	p_1	p_2
Systolic pressure (mm/hg)	127.14 ± 17.04	133.81 ± 13.15	122 ± 12.29*	0.740	**0.038**
Diastolic pressure (mm/hg)	77.14 ± 9.51	79.54 ± 14.46	73 ± 8.23*	0.230	**0.026**

Values are expressed as mean ± standard deviation; NW: Nordic walking; p_1 value: difference with controls and before NW exercise; p_2 value: difference with before and after NW exercise value; *:$p<0.05$ statistically significant.

demonstrated in Figures 1A and 1B. Statistically insignificant changes were observed in the oxidative stress indices ($p>0.05$).

Serum Exercise (irisin and leptin) Levels

The serum irisin and leptin of the participants are demonstrated in Figure 1C. The acute effects of NW exercise caused no significant changes in irisin and leptin levels ($p>0.05$).

Table 3. Functional fitness components of the participants

Parameters	Controls (n=12)	The NW exercise (n=11)	p
Cooper 12-min run/walk test (m)	1310 ± 102.79	1236 ± 179.81	0.530
VO_{2max} (L/dk)	18.01 ± 2.31	16.36 ± 4	0.530
Sit and reach test (cm)	3.90 ± 7.02	2.61 ± 6.85	0.740
Grip strength (right) (bar)	22.18 ± 4.22	19.68 ± 6.32	0.402
Grip strength (left) (bar)	21.75 ± 3.64	18.55 ± 6.80	0.369

Values are expressed as mean ± standard deviation; NW: Nordic walking; VO_{2max}: Maximum oxygen uptake capacity.

Table 4. Biochemical data of the participants

| Parameters	Controls (n=12)	The NW exercise (n=11)	p
Glucose (mmoL/L)	105.89 ± 20.34	96 ± 10.73	0.243
Insulin (pmol/L)	12.13 ± 5.55	11.58 ± 4.65	0.720
HOMA-IR	3.27 ± 1.90	2.73 ± 1.28	0.549
Albumin (g/dL)	46.6 ± 2.59	45.5 ± 2.38	0.278
Cholesterol(mmoL/L)	213.33 ± 36.79	209.8 ± 31.42	0.661
Triglycerides (mmoL/L)	157.22 ± 71.49	107.6 ± 34.63	0.095
Creatine kinase (U/L)	79.38 ± 27	71.6 ± 24.44	0.515
Fibrinogen (mmoL/L)	291.5 ± 37	334.7 ± 80.58	0.315
LDL (mmoL/L)	120 ± 23.39	125.8 ± 31.74	0.549
ALP (U/L)	75.44 ± 19.79	69.9 ± 9.61	0.549
LDH (U/L)	180.33 ± 26.12	175.8 ± 16.27	0.780
Phosphor (mg/dL)	3.58 ± 0.45	3.75 ± 0.59	0.842
Magnesium (mg/mL)	2.11 ± 0.13	2.03 ± 0.14	0.243
HDL (mmoL/L)	58.56 ± 17.59	62.5 ± 7.82	0.315
VLDL cholesterol (mmoL/L)	31.33 ± 14.45	21.5 ± 6.92	0.095

Values are expressed as mean ± standard deviation; NW: Nordic walking; LDL: Low-density lipoprotein; HDL: High-density lipoprotein; ALP: Alkaline phosphatase; VLDL: Very low-density lipoprotein; LDH: Lactate dehydrogenase.

DISCUSSION

NW is increasingly recognized as an effective form of physical activity, particularly among middle-aged and older adults in Central and Northern Europe. The positive effects of NW on cardiovascular health, aerobic capacity, and blood pressure regulation have been widely documented, given its potential to be integrated into daily routines and its suitability for women (13, 14). This study aimed to investigate the acute effects of a single session of NW on selected physiological and biochemical markers in post-menopausal women with pre-hypertension.
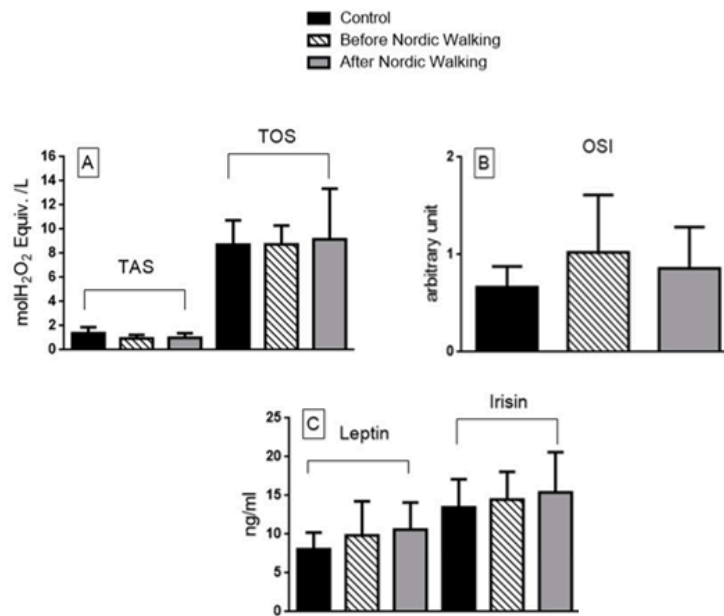
Figure 1. Total antioxidant status (TAS) and total oxidant status (TOS) values of the participants. **B**. Oxidative stress index (OSI) values of the participants. . **C**. Irisin and leptin levels values of the participants. Mean ± standard deviation are used to express values.

Table 5. Whole blood count analyses of the participants

Parameters	Controls (n=12)	The NW exercise (n=11)	p
WBC (k/uL)	7.08 ± 1.79	6.89 ± 1.26	0.968
NEU (%)	58.66 ± 7.21	46.23 ± 16.36	0.053
LYM (%)	31.67 ± 7	39.04 ± 9.41	0.079
MONO (%)	5.94 ± 1.36	5.95 ± 1.24	0.968
BASO (%)	0.53 ± 0.22	0.44 ± 0.23	0.400
EO (%)	3.2 ± 1.66	2.86 ± 2.89	0.182
Hb (gm/dL)	14.1 ± 0.86	13.9 ± 0.67	0.549
MCV (fL)	89.77 ± 2.62	90.35 ± 3.79	0.842
MCH (pg)	29.81 ± 0.93	29.76 ± 1.19	0.968
MCHC (g/dL)	33.21 ± 0.69	32.94 ± 0.81	0.661
RDW (%)	13.04 ± 0.71	13.26 ± 0.6	0.720
PLT (k/uL)	260.44 ± 74.62	272.6 ± 72.59	0.780
PCT (ng/mL)	0.25 ± 0.05	0.24 ± 0.06	0.842

Mean ± standard deviation are used to express values. WBC: White blood cell; NEU: neutrophil; LYM: Lymphocyte; MONO: Monocyte; BASO: Basophil; EO: Eosinophil; Hb: Hemoglobin; MCV: Mean corpuscular volume; MCH: Mean corpuscular hemoglobin; MCHC: Mean corpuscular hemoglobin concentration; RDW: Red blood cell distribution width; PLT: Platelet count; PCT: Procalcitonin.

Table 6. The participants' EI values under various shear stresses

Shear stress (Pa)	The EI values of the participants at different shear stresses		
	Before the NW exercise (n=11)	After the NW exercise (n=11)	p
0.30	0.061 ± 0.02	0.059 ± 0.01	0.646
0.53	0.125 ± 0.03	0.125 ± 0.02	0.533
0.95	0.222 ± 0.03	0.225 ± 0.03	0.799
1.69	0.562 ± 0.03	0.563 ± 0.02	0.878
3.00	0.425 ± 0.02	0.430 ± 0.02	0.625
5.33	0.503 ± 0.01	0.506 ± 0.01	0.449
9.49	0.562 ± 0.01	0.563 ± 0.01	0.929
16.87	0.603 ± 0.01	0.605 ± 0.01	0.385
30.00	0.629 ± 0.01	0.633 ± 0.01	0.043*
Hct (%)	47.10 ± 3.30	49.64 ± 3.32	0.0086*

Mean ± standard deviation are used to express values. NW: Nordic walking ; Hct: Hematocrit; * p-value < 0.05 statistically significant.

The findings of this study indicate that a single session of NW did not lead to significant changes in oxidative stress indices, serum irisin, and leptin levels in pre-hypertensive post-menopausal women. Additionally, no significant differences were found between the groups in physical fitness components such as flexibility, strength, and aerobic capacity, which implies that the participants had similar physical fitness characteristics. The participants' VO_{2max} values suggest that post-menopausal women generally have low aerobic capacity, which is consistent with a sedentary lifestyle (25). This may have implications for their metabolic and vascular responses to exercise, potentially blunting the acute biochemical adaptations expected from physical activity.

In terms of blood pressure, we noted a significant reduction post-exercise, which aligns with the well-documented phenomenon of post-exercise hypotension (PEH). The lack of knowledge about the regulation of hypertension by physical exercise has resulted in contradictory findings; for example, acute aerobic exercise decreases resting blood pressure by 5–7 mmHg in individuals with hypertension after a single session, with effects that are immediate and can persist for up to 24 h in ambulatory situations during daytime (26). Although the mechanisms underlying PEH are multifactorial, they likely involve alterations in autonomic regulation, vascular resistance, and endothelial function. On the other hand, long-term aerobic exercise training reduces resting blood pressure more in individuals with hypertension (27). Similarly, Latosik et al. evaluated the effects of an 8-week supervised NW program on systolic blood pressure in postmenopausal women with systolic hypertension, and their findings demonstrated a significant reduction in SBP, along with improvements in both lower and upper body strength among participants who engaged in the NW training. The 8-week NW regimen may effectively reduce systolic hypertension by directly lowering SBP and enhancing maximal aerobic capacity (28). Consistent with the existing literature, our findings contribute to the growing body of evidence suggesting that even a single session of NW may induce favorable cardiovascular responses in pre-hypertensive individuals. However, to fully elucidate the underlying mechanisms, further long-term studies with larger sample sizes are warranted.

Our results indicate that a single NW session led to statistically significant improvements in erythrocyte deformability at high shear stress (30.00 Pa) and Hct levels. On the other hand, erythrocyte deformability was measured at 9 different shear stresses between 0.3 and 30 Pa, representing the shear stress levels that blood encounters at different regions of circulation. It is known that erythrocyte deformability is affected by membrane skeleton elasticity, cytoplasmic viscosity and cell geometry (surface-volume ratio), and polyunsaturated fatty acids play a key role in the structure and functioning of cell membranes (6, 7). To summarize, erythrocyte deformability can be affected in the circulatory system through a variety of mechanisms. Our findings suggest that even a single moderate-intensity bout of NW may positively influence the hemorheological properties and blood oxygen transport in our study. The increase in Hct may be due to the transient hemoconcentration resulting from the plasma volume shifts during exercise, a commonly observed phenomenon in acute exercise studies (29). Since greater erythrocyte deformability enhances oxygen transport to muscle capillaries even at high levels of Hct, it is possible to interpret the increase in RBC

deformability that we observed in response to NW exercise in our case as an adaptive mechanism (12).

Previous studies have shown that the effects of exercise on RBC deformability vary depending on exercise type, intensity, and subject characteristics. Moderate-intensity one-session aerobic exercise, such as NW, may enhance RBC flexibility via mechanisms involving membrane fluidity and the nitric oxide (NO) signaling pathway (30). Tomschi et al. reported no significant sex diversity in RBC deformability among elite athletes (31). In agreement with our findings, a 4-week regimen of NW exercise resulted in an enhancement of erythrocyte deformability in pre-diabetic individuals, as previously shown in our laboratory (21). However, the current research is the first to address the influence of a single session of NW exercise on blood rheology in patients with pre-hypertensive post-menopausal women. One session of NW exercise under the supervision of a physiotherapist was shown to improve the deformability values in the current study. A statistically significant change in RBC deformability was only observed at an exceptionally high shear stress, which diminishes the practical relevance of this finding. However, because this was a pilot study reporting hemorheological changes in participants, further research on this topic involving larger populations is also needed.

On the other hand, the serum levels of oxidative stress markers (TAS, TOS, and OSI) did not significantly change after a single NW session. There are a limited number of articles examining the connection between NW exercise and oxidative stress. Furthermore, the effect of long-term NW exercise was also investigated in these studies. Cebula et al. demonstrated that 6 weeks of NW exercise generated an improvement in the antioxidant defense, while the TOS levels did not significantly change (32). However, Kortas et al. demonstrated that 3 times/a week, 12 weeks of NW training caused a significant reduction in oxidative stress (9). Pilch et al. showed a significant increment in the TAS levels after 12 weeks of NW with no statistically significant changes in the TOS levels (8). Our results are particularly notable as this is the first article to examine the acute effects of NW exercise in post-menopausal patients with pre-hypertension. However, in a previous study conducted in our laboratory, it was found that a single eccentric isokinetic exercise session had no effect on oxidative stress measures (22). This is in agreement with several acute exercise studies reporting no immediate alterations in the oxidative status following moderate-intensity exercise. When evaluated in the context of existing literature, the lack of change in TAS, TOS, and OSI levels following a single session of exercise may be speculated to result from the exercise duration and intensity

not reaching a threshold sufficient to elicit a measurable impact on oxidative stress mechanisms.

Similarly, the adipokines, irisin and leptin did not show significant changes after the exercise session. Leptin is involved in appetite regulation and energy homeostasis, with levels typically elevated in obesity and reduced following sustained exercise or weight loss. Similar to our findings, obese women's leptin levels were not significantly changed by 45 minutes of walking at 60-80% HRmax (33). Additionally, leptin concentrations did not change after exercise sessions lasting 60 minutes (34). However, acute exercise interventions, particularly those of short duration or lower intensity, often fail to elicit measurable changes in leptin levels. Our findings are consistent with those of previous studies in which leptin concentrations remained stable following a single bout of aerobic exercise in women.

Irisin, a myokine linked to energy expenditure and metabolic regulation, has shown inconsistent responses to exercise. Some studies suggest increases in irisin levels following acute high-intensity or long-duration aerobic exercise, whereas others report no significant changes. A meta-analysis by Fox et al. in 2017 found that irisin levels typically rose within 15 minutes, referred to as "immediate" -after an acute exercise session (35). Similarly, Rashti et al. showed that post-menopausal women's serum irisin levels were considerably increased by vigorous concurrent circuit exercise, which was performed three times a week for 50–65 minutes per session over a period of 10 weeks (36). However, in our study, conducted at 40–55% HRmax, the exercise intensity and session may have been insufficient to stimulate significant irisin release. Furthermore, individual variability in fitness levels and muscle mass may also influence the irisin response.

CONCLUSION

In conclusion, a single session of moderate-intensity NW exercise produced significant improvements in erythrocyte deformability and hematocrit levels, suggesting beneficial acute hemorheological adaptations in post-menopausal women with pre-hypertension. However, no significant changes were observed in the oxidative stress markers, leptin, or irisin levels. The observed reduction in blood pressure may reflect post-exercise hypotension. These findings emphasize the potential of NW as a non-pharmacological strategy for vascular health promotion in this population. Our results could be used as a guide for coaches and exercise physiologists in future research using this workout regimen.

STUDY LIMITATIONS

The limitations of our study include the small sample size and the focus on the effects of a single session. The lack of post-exercise blood lipid profile assessment represents a limitation of this study. Incorporating such analyses—particularly focusing on the composition of circulating fatty acids—could have offered a more comprehensive insight into the mechanisms underlying exercise-induced changes in erythrocyte deformability. Future research should include more detailed investigations with post-exercise lipid profiling to better elucidate these mechanisms. Although a significant change was observed at a single shear stress level of RBC deformability, future studies with repeated measurements and larger sample sizes are needed to confirm this finding.

Author Details

Emine Kilic-Toprak
[1] Department of Physiology, Faculty of Medicine, Pamukkale University, Kinikli, Denizli, Turkiye

0000-0002-8795-0185   ✉ ektoprak@pau.edu.tr

Ebru Tekin
[2] Department of Therapy and Rehabilitation, Bigadic Vocational School, Balikesir University, Bigadic, Balikesir, Turkiye

0000-0002-6984-1110

Yalin Tolga Yaylali
[3] Department of Cardiology, Faculty of Medicine, Pamukkale University, Denizli, Turkiye

0000-0002-8452-923X

Fatma Unver
[4] Faculty of Physiotherapy and Rehabilitation, Pamukkale University, Kinikli, Denizli, Turkiye

0000-0002-3100-0818

Aysegul Cort
[5] Department of Biochemistry, Faculty of Medicine, Pamukkale University, Kinikli, Denizli, Turkiye

0000-0001-8946-7173

Melek Bor-Kucukatay
[1] Department of Physiology, Faculty of Medicine, Pamukkale University, Kinikli, Denizli, Turkiye

0000-0002-9366-0205

REFERENCES

1. Materson BJ, Garcia-Estrada M, Degraff SB, Preston RA. Prehypertension is real and can be associated with target organ damage. J Am Soc Hypertens 2017; 11: 704-8.

2. Egan BM, Stevens-Fabry S. Prehypertension–prevalence, health risks, and management strategies. Nat Rev Cardiol 2015; 12(5): 289-300.

3. Zaydun G, Tomiyama H, Hashimoto H, Arai T, Koji Y, Yambe M, et al. Menopause is an independent factor augmenting the age-related increase in arterial stiffness in the early postmenopausal phase. Atherosclerosis 2006; 184(1): 137-42.

4. Skórkowska-Telichowska K, Kropielnicka K, Bulińska K, Pilch U, Woźniewski M, Szuba A, et al. Nordic walking in the second half of life. Aging Clin Exp Res 2016; 28: 1035-46.

5. Bla´ha M, Rencova´ E, Bla´ha V, Maly´ R, Blazek M, Studnicka J, et al. The importance of rheological parameters in the therapy of microcirculatory disorders. Clin Hemorheol Microcirc 2009; 42: 37-46.

6. Connes P, Simmonds MJ, Brun JF, Baskurt OK. Exercise hemorheology: classical data, recent findings and unresolved issues. Clin Hemorheol Microcirc 2013; 53(1-2): 187-99.

7. Cicco G, Pirrelli A. Red blood cell (RBC) deformability, RBC aggregability and tissue oxygenation in hypertension. Clin Hemorheol Microcirc 1999; 21: 169-77.

8. Pilch W, Tota Ł, Piotrowska A, Śliwicka E, Czerwińska-Ledwig O, Zuziak R, et al. Effects of nordic walking on oxidant and antioxidant status: levels of calcidiol and proinflammatory cytokines in middle-aged women. Oxid Med Cell Longev 2018; 2018: 6468234.

9. Kortas J, Kuchta A, Prusik K, Prusik K, Ziemann E, Labudda S, et al. Nordic walking training attenuation of oxidative stress in association with a drop in body iron stores in elderly women. Biogerontology 2017; 18: 517-24.

10. Perakakis N, Triantafyllou GA, Fernández-Real JM, Huh JY, Park KH, Seufert J, et al. Physiology and role of irisin in glucose homeostasis. Nat Rev Endocrinol 2017; 13(6): 324-37.

11. Kohrt WM, Landt M, Birge SJ Jr. Serum leptin levels are reduced in response to exercise training, but not hormone replacement therapy, in older women. J Clin Endocrinol Metab 1996; 81: 3980-5.

12. Kraemer RR, Johnson LG, Haltom R, Kraemer GR, Hebert EP, Gimpel T, et al. Serum leptin concentrations in response to acute exercise in postmenopausal women with and without hormone replacement therapy. Proc Soc Exp Biol Med 1999; 221: 171-7.

13. Piotrowicz E, Zieliński T, Bodalski R, Rywik T, Dobraszkiewicz-Wasilewska B, Sobieszczańska-Małek M, et al. Home-based telemonitored Nordic walking training is well accepted, safe, effective and has high adherence among heart failure patients, including those with cardiovascular implantable electronic devices: a randomised controlled study. Eur J Prev Cardiol 2015; 22: 1368-77.

14. Muollo V, Rossi AP, Milanese C, Zamboni M, Rosa R, Schena F, et al. Prolonged unsupervised Nordic walking and walking exercise following six months of supervision in adults with overweight and obesity: A randomised clinical trial. Nutr Metab Cardiovasc Dis 2021; 31: 1247-56.

15. Alzahrani E, Alyazedi FM. The impact of a 10-week military training course on Saudi medical recruits' fitness and physical activity levels. Cureus 2023; 15(10): e46593.

16. López-Miñarro PÁ, Vaquero-Cristóbal R, Muyor JM, Espejo-Antúnez L. Related validity of sit-and-reach test as a measure of hamstring extensibility in older women. Nutr Hosp 2015; 32(1): 312-7.

17. Wang YC, Bohannon RW, Li X, Sindhu B, Kapellusch J. Hand-grip strength: normative reference values and equations for individuals 18 to 85 years of age residing in the United States. J Orthop Sports Phys Ther 2018; 48(9): 685-93.

18. Gulati M, Shaw LJ, Thisted RA, Black HR, Bairey Merz CN, Arnsdorf MF. Heart rate response to exercise stress testing in asymptomatic women: the st. James women take heart project. Circulation 2010; 122: 130-7.

19. Baskurt OK, Boynard M, Cokelet GC, Connes P, Cooke BM, Forconi S, et al. International expert panel for standardization of hemorheological methods. New guidelines for hemorheological laboratory techniques. Clin Hemorheol Microcirc 2009; 42: 75-97.

20. Hardeman MR, Goedhart P, Shin S. Methods in hemorheology. In: Baskurt OK, Hardeman MR, Rampling MR, Meiselman HJ, eds. Handbook of Hemorheology and Hemodynamics. Netherlands: IOS Press; 2007: 242-66.

21. Ozdamar M, Kilic Erkek O, Tumkaya S, Ozdamar HC, Ozdamar A, Pakyurek H et al. Examination of the effectiveness of 12-week Nordic Walking exercise in prediabetic individuals. Pam Med J 2022; 15: 285-301.

22. Kilic-Toprak E, Unver F, Kilic-Erkek O, Korkmaz H, Ozdemir Y, Oymak B, et al. Increased erythrocyte aggregation following an acute bout of eccentric isokinetic exercise does not exceed two days. Biorheology 2018; 55: 15-24.

23. Erel O. A new automated colorimetric method for measuring total oxidant status. Clin Biochem 2005; 38(12): 1103-11.

24. Erel O. A novel automated direct measurement method for total antioxidant capacity using a new generation, more stable ABTS radical cation. Clin Biochem 2004; 37(4): 277-85.

25. Kaminsky LA, Arena R, Myers J. Reference standards for cardiorespiratory fitness measured with cardiopulmonary exercise testing: data from the fitness registry and the importance of exercise national database. Mayo Clin Proc 2015; 90(11): 1515-23.

26. Pescatello LS, Blanchard BE, Tsongalis GJ, Maresh CM, Griffiths B, Thompson PD. The GNAS 393 T>C polymorphism and the blood pressure response immediately following aerobic exercise among men with elevated blood pressure. Vasc Dis Prev 2009; 6: 56-64.

27. Thompson PD, Crouse SF, Goodpaster B, Kelley D, Moyna N, Pescatello L. The acute versus the chronic response to exercise. Med Sci Sports Exerc 2001; 33: S438-45

28. Latosik E, Zubrzycki IZ, Ossowski Z, Bojke O, Clarke A, Wiacek M, et al. Physiological responses associated with nordic-walking training in systolic hypertensive postmenopausal women. J Hum Kinet 2014; 43: 185-90.

29. Brun JF. Exercise hemorheology as a three acts play with metabolic actors: is it of clinical relevance? Clin Hemorheol Microcirc 2002; 26(3): 155-74.

30. Suhr F, Brenig J, Müller R, Behrens H, Bloch W, Grau M. Moderate exercise promotes human RBC-NOS activity, NO production and deformability through Akt kinase pathway. PLoS One 2012; 7: e45982.

31. Tomschi F, Bloch W, Grau M. Impact of type of sport, gender and age on red blood cell deformability of elite athletes. Int J Sports Med 2018; 39: 12-20.

32. Cebula A, Tyka A, Pilch W. Effects of 6-week Nordic walking training on body composition and antioxidant status for women 55 years of age. Int J Occup Med Environ Health. 2017; 30: 445-54.

33. Sari R, Balci MK, Balci N, Karayalcin U. Acute effect of exercise on plasma leptin level and insulin resistance in obese women with stable caloric intake. Endocr Res 2007; 32: 9-17.

34. Bouassida A, Zalleg D, Bouassida S, Zaouali M, Feki Y, Zbidi A, et al. Leptin, its implication in physical exercise and training: a short review. J Sports Sci Med 2006; 5: 172-81.

35. Fox J, Rioux BV, Goulet EDB, Johanssen NM, Swift DL, Bouchard DR, et al. Effect of an acute exercise bout on immediate post-exercise irisin concentration in adults: A meta-analysis. Scand J Med Sci Sports 2018; 28: 16-28.

36. Rashti BA, Mehrabani J, Damirchi A, Babaei P. The influence of concurrent training intensity on serum irisin and abdominal fat in postmenopausal women. Prz Menopauzaly 2019; 18: 166-73.
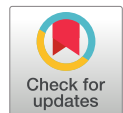
Experimed

Research Article

Open Access

Cytotoxic Effect of Fenugreek (Trigonella foenum-graecum) Seed Extracts on the Wnt Signaling Pathway in the K562 Cell Line

Can Vuruskan [1] , Burcu Cerci Alkac [1] , Tuba Oz [2] , Melek Pehlivan [3] , Mustafa Soyoz [1] ✉

[1] Department of Medical Biology, Faculty of Medicine, Izmir Katip Celebi University, Cigli, Izmir, Turkiye
[2] Department of Toxicology, Poznan University of Medical Sciences, Poznan, Poland
[3] Department of Medical Laboratory, Vocational School of Health Services, Izmir Katip Celebi University, Izmir, Turkiye

Abstract

Objective: Researchers have established that the fenugreek plant exhibits anti-proliferative effects against various types of cancer, highlighting its potential as a valuable source for the development of new anticancer drugs. This study attempted to assess the anti-cancer effects of fenugreek on the K562 chronic myeloid leukemia (CML) cells due to the Wnt signaling pathway.

Materials and Methods: The cytotoxic effect of Fenugreek was performed by 2,3-bis(2-methoxy-4-nitro-5-sulfophenyl)-2H-tetrazolium-5-carboxanilide (XTT) assay. We used reverse transcription-polymerase chain reaction (RT-PCR) to determine gene expression, and western blot was used to detect β-catenin, c-Jun N-terminal kinase (JNK), calcium/calmodulin-dependent protein kinase (CamK), and protein kinase C (PKC) proteins.

Results: The IC_{50} value of fenugreek extract was 717 g/mL after 24 h, and an *in vitro* cytotoxic effect was observed on K562 cell lines. JNK, PKC, CamK, and β-catenin protein levels were reduced in fenugreek extract-treated cells by 81%, 20%, 7%, and 26%, respectively.

Conclusion: According to our findings, fenugreek can affect both canonical and non-canonical pathways in K562 cells, particularly via the JNK protein in the planar cell polarity (PCP) pathway. These data corroborates our hypothesis that fenugreek extract possesses adjuvant compounds beneficial for CML treatment.

Keywords   Fenugreek · Chronic myeloid leukemia · Wnt signaling · Plant extract

✉ Corresponding author: Mustafa Soyoz mustafa.soyoz@ikcu.com

INTRODUCTION

Chronic myeloid leukemia (CML) is a hematological malignancy characterized by the presence of Philadelphia chromosome, resulting in the expression of the BCR-ABL1 fusion protein. This oncoprotein promotes the uncontrolled proliferation and impaired apoptosis of hematopoietic cells, leading to leukemogenesis (1). Although tyrosine kinase inhibitors (TKIs) have dramatically improved CML treatment, resistance to these drugs remains a major clinical challenge (2). This resistance is partly attributed to aberrant signaling pathways, such as the Wnt/β-catenin pathway, which plays a crucial role in cellular renewal and is often dysregulated in various cancers, including CML (3). When activated, Wnt signaling prevents β-catenin phosphorylation, resulting in its accumulation and enhanced leukemia progenitor cell survival (4). As a key player in CML pathogenesis, β-catenin presents a promising therapeutic target.

Fenugreek (Trigonella foenum-graecum L.), a widely distributed plant used in traditional medicine, has garnered attention for its pharmacological properties, including anticancer effects (5). Recent studies have demonstrated that fenugreek extracts exhibit cytotoxicity in various cancer cell lines, including CML cells, through multiple bioactive compounds such as flavonoids and alkaloids (6, 7). While the therapeutic potential of fenugreek in CML has been suggested, its specific impact on Wnt signalling in this context remains unexplored. This study aims to investigate how Fenugreek modulates Wnt/β-catenin signaling in K562 CML cells, providing new insights into its potential as an adjunct therapy in overcoming TKI resistance. By evaluating the effects of Fenugreek on β-catenin expression, along with key signaling proteins such as c-Jun N-terminal kinase (JNK), calcium/calmodulin-dependent protein kinase (CamK), and protein kinase C (PKC), this research fills a critical gap in the literature regarding the modulation of Wnt pathways in CML treatment. *In vitro* studies have shown a cytotoxic effect of fenugreek extracts on several cancer cells (7).

The Wnt/β-catenin pathway is essential for the self-renewal and proliferation of leukemic stem cells (LSCs) in CML (8). Fenugreek may exert anti-leukemic effects by modulating Wnt signaling, potentially reducing LSC self-renewal and proliferation. The presence of specific miRNAs induced by Fenugreek could target Wnt signaling components, thereby influencing the pathway's activity (9).

In this work, the Wnt signaling pathway was investigated in relation to the possible anticancer effects of fenugreek extract on K562 cells. Both mRNA and protein levels demonstrated the amounts of β-catenin expression. JNK, CamK, and PKC proteins were detected by Western blot.

MATERIALS AND METHODS

Plant Material

Fenugreek extract was purchased from a certified company called INDUS Biotech Company (India). The extract Lot number was FE0819030016. Then, 1 mg fenugreek extract was resolved in 1 mL RPMI (1 mg/mL) and diluted at concentrations between 300 and 800 μg/mL.

Cell Culture

Penicillin/streptomycin, L-glutamine, and fetal bovine serum (FBS) enriched RPMI medium was used to grow K562 cells that were incubated at 37 °C with 5% CO_2.

2,3-bis(2-methoxy-4-nitro-5-sulfophenyl)-2H-tetrazolium-5-carboxanilide (XTT) Cell Viability Assay

Cell counts were ascertained using a hemocytometer through the trypan blue exclusion technique. The assessment of cell proliferation and vitality was conducted using XTT test from Biological Industries, Israel. K562 cells (5×10^3 cells/well) were cultivated in a 96-well plate using this procedure. Subsequently, the wells received a medium containing varying doses of fenugreek extract (300, 400, 500, 600, 700, and 800 μg/mL) for a 24-h incubation period. A 50uL of the XTT solution was dispensed into each well. Following the incubation at 37 °C for 2-4 hours, the formazan crystals were assessed at 450 and 630 nm using a microplate reader (PG Instruments). Untreated cells were used as the control group. All experiments were conducted in duplicate.

RNA Extraction, cDNA Synthesis, and Reverse Transcription-Polymerase Chain Reaction (RT-PCR) Assay

K562 cells (1×10^6 cells/well) were cultured in 6-well plates and exposed to half maximal inhibitory concentration (IC_{50}) of fenugreek extract for 24 h (IC_{50}=717 μg/mL). Harvesting of the cells was performed by centrifugation and the medium was removed. Thermo Scientific GeneJET RNA Purification Kit was used for RNA extraction, followed by the cDNA synthesis with A.B.T.™ cDNA Synthesis Kit. A.B.T.™ 2X qPCR SYBR-Green Master Mix was used for RT-PCR and the primer sequences are shown in Table 1. The threshold cycle (Ct) values of β-catenin in all samples were normalized to β-actin.

Table 1. RT-PCR primer sets

Genes	Forward (5'–3')	Reverse (5'–3')
β-actin	CTTCCTGGGCATGGAGTCCTG	GGAGCAATGATCTTGATCTTC
β-catenin	TCTGAGGACAAGCCACAAGATTACA	TGGGCACCAATATCAAGTCCAA

Western Blot Analysis

β-actin, β-catenin, JNK antibodies were purchased from Cell Signaling Technology, USA. PKC and CaMK were obtained from Santa Cruz, USA. K562 cells (1×10^6 cells/well) were subjected to fenugreek extract treatment (IC_{50}=717 μg/mL) for 24 h, while control cells remained untreated. Following incubation, the K562 cells were collected via centrifugation, and the media was discarded. The cell lysates were prepared using RIPA lysis buffer and concentrated for 10 min at 4°C at 12,000 × g. The protein was measured using the Bradford technique and then transferred to a PVDF membrane after being loaded onto a 10% SDS-PAGE gel. Upon preliminary antibody incubation, secondary antibody treatment, and protein band detection with Luminata Forte Western HRP Substrate (Millipore, USA), the membrane was considered ready for use. All experiments were performed in duplicate.

Statistical Analyses

We used SPSS 11 (SPSS Inc., Chicago, IL, USA) and one-way ANOVA to analyze the data. GraphPad Prism 9 from GraphPad Software, Inc. was used to construct the graphs. ImageJ was used for the quantitative evaluation of the Western blot picture (Image Media Cybernetics Inc.) ($p < 0.05$).

RESULTS

### Fenugreek Had a Cytotoxic Effect on K562 Cells

The fenugreek extract was tested for its effect on K562 cell survival. Over the course of 24 h, K562 cells were exposed to the fenugreek extract at doses ranging from 300 to 1000 μg/mL. The *in vitro* cytotoxicity of fenugreek extracts on K562 cell lines was assessed using the XTT assay. Following 24 h of treatment with the extract, a decrease was seen in the viability of K562 cells. IC_{50} value of the fenugreek extract was observed to be 717 μg /mL for 24 h (Figure 1).

The Difference in β-catenin Gene Expression Was Detected Between Fenugreek-treated and Untreated Cells

Following total RNA isolation and cDNA synthesis, expression changes of β-catenin and β-actin genes were analyzed by RT-PCR. The expression of β-catenin was diminished in the treated cells compared with the untreated cells (Figure 2).
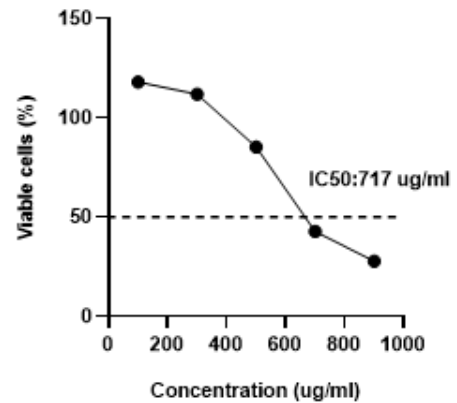
Figure 1. A 24-h XTT activity experiment evaluating the cytotoxic effects of different dosages of fenugreek on K562 cells.
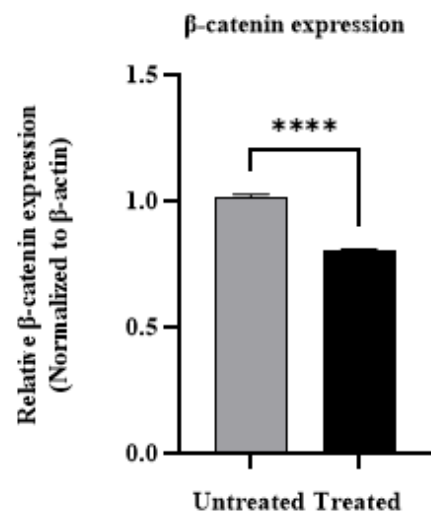
Figure 2. Effects of 717 μg/mL fenugreek extract on β-catenin gene expression of the K562 cell line at 24 h. *$p < 0.001$. (Untreated 1.013 ± 0.012, treated 0.8 ± 0.008). Data represent the mean ± standard deviation of duplicated experiments.

Protein Expression Changes Between the Fenugreek-treated and Untreated Groups

β-catenin, SAPK/JNK, PKC, and CAMK expression levels were normalized to β-actin levels. The SAPK/JNK p54 and β-catenin expression levels were significantly lower after Fenugreek treatment compared with the untreated group (Figure 3a, 3b).

DISCUSSION

Tyrosine kinase inhibitors are widely used in CML therapy. However, most of the patients can develop resistance to TKI. The studies mainly focused on overcoming drug resistance and disease progression and tried to find new drug agents and
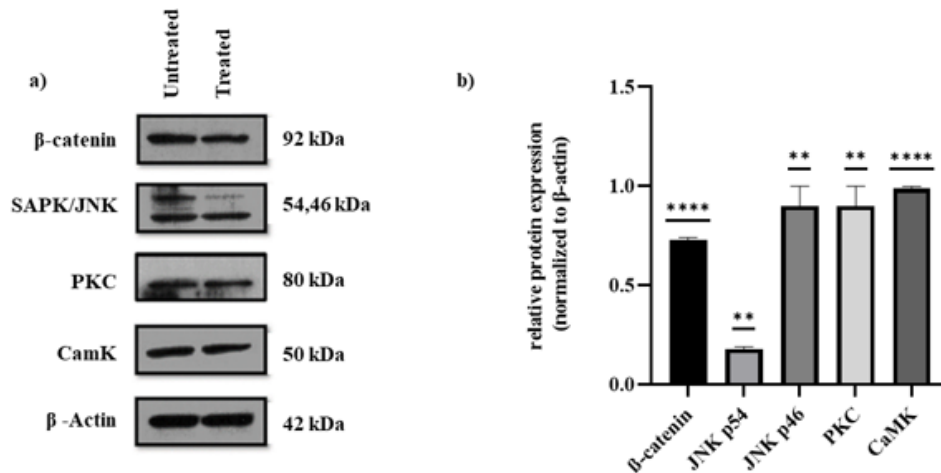
Figure 3. Analysis of fenugreek extract in K562 cells by Western blotting after 24 h of treatment (IC$_{50}$=717 μg/mL) a) Representative immunoblots of experiments. b) Relative protein expression. **p<0.01 ***p=0.005; ****p<0.001. Data represent the mean ± standard deviation of duplicated experiments.

natural additives or the effect of the combined applications (10).

Fenugreek is a medicinal plant that has been used since antiquity to treat diseases such as excessive cholesterol (11), diabetes (12), gastrointestinal disorders (13), and wound inflammation (14). Recent research has highlighted the biological activity and medicinal qualities of this species, primarily through investigations of alkaloids, flavonoids, steroids, and bioactive metabolites, including saponins and diosgenin (15). There is evidence that fenugreek possesses anti-cancer capabilities because of the functional chemical elements that it contains. Alsemari et al. demonstrated that the water extract derived from fenugreek seeds was cytotoxic on many cancer cell lines (16). Khalil et al. reported the anti-apoptotic effects of the fenugreek methanol extract in HepG2 cells (IC$_{50}$ = 1.000 μg/mL) (17). Previous research has shown that different fenugreek extracts can have cytotoxic effects and trigger apoptosis on breast cancer MCF-7 cells (18-20). Al-Oqail et al. showed the cytotoxic effect of the seed oil of fenugreek on epidermoid cancer cells and MCF-7 cells (21). We have also found that fenugreek extracts are cytotoxic to K562 cells. The Wnt signaling pathway is considered significant in controlling the mechanisms of cell proliferation, development, and differentiation (22). Abnormal Wnt signaling is associated with cancer. The effect of flavonoids such as luteolin, quercetin, trigonelline, and vitexin in fenugreek on the Wnt pathway was investigated. Chen et al. found that trigonelline reduced cell death via the Wnt pathway in human mesangial cells. They have also revealed that trigonelline modulates additional elements of the signaling cascade (23, 24). Pandurangan et al. demonstrated the effects of luteolin on

human CRC cells. Research has shown that luteolin can inhibit the growth of human colorectal cancer cells by reducing β-catenin expression (25). Moreover, several effects of luteolin were demonstrated by different research groups by both *in vitro* and *in vivo* experiments (26-28).

In this study, major regulators of the Wnt signaling pathway were examined based on protein expression in K562 cells treated with fenugreek extracts. While for Wnt/Ca²⁺ signaling PKC and CamKII, for Wnt/planar cell polarity (PCP) pathway JNK was investigated and for Wnt/β-catenin signaling β-catenin expressions were analyzed. In our study, we found that the expression levels of β-catenin, which is the major regulator in the canonical pathway, was decreased in K562 cells treated with fenugreek. The canonical pathway is a well-studied and proven pathway for the development of CML treatment strategies (29). Activated Wnt/β-catenin signaling promotes leukemogenesis by mediating LSC self-renewal and drug resistance (30). The BCR-ABL1 oncogene can promote β-catenin during the blast phase of the disease. Hence, the reduction in the Wnt/β-catenin pathway holds great significance in inhibiting the growth of leukemic stem cells that are associated with CML (31).

The PKC and CaMK genes play important roles in the non-canonical Wnt/Ca²⁺ pathway in hematological malignances (32). Experimental and clinical evidence both point to the possibility that PKC inhibitors could be useful in CML treatment (33). In addition, CaMKs reduce carcinogenesis and leukemia formation (34). The increased level of JNK protein in the PCP pathway was the most compelling finding after using fenugreek in CML cells. Na et al. discovered increased JNK expression in nilotinib-resistant CML cells (35). They

discovered that using a JNK inhibitor increased the sensitivity of K562 cells to nilotinib. As a result, the decrease in JNK expression observed in our findings may be important in CML progression. To determine the mechanism that is responsible for this decrease in JNK, additional research is required.

Currently, there is no available literature regarding the impact of fenugreek seed extract on the Wnt pathway in K562 cells. For this reason, our work is important to show the effect of an herbal extract on the Wnt signaling pathway. The anti-cancer properties of fenugreek seed extract will be investigated in further studies for its ingredient beneficial to CML therapy.

Author Details

Can Vuruskan
[1] Department of Medical Biology, Faculty of Medicine, Izmir Katip Celebi University, Cigli, Izmir, Turkiye

0000-0003-1266-9898

Burcu Cerci Alkac
[1] Department of Medical Biology, Faculty of Medicine, Izmir Katip Celebi University, Cigli, Izmir, Turkiye

0000-0002-7477-1073

Tuba Oz
[2] Department of Toxicology, Poznan University of Medical Sciences, Poznan, Poland

0000-0003-4366-8927

Melek Pehlivan
[3] Department of Medical Laboratory, Vocational School of Health Services, Izmir Katip Celebi University, Izmir, Turkiye

0000-0001-8755-4812

Mustafa Soyoz
[1] Department of Medical Biology, Faculty of Medicine, Izmir Katip Celebi University, Cigli, Izmir, Turkiye

0000-0001-5159-6463   ✉ mustafa.soyoz@ikcu.com

REFERENCES

1. Cortes J, Lang F. Third-line therapy for chronic myeloid leukemia: current status and future directions. J Hematol Oncol 2021; 14(1): 44.

2. Braun TP, Eide CA, Druker BJ. Response and resistance to BCR-ABL1-targeted therapies. Cancer Cell 2020; 37(4): 530-42.

3. Grassi S, Palumbo S, Mariotti V, Liberati D, Guerrini F, Ciabatti E, et al. The WNT pathway is relevant for the BCR-ABL1-independent resistance in chronic myeloid leukemia. Front Oncol 2019; 9: 532.

4. Chiarini F, Paganelli F, Martelli AM, Evangelisti C. The role played by Wnt/β-catenin signaling pathway in acute lymphoblastic leukemia. Int J Mol Sci 2020; 21(3): 1098.

5. Khan F, Negi K, Kumar T. Effect of sprouted fenugreek seeds on various diseases: A review. J. Diabetes Metab Disord Control 2018; 5: 119-125.

6. Ahmad A, Alghamdi SS, Mahmood K, Afzal M. Fenugreek a multipurpose crop: potentialities and improvements. Saudi J Biol Sci 2016; 23(2): 300-10.

7. Shabbeer S, Sobolewski M, Anchoori RK, Kachhap S, Hidalgo M, Jimeno A, et al. Fenugreek: a naturally occurring edible spice as an anticancer agent. Cancer Biol Ther 2009; 8(3): 272-78.

8. Müschen M. WNT/β-Catenin Signaling in Leukemia. In: Goss K, Kahn M. (eds) Targeting the Wnt pathway in cancer. Springer, New York, NY. 2011. p.129–42.

9. Pehlivan M, Soyoz M, Cerci B, Karahan Coven HI, Yuce Z, Sercan, H. sFRP1 expression induces miRNAs that modulate Wnt signaling in chronic myeloid leukemia cells. Mol Biol 2020; 54(4): 626-33.

10. Bavaro L, Martelli M, Cavo M, Soverini S. Mechanisms of disease progression and resistance to tyrosine kinase inhibitor therapy in chronic myeloid leukemia: an update. Int J Mol Sci 2019; 20(24): 6141.

11. Sharma RD, Raghuram TC, Rao NS. Effect of fenugreek seeds on blood glucose and serum lipids in type I diabetes. Eur J Clin Nutr 1990; 44(4): 301-6.

12. Losso JN, Holliday DL, Finley JW, Martin RJ, Rood JC, Yu Y, et al. Fenugreek bread: a treatment for diabetes mellitus. J Med Food 2009; 12(5): 1046-49.

13. Pandian RS, Anuradha CV, Viswanathan P. Gastroprotective effect of fenugreek seeds (Trigonella foenum graecum) on experimental gastric ulcer in rats. J Ethnopharmacol 2002; 81(3): 393-97.

14. Uemura T, Hirai S, Mizoguchi N, Goto T, Lee JY, Taketani K, et al. Diosgenin present in fenugreek improves glucose metabolism by promoting adipocyte differentiation and inhibiting inflammation in adipose tissues. Mol Nutr Food Res 2010; 54(11): 1596-608.

15. Chaudhary S, Chaudhary PS, Chikara SK, Sharma MC, Iriti M. Review on fenugreek (Trigonella foenum-graecum L.) and its important secondary metabolite diosgenin. Not Bot Horti Agrobot Cluj-Napoca 2018; 46(1): 22-31.

16. Alsemari A, Alkhodairy F, Aldakan A, Hohanna MA, Bahoush E, Shinwari Z, et al. The selective cytotoxic anti-cancer properties and proteomic analysis of Trigonella Foenum-Graecum. BMC Complement Med Ther 2014; 14: 114.

17. Khalil MI, Ibrahim MM, El-Gaaly GA, Sultan AS. Trigonella foenum (Fenugreek) induced apoptosis in hepatocellular carcinoma cell line, HepG2, mediated by upregulation of p53 and proliferating cell nuclear antigen. BioMed Res Int 2015; 2015: 914645.

18. Alshatwi AA, Shafi G, Hasan TN, Syed NA, Khoja KK. Fenugreek induced apoptosis in breast cancer MCF-7 cells mediated independently by Fas receptor change. Asian Pac J Cancer Prev 2013; 14(10): 5783-8.

19. Khoja KK, Howes MJR, Hider R, Sharp PA, Farrell IW, Latunde-Dada GO. Cytotoxicity of fenugreek sprout and seed extracts and their bioactive constituents on MCF-7 breast cancer cells. Nutrients 2022; 14(4): 784.

20. Sebastian KS, Thampan RV. Differential effects of soybean and fenugreek extracts on the growth of MCF-7 cells. Chem Biol Interact 2007; 170(2): 135-43.

21. Al-Oqail MM, Farshori NN, Al-Sheddi ES, Musarrat J, Al-Khedhairy AA, Siddiqui M A. In vitro cytotoxic activity of seed oil of fenugreek against various cancer cell lines. Asian Pac J Cancer Prev 2013; 14(3): 1829-32.

22. Liu A, Chen S, Cai S, Dong L, Liu L, Yang Y, et al. Wnt5a through noncanonical Wnt/JNK or Wnt/PKC signaling contributes to the differentiation of mesenchymal stem cells into type II alveolar epithelial cells in vitro. PLoS One 2014: 9(3): e90229.

23. Chen C, Shi Y, Ma J, Chen Z, Zhang Mi Zhao Y. Trigonelline reverses high glucose-induced proliferation, fibrosis of mesangial cells via modulation of Wnt signaling pathway. Diabetol Metab Syndr 2022; 14(1): 28.

24. Tewari D, Jóźwik A, Łysek-Gładysińska M, Grzybek W, Bialek WA, Bicki J, et al. Fenugreek (Trigonella foenum-graecum L.) seeds dietary supplementation regulates liver antioxidant defense systems in aging mice. Nutrients 2020; 12(9): 2552.

25. Pandurangan AK, Dharmalingam P, Sadagopan SKA, Ramar M, Munusamy A. Luteolin induces growth arrest in colon cancer cells through involvement of Wnt/β-catenin/GSK-3β signaling. J Environ Pathol Toxicol Oncol 2013; 32(2): 131-9

26. Ashokkumar P, Sudhandiran G. Luteolin inhibits cell proliferation during Azoxymethane-induced experimental colon carcinogenesis via Wnt/β-catenin pathway. Invest New Drugs 2011; 29: 273-84.

27. Wang B, Wang S, Ding M, Lu H, Wu H, Li Y. Quercetin regulates calcium and phosphorus metabolism through the Wnt signaling pathway in broilers. Front Vet Sci 2022; 8: 786519.

28. Kim H, Seo EM, Sharma AR, Ganbold B, Park J, Sharma G, et al. Regulation of Wnt signaling activity for growth suppression induced by quercetin in 4T1 murine mammary cancer cells. Int J Oncol 2013; 43(4): 1319-25.

29. Yao H, Ashihara E, Maekawa T. Targeting the Wnt/β-catenin signaling pathway in human cancers. Expert Opin Ther Targets 2011; 15(7): 873-87.

30. Zhou J, Tian H, Zhi X, Xiao Z, Chen T, Yuan H, et al. Activating transcription factor 5 (ATF5) promotes tumorigenic capability and activates the Wnt/b-catenin pathway in bladder cancer. Cancer Cell Int 2021; 21(1): 660.

31. Pepe F, Bill M, Papaioannou D, Karunasiri M, Walker A, Naumann E, et al. Targeting Wnt signaling in acute myeloid leukemia stem cells. Haematologica 2022; 107(1): 307-11.

32. Mencalha AL, Corrêa S, Abdelhay E. Role of calcium-dependent protein kinases in chronic myeloid leukemia: combined effects of PKC and BCR-ABL signaling on cellular alterations during leukemia development. Onco Targets Ther 2014; 7: 1247-54.

33. Robert G, Ben Sahra I, Puissant A, Colosetti P, Belhacene, Gounon P, et al. Acadesine kills chronic myelogenous leukemia (CML) cells through PKC-dependent induction of autophagic cell death. PloS one 2009; 4(11): e7889.

34. Cui C, Wang C, Cao M, Kang X. Ca2+/calmodulin-dependent protein kinases in leukemia development. J Cell Immunol 2021; 3(3): 144-50

35. Na YJ, Yu ES, Kim DS, Lee DH, Oh SC, Choi CW. Metformin enhances the cytotoxic effect of nilotinib and overcomes nilotinib resistance in chronic myeloid leukemia cells. Korean J Intern Med 2021; 36: 196-206
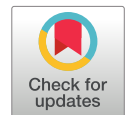
Experimed

Research Article

The Apex of the Mastoid Process as a Fixed Point in Determining the Location of the Entry of the Facial Nerve to the External Base of the Skull

Gulnara Kerimzade [1] ⓘ ✉, Nariman Movsumov [1] ⓘ

[1] Department of Human Anatomy and Medical Terminology of Azerbaijan Medical University, Baku, Azerbaijan

Abstract

Objective: This study examined how the stylomastoid foramen (SMF) relates anatomically to the mastoid process apex, analyzing variations by cranial type (brachy-, meso-, dolichocranic) and age groups, aiming to guide facial nerve blocks and surgical access.

Materials and Methods: Researchers measured the distance from the SMF left to the mastoid apex and the α-angle between SMF axis and the Frankfurt horizontal plane in 159 dry human skulls, categorized by the cephalic index and six age brackets.

Results: Significant differences were found across cranial types and age groups. Dolichocranic skulls exhibited the longest SMF–apex distance, while brachycranic skulls had the deepest SMF position and largest α-angle. The middle-age groups and dolichocranic types displayed lower α-angles, indicating morphological shifts with age and skull shape.

Conclusion: The mastoid apex is a reliable landmark for locating the SMF, but its spatial relationship varies with cranial morphology and age. These insights may improve the accuracy of facial nerve blockade and reduce risks during parotid or mastoid surgery.

Keywords Stylomastoid foramen · Mastoid process · Brachycranes dolichocranic · Mesocranes

INTRODUCTION

The facial nerve exits the skull through the stylomastoid foramen (SMF), located between the mastoid and styloid processes, and enters the parotid gland where it is divided into extracranial branches (1-3). Due to the narrow and variable anatomy of this region, the precise localization of the SMF is crucial in clinical procedures such as facial nerve blocks, parotidectomy, and facial reanimation surgeries (4-6). Inaccurate identification of the SMF can result in nerve damage and surgical complications. Although previous studies have proposed various soft tissue landmarks such as the posterior belly of the digastric muscle, retromandibular vein, and the external carotid artery for localizing the SMF, their variability limits surgical precision (7). The apex of the mastoid process is a more constant and reproducible bony landmark that may be more reliable during surgery. Despite the clinical relevance, few studies have evaluated the topographic relationship between the SMF and the mastoid apex across different cranial types and ages. Earlier studies have not considered the skull morphology (brachycranic, dolichocranic, mesocranic) or developmental and degenerative changes related to age (8, 9).

This study aimed to evaluate the anatomical correlation between the SMF and the mastoid apex in different cranial types and age groups by measuring both the linear distance and α-angle formed with the Frankfurt horizontal plane. The findings may aid in safer surgical planning and targeted facial nerve blocks.

MATERIALS AND METHODS

Study Sample

A total of 159 certified dry human skulls were analyzed. All skulls were obtained from the Department of Human Anatomy and Medical Terminology, Azerbaijan Medical University (Baku, Azerbaijan). The age and cranial measurements were determined from the accompanying anthropological records.

Ethical approval was granted by the University's Ethics Board (Approval No: AMU-2023-102).

Cranial Classification

Cranial types were defined using the cephalic index (Figure 1):

- Cephalic Index = Cranial width/Cranial length × 100

- Brachycranic: ≥ 81.0

- Mesocranic: 76.0–80.9

- Dolichocranic: ≤ 75.9

Skulls were divided into 6 age groups: Group I: 7–12 years, Group II: 13–16 years, Group III: 17–21 years, Group IV: 22–35 years, Group V: 36–60 years, and Group VI: 61–74 years (Table 1).
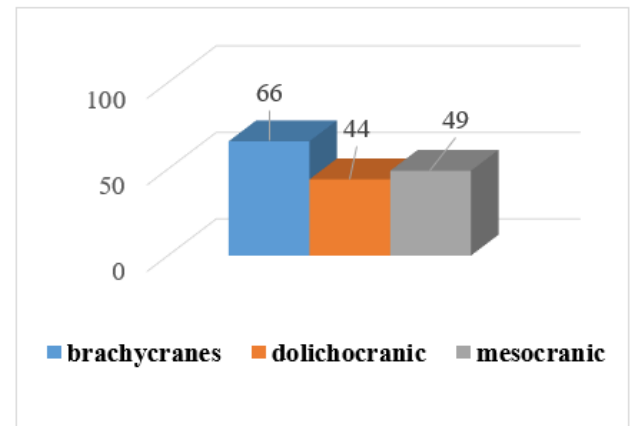

Figure 1. Distribution of skulls based on the width index

Table 1. Distributions according to age groups and skull width

Age groups	Brachycrane	Dolichocrane	Mesocrane
I	20	4	4
II	14	4	5
III	14	4	9
IV	5	8	9
V	9	19	18
VI	4	5	4
Total	66	44	49

Morphometric Measurements

Measurements taken were as follows; 1. Linear distance from the left of the SMF (midpoint of its oval shape) to the apex of the mastoid process (Figure 2). 2. α-angle between the SMF–mastoid apex line and the Frankfurt horizontal plane (established between the anatomical landmarks) (Figure 3).

All measurements were taken three times using a digital sliding caliper (accuracy 0.01 mm), and the mean values were recorded to reduce intra-observer variability.

Statistical Analyses

All numerical data were recorded and subjected to statistical processing using variation and dispersion methods with IBM SPSS Statistics for Windows, version 26.0 (IBM Corp., Armonk, NY, USA). For each group, the following parameters were calculated: arithmetic mean (M), standard error of the mean (SEM), 95% confidence interval (95% CI), median (Med), quartiles (Q1, Q3), and minimum and maximum values. Differences between the groups were assessed using analysis of variance (ANOVA) with the Fisher F-test. Pairwise comparisons were performed using the Student's t-test
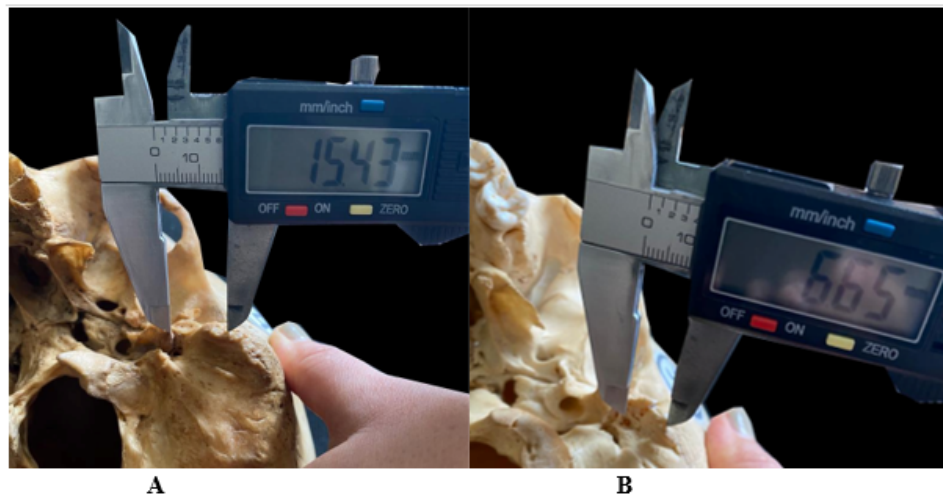
Figure 2. Distance from the stylomastoid foramen to the apex of the mastoid process. A: Mesocrane, 12 years; B: Dolichocrane, 56 years
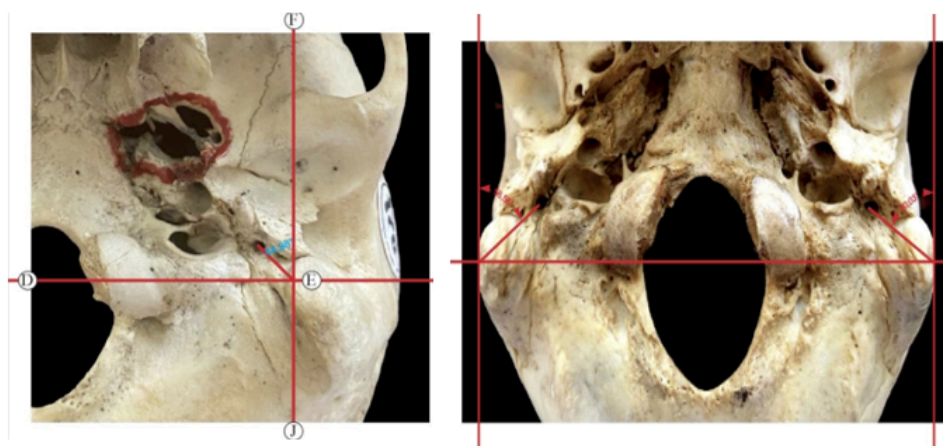

Figure 3. Determination of α-angle. A: 20-year-old mesocranial skull (α = 44.98°); B: 56-year-old brachycranial skull (α = 56.56°).

with Bonferroni correction. For comparisons between two independent groups, the non-parametric Mann–Whitney U test was used, and for comparisons among three or more groups, the Kruskal–Wallis H test was applied.

Statistical significance level was accepted as p<0.05, at which point the null hypothesis was rejected.

RESULTS

The statistical analysis of the distance between the stylomastoid foramen and the apex of the mastoid process in skulls with different cranial width indices is summarized in Table 2. A statistically significant difference was observed between the right (P_H=0.030) and left (P_H=0.007) sides among the three cranial types. The greatest mean distances were found in the dolichocranic skulls (right: 12.8 ± 0.3 mm; left: 13.1 ± 0.2 mm), and the shortest in the brachycranic skulls (right: 11.3 ± 0.4 mm; left: 11.4 ± 0.4 mm). The Mann–Whitney U test confirmed statistically significant differences

between the brachycranic and dolichocranic skulls (right: PU=0.012 left: P_U=0.004) and between the dolichocranic and mesocranic skulls on the left side (P_U=0.012). Analysis of α-angle according to cranial type showed a significant variation on the left side (P_H<0.001) (Table 3). The largest mean angle was observed in brachycranic skulls (64.5° ± 0.4°), and the smallest was observed in dolichocranic skulls (59.8° ± 1.7°). Comparisons between brachycranic and dolichocranic (P_U=0.001) and brachycranic and mesocranic skulls (P_U=0.001) revealed statistically significant differences.

Age-related analysis of the distance between the mastoid apex and the stylomastoid foramen showed significant changes in the brachycranic skulls across all age groups, on both the right and left sides (P_H<0.001) (Table 4 and Table 5). The shortest distance was noted in age group I (right: 8.2 ± 0.4 mm; left: 8.1 ± 0.5 mm), increasing in groups IV and V. Significant differences were found when comparing age group I to groups II–V (P_U<0.001), and between groups II–V, IV–VI, and V–VI.

Table 2. Statistical analysis of the distance (mm) between the apex of the mastoid process and the stylomastoid foramen in different types of dry skulls

Skull types	n	Side	M ± SEM	Min-Max	Med	Q_1	Q_3	P_H	P_{U1}	P_{U2}
Brachycrane	66	Right	11.3 ± 0.4	5.0-19.0	12.0	9.0	14.0	0.030	0.012	
		Left	11.4 ± 0.4	4.0-17.0	12.0	9.0	14.0	0.007	0.004	
Dolichocrane	44	Right	12.8 ± 0.3	9.0-18.0	13.0	11.0	14.0	0.030	0.012	
		Left	13.1 ± 0.2	9.0-16,0	13.0	12.0	14.0	0.007	0.004	0.021
Mesocrane	49	Right	12.4 ± 0.3	6.0-19.0	13.0	11.0	14.0	0.030		
		Left	12.2 ± 0.3	8.0-15.0	12.0	11.0	14.0	0.007		0.021

P_H: p value in all groups; P_{U1} and P_{U2}: p values differential integrity between the two respective groups; M: Mean; SEM: standard error of the mean; Min: Minimum; Max: Maximum; Med: Median; Q_1: first quartile; Q_3: third quartile.

Table 3. Statistical analysis of the α-angle (M°) in different types of dry skulls by the width index

Skull types	n	Side	M ± SEM	Min-Max	Med	Q_1	Q_3	P_H	P_{U1}	P_{U2}
Brachycrane	66	Right	62.5 ± 0.4	55.2-72.9	62.5	60.1	62.7			
		Left	64.5 ± 0.4	53.9-75.4	64.4	62.8	66.2	<0.001	0.001	0.001
Dolichocrane	44	Right	62.2 ± 0.6	54.6-71.0	62.5	59.5	64.7			
		Left	59.8 ± 1.7	34.5-79.8	61.9	58.8	65.3	<0.001	0.001	
Mesocrane	49	Right	63.7 ± 0.5	56.6-72.7	63.2	62.2	64.1			
		Left	62.7 ± 0.7	45.0-75.4	62.6	61.1	64.5	<0.001		0.001

P_H: p value in all groups; P_{U1} and P_{U2}: p values differential integrity between the two respective groups; M: Mean; SEM: standard error of the mean; Min: Minimum; Max: Maximum; Med: Median; Q_1: first quartile; Q_3: third quartile.

In dolichocranic skulls, changes across age groups were less pronounced but still statistically significant when comparing group II vs. III (P_U=0.050), III vs. IV (P_U=0.023), and III vs. V (P_U=0.017) on the right side.

In mesocranic skulls, statistically significant differences were observed across all age groups on both sides (right: P_H=0.023; left: P_H=0.048). The shortest distances were recorded in group I (right: 8.5 ± 0.5 mm; left: 9.0 ± 1.0 mm), gradually increasing and then declining again in group VI.

Pairwise comparisons between age groups revealed significant differences in mesocranic skulls: I vs. III (left: P_U=0.040), I vs. IV (right: P_U=0.026; left: P_U=0.039), I vs. V (left: P_U=0.033), III vs. VI (P_U=0.037), IV vs. V (right: P_U=0.033), IV vs. VI (right: P_U=0.010; left: P_U=0.029), and V vs. VI (right: P_U=0.016; left: P_U=0.023).

The α-angle also varied with age. In the brachycranic skulls, a statistically significant difference on the left side was observed across the age groups (P_H=0.017), with the smallest angle in group IV. In the dolichocranic skulls, the smallest α-angle was recorded on the right side in group IV (P_H=0.003). In mesocranic skulls, variation in α across age groups on the left side was also significant (P_H=0.042).

DISCUSSION

Recent anatomical studies have proposed several fixed bony and vascular landmarks to localize the facial nerve trunk and the stylomastoid foramen. These include the posterior belly of the digastric muscle, the retromandibular vein, the angle of the mandible, the external carotid artery, and the C_1 vertebra (11, 12). Pereira et al. (13) recommended a triangular reference formed by the temporomandibular joint, mastoid process, and mandibular angle for nerve trunk identification.

Among these, the apex of the mastoid process has a distinct anatomical role. Al-Qahtani et al. (14) observed that the facial nerve trunk lies midway between the mastoid apex and the osteochondral junction of the external auditory canal (mean distances: 9.2 ± 1.58 mm and 10.3 ± 1.79 mm). Similarly, Grayling et al. (15) measured distances of 9.35 ± 1.67 mm on the right and 9.18 ± 2.05 mm on the left.

Given the variability in the extracranial branches of the facial nerve, our study focused on its proximal (truncal) portion using dry skulls. Our findings confirm that cranial type significantly influences both the distance from the mastoid apex to the stylomastoid foramen and α-angle. In dolichocranic skulls, the foramen is positioned closer to the surface, whereas in brachycranic skulls, it lies deeper. α-angle was smaller in the dolichocranic and larger in the brachycranic skulls.

With aging, especially in brachycranic and mesocranic skulls, the distance from the mastoid apex to the stylomastoid foramen initially increases and then decreases after 60 years.

Table 4. Statistical analysis of the distance (mm) between the apex of the styloid process and the stylomastoid foramen of dry skulls in different age groups

Skull	Age groups	n	Side	M ± SEM	Min-Max	Med	Q_1	Q_3	P_{H1}	P_{H2}
Brachycrane	I	20	R	8.2 ± 0.4	5.0-11.0	8.5	7.0	9.0	right<0.001	
			L	8.1 ± 0.5	4.0-12.0	8.0	6.5	9.5	Left <0.001	
	II	14	R	11.6 ± 0.4	8.0-14.0	11.5	11.0	13.0		
			L	11.4 ± 0.6	7.0-17.0	11.5	10.0	12.0		
	III	14	R	12.9 ± 0.7	8.0-19.0	13.5	12.0	14.0		
			L	13.6 ± 0.8	10.0-17.0	13.5	11.0	16.0		
	IV	5	R	14.4 ± 0.4	14.0-16.0	14.0	14.0	14.0		
			L	13.6 ± 0.4	13.0-15.0	13.0	13.0	14.0		
	V	9	R	13.1 ± 0.4	12.0-15.0	13.0	12.0	14.0		
			L	14.1 ± 0.5	11.0-15.0	15.0	14.0	15.0		
	VI	4	R	12.0 ± 3.0	9.0-15.0	12.0	9.0	15.0		
			L	11.0 ± 1.0	10.0-13.0	11.0	10.0	12.0		
Dolichocrane	I	4	R	14.2 ± 0.4	13.5-16.0	13.8	11.9	13.9		
			L	12.1 ± 0.3	12.3-14.7	11.7	10.5	13.5		
	II	4	R	13.0 ± 0.9	11.0-15.0	13.0	11.5	14.5		
			L	13.0 ± 0.4	12.0-14.0	13.0	12.5	13.5		
	III	4	R	10.0 ± 0.6	9.0-12.3	10.0	9.0	11.0		
			L	11.7 ± 0.3	10.5-14.0	12.0	11.0	12.0		
	IV	8	R	12.9 ± 0.6	11.0-16.0	12.5	11.5	14.0		
			L	13.6 ± 0.4	12.0-15.0	13.5	13.0	14.5		
	V	19	R	13.3 ± 0.5	10.0-18.0	13.0	12.0	15.0		
			L	13.4 ± 0.4	11.0-16.0	13.0	12.0	15.0		
	VI	5	R	12.2 ± 0.8	10.0-14.0	12.0	11.0	14.0		
			L	12.4 ± 1.0	9.0-15.0	13.0	12.0	13.0		
Mesocrane	I	4	R	8.5 ± 0.5	6.0-11.0	8.5	6.0	11.0		Right - 0.023
			L	9.0 ± 1.0	8.0-10.0	9.0	8.0	10.0		Left - 0.048
	II	5	R	12.2 ± 1.2	10.0-16.0	11.0	10.0	14.0		
			L	11.8 ± 0.9	9.0-14.0	12.0	11.0	13.0		
	III	9	R	13.3 ± 0.9	10.0-19.0	14.0	11.0	14.0		
			L	12.7 ± 0.5	10.0-15.0	13.0	12.0	13.0		
	IV	9	R	13.3 ± 0.3	12.0-15.0	13.0	13.0	14.0		
			L	12.9 ± 0.5	10.0-14.0	13.0	12.0	14.0		
	V	18	R	12.3 ± 0.3	10.0-14.0	12.0	11.0	13.0		
			L	13.3 ± 0.4	8.0-14.0	12.0	11.0	14.0		
	VI	4	R	10.0 ± 0.6	9.0-11.0	10.0	9.0	11.0		
			L	10.3 ± 0.3	10.0-11.0	10.0	10.0	11.0		

P_{H1}: p values in brachycranes; P_{H2}: p values in mesocranes difference integrity between all age groups; M: Mean; SEM: standard error of the mean; Min: minimum; Max: maximum; Med: median; Q_1: first quartile; Q_3: third quartile; R: right; L: left.

In contrast, age-related changes in the dolichocranic skulls were less pronounced.

Our α-angle findings support earlier studies (16) although previous research did not consider cranial index or age-related morphology. The α-angle data align with those of Sharma and Varshney (17), who analyzed 100 skulls and proposed its utility for locating the stylomastoid foramen in clinical procedures, such as facial nerve blocks.

CONCLUSIONS

The apex of the mastoid process serves as a reliable anatomical landmark for locating the stylomastoid foramen.

Table 5. Statistical analysis of α-angle (M0) in brachycrane, dolichocrane and mesocrane dry skulls in different age groups

Skull	Age groups	n	Side	M ± SEM	Min-Max	Med	Q_1	Q_3	P_{H1}	P_{H2}	P_{H3}
Brachycrane	I	20	R	62.5 ± 0.3	60.1-67.7	62.5	62.0	62.6			
			L	65.1 ± 0.6	54.3-68.1	66.1	64.9	66.2	0.017		
	II	14	R	63.8 ± 0.9	58.5-69.7	63.8	61.4	66.7			
			L	65.6 ± 0.7	62.5-70.6	64.4	63.5	66.5	0.017		
	III	14	R	61.4 ± 0.9	58.5-68.8	60.9	58.5	63.3			
			L	64.5 ± 1.0	61.7-75.4	63.6	62.0	64.5	0.017		
	IV	5	R	62.3 ± 2.8	56.6-72.9	61.3	59.5	61.3			
			L	60.8 ± 1.8	53.9-63.9	61.9	61.9	62.7	0.017		
	V	9	R	61.6 ± 1.7	55.2-69.4	63.2	56.6	64.5			
			L	63.6 ± 1.5	56.5-70.0	64.5	60.0	66.1	0.017		
	VI	4	R	65.3 ± 2.8	62.5-68.1	65.3	62.5	68.1			
			L	64.4 ± 1.0	63.4-67.4	64.4	63.4	65.4	0.017		
Dolichocrane	I	4	R	62.8 ± 0.3	60.1-66.3	62.5	62.0	62.6		0.003	
			L	66.3 ± 0.4	64.3-68.1	66.1	64.9	66.2			
	II	4	R	57.6 ± 1.1	54.6-59.5	58.1	56.1	59.0		0.003	
			L	66.0 ± 0.9	64.5-68.4	66.6	64.5	67.5			
	III	4	R	62.5 ± 3.7	58.0-69.9	59.7	58.0	69.0		0.003	
			L	64.9 ± 5.3	58.5-75.3	60.8	58.5	75.3			
	IV	8	R	60.0 ± 0.8	57.0-64.4	59.8	58.4	61.2		0.003	
			L	62.0 ± 1.1	59.8-68.7	61.2	59.8	62.7			
	V	19	R	62.9 ± 0.5	58.6-68.0	62.7	62.2	64.4		0.003	
			L	61.6 ± 2.2	34.5-79.8	62.7	59.0	65.6			
	VI	5	R	66.8 ± 1.4	62.3-71.0	67.1	65.3	68.1		0.003	
			L	63.8 ± 3.1	53.5-72.8	65.3	61.9	65.4			
Mesocrane	I	4	R	62.6 ± 0.1	60.6-63.6	63.6	62.6	63.6			
			L	65.5 ± 0.3	65.2-67.0	65.5	65.2	66.8			0.042
	II	5	R	62.7 ± 0.8	59.7-64.3	63.4	62.5	63.8			
			L	61.7 ± 0.8	58.5-62.6	62.4	62.3	62.5			0.042
	III	9	R	64.3 ± 1.8	56.6-72.5	62.2	61.2	68.8			
			L	60.7 ± 2.7	45.0-75.4	61.2	61.1	63.5			0.042
	IV	9	R	63.7 ± 0.5	61.2-65.3	64.5	62.4	64.5			
			L	62.7 ± 1.1	54.3-65.0	63.6	62.6	64.5			0.042
	V	18	R	62.9 ± 0.5	56.7-67.2	63.2	62.2	64.3			
			L	62.4 ± 0.7	57.5-70.7	62.2	60.3	64.3			0.042
	VI	4	R	69.0 ± 3.3	62.5-72.7	72.0	62.5	72.7			
			L	69.6 ± 3.1	63.4-72.8	72.4	63.4	72.8			0.042

p values in difference integrity between all age groups in P_{H1}-brachycranes; P_{H2}-dolichocranes; P_{H3}-mesocranes; M: mean; SEM: standard error of the mean; Min: minimum; Max: maximum; Med: median; Q_1: first quartile; Q_3: third quartile; R: right; L: left.

In dolichocranic skulls, the foramen lies more superficially, with a greater distance to the mastoid apex and a smaller α-angle. In brachycranic skulls, it is located deeper, with a larger α-angle. Age significantly affects these parameters in brachycranic and mesocranic skulls, particularly after 60 years. These morphometric patterns should be considered in clinical and surgical approaches to the facial nerve.

16. Kutoğlu T, Çetkin M, Turan Ö, Bayko S, Yarkan İS. Morphometric and topographic features of stylomastoid foramen and its clinical significance in facial nerve block. J Neurol Surg B Skull Base 2021; 82(S 03): e271-e277.

17. Sharma N, Varshney R. Morphometry of stylomastoid foramen and its clinical application in facial nerve block. Saudi J Anaesth 2015; 9(1): 60–3.
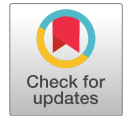
Author Details

Gulnara Kerimzade
[1] Department of Human Anatomy and Medical Terminology of Azerbaijan Medical University, Baku, Azerbaijan

0000-0002-3460-0130   kerimzade73@list.ru

Nariman Movsumov
[1] Department of Human Anatomy and Medical Terminology of Azerbaijan Medical University, Baku, Azerbaijan

0009-0004-5566-5234

REFERENCES

1. Seneviratne SO, Patel BC. Facial Nerve Anatomy and Clinical Applications. In: StatPearls. Treasure Island (FL): StatPearls Publishing; 2024.

2. Takezawa K, Townsend G, Ghabriel M. The facial nerve: anatomy and associated disorders for oral health professionals. Odontology 2018; 106(2):103-6.

3. Phillips CD, Bubash LA. The facial nerve: anatomy and common pathology. Semin Ultrasound CT MR 2002; 23(3): 202-17.

4. Celik O, Eskiizmir G. The role of facial canal diameter in the pathogenesis and grade of Bell's palsy: a study by high resolution computed tomography. Braz J Otorhinolaryngol 2017; 83(3): 261-8

5. Shadlinsky VB, Abdullayev AS. Anthropology with the basics of morphology, Baku. Shahhafchi Chap Poligrafiya 2019; 413 p.

6. Ghosh S. K. Variations in the morphology of stylomastoid foramen: a possible solution to the conundrum of unexplained cases of Bell's palsy. Folia Morphol 2021; 80(1): 97-105

7. Karaca H, Soydan L. Measurement of the depth of facial nerve at the level of stylomastoid foramen using MR imaging in Bell's palsy. Clin Imaging 2019; 58: 34-8.

8. Serdar B, Rohat, Evren B, Mustafa D. The precise location of the stylomastoid foramen and clinical implication for facial nerve block. Med Records-Int Med J 2022; 4(3): 355-60.

9. Le QT, Tran QH, Pham DD, Phan-Tran TT, Tran DK. An anatomical study of main body and branches of facial nerve. J Med Pharm Chem Res 2024; 6(9): 1450-9.

10. Shadlinski VB, Movsumov NT, Gasimov ShI, Shadlinskaya SV. Human anatomy (Volume I). Baku 2024, 562 p.

11. Ghannam MG, Singh P. Anatomy, head and neck, salivary glands. In: StatPearls. Treasure Island (FL): StatPearls Publishing; 2024.

12. Sani Jahormi MS, Kalani N, Ghaedi M, Taheri L, Zabetian H, Sahraei R. Comparison of two drugs, ephedrine and lidocaine, on pain caused by propofol injection in patients undergoing elective surgery. Navid No 2023; 26(85): 49-55.

13. Pereira JA, Merí A, Potau JM, Prats Galino A, Sancho JJ, Sitges-Serra A. A simple method for safe identification of the facial nerve using palpable landmarks. Arch Surgery 2004; 139: 745-7.

14. Al-Qahtani KH, AlQahtani FM, Muqat MM, AlQahtani MS, Al-Qannass AM, Islam T, et al. A new landmark for the identification of the facial nerve during parotid surgery: A cadaver study. Laryngoscope Investig Otolaryngol 2020; 5(4): 689-93.

15. Greyling LM, Glanvill R, Boon JM, Schabort D, Meiring JH, Pretorius JP, et al. Bony landmarks as an aid for intraoperative facial nerve identification. Clin Anat 2007; 20(7): 739-44.

Experimed

Research Article

Identifying Hub Genes and miRNAs Associated with Mesial Temporal Lobe Epilepsy

Simay Bozkurt [1] , Omer Faruk Duzenli [1,2] , Emrah Yucesan [2]

[1] Department of Neuroscience, Institute of Neurological Sciences, Istanbul University, Cerrahpasa, Istanbul, Turkiye
[2] Department of Neurogenetics, Institute of Neurological Sciences, Istanbul University, Cerrahpasa, Istanbul, Turkiye

Abstract

Objective: Mesial temporal lobe epilepsy (MTLE) is a form of focal epilepsy. Recent studies indicate that microRNAs (miRNAs) are involved in the pathogenesis of MTLE. The purpose of this study was to determine differentially expressed genes (DEGs) and their regulatory miRNAs using bioinformatics analysis.

Materials and Methods: The GSE186334 gene expression dataset was retrieved from the Gene Expression Omnibus (GEO) database. DEGs between MTLE and control samples were determined using GEO2R with $p<0.05$ and $|logFC|<-1$, $|logFC|>1$ as the threshold. Metascape was used for functional enrichment and gene ontology (GO) analysis. Protein-protein interactions (PPIs) were generated using the STRING database and visualized with Cytoscape. The top 10 highly connected genes were identified as hub genes. Candidate miRNAs targeting these genes were predicted using the miRDB, miRWalk, TargetScan and miRNet databases.

Results: A total of 547 DEGs were found, comprising 380 upregulated and 167 downregulated genes. PPI analysis revealed 10 hub genes: *IL6*, *IL1B*, *TNF*, *CCL2*, *CCL3*, *CCL4*, *CXCL8*, *IL1A*, *CD86*, and *CD40LG*. miR-15a-5p and the hsa-let-7 family of miRNAs were predicted as potential regulators.

Conclusion: Key hub genes and regulatory miRNAs involved in MTLE were identified. The enrichment of proinflammatory genes indicates a significant role of neuroinflammation. miRNAs such as miR-15a-5p and the hsa-let-7 family may critically regulate these pathways. These insights could support the development of new diagnostic biomarkers and therapeutic strategies, pending experimental validation.

Keywords miRNAs · Mesial temporal lobe epilepsy · DEGs · Bioinformatics

INTRODUCTION

Epilepsy is a chronic neurological disorder characterized by recurrent, unprovoked seizures due to irregular electrical discharges in the brain. It is broadly classified into focal and generalized types based on the origin and spread of the epileptic activity. Although different brain regions can be affected depending on the type of epilepsy, the temporal lobes are the most common sites of epileptogenic activity.

Temporal lobe epilepsy (TLE) is one of the most common forms of intractable epilepsy, accounting for approximately 60% of all focal epilepsies (1). TLE can be classified into two types according to the anatomical origin of seizure onset: mesial temporal lobe epilepsy (MTLE) and lateral temporal lobe epilepsy (LTLE). MTLE accounts for approximately 80% of all TLE cases and originates from the mesial part of the temporal lobe. The hippocampus, amygdala, and parahippocampal gyrus are key structures involved in the onset or propagation of seizures (1). Despite the involvement of multiple regions, the most common neuropathological finding in MTLE is hippocampal sclerosis (HS) (2).

TLE is frequently resistant to anti-epileptic drugs (AEDs), making non-pharmacological approaches crucial for disease management. These include surgical interventions and neurostimulation techniques. TLE exhibits both clinical and genetic heterogeneity. Although most TLE cases are sporadic, advancements in genetic testing have identified the familial forms of the disorder (3).

Familial TLE is classified into three distinct groups: familial lateral temporal lobe epilepsy (FLTLE), familial mesial temporal lobe epilepsy (FMTLE), and FMTLE with HS. This heterogeneity complicates efforts to elucidate the genetic basis of the disease. Linkage analysis has associated FMTLE with chromosome 4q (4), while another study indicated that chromosome 18p may contribute to hippocampal sclerosis in FMTLE (5). However, these studies did not identify a specific disease-causing gene.

Several studies have demonstrated that neuroinflammation, ion channel changes, and epigenetic factors play an important role in the pathogenesis of MTLE (6). Along with these factors, recent research has indicated that MTLE has a complex genetic basis, likely influenced by both monogenic and polygenic factors. Candidate genes such as *SCN1A, SCN1B, LGI1*, and *DNA2* have been implicated in various forms of epilepsy, including MTLE (7). These genes are involved in neuronal excitability, synaptic transmission, and neurodevelopmental processes, which are critical in seizure pathophysiology. In a study examining the *SCN1A* mRNA expression levels in hippocampal biopsy samples of MTLE-HS patients with a

history of febrile seizures, it was found that a variation in *SCN1A* increases susceptibility to the disease (8). In another study, *LGI1* was identified as a candidate pathogenic gene in FMTLE through whole-exome sequencing (WES) analysis. In addition to the above-mentioned processes, an increasing number of studies have focused on the role of mitochondrial functions in epileptogenesis (9). An example of these studies is the detection of mitochondrial single or multiple deletions in the hippocampus of MTLE patients using the clinical-grade high-sensitivity assay. Autophagy as another cellular process plays a significant role in the pathophysiology of MTLE. The bioinformatics analysis study determined 40 autophagy-related genes associated with MTLE. In particular, it has been suggested that *BNIP, SQSTM1, VEGFA,* and *WIPI2* may play critical roles in the onset phase and progression of MTLE by regulating the autophagy pathway (10). Additionally, epigenetic modifications and regulatory elements, such as non-coding RNAs, have gained attention for their potential role in epilepsy-related gene expression changes. Among these, microRNAs (miRNAs) are key post-transcriptional regulators that may contribute to neuronal hyperexcitability and neuroinflammation, both of which are central to MTLE pathogenesis (11). Considering the above-mentioned points, genetic factors are involved in the etiopathogenesis of MTLE.

Rapid advancements in high-throughput sequencing, multi-omics technologies, and bioinformatics have significantly enhanced the identification of disease-associated genes and molecular pathways, paving the way for novel diagnostic strategies and precision medicine approaches. Researchers have also inevitably investigated the aforementioned genomic approaches in MTLE studies. In this study, we analyzed the human hippocampus microarray dataset GSE186334 from the Gene Expression Omnibus (GEO) to identify differentially expressed genes (DEGs) between MTLE non-HS patients and healthy individuals using bioinformatics approaches. Further investigation of the genetic mechanisms underlying MTLE may enable the identification of genetic biomarkers, particularly microRNAs, which could contribute to early diagnosis and disease monitoring.

MATERIALS AND METHODS

Microarray Data Selection and Preprocessing

The dataset GSE186334 was retrieved from the GEO database. The dataset was obtained using the GPL20301 Illumina HiSeq 4000 platform (Homo sapiens) and contained 68 samples, which included cortical and hippocampal tissues. To reduce heterogeneity and enhance the specificity of our analysis, we selected hippocampal tissue samples from five MTLE non-HS patients and five healthy controls. The raw gene expression

data were downloaded and preprocessed for downstream analysis. The overall workflow of this study is illustrated in Figure 1.

Identification of DEGs

DEGs between MTLE non-HS patients and healthy controls were identified using the GEO2R analysis tool. GEO2R applies the DeSeq2 package in a web-based interface to perform the detection of DEGs and statistical analysis. The significance threshold for DEGs was set at |logFC| > 1 to identify upregulated genes and |logFC| < –1 to identify downregulated genes, with an adjusted p value < 0.05 to control for the false discovery rate (FDR) (Supplementary Data).

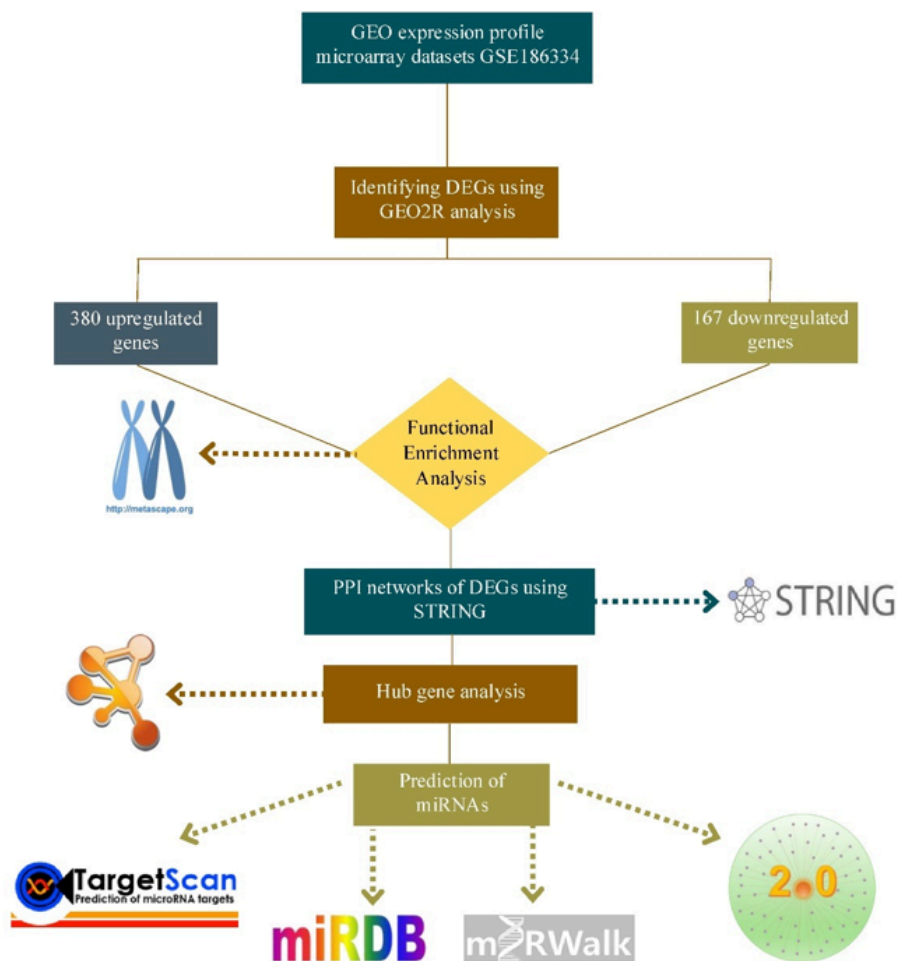## Functional Enrichment Analysis of DEGs

To examine the biological significance of the identified DEGs, Gene Ontology (GO) term enrichment analysis and Kyoto Encyclopedia of Genes and Genomes (KEGG) pathway analysis were performed using Metascape. GO enrichment analysis

categorized the DEGs into three domains: biological processes (BP), molecular functions (MF), and cellular components (CC). KEGG pathway analysis identified relevant biological pathways that may be associated with MTLE pathogenesis.

Enrichment analysis was conducted to determine the statistical significance of the GO and KEGG terms. Pathways and processes with a p value <0.05 were considered significantly enriched. The results are shown with bar plots created in Metascape.

Analysis of Hub Genes and Protein–Protein Interaction Networks

To elucidate the interactions among the identified DEGs, a protein-protein interaction (PPI) network was constructed using the STRING database. The minimum required interaction score was set to 0.4 (medium confidence) to obtain a reliable interaction network.

Figure 1. Overview of the study workflow. This figure illustrates the step-by-step methodology employed in the study, from dataset selection and preparation to identification of DEGs, enrichment analysis, construction of PPI networks, identification of hub genes, and miRNA-target interaction analysis.

Table 1. List of hub genes identified by cytoHubba based on MCC scores.

Rank	Name	Score
1	IL6	10328720136
2	TNF	10328714915
3	IL1B	10313756120
4	CXCL8	8184967523
5	CCL2	8098327608
6	CCL3	8076782887
7	IL1A	8071313809
8	CCL4	8006342400
9	CD86	7845516145
10	CD40LG	7838944014

Table 2. Degree and betweenness centrality values of the predicted miRNAs identified through the miRNet network analysis.

ID	Degree	Betweenness
hsa-miR-92b-3p	4	2.532757
hsa-mirR-7-5p	7	11.40184
hsa-miR-24-3p	6	23.63709
hsa-miR-23a-3p	4	1.999872
hsa-miR-214-3p	4	7.144143
hsa-miR-21-5p	5	4.099107
hsa-miR-191-5p	5	4.099107
hsa-miR-18a-5p	4	2.385981
hsa-miR-17-5p	5	15.50011
hsa-miR-16-5p	5	3.741408
hsa-miR-15a-5p	5	3.741408
hsa-miR-155-5p	5	5.229643
hsa-miR-124-3p	5	3.741408
hsa-miR-107	5	11.5035
hsa-miR-101-3p	4	2.881928
hsa-miR-1-3p	4	1.675764
hsa-let-7e-5p	4	2.580618
hsa-let-7b-5p	5	4.431913
hsa-let-7a-5p	5	4.672408

The PPI network was further analyzed using Cytoscape software (version 3.10.1). The cytoHubba plugin was used to identify hub genes—key nodes with high connectivity in the network. Hub genes were ranked based on maximum clique centrality (MCC), which indicates their potential functional significance within the MTLE molecular network. The MCC scores of the identified hub genes are presented in Table 1.

Prediction of miRNAs Targeting Hub Genes

To explore potential post-transcriptional regulatory mechanisms, hub genes were analyzed using miRNA-target prediction tools, including miRDB (http://mirdb.

org/), TargetScan (https://www.targetscan.org/), and miRWalk (http://mirwalk.umm.uni-heidelberg.de/). In addition, we used miRNet 2.0 to identify miRNAs that target hub genes and visualized the miRNA-target regulatory network. miRNAs with a degree of 3 or over were displayed and selected as top candidates based on their degree in the interaction network. The degree reflects the regulatory potential through the target connectivity. Although the cutoff is not biologically fixed, it helps reduce the noise and highlight miRNAs with a broader influence. The relevant literature also supported the biological roles of the selected miRNAs. Due to the small sample size, a relatively low degree cutoff was chosen to avoid excluding potentially important miRNAs. The aforementioned tools use different algorithms to predict miRNA binding sites on gene transcripts, providing complementary insights into gene-miRNA interactions. The degree and betweenness centrality values of the identified miRNAs are presented in Table 2.

RESULTS

Screening of DEGs

As a result of the filtering performed, 547 differently expressed genes were found between MTLE non-HS and controls. This included 380 upregulated and 167 downregulated genes.

Functional Enrichment Analysis

Enrichment analysis was performed separately for upregulated and downregulated genes. According to the results of the GO and KEGG analysis, the upregulated genes were found to be particularly enriched in NGF-stimulated transcription and IL-10 signaling pathways (Figure 2), whereas the downregulated genes were primarily enriched in the neuronal system pathway and the regulation of synaptic transmission processes (Figure 3).

PPI Network Analysis of the DEGs

The STRING database was employed to analyze the PPI specific to the target genes. Cytoscape 3.10.1 was used to visualize the PPI networks. Based on the PPI data, the top 10 genes with the highest degree of interaction were selected as hub genes (Figure 4). In cytoHubba, red indicates the highest interaction intensity, while yellow represents genes with lower interaction levels.

Construction of Potential miRNA-target Regulatory Networks

We identified miRNAs targeting the key genes using the miRNet database (Figure 5). We found that hsa-miR-7-5p had the highest degree (degree 7). We presumed that the hsa-

let-7 miRNA family could be the most critical miRNA in MTLE pathophysiology.

DISCUSSION

Epilepsy is a neurological disorder that causes recurrent seizures due to abnormal electrical activity in the brain. MTLE is the most common type of refractory epilepsy (1). HS is an important pathology of MTLE. The diagnosis and follow-up of the disease involve electroencephalogram (EEG), various neuroimaging analyses, and genetic tests. Apart from these methods, most studies have focused on the role of miRNAs in diagnosis and monitoring. Although it is not yet in clinical practice, there are numerous studies in the literature supporting its potential clinical use (12). Based on the analysis of the datasets, our study enables the elucidation of the molecular and genetic basis of MTLE by identifying associated with MTLE and the miRNAs targeting these genes.

This study screened MTLE non-HS and postmortem control expression datasets and identified 547 DEGs. We found that all of the hub genes were upregulated and related to inflammation-associated cytokines and chemokines.

As shown in Figure 5, *interleukin1A (IL1A)* emerges as a key gene in our study, primarily due to its central position in the miRNA interaction network. This centrality shows suggests a potentially significant regulatory role in the molecular landscape of epilepsy. The IL-1α protein encoded by the *IL1A* gene is a proinflammatory cytokine that plays a pivotal role in immune responses and inflammation, both in the periphery and within the central nervous system (CNS). IL-1α is constitutively expressed in glial cells and can be rapidly released upon neuronal injury or infection, serving as an early mediator of neuroinflammation. In the CNS, IL-1α participates in the modulation of blood-brain barrier permeability, leukocyte recruitment, and the activation of astrocytes and microglia—processes closely associated with seizure susceptibility and epileptogenesis (13).

Recent experimental studies have demonstrated that IL-1α may contribute to neuronal hyperexcitability by enhancing
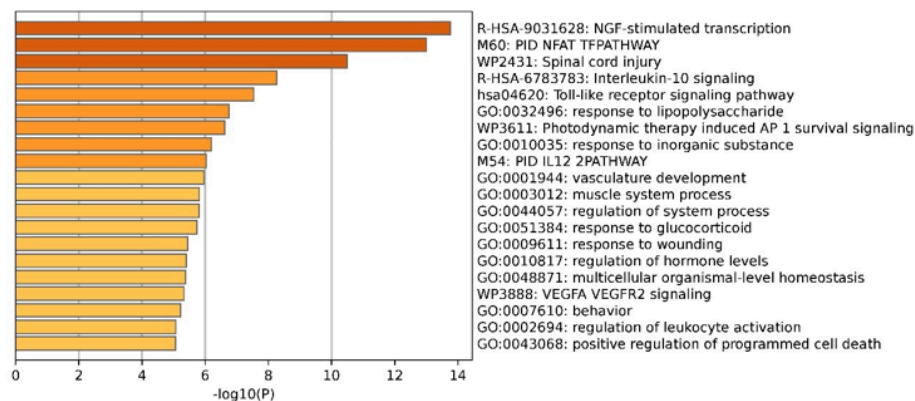

Figure 2. Enrichment analysis of downregulated genes reveals disrupted neuronal functions. GO and KEGG pathway enrichment analyses indicated that the downregulated DEGs in MTLE non-HS samples were significantly involved in the neuronal system, including the regulation of synaptic transmission and other neural processes, suggesting functional impairments relevant to epilepsy pathogenesis.
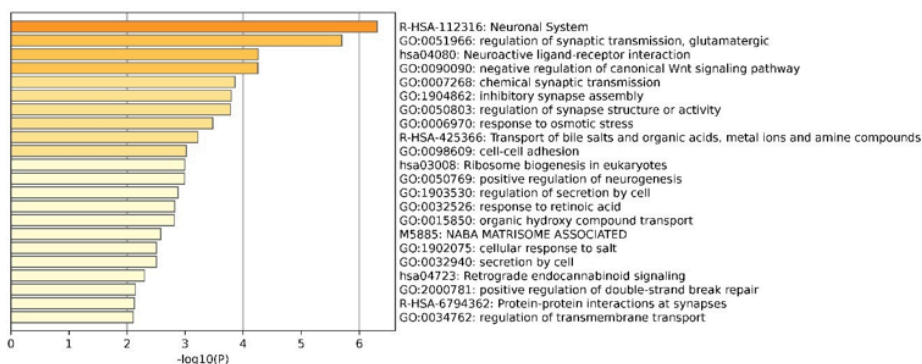

Figure 3. Enrichment analysis of upregulated genes highlights inflammation-related pathways. GO and KEGG analysis of upregulated DEGs demonstrated enrichment in pathways such as nerve growth factor (NGF)-stimulated transcription and IL10 signaling, indicating enhanced inflammatory and immune responses in MTLE non-HS patients.
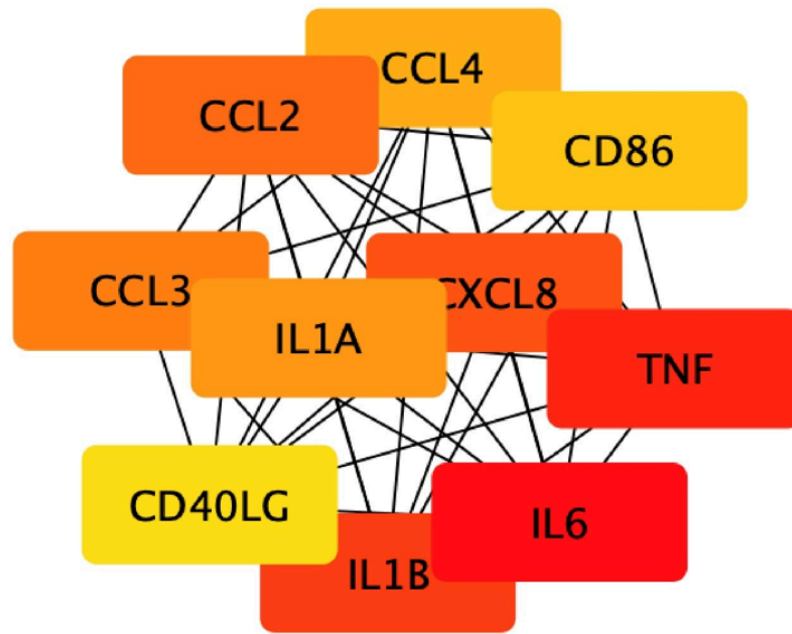
Figure 4. Identification of hub genes within the PPI network of DEGs. Using Cytoscape and the cytoHubba plugin, the top 10 hub genes were determined based on their of interaction and centrality within the constructed protein-protein interaction network. Genes with the highest interaction scores are visualized in red, indicating their potential importance in MTLE pathophysiology.
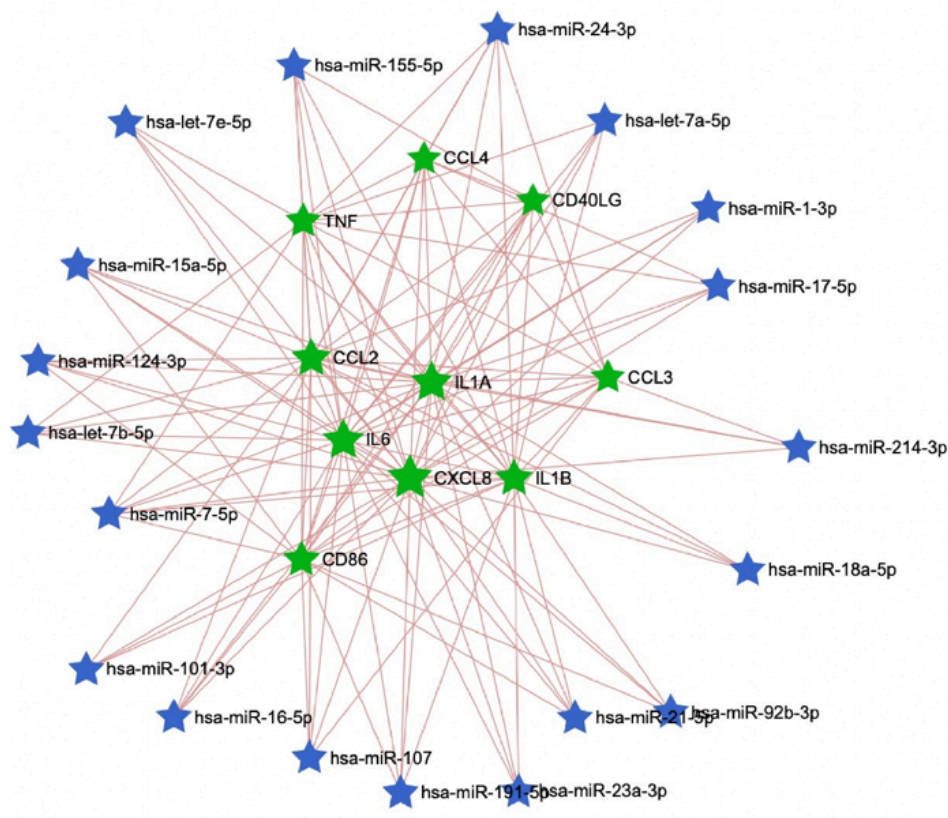
Figure 5. The miRNA-target network underscores the regulatory roles of key miRNAs in MTLE. The figure presents an miRNA-hub gene interaction network generated via miRNet 2.0. miRNAs with three or more connections are shown, with hsa-miR-7-5p and the hsa-let-7 family appearing as prominent regulators, suggesting their crucial roles in the post-transcriptional control mechanisms associated with MTLE.

glutamate release and reducing GABAergic inhibition, thereby altering the excitatory-inhibitory balance in favor of seizures. Although the body of research specifically addressing the role of IL-1α in epilepsy remains limited, accumulating evidence indicates that IL-1α, in conjunction with IL-1β and its receptor (IL-1R1), may activate intracellular signaling cascades such as the NF-κB and MAPK pathways (14). These pathways are implicated in the chronic inflammatory state observed in TLE, particularly in patients with HS. Moreover, polymorphisms in the *IL1A* gene have been associated with an increased risk of various inflammatory diseases, and emerging data suggest a possible link with seizure susceptibility, although the findings are still inconclusive and require further validation in large-scale cohorts. As neuroinflammatory responses are increasingly recognized as key modulators in the pathophysiology of MTLE, IL-1α represents a candidate molecule of interest that may not only deepen our understanding of the molecular mechanisms of epileptogenesis but also serve as a potential biomarker or therapeutic target (15).

A type I membrane protein, produced by the *CD86* gene, is part of the immunoglobulin superfamily. *CD86* is continuously expressed on antigen-presenting cells, dendritic cells, macrophages, and B cells. In the brain, *CD86* is expressed by microglia. This also shows that *CD86* plays a role in the brain's defense mechanism. There are few studies investigating the role of *CD86* in the mechanism of epilepsy.

Consistent with the results of our study, *CD86* was upregulated in a mouse model treated with kainic acid and pilocarpine. A study on the inflammatory mechanism in epilepsy found that the upregulation of 11 genes, including *CD86,* was reported to reduce the risk of the disease (16).

CXCL8 (also known as *IL8*) and *IL1B*, both have potential roles in neuroinflammation and neuroprotection. Many studies have found that altered levels of *IL8* and *IL1B* are associated with different types of epilepsy, including MTLE (17). As an example of these studies, it can be given that in patients with MTLE, it was found that *IL1B* and *IL8* were at elevated levels in the temporal cortex tissue (18).

The CD40LG gene encodes a transmembrane protein called the cluster of differentiation 40 (CD40) ligand, a member of the tumor necrosis factor (TNF) superfamily, found on the surface of T cells. CD40L binds to its receptor CD40, and CD40L-CD40 signaling is involved in various processes within the cell. These interactions play a critical role in the CNS. Although this signaling pathway has been investigated in various neurodegenerative diseases and other neurological conditions, it has been relatively understudied in epilepsy. Plasma CD40 levels and *CD40* mRNA expression levels were

significantly increased in the leukocytes of patients with post-stroke epilepsy. When brain samples from patients with TLE were examined for this signaling using an immunohistology approach, it was found that *CD40* expression levels were highly expressed in the hippocampal regions (19). These findings support further investigation of CD40LG/CD40 signaling in epilepsy.

TNF plays a significant role in both human health and disease. *TNF* is continuously expressed in the normal brain. In the CNS, this cytokine regulates various processes such as neurogenesis, neuroinflammation, synaptic plasticity, and transmission (20). Epilepsy can occur when there is an imbalance between excitation and inhibition neurotransmitters. Therefore, TNF-regulated excitatory synaptic transmission is a key step in the control of epileptic seizure development (21). This cytokine, which we found to be upregulated in our study, has an exact mechanism in epileptogenesis that has not yet been elucidated, although it has been investigated in various animal and human studies in the literature. In a study in which a limbic epilepsy mouse model was created, they showed that an increase in hippocampal TNF-α mRNA levels triggered seizures (22).

In another study in which a status epilepticus (SE) rat model was established, it was shown that dynamic TNF-α expression levels were up-regulated. Furthermore, in the same study, children with MTLE were examined, and the same results were found. This study showed that upregulation of TNF-α is associated with the development of MTLE (23). Our study found that there are 10 miRNAs that target TNF-α. Considering all these results, it is hypothesized that investigating TNF-α could be important for elucidating the underlying mechanisms of MTLE.

CCL2, CCL3, and CCL4 are chemokines that play significant roles in the epileptogenesis processes. Chemokines can stimulate the movement and activation of leukocytes toward the sites of inflammation (24). Inflammation and oxidative stress are known to be important in the mechanism of epilepsy. The release of inflammatory molecules and oxidative stress-induced free radicals in the epileptic focus may induce or maintain epileptic activity (25). In a study conducted in 2022 to investigate inflammatory parameters, brain samples from drug-resistant MTLE patients and the autopsy control group were compared. The study found that *CCL2, CCL3*, and *CCL4* were upregulated in patients (26).

IL6 is another cytokine that exhibits both pro-inflammatory and anti-inflammatory activities. IL6 is involved not only in the immune response but also in many biological and physiological processes, including the nervous system (27). In epilepsy, which we investigated in our study, it was reported

in the literature that IL6 is involved in epileptogenesis. In many studies in the literature comparing healthy controls and patients, increased levels of IL6 expression have been found in the cerebrospinal fluid (CSF), blood plasma, and blood serum samples. A study in 2022 showed that increased IL6 expression levels in CSF and serum in early-onset refractory status epilepticus can be used as a marker for early diagnosis (28). Similar results are available in the context of MTLE.

The underlying cause of a disease with a complex pathophysiology such as epilepsy requires further investigation of miRNAs to elucidate their role and apply them in practice for diagnosis. In the literature, the number of mRNAs affected by miRNAs and, consequently, the number of genes targeted by miRNAs is quite high, which is common for miRNAs. We created an miRNA-target network using miRNet 2.0 to examine potential miRNAs in MTLE.

We found that miR-15a-5p targets *CCL2, IL1A, IL6,* and *CD86*. Children with TLE exhibited significantly lower expression of miR-15a-5p than the healthy control group. The study also investigated the function of hippocampal neurons in primary neuron cultures. Primary hippocampal neurons isolated from newborn rats were cultured to mimic the TLE condition. The results showed that the expression level of miR-15a-5p was decreased in the hippocampal cells. Moreover, in cultures overexpressing miR-15a-5p, TLE-induced apoptosis and reduced cell viability were rescued (29). Therefore, it is suggested that the mentioned miRNA might be used as a potential diagnostic marker. Additionally, we found that the hsa-let-7 miRNA family (hsa-let-7a-5p, hsa-let-7b-5p and hsa-let-7e-5p) targets *IL6*. In a study, *IL6* was upregulated, while hsa-let-7a-5p was downregulated in patients with MTLE (30). We propose that *IL6,* which had the highest score according to the MCC algorithm in our study, and hsa-let-7a-5p, which targets it, should be investigated in the development of MTLE.

Although our findings highlight several inflammatory genes and miRNAs potentially associated with MTLE, it is important to interpret these associations with caution. The upregulation of cytokines such as IL-1α, IL-1β, and TNF does not necessarily indicate a causal role in epileptogenesis. Further experimental studies are required to determine their specific function and impact on MTLE pathogenesis.

CONCLUSION

In conclusion, our study highlights the potential role of specific cytokines and chemokines—including TNF-α, IL6, IL1A/B, CD86, CD40LG, and CCL family members—in the pathogenesis of MTLE, particularly in non-HS cases. These molecules, many of which are central to neuroinflammatory processes, were consistently upregulated, suggesting a robust

link between chronic inflammation and epileptogenic activity. Moreover, our miRNA-target network analysis revealed several miRNAs, notably miR-15a-5p and members of the hsa-let-7 family that may serve as upstream regulators of these inflammatory genes.

Although the causal relationship between neuroinflammation and MTLE remains uncertain—whether neuroinflammation precedes or follows seizure activity—our findings provide further evidence supporting the involvement of immune-related molecular pathways in epileptogenesis. This underscores the need for more targeted research to clarify the temporal and mechanistic dynamics of these processes.

Note that our findings were based on a relatively small number of hippocampal tissue samples, given the limited accessibility of RNA-seq data from this specific brain region. While this enhances the value of the dataset, the limited sample size may affect the generalizability of the results. Therefore, the associations identified in this study should be interpreted with caution and further validated in larger, more comprehensive datasets.

Importantly, the identification of miRNAs associated with these inflammatory mediators opens up new avenues for the development of minimally invasive biomarkers for early diagnosis, prognosis, and possibly therapeutic intervention. Future studies with larger cohorts and experimental validation are warranted to confirm the diagnostic and therapeutic utility of these candidate molecules in clinical settings.

Our findings contribute to the growing body of evidence supporting the integration of transcriptomic and miRNA-based approaches in the study of complex neurological disorders such as MTLE.

Author Details

Simay Bozkurt
[1] Department of Neuroscience, Institute of Neurological Sciences, Istanbul University, Cerrahpasa, Istanbul, Turkiye

 0000-0002-9185-4225

Omer Faruk Duzenli
[1] Department of Neuroscience, Institute of Neurological Sciences, Istanbul University, Cerrahpasa, Istanbul, Turkiye

[2] Department of Neurogenetics, Institute of Neurological Sciences, Istanbul University, Cerrahpasa, Istanbul, Turkiye

 0000-0002-2938-711X

Emrah Yucesan
[2] Department of Neurogenetics, Institute of Neurological Sciences, Istanbul University, Cerrahpasa, Istanbul, Turkiye

 0000-0003-4512-8764   ✉ emrah.yucesan@iuc.edu.tr

REFERENCES

1. William C. McIntosh, Joe M. Das. Temporal Seizure. In: StatPearls. 2023.

2. Baulac M. MTLE with hippocampal sclerosis in adult as a syndrome. Rev Neurol 2015; 171(3): 259-66.

3. Liu C, Qiao XZ, Wei ZH, Cao M, Wu ZY, Deng YC. Molecular typing of familial temporal lobe epilepsy. World J Psychiatry 2022; 12(1): 98-107.

4. Hedera P, Blair MA, Andermann E, Andermann F, D'agostino D, Taylor KA, et al. Familial mesial temporal lobe epilepsy maps to chromosome 4q13.2-q21.3. Neurology 2007; 68(24): 2107-12.

5. Maurer-Morelli C V., Secolin R, Morita ME, Domingues RR, Marchesini RB, Santos NF, et al. A locus identified on chromosome18p11.31 is associated with hippocampal abnormalities in a family with mesial temporal lobe epilepsy. Front Neurol 2012; 3: 124.

6. Leal B, Chaves J, Carvalho C, Rangel R, Santos A, Bettencourt A, et al. Brain expression of inflammatory mediators in Mesial Temporal Lobe Epilepsy patients. J Neuroimmunol 2017; 313: 82-8.

7. Ruffolo G, Martinello K, Labate A, Cifelli P, Fucile S, Di Gennaro G, et al. Modulation of GABAergic dysfunction due to SCN1A mutation linked to Hippocampal Sclerosis. Ann Clin Transl Neurol 2020; 7(9): 1726-31.

8. Silvennoinen K, Gawel K, Tsortouktzidis D, Pitsch J, Alhusaini S, van Loo KMJ, et al. SCN1A overexpression, associated with a genomic region marked by a risk variant for a common epilepsy, raises seizure susceptibility. Acta Neuropathol 2022; 144(1): 107-27.

9. Gurses C, Azakli H, Alptekin A, Cakiris A, Abaci N, Arikan M, et al. Mitochondrial DNA profiling via genomic analysis in mesial temporal lobe epilepsy patients with hippocampal sclerosis. Gene 2014; 538(2): 323-7.

10. Yang M, Li Y, Liu X, Zou S, Lei L, Zou Q, et al. Autophagy-related genes in mesial temporal lobe epilepsy: an integrated bioinformatics analysis. Acta Epileptol 2024; 6(1): 16.

11. Martinez B, Peplow P V. MicroRNAs as potential biomarkers in temporal lobe epilepsy and mesial temporal lobe epilepsy. Neural Regen Res 2023; 18(4): 716-26.

12. Pagni S, Mills JD, Frankish A, Mudge JM, Sisodiya SM. Non-coding regulatory elements: Potential roles in disease and the case of epilepsy. Neuropathology Appl Neurobiol 2022; 48(3): e12775.

13. Zhukova JV, Lopatnikova JA, Alshevskaya AA, Sennikov SV. Molecular mechanisms of regulation of IL-1 and its receptors. Cytokine Growth Factor Rev 2024; 80: 59-71.

14. Kang H, Dong Y, Peng R, Liu H, Guo Q, Song K, et al. Inhibition of IRE1 suppresses the catabolic effect of IL-1β on nucleus pulposus cell and prevents intervertebral disc degeneration in vivo. Biochem Pharmacol 2022; 197: 114932.

15. Saghazadeh A, Gharedaghi M, Meysamie A, Bauer S, Rezaei N. Proinflammatory and anti-inflammatory cytokines in febrile seizures and epilepsy: Systematic review and meta-analysis. Rev Neurosci 2014; 25(2): 281-305.

16. Mu J, Cao C, Gong Y, Hu G. Relationship between inflammation/immunity and epilepsy: A multi-omics mendelian randomization study integrating GWAS, eQTL, and mQTL data. Epilepsy and Behavior 2024; 161.

17. Uludag IF, Duksal T, Tiftikcioglu BI, Zorlu Y, Ozkaya F, Kirkali G. IL-1β, IL-6 and IL1Ra levels in temporal lobe epilepsy. Seizure 2015; 26: 22-5.

18. Strauss KI, Elisevich KV. Brain region and epilepsy-associated differences in inflammatory mediator levels in medically refractory mesial temporal lobe epilepsy. J Neuroinflammation 2016; 13(1): 270.

19. Pototskiy E, Vinokuroff K, Ojeda A, Major CK, Sharma D, Anderson T, et al. Downregulation of CD40L-CD40 attenuates seizure susceptibility and severity of seizures. Sci Rep 2021; 11(1): 17262.

20. Gonzalez Caldito N. Role of tumor necrosis factor-alpha in the central nervous system: a focus on autoimmune disorders. Front Immunol 2023; 14: 1213448.

21. Casillas-Espinosa PM, Powell KL, O'Brien TJ. Regulators of synaptic transmission: roles in the pathogenesis and treatment of epilepsy. Epilepsia 2012; 53(9): 41-58.

22. Patel DC, Wallis G, Jill Dahle E, McElroy PB, Thomson KE, Tesi RJ, et al. Hippocampal TNFα signaling contributes to seizure generation in an infection-induced mouse model of limbic epilepsy. eNeuro 2017; 4(2): ENEURO.0105-17.2017.

23. Ashhab MU, Omran A, Kong H, Gan N, He F, Peng J, et al. Expressions of tumor necrosis factor alpha and MicroRNA-155 in immature rat model of status epilepticus and children with mesial temporal lobe epilepsy. J Mol Neurosci 2013; 51(3): 950-8.

24. Deshmane SL, Kremlev S, Amini S, Sawaya BE. Monocyte chemoattractant protein-1 (MCP-1): An overview. J Interferon Cytokine Res 2009; 29(6): 313-26.

25. Khaboushan AS, Pahlevan-Fallahy MT, Shobeiri P, Teixeira AL, Rezaei N. Cytokines and chemokines profile in encephalitis patients: A meta-analysis. PLoS One 2022; 17(9): e0273920.

26. Aulická S, Česká K, Šána J, Siegl F, Brichtová E, Ošlejšková H, et al. Cytokine-chemokine profiles in the hippocampus of patients with mesial temporal lobe epilepsy and hippocampal sclerosis. Epilepsy Res 2022; 180: 106858.

27. Erta M, Quintana A, Hidalgo J. Interleukin-6, a major cytokine in the central nervous system. Int J Biol Sci 2012; 8(9): 1254-66.

28. Kwack DW, Kim DW. The increased interleukin-6 levels can be an early diagnostic marker for new-onset refractory status epilepticus. J Epilepsy Res 2022; 12(2): 78-81.

29. Li N, Pan J, Liu W, Li Y, Li F, Liu M. MicroRNA-15a-5p serves as a potential biomarker and regulates the viability and apoptosis of hippocampus neuron in children with temporal lobe epilepsy. Diagn Pathol 2020; 15(1): 46.

30. Srivastava A, Dixit AB, Paul D, Tripathi M, Sarkar C, Chandra PS, et al. Comparative analysis of cytokine/chemokine regulatory networks in patients

with hippocampal sclerosis (HS) and focal cortical dysplasia (FCD). Sci Rep 2017; 7(1): 15904.